

Introducing, Examining and Optimising Flow Diversion Structure as an Innovative Countermeasure against Local Scour around Bridge Piers

by Mohsen Ranjbar-Zahedani

Thesis submitted in fulfilment of the requirements for
the degree of

Doctor of Philosophy

under the supervision of Associate Professor Hadi Khabbaz

University of Technology Sydney
Faculty of Engineering and Information Technology

September 2019

CERTIFICATE OF ORIGINAL AUTHORSHIP

I, Mohsen Ranjbar-Zahedani declare that this thesis, is submitted in fulfilment of the requirements for the award of PhD degree, in the School of Civil and Environmental Engineering, Faculty of Engineering and Information Technology at the University of Technology Sydney.

This thesis is wholly my own work unless otherwise referenced or acknowledged. In addition, I certify that all information sources and literature used are indicated in the thesis.

This document has not been submitted for qualifications at any other academic institution.

This research is supported by the Australian Government Research Training Program.

Signature: Production Note:
Signature removed prior to publication.

Date: 06/04/2020

*Sincerely dedicated to
my wonderful wife*

Acknowledgement

Studying PhD abroad was a challenging but valuable experience for me, and it could not be completed without the support and guidance that I received from many people. Hence, I wish to express my sincere appreciations to those who helped me during this experience.

I greatly appreciate my supervisor, Associate Professor Hadi Khabbaz, for the nonstop support of my PhD study and his patience, motivation, and knowledge. It is my grand chance of expressing my truthful thankfulness to my external supervisor Professor Alireza Keshavarzi for his leadership, expert suggestions, continuous and strong support, and warm encouragement during my PhD study. Besides, I would like to have special thanks to my knowledgeable co-supervisor Associate Professor James Edward Ball, for his valuable advice and constant support from the commencement of this project to the end.

I gratefully acknowledge financial support from the Graduate Research School at the University of Technology Sydney (UTS) during my PhD study.

The major parts of my experimental tests have been conducted at the University of Wollongong (UOW) and also Western Sydney University (WSU). Therefore, I would like to greatly appreciate Associate Professor Brian Jones from the School of Earth and Environmental Sciences at UOW, who kindly permitted me to have access to their laboratory. I would also like to have exceptional thanks to Professor Bijan Samali, the director of the Centre for Infrastructure Engineering at WSU for granting me to have access to the advanced hydraulic laboratory at WSU.

Furthermore, I am very thankful to my friends and technical staff especially, Mr Rami Haddad, Mr Peter Tawadros, Mr James Tawadros, Dr Farshad Oveissi, Dr Lam Nguyen, and Mr Geoff Hurt who assisted and supported me to set-up the flume, assemble the required apparatus, design the experimental tests and build the physical models. I also want to thank my friend, Dr Mehdi Aghayarzadeh, for his friendship and frequent help and support.

My deepest and sincere gratitude goes to my dearest parents and my beloved siblings. Their unconditional love, support and encouragement have led me through the challenges of life. I would like to appreciate them with all my heart, sincerely.

Last but not least, I am really indebted to my wonderful wife, Shabnam, for being an endless source of love and encouragement. Her understanding of the demands required to complete this work has been inspirational. She supported me since I intended to commence this journey and travelled along thousands of miles away from our home country to make my dream come true.

List of Publications

- **Journal Papers**

1. **Ranjbar-Zahedani, M.**, Keshavarzi, A., Khabbaz, H. & Ball, J. 2018, 'Protecting bridge pier against local scour using flow diversion structure', *Proceedings of the Institution of Civil Engineers-Water Management*, vol. 171, No. 5, pp. 271-280.
2. **Ranjbar-Zahedani M.**, Keshavarzi A, Khabbaz H, & Ball J., 'Optimising Triangular Prism Flow Diversion Structure as an Effective Local Scour Countermeasure around a Pier'. Accepted for publication in the Journal of Hydraulic Research.

- **Peer-Reviewed Conference Papers**

3. **Ranjbar-Zahedani, M.**, Keshavarzi, A. & Khabbaz, H. 2017, 'Control of local scour at vicinity of bridge piers using flow diversion structure', *Proceedings of the 37th IAHR World Congress*, Kuala Lumpur, Malaysia.
4. **Ranjbar-Zahedani, M.**, Keshavarzi, A., Khabbaz, H., & Ball, J. 2019, 'Submerged flow diversion structure as an effective countermeasure to protect bridge piers from scour', *9th Australian Small Bridges Conference*, Gold Coast, Australia.
5. **Ranjbar-Zahedani, M.**, Keshavarzi, A., Khabbaz, H., & Ball, J. 2019, 'Flow structures around a circular bridge pier with a submerged prism at upstream', *Proceedings of the 4th World Congress on Civil, Structural, and Environmental Engineering (CSEE'19)*, Rome, Italy

- **Other Papers, Not Directly Related, to this Study**

6. Keshavarzi, A., Shrestha, C.K., **Ranjbar-Zahedani, M.**, Ball, J. & Khabbaz, H. 2017, 'Experimental study of flow structure around two in-line bridge piers', *Proceedings of the Institution of Civil Engineers - Water Management*, vol. 171, No. 6, pp. 311-327.
7. Keshavarzi, A., Shrestha, C.K., Melville, B., Khabbaz, H., **Ranjbar-Zahedani, M.** & Ball, J. 2018, 'Estimation of maximum scour depths at upstream of front and rear piers for two in-line circular columns', *Environmental Fluid Mechanics*, vol. 18, no. 2, pp. 537-50

Table of Contents

CERTIFICATE OF ORIGINAL AUTHORSHIP	I
Acknowledgement.....	III
List of Publications	V
Table of Contents	VI
List of Figures	X
List of Tables.....	XVI
Abstract	XVII
CHAPTER 1. Introduction	1
1.1. Background	2
1.2. Problem Statement	2
1.3. Research Objectives	3
1.4. Research Significance and Innovation	5
1.5. Research Methodology.....	5
1.6. Scope and Limitations.....	6
1.7. Layout of Thesis.....	7
CHAPTER 2. Literature Review	9
2.1. Introduction	10
2.2. Analysis of Bridge Collapses	10
2.3. Bridge Scour	12
2.3.1. General Scour.....	13
2.3.2. Contraction Scour.....	13
2.3.3. Local Scour	13
2.4. Classification of Studies on Local Scour around Bridge Piers	15
2.5. Turbulent Flow Field and Local Scour Mechanism around Piers	15
2.5.1. Turbulent Flow.....	16
2.5.2. Local Scour Mechanism around a Single Pier	17

2.5.3. Group of Piers	21
2.6. Countermeasures against Local Scour around Bridge Piers	27
2.6.1. Local Scour Countermeasures Using Armouring Devices	27
2.6.2. Local Scour Countermeasures Using Flow Altering Devices.....	36
2.7. Summary	53
CHAPTER 3. Preliminary Experimental Investigation of Flow Diversion Structure as a Pier Scour Countermeasure	55
3.1. Introduction	56
3.2. Selection the Shape of Flow Diversion Structure	56
3.3. Experimental Setup and Procedure	59
3.3.1. Laboratory Flume.....	59
3.3.2. Design of Experiment Conditions.....	60
3.3.3. Experimental Procedure	61
3.4. Results and Discussion.....	64
3.4.1. Determination of the Maximum Scour Depth.....	65
3.4.2. Determination of the Scour Hole Volume	70
3.4.3. Flow Field Analysis	71
3.4.4. Performance of the Proposed Flow Diversion Structure.....	78
3.5. Summary	79
CHAPTER 4. Experimental Optimisation of Hydrodynamic Performance of Flow Diversion Structure to Reduce Local Scour	81
4.1. Introduction	82
4.2. Review of Bridge Pier Protection against Local Scour.....	82
4.3. Materials and Methods.....	85
4.3.1. Dimensional Analysis and Definition of Dimensionless Variables.....	85
4.3.2. Experimental Design Using Taguchi's Method.....	88
4.4. Experimental Setup and Procedure	92
4.4.1. Flume and Its Components	92
4.4.2. Designing Experiment Conditions	93
4.4.3. Procedure of Local Scour Experiments.....	99

4.5. Results and Discussion.....	102
4.5.1. Sensitivity Analysis of the Dimensionless Parameters	104
4.5.2. Analysis of Variance (ANOVA) for Maximum Scour Depth	107
4.5.3. Analysis of Scour-Hole Volume	109
4.5.4. Confirmation Test	112
4.6. Conceptual Field Application of FDS.....	115
4.7. Conclusions.....	116
CHAPTER 5. Flow Field around a Circular Pier with Optimised Flow Diversion Structure at Upstream	117
5.1. Introduction.....	118
5.2. Review of Flow Structures near Bridge Piers.....	118
5.3. Experimental Setup and Procedure	119
5.3.1. Flume and Its Components	119
5.3.2. Physical Models of Bridge Pier and Flow Diversion Structures.....	120
5.3.3. Hydraulic Conditions	122
5.3.4. Particle Image Velocimetry (PIV)	123
5.3.5. Procedure of Flow Field Experiments.....	124
5.3.6. Image Processing	127
5.3.7. MATLAB Programming for PIV Data Analysis	127
5.4. Results and Discussion.....	128
5.4.1. Time Average Velocity Components.....	129
5.4.2. Flow Pattern	137
5.4.3. Turbulence Intensity Components	142
5.4.4. Turbulent Kinetic Energy.....	149
5.4.5. Reynolds Shear Stress	153
5.5. Conclusions.....	157
CHAPTER 6. Conclusions	158
6.1. Summary	159
6.2. Conclusions.....	160
6.2.1. Proof of Concept	160

6.2.2. Optimisation of Concept	161
6.2.3. Flow Field	163
6.3. Recommendations	165
References	167
APPENDIX A. The Captured Models of Scour Holes and Photographs of Scour Tests.....	180
APPENDIX B. Flow Field Plots.....	207
B.1. Plots of Streamwise Velocity Component.....	208
B.2. Plots of Vertical Velocity Component	220
B.3. Plots of Absolute Flow Velocity and Streamlines.....	232
B.4. Plots of Streamwise Turbulence Intensity	244
B.5. Plots of Vertical Turbulence Intensity.....	256
B.6. Plots of Turbulent Kinetic Energy.....	268
B.7. Plots of Reynolds Shear Stress	280
APPENDIX C. F-Distribution Table.....	292
APPENDIX D. Developed Code in MATLAB for PIV Data Analysis.....	295

List of Figures

Figure 1.1. Schematic diagram of a flow diversion structure	4
Figure 2.1. Various types of potential scour around bridge piers (modified from Melville & Coleman, 2000)	12
Figure 2.2. Local scour around bridge piers (taken by the candidate).....	14
Figure 2.3. Temporal velocity fluctuations at a point in turbulent flow	16
Figure 2.4. Main features of flow around a bridge pier (Hamill, 1998)	18
Figure 2.5. Two circular piers in cross-flow; a) tandem configuration; b) side-by-side configuration; c) staggered configuration	21
Figure 2.6. Tandem piers flow classification (modified from Sumner, 2010).....	22
Figure 2.7. Alternative armouring devices for pier scour protection (Melville & Coleman, 2000)	28
Figure 2.8. Collar on pier (modified from Kumar et al., 1999)	36
Figure 2.9. Bridge Pier with Slot; a) slot near bed; b) slot near water surface (modified from Chiew, 1992)	38
Figure 2.10. Bridge Pier with Slot; a) straight slot; b) T-shaped slot; c) Y-shaped slot (modified from Hajikandi & Golnabi, 2017)	39
Figure 2.11. Sacrificial piles upstream of a circular pier (Melville & Hadfield, 1999)..	40
Figure 2.12. Transverse sacrificial piles upstream of a pier (modified from Haque et al., 2007)	41
Figure 2.13. The use of Iowa vanes as a pier scour countermeasure (modified from Melville & Coleman, 2000)	42
Figure 2.14. Schematic of a delta wing (modified from Gupta & Gangadharaiah, 1992)	43
Figure 2.15. Permeable sheet pile upstream of a pier (Parker et al., 1998)	44
Figure 2.16. Internal openings through the pier (modified from El-Razek et al., 2003)	45
Figure 2.17. Surface guide panel; a) side view; b) plan view (modified from Huang et al., 2005).....	46

Figure 2.18. Threaded pier - helical wires or cables wrapped spirally on the pile to form thread (modified from Dey et al., 2006)	47
Figure 3.1. Wake width behind different structures (Roshko 1954).....	57
Figure 3.2. Schematic diagram of the preliminary experimental setup	61
Figure 3.3. Schematic diagram of grid points positions for measuring velocity components (longitudinal view).....	63
Figure 3.4. Photographs of measuring velocity components by ADV; a) control test; b) test with $d/D=1.5$	63
Figure 3.5. Scour depth vs. normalised distance to the pier; a) maximum scour depth; b) trend of maximum scour depth reduction	66
Figure 3.6. Maximum scour depth vs. normalised distance a) maximum scour depth at rear pier and b) maximum scour depth reduction at rear pier for the two in-line piers case.....	69
Figure 3.7. Scour hole volume against normalised distance; a) scour hole volume; b) scour hole volume reduction	71
Figure 3.8. Comparison plot of streamwise velocity component (u) in Test 1 (without FDS) and Test 4 (FDS with $d/D=1.5$)	73
Figure 3.9. Contour plots of time-averaged streamwise velocity component; a) Test 1; b) Test 4.....	74
Figure 3.10. Comparison of the depth-averaged of u in Test 1 and Test 4.....	75
Figure 3.11. Comparison plot of vertical velocity component (w) in Test 1 (without FDS) and Test 4 (with FDS)	76
Figure 3.12. Contour plots of time-averaged vertical velocity component; a) Test 1; b) Test 4.....	77
Figure 3.13. Comparison of the depth-averaged of w in Tests 1 and 4	77
Figure 3.14. Contour plots of mean flow velocity and streamlines; a) Test 1; b) Test 4	78
Figure 3.15. Streamlines diversion by triangular flow diversion structure.....	79
Figure 4.1. Schematic diagram of the pier and the flow diversion structure (FDS)	84

Figure 4.2. The effect of clear distance between the pier and FDS or between two in-line piers on local scour reduction around the rear pier	87
Figure 4.3. Schematic diagram of the laboratory flume.....	93
Figure 4.4. Sieve analysis of the sand used.....	95
Figure 4.5. Local scour depth variation with flow intensity (after Melville & Coleman, 2000)	96
Figure 4.6. Schematic diagram of pier and FDSs used in this experimental study.....	98
Figure 4.7. a) A photograph of an FDS; b) a photograph of pier on its position in the plexiglass sheets	100
Figure 4.8. A typical photograph of the test preparation (Test 10).....	100
Figure 4.9. Photographs of Artec Eva 3D scanner.....	101
Figure 4.10. Main-effect plots of the maximum pier scour depth	105
Figure 4.11. Effects of the height of FDS on the maximum pier scour depth	107
Figure 4.12. Main-effect plots of the scour-hole volume.....	110
Figure 4.13. Photographs of scour-hole; a) control test; b) optimum test.....	113
Figure 4.14. 3D models of scour-hole; a) control test; b) optimum test.....	114
Figure 5.1. Flow field around a bridge pier	119
Figure 5.2. A photograph of the flume and its components.....	120
Figure 5.3. a) FDS models; b) installation of the models into the plexiglass sheets on the flume bed.....	122
Figure 5.4. Schematic diagram of the PIV technique (Goharzade & Molki, 2014)	123
Figure 5.5. Experimental setup; a) a schematic diagram of the pier and FDS; b) different planes of PIV measurements (plan view).....	125
Figure 5.6. A photograph of experimental set up and PIV system in the laboratory....	125
Figure 5.7. Normalised streamwise velocity for the single pier case at $Y/D = 0$	131
Figure 5.8. Normalised streamwise velocity for the single pier case and FDS with $H/y=0.25$ at $Y/D = 0$	131

Figure 5.9. Normalised streamwise velocity for the single pier case and FDS with $H/y=0.50$ at $Y/D = 0$	132
Figure 5.10. Normalised streamwise velocity for the single pier case and FDS with $H/y=0.75$ at $Y/D = 0$	132
Figure 5.11. Normalised streamwise velocity for the single pier case and FDS with $H/y>1$ at $Y/D = 0$	133
Figure 5.12. Normalised vertical velocity for the single pier case at $Y/D = 0$	134
Figure 5.13. Normalised vertical velocity for the single pier case and FDS with $H/y=0.25$ at $Y/D = 0$	135
Figure 5.14. Normalised vertical velocity for the single pier case and FDS with $H/y=0.50$ at $Y/D = 0$	135
Figure 5.15. Normalised vertical velocity for the single pier case and FDS with $H/y=0.75$ at $Y/D = 0$	136
Figure 5.16. Normalised vertical velocity for the single pier case and FDS with $H/y>1$ at $Y/D = 0$	136
Figure 5.17. Normalised absolute flow velocity and Streamlines in wide frame at $Y/D = 0$; a) single pier case; b) single pier case and FDS with $H/y=0.25$	139
Figure 5.18. Normalised absolute flow velocity and Streamlines in tight frame at $Y/D = 0$; a) single pier case; b) single pier case and FDS with $H/y=0.25$	140
Figure 5.19. Normalised absolute flow velocity and Streamlines for the single pier case and FDS with $H/y=0.50$ at $Y/D = 0$	141
Figure 5.20. Normalised absolute flow velocity and Streamlines for the single pier case and FDS with $H/y=0.75$ at $Y/D = 0$	141
Figure 5.21. Normalised absolute flow velocity and Streamlines for the single pier case and FDS with $H/y>1$ at $Y/D = 0$	142
Figure 5.22. Normalised streamwise turbulence intensity for the single pier case at $Y/D = 0$	144
Figure 5.23. Normalised streamwise turbulence intensity for the single pier case and FDS with $H/y=0.25$ at $Y/D = 0$	144

Figure 5.24. Normalised streamwise turbulence intensity for the single pier case and FDS with $H/y=0.50$ at $Y/D = 0$	145
Figure 5.25. Normalised streamwise turbulence intensity for the single pier case and FDS with $H/y=0.75$ at $Y/D = 0$	145
Figure 5.26. Normalised streamwise turbulence intensity for the single pier case and FDS with $H/y>1$ at $Y/D = 0$	146
Figure 5.27. Normalised vertical turbulence intensity for the single pier case at $Y/D = 0$	147
Figure 5.28. Normalised vertical turbulence intensity for the single pier case and FDS with $H/y=0.25$ at $Y/D = 0$	147
Figure 5.29. Normalised vertical turbulence intensity for the single pier case and FDS with $H/y=0.50$ at $Y/D = 0$	148
Figure 5.30. Normalised vertical turbulence intensity for the single pier case and FDS with $H/y=0.75$ at $Y/D = 0$	148
Figure 5.31. Normalised vertical turbulence intensity for the single pier case and FDS with $H/y>1$ at $Y/D = 0$	149
Figure 5.32. Normalised turbulent kinetic energy for the single pier case at $Y/D = 0$.	150
Figure 5.33. Normalised turbulent kinetic energy for the single pier case and FDS with $H/y=0.25$ at $Y/D = 0$	151
Figure 5.34. Normalised turbulent kinetic energy for the single pier case and FDS with $H/y=0.50$ at $Y/D = 0$	151
Figure 5.35. Normalised turbulent kinetic energy for the single pier case and FDS with $H/y=0.75$ at $Y/D = 0$	152
Figure 5.36. Normalised turbulent kinetic energy for the single pier case and FDS with $H/y>1$ at $Y/D = 0$	152
Figure 5.37. Normalised Reynolds Shear Stress for the single pier case at $Y/D = 0$	154
Figure 5.38. Normalised Reynolds Shear Stress for the single pier case and FDS with $H/y=0.25$ at $Y/D = 0$	154
Figure 5.39. Normalised Reynolds Shear Stress for the single pier case and FDS with $H/y=0.50$ at $Y/D = 0$	155

Figure 5.40. Normalised Reynolds Shear Stress for the single pier case and FDS with $H/y=0.75$ at $Y/D = 0$	155
Figure 5.41. Normalised Reynolds Shear Stress for the single pier case and FDS with $H/y>1$ at $Y/D = 0$	156

List of Tables

Table 2.1. Number of failed bridges vs. Causes of failure, by 10 year intervals (modified from Lee et al., 2013).....	11
Table 2.2. Summary of flow field results for the longitudinal plane at centreline (after Keshavarzi et al., 2017).....	24
Table 2.3. Equations for sizing riprap around bridge piers.....	29
Table 2.4. Methods to estimate riprap extent, grading and filter requirements (after Melville & Coleman, 2000)	33
Table 2.5. Summary of different flow-altering devices as a pier scour countermeasure	51
Table 3.1. Shape factors for different pier shapes (modified from Melville & Coleman 2000)	58
Table 3.2. Characteristics of the preliminary tests	64
Table 3.3. Tests conditions and scour depth characteristics	65
Table 3.4. Scour depth characteristics at rear pier in tandem arrangement (after Keshavarzi et al., 2018).....	68
Table 3.5. Scour hole volume characteristics.....	70
Table 4.1. Experimental variables and their values and levels	88
Table 4.2. Experimental design based on Taguchi's method.....	90
Table 4.3. Mutually orthogonal of any two variables' weighing factors	91
Table 4.4. The results of local scour tests	103
Table 4.5. Variable level averages for the maximum pier scour depth (mm).....	104
Table 4.6. Comparison of the best d/D for different cases and hydraulic conditions ...	106
Table 4.7. Analyses of variance for the maximum scour depth.....	109
Table 4.8. Variable level averages for the scour-hole volume (1000 mm ³)	110
Table 4.9. Analyses of variance for the scour-hole volume.....	111
Table 5.1. Flow conditions for experimental tests on flow field	122
Table 5.2. The details of the flow field tests configurations.....	126

Abstract

Previous studies have shown that local scour around bridge piers and abutments is a common cause of waterway bridge failures, and around 60% of bridge collapses are due to this phenomenon. To control and reduce local scour, different engineering methods have been proposed by the researchers which can be classified into two distinct categories, including (i) armouring devices, which is a conventional way, and (ii) flow-altering devices. Armouring devices such as riprap is placed around a pier to armour the riverbed grains against shear stresses and reduces the local scour. However, riprap layers often fail to protect bridges during floods because it cannot be stable to withstand the high approaching stream velocities. The second category is flow-altering devices that change the flow field around the bridge piers in a manner that reduces the potential for erosion.

In this study, a new flow-altering device named flow diversion structure (FDS) has been introduced and experimentally examined and optimised. Different criteria were considered to select the shape of this FDS including diverting streamlines from the vicinity of pier, creating a relatively wide wake region behind the FDS, and having a low amount of local scour around itself. Theoretically, by comparison different shapes according to the above criteria, triangular prism was recognised as a proper shape. The effectiveness of this innovative countermeasure was examined through a wide-ranging series of experimental studies. Firstly, a number of preliminary laboratory tests were conducted to prove whether proposed FDS can reduce the local scour around a circular bridge pier. An introductory FDS was built with a lateral base of $0.2D$, longitudinal base of $0.5D$ (where D is the pier diameter), and full-depth (unsubmerged) height. Seven tests were conducted for situations of a single pier and a single pier plus the FDS, which was installed at six alternative locations upstream of the pier (namely $d/D = 0.5, 1.0, 1.5, 2.0, 2.5$ and 3.5 , where d is the clear distance between the pier and FDS). All tests were conducted under steady state and clear-water scour conditions. After achieving the equilibrium bed condition, the bed profile was measured, and the maximum scour depth and volume of the scour hole were determined for each experimental test. In addition, to determine the influence of the FDS on the flow field upstream of the pier, the velocity components were measured by an Acoustic Doppler Velocimetry (ADV). Analysis of the results indicated that the proposed FDS could change both the magnitude and direction of the velocity components upstream of the pier, and consequently reduce the scour depth around the pier

up to 38%. Besides, the clear distance between the pier and the FDS affected the performance of this new countermeasure.

Secondly, to optimise the dimensions of FDS including the lateral base (B), longitudinal base (L), and height (H), and its clear distance from the upstream face of a circular pier (d), different FDS dimensions and locations were examined experimentally. Taguchi's method, which is an efficient statistical approach to design experimental tests, was employed here to determine the parameter combination to minimise the numbers of alternative tests. Therefore, 27 FDSs were tested to find the optimum size and installation location of the FDS. An advanced technology of 3-D printing was employed to build accurate physical models. At the end of each test, to measure the topography of the scoured bed a precise 3-D scanner was used. Similar to the preliminary tests, these experiments were also conducted in a steady flow and under clear water scour conditions. However, the hydraulic conditions were adjusted in such a way to produce almost maximum possible local scour. After achieving equilibrium condition, the scour hole was scanned, and the maximum scour depth and the volume of the scour hole were extracted from the 3-D model for each experimental test. The outcomes clearly demonstrated that the best lateral base, longitudinal base, and height of FDS were equals to $0.4D$, $0.6D$, and $0.25y$ (where y is the water depth), respectively. Furthermore, the best clear distance between FDS and the pier is approximately between $1D$ and $1.5D$. In the optimum situation, the scour depth and the volume of the scour hole around the pier reduced by 40% and 60%, respectively.

Finally, to find out how the optimised FDS affected the flow field around a circular pier, an experimental study of flow field was conducted using a Particle Image Velocimetry (PIV) system. All tests were conducted under fixed bed condition with no sediment. The optimised FDS was installed at the best location upstream of the pier ($d/D = 1.5$), and the velocity components were measured at five vertical planes (i.e., $Y/D = 0, 1, 2, 3$ and 4 , where Y is the transverse direction). A similar test was carried out with only a single pier as a control test. The PIV images, collected during the individual experiments, were processed to determine the streamwise (u) and vertical (w) velocity components. A code was developed using MATLAB software to calculate the turbulence characteristics of the flow. Analysis of the results indicated that the optimised FDS significantly affected the flow field and changed the complicated vortices systems, including down-flow, horseshoe vortex, and wake vortex around the pier. Consequently, the pier-scour was significantly reduced by the substantial changes in the flow field. This novel device is a simple and easy option for mitigating local scour around the piers supporting existing and new bridges.

CHAPTER 1

Introduction



The screenshot shows the BBC News Magazine website interface. At the top, the BBC logo is on the left, and navigation links for 'Sign in', 'News', 'Sport', 'Weather', 'Capital', 'TV', and 'Radio' are on the right. Below this is a red and orange header with 'NEWS' in white and 'Magazine' in white on an orange background. The main content area is titled 'News Front Page' and includes a world map icon, a 'Page last updated at 14:26 GMT, Monday, 23 November 2009' timestamp, and links for 'E-mail this to a friend' and 'Printable version'. The featured article is titled 'Can you stop bridges collapsing in floods?' and includes a photograph of a bridge over a river. Below the photo is a sub-headline 'Older bridges are often not on piles driven into the riverbed' and a section titled 'WHO, WHAT, WHY?' with the text 'The Magazine answers...'. The article body begins with 'A number of bridges have collapsed or are on the verge of giving way in the Cumbrian floods. But is there any way to guarantee this doesn't happen?'. A left-hand navigation menu lists various categories: Africa, Americas, Asia-Pacific, Europe, Middle East, South Asia, UK (with sub-links for England, Northern Ireland, Scotland, Wales, UK Politics, and Education), Magazine (highlighted), Business, Health, Science & Environment, Technology, Entertainment, and Also in the news.

1.1. Background

Bridges on waterways are essential structures for transportation. However, every year, many bridges collapse all over the world. Examples of these collapses are Bishopsford Road Bridge in England (2019), Nanfang'ao Bridge in Republic of China (2019), Rail Bridge in Romania (2018), Provincial Road Ksanthi-Iasmos at Kompsatos river crossing in Greece (2017), Pfeiffer Canyon Bridge in the United States (2017), etc. (see https://en.wikipedia.org/wiki/List_of_bridge_failures for more information).

Collapse of a bridge causes several problems to the public safety and the transportation system as well as imposes enormous financial losses and environmental damages. In addition, it may destroy the reputation of bridge asset management authorities. Accordingly, a key desire would be to reduce the risk of waterway bridge collapse. To achieve this desire, reasons for waterway bridge collapses should be well-understood. While several studies conducted on the various reasons that led to collapse of bridges are discussed in the literature analysis presented later, it is necessary to overview these studies in discussing the problem investigated herein.

The following section provides a brief description of the main causes of waterway bridge failure.

1.2. Problem Statement

While there are many causes of bridge collapse, a common theme in studies investigating bridge collapses is local scour of the bridge piers. Smith (1976), Wardhana & Hadipriono (2003), Lagasse et al. (2007) report scour induced collapses as being between 45% and 60%. Therefore, it is identified that an appropriate answer to the question, *how can we stop waterway bridges collapsing?*, would be finding an effective and eco-friendly way to control local scour around bridge piers.

1.3. Research Objectives

As stated in the previous section, a leading concern regarding the stability of bridge foundations is the occurrence of local scour around the piers. Local scour around a bridge pier is a result of flow field and bridge pier interactions that forms a system of complicated vortices around the pier that is explained in Chapter 2. One approach to reduce local scour is to change this vortices system by using a flow altering device. Alternative flow altering devices have been proposed in the literature. These are discussing in detail in Chapter 2. Arising from that discussion, it will be shown that there are no guidelines for the design of these flow altering devices. In this study, a new flow altering device named Flow Diversion Structure (FDS) with a triangular prismatic shape installed upstream of the pier is introduced and discussed. The reasons for selection of a triangular shape for the FDS are presented in Section 3.2. Figure 1.1 illustrates a schematic diagram of the FDS installed upstream of a circular pier. In addition to confirming the FDS is a viable flow altering device, design guidance is required if the FDS is to be deployed in the field.

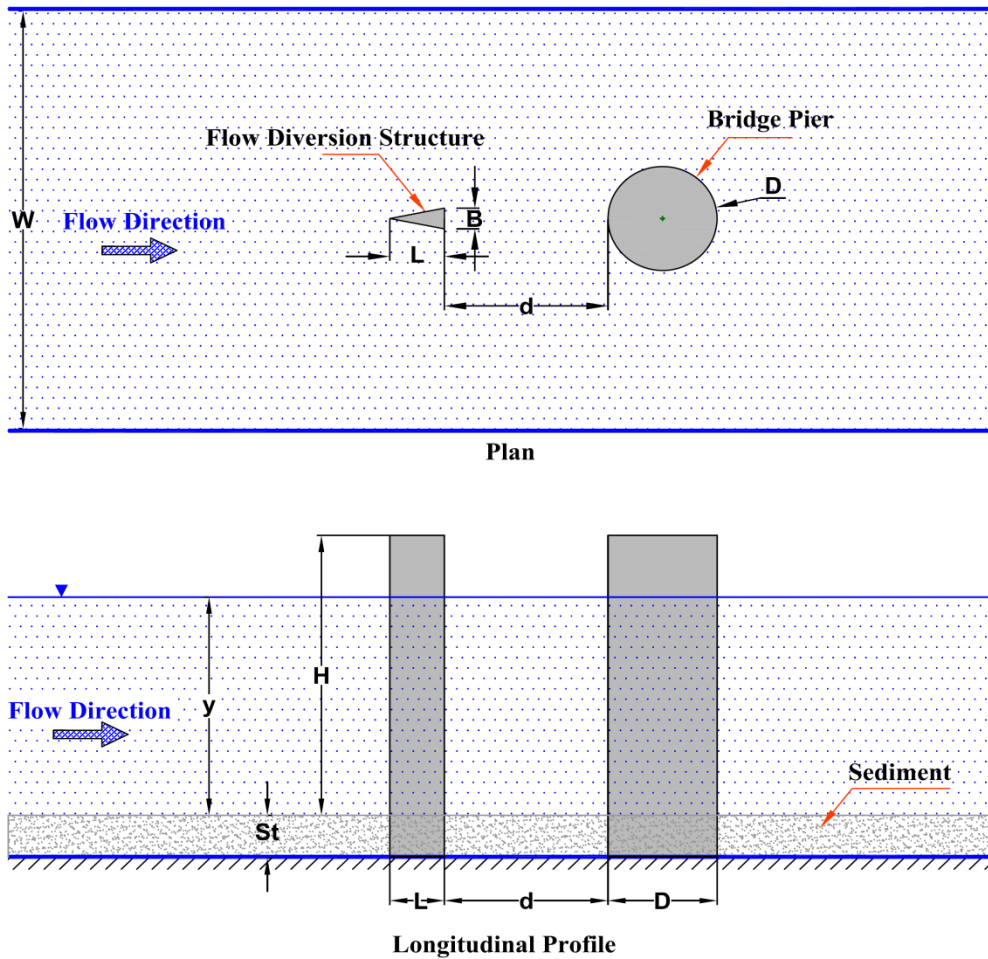


Figure 1.1. Schematic diagram of a flow diversion structure

The main goal herein is to perform an experimental study of the effects of this FDS on both local scour and flow field around a circular pier. To achieve this goal, three specific objectives are planned as follows:

1. Evaluating the effects of the FDS with initial dimensions on local scour and flow field near a circular pier. This objective is considered as a proof of concept for a triangular FDS.
2. Optimising the dimensions and installation location of the FDS to achieve the maximum reduction of local scour. The lateral base (B), longitudinal base (L), and height (H) of the FDS, as well as the clear distance between the pier and the FDS (d) are optimised as a function of pier size and flow conditions. These optimised dimensions and location provide guidance for field applications.

3. Evaluating the effects of the optimised FDS on the flow field around a circular pier.

1.4. Research Significance and Innovation

"Man who overlook water under bridge will find bridge under water" (Neill 1973). This citation highlights the important effects of running water on the stability of bridges; and significantly its impact on piers that support the bridge. Accordingly, this research is focused on the countermeasures against local scour around bridge piers.

Unlike the literature discussing scour mechanism and the associated flow field for bridge piers, there is still inadequate research on local scour countermeasures; and considerably few methods have been suggested to reduce local scour around a pier by changing the flow field at the vicinity of the pier. The previously proposed flow altering devices were not fully discussed, and they have a lack of information and guiding principles associated with their design and performance. Hence, there is no thorough report of their applications in real situations.

In this study, a new flow altering device is introduced to reduce the local scour around a circular bridge pier through the following innovations:

- Proposing and confirming a new shape for a flow altering device, hereafter referred to as FDS, for reducing local scour around a bridge pier.
- Developing design guidance for the FDS dimensions and location. Taguchi's technique was employed to minimise the number of alternative tests required for development of this design guidance
- Employing reliable measurement techniques to capture accurate results such as 3-D scanner for measuring scour-hole topography, and PIV system for measuring instantaneous flow velocity components

1.5. Research Methodology

Because of the complexity of the turbulent flow field and mechanisms of local scour around a bridge pier, most studies in this field are based on the physical modelling. The main hypothesis of this research study is that suitable guidance for the design of a FDS can be obtained through design of a well-structured experimental program. To achieve

this, a program of experimental work is designed and undertaken. As part of this experimental program the effectiveness of the FDS needs to be considered, and the optimal dimensions and location need to be determined.

Three research objectives were identified in Section 1.3. To achieve each of these objectives alternative sets of experiments were required. While details of these experiments are outlined in Chapter 3 to 5, common conditions for all experiments were:

- All tests were conducted under steady state flow condition
- All local scour tests were performed under clear water scour condition (the definition of clear water scour is presented in section 2.2.3.)
- All flow field tests were completed under fixed bed condition (no sediment)

Two types of measuring devices were used in this study for determining flow velocity components. Acoustic Doppler Velocimetry (ADV) was utilised for the first series of tests, while Particle Image Velocimetry (PIV) was employed for the third series of tests. Measurement of velocity components was not needed during the second series of tests. The final bed topographies in the first and second set of the local scour tests were measured using a digital pointer, and a 3-D topography scanner, respectively.

Finally, the local scour data were analysed to evaluate the effects of the proposed FDS on local scour reduction around a circular pier, and to find out the optimum dimensions and the best installation location of FDS to achieve the maximum reduction of local scour. In addition, the measured flow field data were analysed to discover how this FDS could change the flow field around a circular pier, and consequently reduce the local scour.

1.6. Scope and Limitations

The mechanism of pier scour is complex due to the complicated interactions between flow, pier, and sediment. Consequently, a laboratory experimental study is widely considered as one of the most reliable and precise methods of study in the field of pier-scour. Accordingly, this study was planned to be conducted experimentally. However,

limitations on experimental investigations arise from the available facilities, time, and budget. The limitations for this study were:

- The flow condition was steady state
- Local scour tests were conducted under clear water scour condition
- Local scour tests were carried out using cohesion-less and uniform sand
- Only a single circular pier model was employed for studying the effects of the FDS on local scour and flow field around a bridge pier

1.7. Layout of Thesis

While there are six chapters in this thesis, the purpose of individual chapters differs.

In the first chapter, a general background to the research undertaken is presented. This background includes the objectives and through this the significance of the research. As presented will be an overview of the investigation methodology and, through the discussion of the methodology, the innovation within the project. Finally, an overview of the information that will be developed during the research is presented.

A critical component of the research is an analysis of the literature highlighting the lack of data and information regarding the problem being investigated. This analysis of the published literature on local scour is presented in Chapter 2. Included in this analysis is the definition of local scour and flow characteristics influencing the presence and magnitude of local scour. Furthermore, the need for countermeasures protecting piers against local scour is discussed with alternative approaches, including armouring devices and flow altering devices, for providing that protection. Of critical importance to this project is the analysis showed, for the flow altering devices previously investigated, that there are no guidelines for design of them. In this study, a flow altering device is studied for a suitable shape and the development of guidance for design. This is investigated in the following three chapters.

The methodology for the investigation consisted of three components. The first of these components was a series of tests aimed at confirming a triangular shaped prism located upstream of a pier would mitigate local scour at the pier. These tests are described in Chapter 3 where the “proof of concept” is presented.

Following the “proof of concept”, a series of tests was designed to investigate the optimal size and location of the FDS. Due to the number of parameters being considered, Taguchi’s method was used in the design of a feasible test series. This design and the results of the test series are described in Chapter 4. Also presented in Chapter 4 is a conceptual field application of the FDS.

The final component of the investigation was consideration of the flow fields with and without the FDS. PIV techniques were used in this part of the investigation. These techniques and the results obtained are presented in Chapter 5.

A summary of the outcomes from the investigation are presented in Chapter 6. Also presented in Chapter 6 are suggestions developed during this investigation for further research in this topic.

Finally, some additional materials relevant to the investigation are included as appendices.

CHAPTER 2

Literature Review

"Man who overlook water under bridge will find bridge under water" (Neill 1973)



2.1. Introduction

As stated in the previous chapter, for reducing the risk of waterway bridge collapses, it is necessary to well-understood the reasons for this problem. In this chapter, initially, an analysis of bridge collapses to find the main reason for this problem is presented. As will be discussed, the main reason for bridge collapses is scour. Then, the definition and types of bridge scour will be stated. After that, a classification of the bridge scour studies will be presented, followed by the analysis of published literature on bridge scour mechanism and countermeasures that are related to the objectives of the current research study. Finally, a summary to highlight the lack of data and information regarding the problem being investigated will be presented.

2.2. Analysis of Bridge Collapses

Smith (1976) analysed 143 cases of bridge collapse in different countries from 1961 to 1975. He reported that about 70 bridges collapsed during the flood, about 45% of which were due to local scour of the bridge piers.

Melville (1992) reported that in New Zealand, 29 bridges collapsed as a result of abutment scour during the years 1960 to 1984. In addition, every year in this country at least one severe bridge collapse occurs due to the scour as stated by Melville & Coleman (2000).

Based on Wardhana & Hadipriono (2003), flood and scour were the most common causes of bridge failures at 53% in the United States between 1989 and 2000, whereas overload and lateral impact forces from trucks, barges/ships, and trains contributed 20% of the total bridge failures during the same period.

According to a report by Lagasse et al. (2007), bridge pier scour is the leading cause of 60% of bridge failures in the United States. They stated that “83% of the 583,000 bridges in the National Bridge Inventory (NBI) are built over waterways.” They cited an example from a 1994 storm in Georgia where scour damage occurred to more than 500 bridges. Scour depth ranging from 4 to 6 meters at 31 bridges were reported by report source.

Lee et al. (2013) studied the United States bridge failures between 1980 and 2012 and reported the number of failed bridges versus causes of failure, as presented in Table 2.1. Referring to that study, it can be realized that scour and flood are the most common causes of waterway bridge failures.

**Table 2.1. Number of failed bridges vs. Causes of failure, by 10 year intervals
(modified from Lee et al., 2013)**

Causes of failure	2000-2012	1990-2000	1980-1990	Total	Percent
Flood	40	154	107	301	28.3%
Scour	53	92	55	200	18.8%
Collision	51	55	57	163	15.3%
Overload	37	31	67	135	12.7%
Internal causes ¹	32	36	50	118	11.1%
Environmental degradation	23	22	26	71	6.7%
Fire	12	10	8	30	2.8%
Earthquake	1	11	8	20	1.9%
Wind	8	8	1	17	1.6%
Others ²	2	3	2	7	0.7%
Total	259	422	381	1062	100%

Bridge failures that happened in USA during the years 2000 - 2012 were analysed by Taricska (2014). He concluded that both scour, and flood individually was higher than any other single cause of failure, and together, combined for nearly 50% of all bridge failures over the timeframe studied.

The history of the bridge failures indicates that among all the causes, scour is a significant and common cause of waterway bridge failures.

1- Internal causes consist of faulty design, error in construction, low quality materials, and lack of maintenance.

2 - The causes of seven failures are not distinctly defined in the data sources and are listed as 'others'.

2.3. Bridge Scour

Bridge scour is a specific form of waterway erosion. Van Rijn (1993) stated that the scour process near a bridge pier is related to three effects including (i) local disturbance of the flow field, (ii) local reduction of cross-section, and (iii) general lowering of river bed near the bridge site during floods. Melville & Coleman (2000) defined bridge scour as *“the lowering of the level of the riverbed by water erosion such that there is a tendency to expose the foundations of a bridge. The amount of this reduction below an assumed natural level (generally the level of the riverbed prior to the commencement of the scour) is termed the depth of scour or scour depth.”* They stated that three different types of scour can happen at a bridge; there are

- General scour
- Contraction scour
- Local scour

These types of bridge scour are depicted in Figure 2.1. One or some of the different scour types may happen simultaneously at a particular bridge.

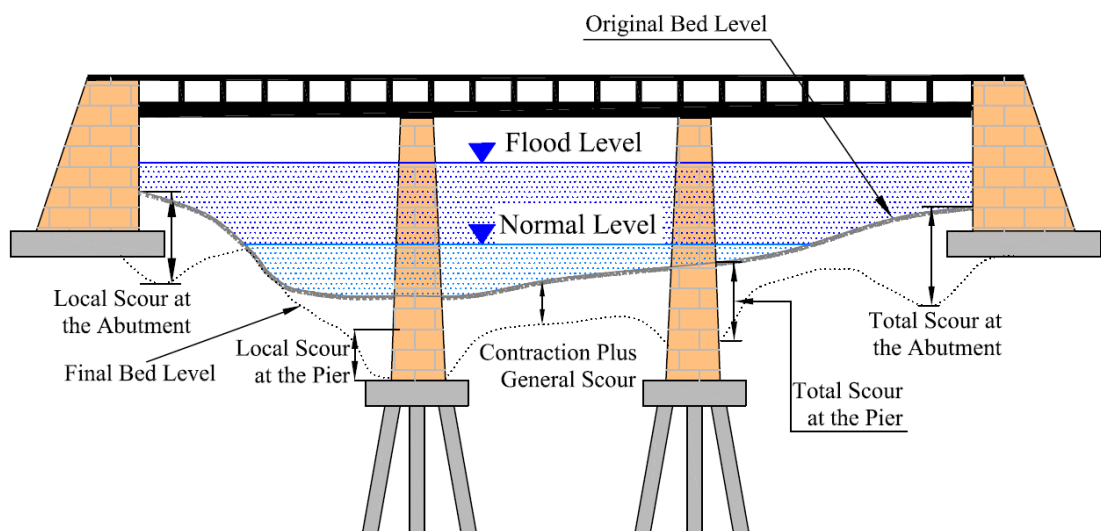


Figure 2.1. Various types of potential scour around bridge piers (modified from Melville & Coleman, 2000)

2.3.1. General Scour

General scour based on Melville & Coleman (2000) is lowering of the overall longitudinal profile of the riverbed attributable to natural or anthropogenic causes. The occurrence of this type of scour is unrelated to the presence of the piers. General scour in a riverbed may occur either as a short-term or long-term phenomenon depending on the time taken for the development of scour.

2.3.2. Contraction Scour

Contraction scour occurs where the cross-section of a river narrows because of the existing of a structure such as bridge piers or abutments in the river. Accordingly, the flow velocity increases along the narrow section and then decreases as the cross-section expands beyond this section. The contraction scour occurs due to this accelerated flow (Melville & Coleman 2000).

2.3.3. Local Scour

Local scour is caused by the interference of the piers and abutments with the flow and is characterised by the formation of the scour holes around the bridge piers or abutments (Melville & Coleman, 2000). Figure 2.2 illustrates the scour hole around bridge piers in Australia.

Of the above classifications, this study focuses on countermeasures against local scour around bridge piers.



Figure 2.2. Local scour around bridge piers (taken by the candidate)

Melville (1975) suggested classifying the local scour based on the amount of sediment transported out (q_{s1}) and supplied in (q_{s2}) of the scour hole. The difference between these two amounts is expressed as the scour hole rate in volume per unit time (q_s).

$$q_s = q_{s1} - q_{s2} \quad (2.1)$$

Accordingly, two distinct types of local scour can be identified as follows:

- **Clear Water Scour**

Clear water scour happens when sediment particles are removed from the scour hole and not replaced. In this type of local scour the sediment feed rate for the scour hole is zero

($q_{s2} = 0$). The maximum amount of local scour is reached when the transport capacity out of the scour hole is zero. This condition is attained when the flow is no longer capable to move sediment particles from the scour hole.

- **Live Bed Scour**

Live bed scour occurs where the scour hole is constantly supplied with material from the sediment load carried by the upstream section. In this type, the rate of sediment transports out (q_{s1}) and in (q_{s2}) of the scour hole are positive. The equilibrium condition is achieved when the capacity for transport of sediment into and out of the scour hole are equalised ($q_{s1}=q_{s2}$).

2.4. Classification of Studies on Local Scour around Bridge Piers

Many researches have been conducted in the field of local scour around bridge piers. These various investigations can be classified into three categories, namely (i) local scour mechanism and flow field, (ii) estimation of local scour, and (iii) countermeasures against local scour. The main objective of this research is reduction of local scour around bridge piers by changing the flow field, which can be incorporated into the first and third categories of the above classification. Therefore, in the following sections, a brief review of some previous studies in these two categories is presented. For this project it is necessary to understand some basic concepts of open channel hydraulics and fluid mechanics; these are presented here.

2.5. Turbulent Flow Field and Local Scour Mechanism around Piers

As stated in several investigations such as Melville & Raudkivi (1977), Chiew (1984), Dargahi (1989), Rajagopalan & Antonia (2005), Kirkil et al. (2008), Debnath et al. (2012), Keshavarzi et al. (2014), Sarkar et al. (2016), and Gautam et al. (2019), factors that influence local scour around a bridge pier includes three dimensional turbulent flow. Therefore, to study the flow field and mechanism of scour around bridge piers, it is

required to know some basic concepts of turbulent flow in open channels which are presented in the next section.

2.5.1. Turbulent Flow

According to Pope (2000), an essential feature of turbulent flows is that the fluid velocity fluctuates significantly and irregularly in both position and time. Generally in hydraulic engineering, u , v and w are used to show the instantaneous velocity components at a point in the streamwise, transverse and vertical directions, respectively. Correspondingly, \bar{u} , \bar{v} and \bar{w} show the mean velocity components; and u' , v' and w' show the velocity fluctuating components. This behaviour can be exemplified by a time history of the velocity components in a typical point, as shown in Figure 2.3; and the following equations (Reynolds decomposition) can be written:

$$u = \bar{u} + u' \quad (2.2)$$

$$v = \bar{v} + v' \quad (2.3)$$

$$w = \bar{w} + w' \quad (2.4)$$

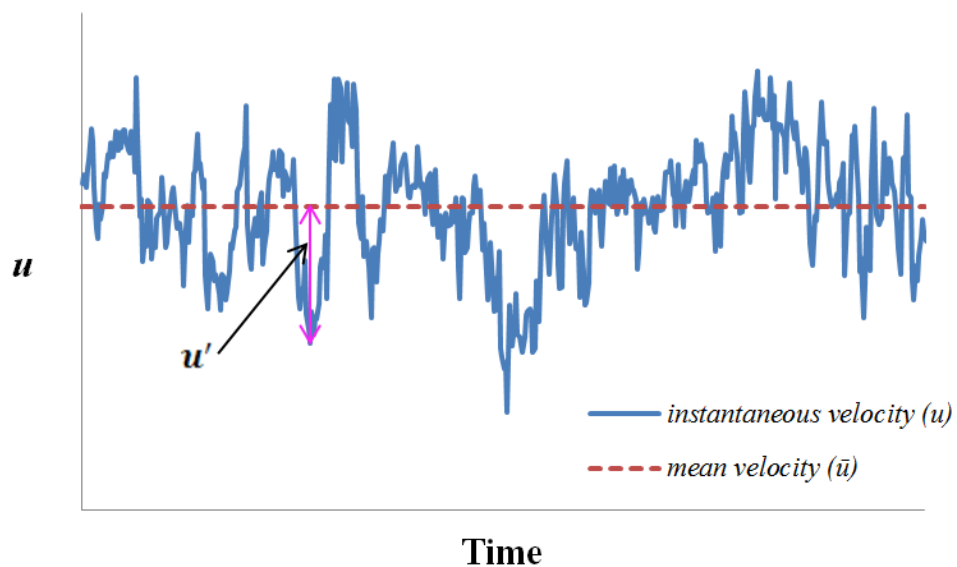


Figure 2.3. Temporal velocity fluctuations at a point in turbulent flow

In the area of fluid dynamics, turbulence intensity (TI) is described as the ratio of the root mean square of the velocity fluctuating components to the mean flow velocity. Turbulent kinetic energy (TKE) is the kinetic energy calculated with turbulent fluctuating velocities. Turbulence intensity (TI) and turbulent kinetic energy (TKE) can be calculated by Equations 2.5 and 2.6, respectively.

$$TI = \sqrt{\frac{1}{3}(\overline{u'^2} + \overline{v'^2} + \overline{w'^2})} \quad (2.5)$$

$$TKE = \frac{1}{2}(\overline{u'^2} + \overline{v'^2} + \overline{w'^2}) \quad (2.6)$$

The velocity fluctuating components can also be utilised to compute the Reynolds Shear Stress. The components of Reynolds Shear Stress are defined as:

$$\tau_{uv} = -\rho\overline{u'v'} \quad (2.7)$$

$$\tau_{vw} = -\rho\overline{v'w'} \quad (2.8)$$

$$\tau_{uw} = -\rho\overline{u'w'} \quad (2.9)$$

The principles of turbulent flow and its characteristics are explained by Pope (2000).

2.5.2. Local Scour Mechanism around a Single Pier

The complicated flow structure at the vicinity of a bridge pier causes the local scour, which is one of the significant reasons for waterway bridge failure. The main feature of this flow field is a system of vortices formed around a bridge pier as schematically illustrated in Figure 2.4.

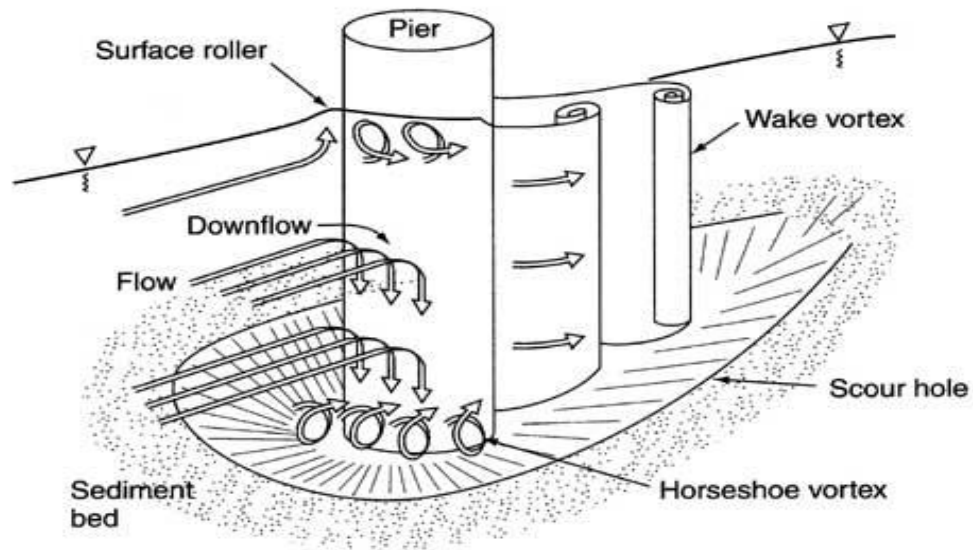


Figure 2.4. Main features of flow around a bridge pier (Hamill, 1998)

As expressed by Melville (1975), a vortices system shaped around a bridge pier including horseshoe vortex and wake vortex, is the leading cause for the local scour. The horseshoe vortex increases the velocity near the bed, leads to a rise in the transport capacity of the sediment particles. The wake vortex suspends the sediment particles and also acts like a vacuum cleaner while moving the bed material downstream.

Melville & Raudkivi (1977) stated that when a bridge pier is placed in a river stream, the flow velocity reduces upstream of the pier and becomes stationary on the upstream surface of the pier. Hence, the upstream flow velocity on the upstream surface of the pier reduces to zero, which results in an increase in pressure. The related pressures are maximum near the surface, and decrease downwards. This difference in pressure forms an adverse pressure gradient on the upstream face of the pier in the vertical direction as a result of approaching boundary layer flow. If this pressure gradient is strong enough, it is capable of causing a downward flow on the upstream face of the pier.

Based on Qadar (1981), scouring vortex due to flow separation in front of a pier is the main cause of the local scour. Chiew (1984) also introduced a concept similar to Melville's (1975) conceptual model. To comprehend the mechanism of local scour, some studies, for example those by Ettema (1980), Dargahi (1989), Ahmed & Rajaratnam (1997), Richardson & Panchang (1998), Melville & Coleman (2000),

Meneghini et al. (2001), Muzzammil & Gangadhariah (2003), Kumar & Kothiyari (2011), and Shrestha (2015) have been performed. In all the above studies, it was concluded that vortices are the most important causes of sediment particle entrainment around the bridge piers.

As discussed by Melville & Coleman (2000), there are four main characteristics of the flow structure at a pier. These include a down-flow and surface roller at the upstream of the bridge pier, a horseshoe vortex at the pier base of the bridge, and wake vortices downstream of the bridge pier, as shown in Figure 2.4.

Based on Muzzammil & Gangadhariah (2003), the boundary layer at the upstream face of a pier undergoes a three-dimensional separation. The downward flow due to negative pressure gradient interacts with the horizontal boundary layer separation close to the river bed. This interaction results in formation of a vortex system. This vortex system wraps around the pier and is swept downstream by the flow. When it is viewed from the top of the pier, the shape of the swept vortex system is the same as a horseshoe. Hence it is popularly known as horseshoe vortex.

Down-flow and horseshoe vortex features around circular piers were experimentally investigated by Unger & Hager (2007). They have concluded that the governing scour agents included the horseshoe vortex inside the continuously increasing scour hole and the down-flow at the upstream surface of the bridge pier. Furthermore, the horseshoe vortex develops with time, and its velocity profile is a function of pier diameter, the approach flow depth, median sediment size and densimetric particle Froude number.

Dey & Raikar (2007) experimentally studied the horseshoe vortex in scour holes around the piers. The results of their study revealed that the horseshoe vortex size becomes larger as the scour hole develops. In addition, the horseshoe vortex circulations increase with the increase in scour hole size.

Ettema et al. (2011) categorised three types of flow structure around bridge piers, based on the ratio of the flow depth (y) to the pier diameter (D) including narrow piers when $y/D > 1.4$, transitional piers when $0.2 < y/D < 1.4$, and wide piers when $y/D < 0.2$.

As stated by Ettema et al. (2011) for narrow piers, a down-flow and up-flow with roller take place at the upstream of the pier as a results of flow impact against the pier face.

The flow converging, contracting, then diverging occurs as the flow passes the pier. The generation, transport and dissipation of the horseshoe vortex also happen at the pier base. In addition, the shear layers detach at pier flanks. Moreover, wake vortices form behind the pier. These flow field features grow as the scour develops. Consequently, in narrow piers, the scour is typically deepest at the face of the pier due to the formation of different flow field features around the pier.

According to Ettema et al. (2011), the features of flow structure in the transitional pier are almost similar to the features described for narrow piers. However, the flow field features start to partially disrupt according to the reducing of water depth and or increasing of pier diameter. Therefore, the capability of flow field features to erode foundation material will reduce.

For the third type of this categorisation, Ettema et al. (2011) presented that as the flow approaches to the pier, the flow velocity reduces and the flow moves along the upstream face of the pier before narrowing and moving around the sides of pier. A partial and weak down-flow occurs at the upstream face of the pier, which may narrowly erode the pier foundation at the pier centre plane. The maximum erosive flow field features which include wake vortices and the part of the horseshoe vortex happen close to the flanks of the pier. Hence, deepest scour occurs at the pier flanks.

Gautam et al. (2019) experimentally studied the flow and turbulence characteristics around simple and complex piers. The complex pier in their study was a circular cylindrical pier resting on an elliptical pile-cap supported by a 2×2 array of pile group. They reported that the flow field around a complex pier is significantly different from that of the simple pier. The results of their study show that the magnitudes of the mean velocity, turbulence intensity and Reynolds Shear Stress for the simple pier case are higher than those of the complex pier.

In addition to the above studies, several other researches have been conducted to investigate the process of local scour, for instance Dargahi (1990), Roulund et al. (2005), Zhao & Huhe (2006), Kirkil et al. (2008), Kirkil et al. (2009), Veerappadevaru et al. (2011), Chang et al. (2013), Beheshti & Ataie-Ashtiani (2016), Sarkar et al. (2016), and Vijayasree et al. (2019). All of these studies prove the interaction of the flow field and the bridge pier as the mechanism of local pier scour.

2.5.3. Group of Piers

Reviewing previously published studies indicates that scour mechanisms and flow fields are more complicated when a group of piers obstructs the flow. In this situation, the piers configuration affects the flow field in addition to other parameters such as the geometry of piers and hydraulics of flow. A number of researchers such as Zdravkovich (1987), Sumner et al. (2000), Meneghini et al. (2001), Lin et al. (2002), Zhou & Yiu (2006), Sumner (2010), Beheshti & Ataie-Ashtiani (2016) among others, have conducted researches in the area of flow field around a group of piers.

The most common case of piers group is two cylinders in cross-flow. The basic patterns of this group are shown in Figure 2.5. According to the scope of this study, a brief review of previous studies for two tandem bridge piers is presented here.

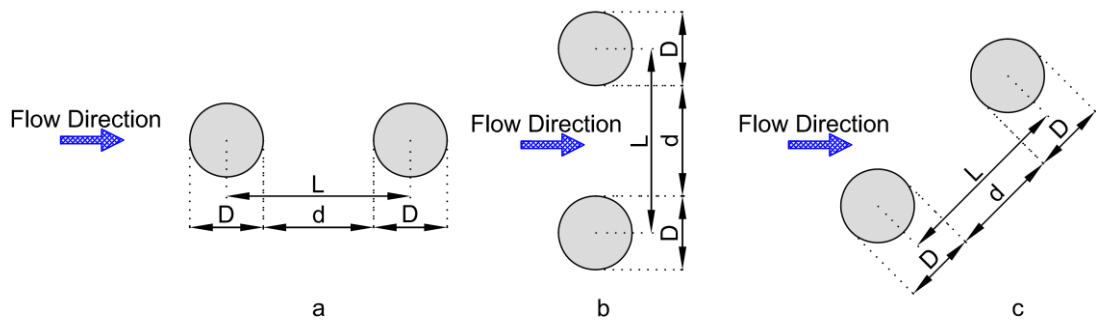


Figure 2.5. Two circular piers in cross-flow; a) tandem configuration; b) side-by-side configuration; c) staggered configuration

As discussed by Zdravkovich (1987), two particular kinds of flow interference can be distinguished for the case of two piers, including proximity interference, and wake interference. The proximity interference takes place when none of the piers is submerged in the wake of the other one. For instance, side-by-side piers belong to this category. The wake interference occurs when one of the piers is placed into the wake region of the other. This type of flow interference might occur only to the downstream pier in tandem and staggered arrangements. Zdravkovich (1987) also stated that a combination of these two flow interference might happen in some regions. Besides, there is another type when the flow interference is negligible, and the flow around each pier in that region is effectively identical to that around a single pier.

Sumer & Fredsøe (2002) discussed that the interference effect for both the wake vortex flow and the horseshoe vortex flow would strongly depend on the pier-group configuration. In the case of the tandem arrangement, the two piers act as a single body, and therefore there is only one wake vortex when $d/D < 0.15$ (where d and D are the pier spacing and diameter, respectively). The d/D needs to be increased by 3, for two wake vortices regime to emerge. For $d/D > 3$, the wake vortex behind the downstream pier is called binary vortex that each vortex, in this case, consists of two vortices (one is formed behind the upstream pier and the other behind the downstream pier).

A comprehensive review of the flow field around two circular piers has been conducted by Sumner (2010). It was stated that, for two piers in a tandem pattern, the upstream pier shields the downstream one from the approach flow. Therefore, the approach flow for the downstream pier would be altered by the wake of the upstream one. Moreover, the wake and vortex region after the upstream pier are affected by the downstream pier. It was also reported that the upstream and downstream piers behave as a turbulence generator and wake stabilizer, respectively. In addition, the piers might act as a single pier or two separate piers depend on their spacing. A classification of flow regimes for two tandem piers including extended-body, re-attachment and co-shedding was reported by Sumner (2010), as shown in Figure 2.6.

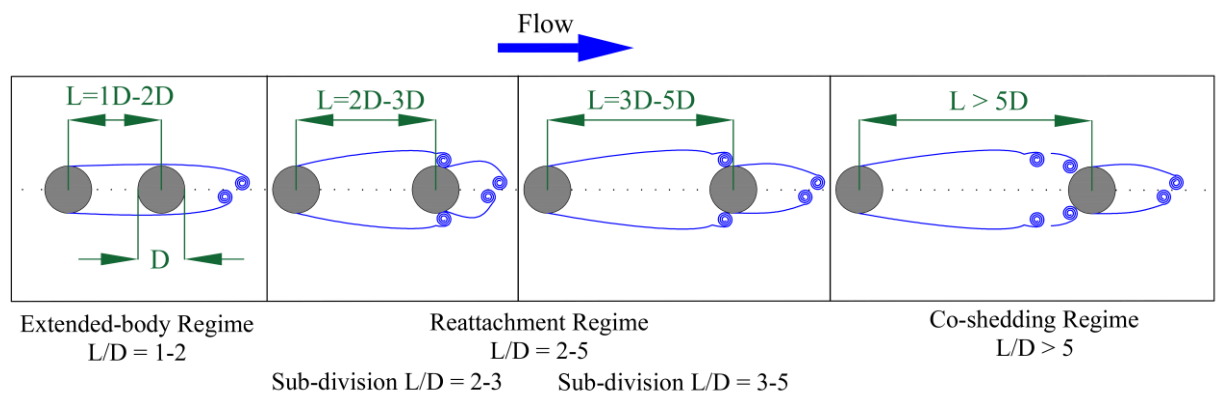


Figure 2.6. Tandem piers flow classification (modified from Sumner, 2010)

The extended body regime occurs when the L/D ratio (L is the space between centres of two piers) is in the domain of $1 < L/D < 1.2-1.8$, as suggested by Zdravkovich (1987). Zhou & Yiu (2006), proposed $1 < L/D < 2$ for occurring the extended body regime. In this regime, two piers perform as a single pier. As reported by Sumner (2010), the downstream pier is placed in the upstream pier's vortex. Additionally, the wake vortex

of the downstream pier happens nearer to the pier in comparison with the case of a single pier.

The distance between two piers in the case of a re-attachment regime is poorly defined. As cited by Shrestha (2015), This distance is between 1.2-1.8 and 3.4-3.8 by Zdravkovich (1987) and between 2 and 5 by Zhou & Yiu (2006). In this regime, the detached shear layers from the upstream pier can re-attach around the downstream pier as shown in Figure 2.6. It is worth mentioning that there is only one vortex street, which is formed behind the downstream pier.

When two piers are apart, the co-shedding regime takes place. According to Zdravkovich (1987) for $L/D > 3.4 - 3.8$, the co-shedding regime occurs, while Zhou & Yiu (2006) reported $L/D > 5$ for the formation of this regime. In this case, the vortices occur at the downstream of both piers. However, the vortices produced by the front pier disturb the vortices in the back of the rear one. Accordingly, the vortices behind the downstream pier become weaker and fade rapidly.

Keshavarzi et al. (2017) used a particle image velocimetry (PIV) technique to study the turbulence characteristics of a single pier and two tandem circular piers. The results of their study have been summarized in Table 2.1 for the longitudinal plane at the centreline. They concluded that the flow field for the case of two tandem piers is more complicated than the single pier. In addition, the flow field has been considerably affected by the distance between two tandem piers. The turbulence characteristics including TI, TKE and RSS for two tandem piers significantly differ from the single pier. Results of their study showed that when $2 \leq L/D \leq 3$, more powerful turbulence flow occurs behind the front pier and as a result, a higher scour depth can be expected around front pier. Accordingly, for the tandem arrangements of two piers, $2 \leq L/D \leq 3$ is the worst condition for the front pier due to stronger turbulence that may produce more scour.

In this research, flow conditions in the experiments were selected to develop similar characteristics to those presented in Table 2.2 for the flow pattern, u/V , w/V , TI_u , TI_w , TKE, and RSS. A detailed discussion of the flow conditions for the experiments is presented in Chapter 5.

Table 2.2. Summary of flow field results for the longitudinal plane at centreline (after Keshavarzi et al., 2017)

Characteristic	Single pier		Two tandem piers					
			US pier 1	Between two piers			DS pier 2	
	US*	DS*		L/D* =1	L/D=2	L/D=3		4 ≤ L/D ≤ 6
Flow Pattern	<ul style="list-style-type: none"> • Flow separation • Downward flow • Clockwise vortex 	<ul style="list-style-type: none"> • Reverse and upward flow at immediate DS side • Flow random direction at wake region • Max. up flow intensity at 2D from Pier DS face 	<ul style="list-style-type: none"> • Similar to single pier 	<ul style="list-style-type: none"> • Wake only behind Pier 2 	<ul style="list-style-type: none"> • Wake is not noticed behind Pier 1 • Reverse and upward flow between 2 Piers 	<ul style="list-style-type: none"> • Flow separation at 1.5D from the DS face of Pier1 • Flow rotation at the immediate DS side of Pier 1 	<ul style="list-style-type: none"> • Flow separation at 2.5D from DS face of Pier 1 • Flow rotation between two piers 	<ul style="list-style-type: none"> • Wake behind the single pier is larger than that of the two tandem piers cases
Time Average Velocity Components	<p>u/V</p> <ul style="list-style-type: none"> • $u/V=1$ at $X/D \geq 1.25$ from US side and then becomes smaller and reduced to 0 at US Pier face 	<ul style="list-style-type: none"> • Reverse flow at the wake close to DS Pier face with $-0.6 \leq u/V \leq 0$ • Max. $u/V=1.2$ occurs at Pier side 	<ul style="list-style-type: none"> • Similar to single pier 	<ul style="list-style-type: none"> • DS of Pier 2 approximately similar to DS of single pier 	<ul style="list-style-type: none"> • Reverse flow between two piers with $-0.5 \leq u/V \leq 0$ 	<ul style="list-style-type: none"> • As the flow approaches Pier 2, positive value of u/V between two piers could be observed 	<ul style="list-style-type: none"> • A gradual increasing in the value of u/V was noticed with increasing in the distance from the DS face of Pier 2 	
	<p>w/V</p> <ul style="list-style-type: none"> • $-0.3 \leq w/V \leq 2$ that negative value shows down-flow and Max. value occurs at US side 	<ul style="list-style-type: none"> • upward flow region extending towards the free surface • heavily fluctuated w near the bed 	<ul style="list-style-type: none"> • down-flow in all the cases of two tandem piers 	<ul style="list-style-type: none"> • upward flow region extending towards the free surface at DS side of Pier 2 	<ul style="list-style-type: none"> • No down-flow at US side of Pier 2, and no horseshoe vortex in this region 	<ul style="list-style-type: none"> • No noticed horseshoe vortex at the base of Pier 2 	<ul style="list-style-type: none"> • Horseshoe vortex in front of Pier 2 with smaller size than that of Pier 1 	<ul style="list-style-type: none"> • Increasing the magnitude of upward flow with increasing in the spacing between two piers

Table 2.2. (cont.) Summary of flow field results for the longitudinal plane at centreline (after Keshavarzi et al., 2017)

Characteristic	Single pier		Two tandem piers					
			US pier 1	Between two piers			DS pier 2	
	US*	DS*		L/D*=1	L/D=2	L/D=3		4 ≤ L/D ≤ 6
TI_u	<ul style="list-style-type: none"> Higher value of TI_u close to the bed and decreasing with increasing the distance towards the free surface 	<ul style="list-style-type: none"> Higher value of TI_u extend to the mid-depth of the flow 	<ul style="list-style-type: none"> Max. value of in the zone close to the bed 	<ul style="list-style-type: none"> For L/D ≤ 4 higher values of TI_u existing close to the bed and the higher value zones extending throughout the gaps. For L/D = 6, the Max. TI_u occurring at a distance of 1.5*D from DS face of Pier 1. As the flow approaching Pier 2, TI_u reducing by 60% of max. value, observing at the DS side of Pier 1. 				<ul style="list-style-type: none"> increasing TI_u with increasing in the spacing between two piers
Turbulence Intensity Components								
TI_w	<ul style="list-style-type: none"> Higher value of TI_w close to the bed and decreasing with increasing the distance towards the free surface 	<ul style="list-style-type: none"> distribution of TI_w similar to the TI_w with approximately the same value 	<ul style="list-style-type: none"> For all values of L/D, approximately the same order and distribution of TI_w 	<ul style="list-style-type: none"> Max. TI_w at the DS side of Pier 2 is about 50% less than that of the single pier 	<ul style="list-style-type: none"> Max. TI_u and TI_w between two piers are approximately the same 			<ul style="list-style-type: none"> increasing TI_w with increasing in the spacing between two piers

Table 2.2. (cont.) Summary of flow field results for the longitudinal plane at centreline (after Keshavarzi et al., 2017)

Characteristic	Single pier		Two tandem piers					
			US pier 1	Between two piers				DS pier 2
	US*	DS*		L/D*=1	L/D=2	L/D=3	4 ≤ L/D ≤ 6	
Turbulent Kinetic Energy	<ul style="list-style-type: none"> • Similar to turbulence intensity 	<ul style="list-style-type: none"> • Max. TKE close to the pier near the bed and about 2 times greater than that of the US side 	<ul style="list-style-type: none"> • Similar to single pier 	<ul style="list-style-type: none"> • increasing TKE behind Pier 1 with increasing in the spacing between two piers • For L/D=3 and 4, higher value of TKE close to the Pier 2 • for L/D>4, the value of TKE decreasing as flow approaching Pier 2 				<ul style="list-style-type: none"> • Increasing TKE with increasing the spacing between two piers up to L/D=3. Further increasing in spacing, decreasing TKE
Reynolds Shear Stresses (RSS)	<ul style="list-style-type: none"> • Increasing RSS with approaching the flow to pier 	<ul style="list-style-type: none"> • $-0.5 \leq \text{RSS} \leq 0.5$ close to pier and extending up to a distance of 3*D from DS face 	<ul style="list-style-type: none"> • Similar to single pier 	<ul style="list-style-type: none"> • higher negative values close to the bed • Decreasing RSS with increasing the spacing between two Piers • Higher values close to Pier 1 and gradually decreasing as flow approaching Pier 2 				<ul style="list-style-type: none"> • Increasing RSS with increasing the spacing between two piers up to L/D=3. Further increasing in spacing, decreasing RSS

*US: upstream, DS: downstream, L/D: normalized spacing with respect to pier diameter

Tl_u and Tl_w : turbulence intensity components in the streamwise and the transverse direction

2.6. Countermeasures against Local Scour around Bridge Piers

To control and reduce the local scour around bridge piers, which is a common cause of waterway bridge failures, different engineering methods have been proposed by researchers. These various types of pier scour countermeasures can be classified into two distinct categories. The first category is associated with using armouring devices; is a traditional solution to deal with pier scour problems. The concept behind this type of scour countermeasure is that materials, such as large stones which are heavier than the riverbed grains, can withstand the elevated shear stresses which occur around bridge piers. The second category is associated with the employment of flow-altering devices. The basic concept for using flow-altering devices is to change the flow field around the bridge pier in a manner that reduces the potential for erosion around the bridge pier. The following sections provide a review of previous studies on countermeasures against local scour around bridge piers.

2.6.1. Local Scour Countermeasures Using Armouring Devices

Riprap is one of the most common pier-scour countermeasures. Other devices such as tetrapods, tetrahedrons, toskanes, grout-filled mats, cable-tied blocks (see Figure 2.7) can be considered as the alternative armouring devices for pier scour protection (Melville & Coleman 2000). So far, several design criteria have been suggested for riprap such as those developed by Brice & Blodgett (1978), Wörman (1989), Parola (1993), Chiew (1995), Chiew & Lim (2000), Lauchlan & Melville (2001), Lim & Chiew (2001), Unger & Hager (2006), Lagasse et al. (2007), Mashahir et al. (2009), Tabarestani & Zarrati (2012), Karimae Tabarestani & Zarrati (2015), Suaznabar et al. (2017), and Karimaei Tabarestani & Zarrati (2019).

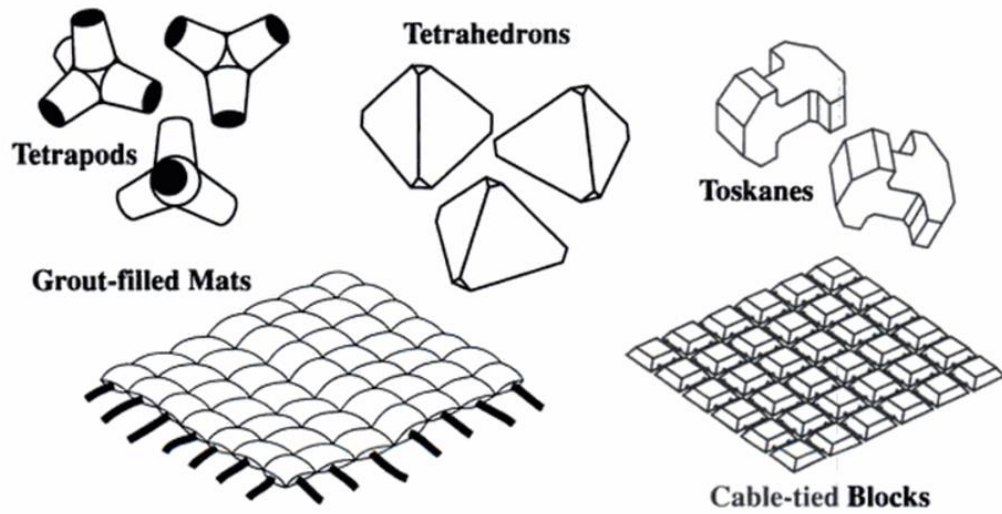


Figure 2.7. Alternative armouring devices for pier scour protection (Melville & Coleman, 2000)

Different equations have been proposed by researchers for sizing riprap and also other design criteria such as riprap extent, grading and filter. These design criteria for riprap are summarised in Tables 2.3 and 2.4.

Table 2.3. Equations for sizing riprap around bridge piers

Methods	Equation	Symbols
Quazi & Peterson (1973)	$\frac{d_{r50}}{y} = \frac{0.85}{(S_s - 1)^{1.25}} Fr^{2.5}$	
Breusers et al. (1977)	$\frac{d_{r50}}{y} = \frac{2.83}{(S_s - 1)} Fr^2$	
Farraday & Charlton (1983)	$\frac{d_{r50}}{y} = 0.547 Fr^3$	
Parola et al. (1989)	$\frac{d_{r50}}{y} = \frac{C^*}{(S_s - 1)} Fr^2$	<p>d_{r50}= median stone size y= mean approach flow depth S_s=specific gravity of riprap stones Fr=Froude No. of the approach flow depth=$V/(gy)^{0.5}$ V= mean approach flow velocity (m/s) C^*= pier shape factor; C^*= 1.0 (rectangular), 0.61 (round-nose)</p>
Breusers & Raudkivi (1991)	$\frac{d_{r50}}{y} = \frac{0.278}{(S_s - 1)^{1.5}} Fr^3$	
David (1994)	$\frac{d_{r50}}{y} = \frac{0.58K_P K_V}{(S_s - 1)} Fr^2$	
Richardson & Davis (1995)	$\frac{d_{r50}}{y} = \frac{0.346f_1^2 f_2^2}{(S_s - 1)} Fr^2$	

Table 2.3. (cont.) Equations for sizing riprap at bridge piers

Methods	Equation	Symbols
Chiew (1995)	$\frac{d_{r50}}{y} = \frac{0.168}{(S_s - 1)^{1.5} U_*^3} Fr^3$ $U_* = \frac{0.3}{K_d K_y} Fr^3$	$K_y = 0.783 \left(\frac{y}{D}\right)^{0.322} - 0.106 \quad 0 \leq \left(\frac{y}{D}\right) < 3$ $K_y = 1 \quad \left(\frac{y}{D}\right) \geq 3$ $K_d = 0.398 \ln\left(\frac{D}{d_{r50}}\right) - 0.034 \left[\ln\left(\frac{D}{d_{r50}}\right)\right]^2 \quad 1 \leq \left(\frac{D}{d_{r50}}\right) < 50$ $K_d = 1 \quad \left(\frac{D}{d_{r50}}\right) \geq 50$ <p> K_y = flow depth factor K_d = sediment size factor </p>
(Parola 1993, 1995)	$\frac{d_{r50}}{y} = \frac{f_1 f_3}{(S_s - 1)} Fr^2$	<p> D_p = pier projected width f_1 = factor for pier shape (1.0 for rectangular and 0.71 for round-nose) f_3 = factor for pier size = $f(D_p/d_{r50})$: </p> $f_3 = 0.83 \quad 4 < \left(\frac{D_p}{d_{r50}}\right) < 7$ $f_3 = 1.0 \quad 7 < \left(\frac{D_p}{d_{r50}}\right) < 14$ $f_3 = 1.25 \quad 20 < \left(\frac{D_p}{d_{r50}}\right) < 33$

Table 2.3. (cont.) Equations for sizing riprap at bridge piers

Methods	Equation	Symbols
Croad (1997)	$\frac{d_{r50}}{y} \left(1 - \frac{2d_{r50}}{y}\right)^{0.5} = \frac{0.641}{A^3(S_s - 1)^{1.5}} Fr^3$ $d_{r50} = 17d_{b50}$	<p>A equals acceleration factor. d_{b50} = is for sediment particles at the bed further details from Croad (1997)</p>
Lauchlan (1999)	$\frac{d_{r50}}{y} = 0.3S_f \left(1 - \frac{Y_r}{y}\right)^{2.75} Fr^{1.2}$	<p>S_f = safety factor, with a minimum recommended value = 1.1 Y_r = placement depth below bed level</p>
Lauchlan & Melville (2001)	$\frac{d_{r50}}{y} = K_Y (0.3Fr^{1.2})$	<p>K_Y = adjustment factors for riprap placement depth</p>

Table 2.3. (cont.) Equations for sizing riprap at bridge piers

Methods	Equation	Symbols
Mashahir et al. (2009)	$\frac{U}{U_c} = \frac{0.3}{K(D/d_{r50}) \times K(y/D) \times K(Rec)}$	<p>U/U_c = critical flow intensity for riprap failure U = flow velocity $U_c = 7.66\sqrt{0.056(SG - 1)gd_{r50}(y/d_{r50})^{(1/6)}}$ $K(D/d_{r50})$, $K(y/D)$ and $K(Rec)$ = sediment size, flow depth, and rectangular pier adjustment factors respectively. SG = specific gravity of riprap stone D_{eff} = Pier effective width</p>
Tabarestani & Zarrati (2012)	$U^2 / (SG - 1)gd_{r50} = 3.8\left(\frac{D_{eff}}{D}\right)^{-1.5}\left(\frac{D}{d_{r50}}\right)^{-0.5}\left(\frac{y}{d_{r50}}\right)^{0.25}$	
Froehlich (2013)	$d_{r50}/y = K_r \times K_b \times K_\omega \times K_p \times K_s \times K_a \times Fr^3$	<p>K_r = factor for slope effect K_b = factor for pier width K_ω = factor for cross-flow shear K_p = factor for transverse pier spacing K_s = factor for pier shape K_a = factor for pier alignment with the flow Fr = Froude number of the flow approaching a bridge pier</p>

Table 2.4. Methods to estimate riprap extent, grading and filter requirements (after Melville & Coleman, 2000)

Methods	Riprap extent		Level	Grading
	Lateral extent	Thickness		
Bonasoundas (1973)	Semi-circular upstream shape (Radius 3b), semi-elliptical downstream shape; overall length 7D	D/3		
Neill (1973)	Project around the nose of the pier by a distance = 1.5D	2d _{r50}	Riprap surface below expected general scour level	
Poey (1974)	1.5 to 2.5D in all directions from the pier face			
Hjorth (1975)	Length = 6.25D, width = 3D, circular arc upstream, triangular shape downstream			
Breusers et al. (1977)	2D from pier face	3d _{r50}	Some distance below bed level to prevent excessive exposure	
Richardson and Davis (1995)	Width > 5D	> 3d _{r50}	Top of riprap at bed level	d _{r50} ≥ 0.5d _{rmax}
Chiew (1995)	$\frac{C_r}{D} \geq 12.5 \frac{V}{V_c} - 2.75$ C _r = width of riprap layer			
Parola (1995)	Semi-circular upstream (radius b _p), triangular downstream; overall length = 7b _p			
Croad (1997)	> 5.5b _p , of which 1.5 b _p is upstream of the upstream face of the pier	2d _{r50}		d _{rmax} ≤ 2 d _{r50} d _{r50} ≤ 2 d _{r15}
Lauchlan (1999)	1 to 1.5b in all directions from the pier face Synthetic filter (if placed) should have lateral extent about 75% of the lateral extent of the riprap layer	2d _{r50} to 3 d _{r50}	A factor for level of placement, Y _r , included in riprap sizing equation	

Referring to Table 2.3, it can be found that different methods offer the dissimilar ranges for sizing riprap at bridge piers. For example, the methods proposed by David (1994), Breusers et al. (1977) and Croad (1997) estimate very large riprap size, while that of Breusers & Raudkivi (1991) calculates very small riprap size. Similarly, with consideration of Table 2.3, the other design criteria produce different results by different methods.

Although several researchers proposed different design criteria for riprap as a local scour countermeasure, riprap stability is still an issue. As referenced by Melville & Coleman (2000), riprap layer at bridge piers can fail due to four mechanisms that were observed during the laboratory studies of Parola (1993), Chiew (1995) and Melville et al. (1997). These four failure mechanisms are the shear failure, winnowing failure, edge failure and bed-form undermining as explained here:

- Shear failure happens where the hydrodynamic force of the flow can move the riprap, and therefore riprap no longer able to protect the riverbed grains.
- Winnowing failure occurs by the turbulence and seepage flows through the voids between the riprap, which can erode the finer riverbed grains. The rivers with sand bed materials have more potential for winnowing failure than the rivers with coarser bed materials.
- Edge failure starts from the border of the riprap layer, where the riprap is not sufficiently extended laterally. Therefore, the eroded riverbed grains at the border of the riprap layer can undermine the riprap.
- Bed-form undermining takes place where the large dunes are formed at the riverbed, which can damage the riprap layer.

The stability of riprap as a local scour protection has been investigated by several researchers. Lauchlan & Melville (2001) studied the effects of bed degradation on riprap protection at bridge piers and reported that riprap protection is not sufficient for bed scouring when the channel bed degrades. As discussed by Yoon & Kim (2001), the stability of riprap scour countermeasure improves in a collective body (sack gabions) rather than as individual riprap.

Chiew (2002) considered the results of investigations conducted over the past 25 years and identified five failure mechanisms related to the use of riprap at bridge piers including shear failure, winnowing failure, edge failure, bed-form induced failure and bed-degradation induced failure. Each of these failure mechanisms has the potential to cause the eventual breakdown of the riprap layer.

For a degrading channel Chiew (2004) investigated riprap stability at bridge pier. He reported that riprap around a pier would eventually develop into a stable mound when the bed shear stress reduces with bed degradation. However, the mound is very vulnerable to another designed flood flow accompanied by large dunes, and this type of riprap instability may be called bed-degradation induced failure.

As mentioned by Beg & Beg (2013), riprap layers often fail to protect bridges during floods due to the general movement of sediment during severe flood conditions. The movement of bed sediment loses the stability of riprap stones.

According to Wang et al. (2017), riprap could only provide limited improvement to the nominal resistance. When the flood is coming, riprap might not be stable to withstand high approaching stream velocities and buoyant forces. Therefore, riprap might be eroded during the flood. The other disadvantages of riprap are influencing on the local ecological system, requiring a regular fix, and having complicated installation as stated by Wang et al. (2017).

2.6.2. Local Scour Countermeasures Using Flow Altering Devices

A number of researchers as cited by Tafarjnoruz et al. (2010) and Singh et al. (2020) have introduced new flow-altering devices or evaluated the performance of the existing devices to prevent local scour around bridge piers. Using the review framework of Tafarjnoruz et al. (2010), recent research in flow-altering devices is presented in the following section.

- **Collar**

Collar is generally a thin circular disk which attached around a pier as shown in Figure 2.8. As stated by Ettema (1980), Dargahi (1990), and Fotherby (1992), the basic mechanism of local score reduction by a collar is that this device shields the sediment bed from the down-flow and horseshoe vortex. As reported by Chiew (1992), the scour depth can be halved for a circular pier with a collar of diameter equal to twice that of the pier. Additionally, he reported that the effectiveness of a collar increases when it is placed below the bed level.

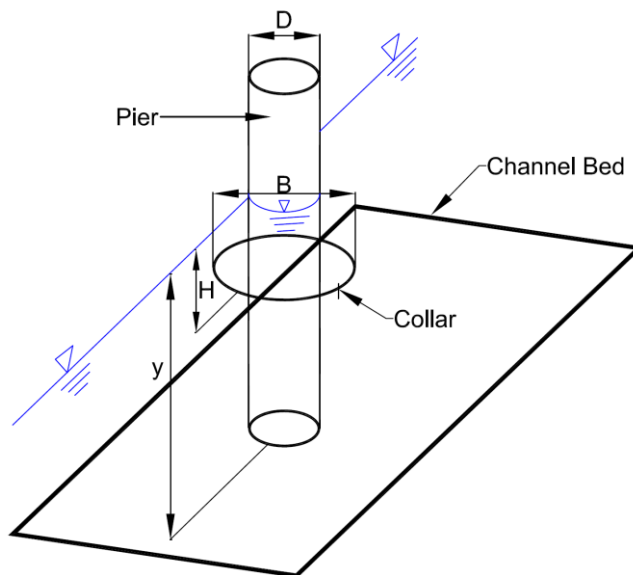


Figure 2.8. Collar on pier (modified from Kumar et al., 1999)

Kumar et al. (1999) proposed Equation (2.10) for estimation the maximum scour depth around a circular bridge pier fitted with a collar for the uniform-sized sediment in clear-water scour condition (see Figure 2.8).

$$\left(\frac{ds_p - ds_c}{ds_p}\right) = 0.057 \left(\frac{B}{D}\right)^{1.612} \left(\frac{H}{y}\right)^{0.837} \quad (2.10)$$

Where, following the nomenclature of Kumar et al. (1999)

ds_p = depth of scour on pier without a collar

ds_c = depth of scour on pier with a collar

B = diameter of collar

D = diameter of circular pier

H = elevation difference between water surface and collar surface

y = depth of water above bed elevation

According to Equation 2.9 and also as discussed by Chiew (1992), Zarrati et al. (2004), Moncada-M et al. (2009), Gogus & Dogan (2010), Kumcu et al. (2014), and Khodashenas et al. (2018) the efficiency of a collar increases by increasing the collar width and by placing it at or below the original bed level. Nevertheless, based on Zarrati et al. (2006), a collar wider than three times of the pier diameter ($B > 3 \times D$) is not practicable. In addition, Zarrati et al. (2004) stated that placing a collar below the original bed level may extend the scour hole around the pier and increase the scour depth downstream of the collar.

Mashahir et al. (2004) investigated the development of scour around a bridge pier protected by a collar as a function of time. They concluded that the collar might delay the scour development around the pier.

Based on Salamatian & Zarrati (2019), a collar may increase the reliability of bridge piers at low flow intensities.

The results of previous studies show that the best effectiveness of a collar achieves when it is placed at or below the bed level. A collar which is placed at or below the bed level does not affect the flow field such as down-flow, horseshow vortex or wake vortex, and just armour the bed sediment. Therefore, it may be concluded that a collar acts as an armouring device, and should not be considered as a flow-altering device. Consequently, collars may fail to protect the bridge due to similar failure mechanisms to other armouring devices.

- **Slot in the Pier**

As presented by Chiew (1992), a slot reduces the local scour either by diverting the down-flow away from the bed or by decreasing the down-flow impinging on the bed. The parameters that affect the performance of a slot are width, length and location of the slot, as shown in Figure 2.9. Chiew (1992) found that a slot with a width of 0.25 pier diameter that located near the water surface or the bed level can reduce the clear-water scour by as much as 20%, whereas a one-half-diameter-wide slot placed near the water surface affords up to 30% of clear-water scour reduction.

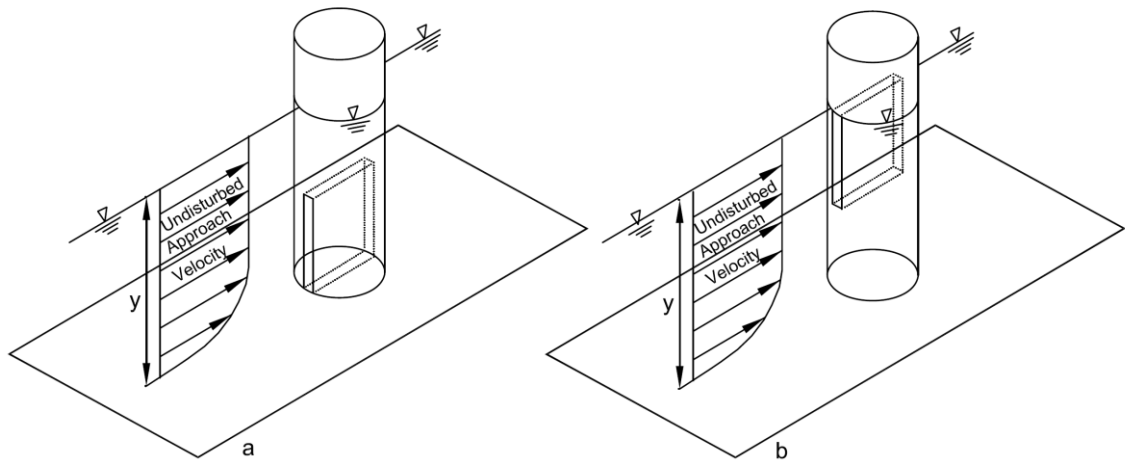


Figure 2.9. Bridge Pier with Slot; a) slot near bed; b) slot near water surface (modified from Chiew, 1992)

Kumar et al. (1999) experimentally studied the effects of slots on the reduction of the local scour around bridge piers and concluded that slots could be effective if the slot

extends into the bed. However, a slot is not effective if the upstream flow direction and slot are not aligned. Similar results have been reported by Heidarpour (2002) and Moncada-M et al. (2009), that the most favourable location of a slot to decrease the local scour is near the bed. Moncada-M et al. (2009) also concluded that the axial scour hole shape depends neither on the length nor on the location of the slot. Based on Kumar et al. (1999) and Grimaldi et al. (2009b), a slot may be more efficient if it is partially fixed into the bed. Hajikandi & Golnabi (2017) experimentally compared the straight, T-shaped, and Y-shaped slots (Figure 2.10) and reported that T-shaped slot is not appropriate configuration. In addition, it is concluded that Y-shaped slot produces deeper scour depths at the pier compared with the straight slot, but since the slope of the scour profiles in the presence of Y-shaped slot is steeper, a smaller scour hole is generated.

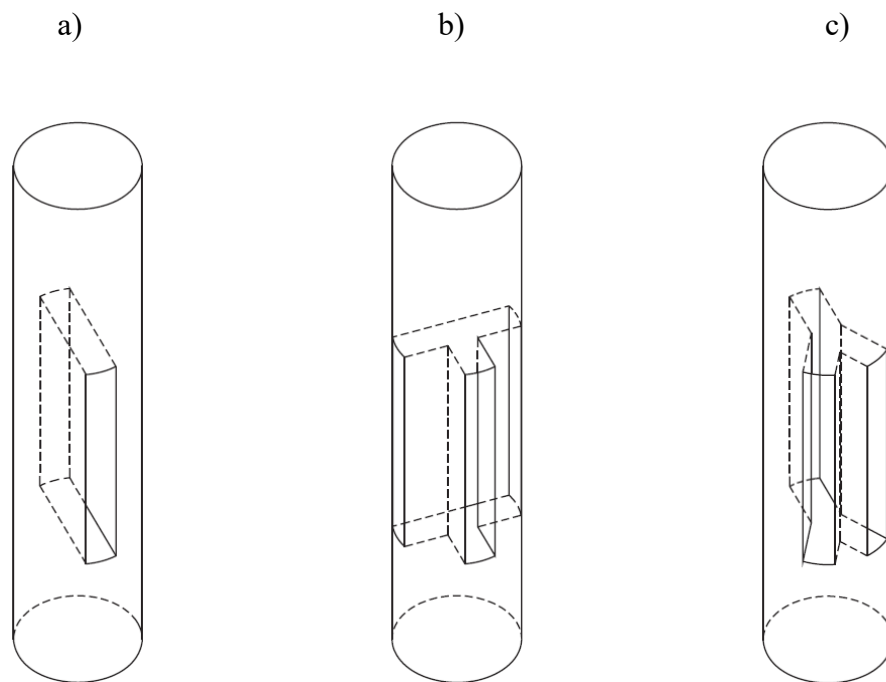


Figure 2.10. Bridge Pier with Slot; a) straight slot; b) T-shaped slot; c) Y-shaped slot (modified from Hajikandi & Golnabi, 2017)

On the other hand, a slot has several limitations. As discussed by Kumar et al. (1999) and Heidarpour et al. (2003), one of the critical weakness of a slot is that its

effectiveness decreases significantly as the angle of attack increases. As mentioned by Melville & Coleman (2000), using the slot as a scour countermeasure depends on the other factors such as the presence of debris that could block the slot, and flow skewness that may render the device ineffective. As discussed by Beg & Beg (2013), a slot cannot be considered as a good scour protection device due to the limitations of this method. They mentioned that slot reduces the strength of pier structure. Also, debris and floating materials can block the slot space. Based on the previous studies, it may be concluded that the disadvantages of a slot are more than its benefits, and also this method may not be applied to the existing piers.

- **Sacrificial Piles**

Sacrificial piles are a single or a group of piles placed upstream of a bridge pier. As presented by Melville & Hadfield (1999), Chiew & Lim (2003), and Haque et al. (2007) the intention of this approach for mitigating local scour is to deflect the high-velocity flow and to create a lower velocity wake area which has less erosive capability. Some parameters including the number of piles, their protrusion (partially or fully submerged) and their configuration affect the efficiency of this method.

Melville & Hadfield (1999) studied the effects of a group of sacrificial piles to protect a bridge pier from local scour, as illustrated in Figure 2.11. As recommended by Melville & Hadfield (1999), sacrificial piles can be used as a scour countermeasure when the flow remains aligned, and the flow intensity is relatively small. They also pointed out that the effectiveness of sacrificial piles is reduced under live-bed condition, due to the passage of bed-forms.

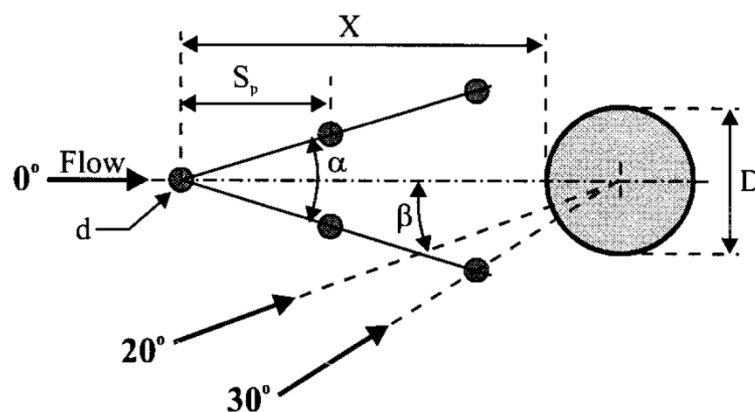


Figure 2.11. Sacrificial piles upstream of a circular pier (Melville & Hadfield, 1999)

Chiew & Lim (2003) proposed sacrificial sill at the upstream of a pier as a local scour countermeasure. Based on their experimental study, they reported the best effectiveness of a sacrificial sill achieved when the "sill is vertical, the sill height is larger than 0.3 times the depth of flow, the clear distance between the pier and sill is 4.4 times the pier width, and the angle of attack is zero."

Haque et al. (2007) suggested a group of transverse sacrificial piles (see Figure 2.12) in order to fill the scour hole around the pier by the scoured materials from the sacrificial piles.

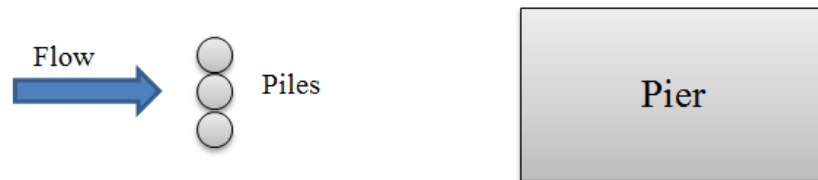


Figure 2.12. Transverse sacrificial piles upstream of a pier (modified from Haque et al., 2007)

The benefit of these sacrificial devices is that they can be applied for both new and already existing bridge piers. However, the size and shape of the sacrificial piles remain unclear in the study of Melville & Hadfield (1999). Furthermore, the installation location, number of piles, their configurations and degree of submergence needs further investigation including, consideration of the potential for a group of sacrificial piles to trap debris during flood events.

- **Iowa Vanes**

Iowa vanes have been proposed by Odgaard & Wang (1987) as a local scour countermeasure. Iowa vanes are vertical plates installed in the stream bed just upstream of the pier and angled outwards. As latter discussed by Odgaard & Wang (1991), the

mechanism of these vanes to reduce the local scour includes producing secondary flow circulation, changing the bed shear stress, and altering hydraulic conditions and sediment transport rate. According to the results of experiments by Parker et al. (1998), Iowa vanes did not perform adequately as a countermeasure against bridge scour under mobile-bed condition. As reported by Melville & Coleman (2000), experimental study has been conducted to investigate the use of Iowa vanes for pier scour reduction under live-bed condition by Lauchlan (1999). His experimental setup is illustrated in Figure 2.13. He concluded that although the maximum scour depth reduction was significant in some tests (30% to 50%), no significant trends were evident in the data. The angle of attack (α) and the streamwise spacing (e) (see Figure 2.13) are important parameters affecting the performance of Iowa vanes.

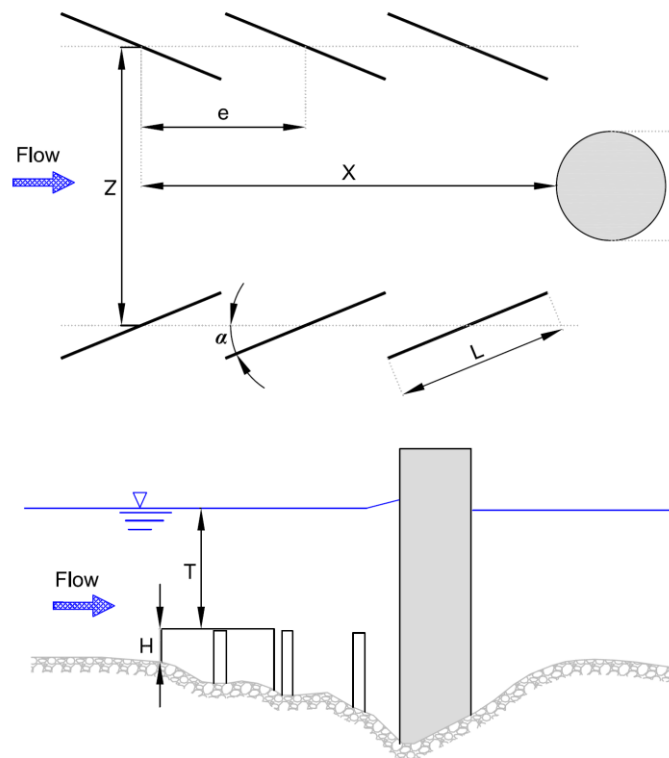


Figure 2.13. The use of Iowa vanes as a pier scour countermeasure (modified from Melville & Coleman, 2000)

- **Delta Wing**

Gupta & Gangadharaiyah (1992) proposed a vane in the shape of a delta wing placed horizontally upstream of the pier with pointed edge directed upstream to reduce the

local scour around a bridge pier (see Figure 2.14). They stated that this device reduces the local scour by barricading the vortex development, and producing counter-rotating vortices against the horseshoe vortex.

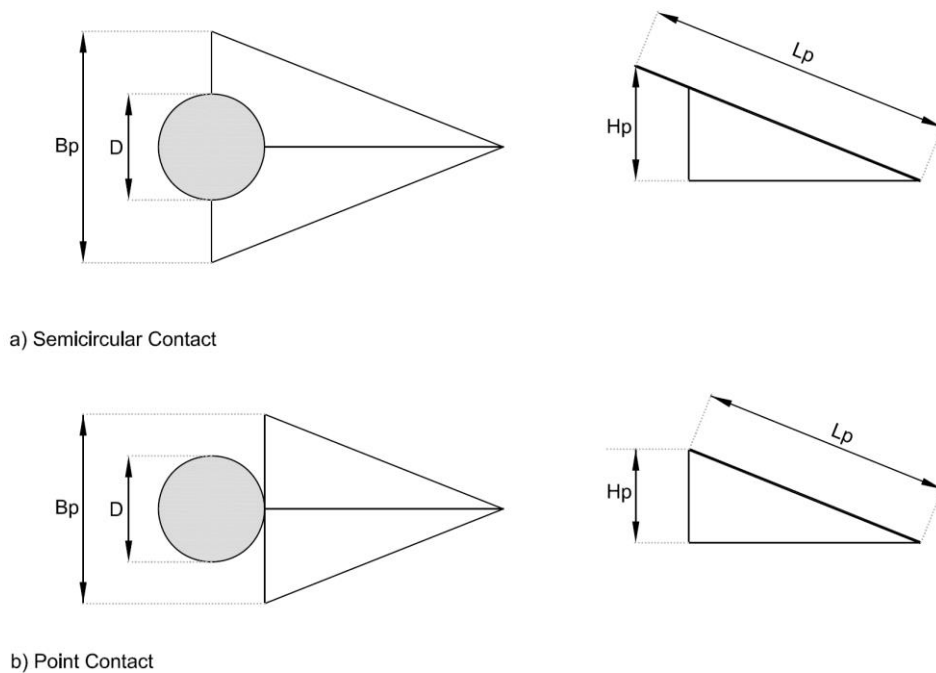


Figure 2.14. Schematic of a delta wing (modified from Gupta & Gangadharaiah, 1992)

- **Pier Group**

A group of three smaller circular piers was studied by Vittal et al. (1994) as a scour-reduction device. They reported that this method is more effective than a solid pier with a full slot of 0.50 times its diameter. In addition, it is as effective as a solid pier with a collar of 3.50 times its diameter. Furthermore, they stated that a collar on a pier group is more efficient than a collar on a solid pier. However, they did not consider the suitability of the method for existing bridges; consideration of the method suggests that it is not applicable for existing bridges.

- **Permeable Sheet Pile**

Permeable sheet pile may be considered as another type of vanes (see Figure 2.15). As reported by Parker et al. (1998), the idea of this method is based on the permeable dikes as river training devices. In fact, this device allows sediment-laden water to pass through a lattice that slows the flow down significantly, thus causing the sediment to settle out. If permeable sheet pile is placed upstream of a pier, some of the near-bed flow would be deflected from the bridge pier thereby reducing the approach velocity which decreases the strength of the horseshoe vortex (Parker et al. 1998). The significant drawback of permeable sheet piles is that they may be blocked by sediment, debris and other floating materials. In this condition, the degree of contraction to the flow cross section increases and consequently more scour happens. Therefore, this method cannot be considered as a suitable local scour protection.

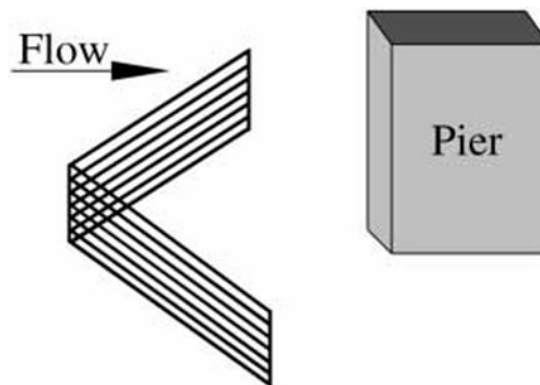


Figure 2.15. Permeable sheet pile upstream of a pier (Parker et al., 1998)

- **Internal Openings through the Pier**

This countermeasure is made by penetrating some tubes inside a pier, as shown in Figure 2.16. As reported by El-Razek et al. (2003) the effectiveness of this method depends on several parameters such as the opening diameter, angle of inclination (α), and Froude number. However, they did not discuss how these tubes affect the flow field around the pier.

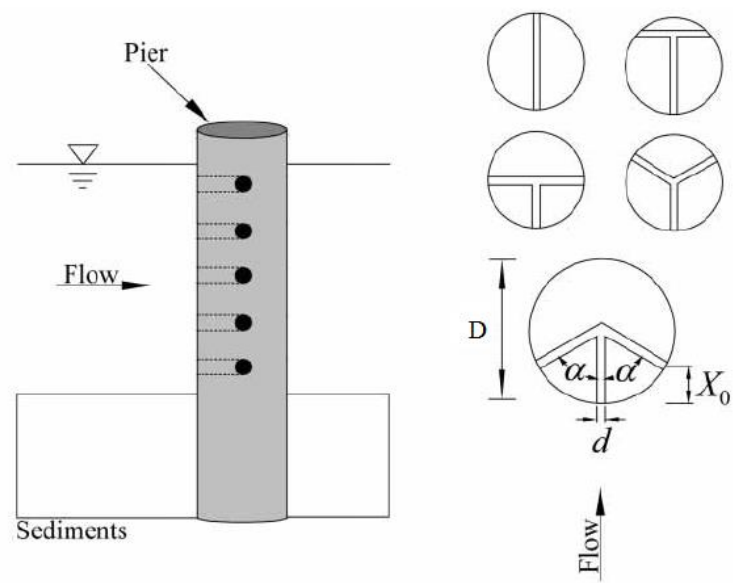


Figure 2.16. Internal openings through the pier (modified from El-Razek et al., 2003)

- **Surface Guide Panels**

Surface guide panels as described by Huang et al. (2005) comprise two vertical panels which are installed upstream of a pier (see Figure 2.17). According to Huang et al. (2005), the upward flow below the guide panels reduces near-bed shear flow and weakens the horseshoe vortex. Moreover, the local sediments deposition at the panels may drop into the scour hole around the pier. these two mechanisms may reduce the local scour around the pier (Huang et al. 2005).

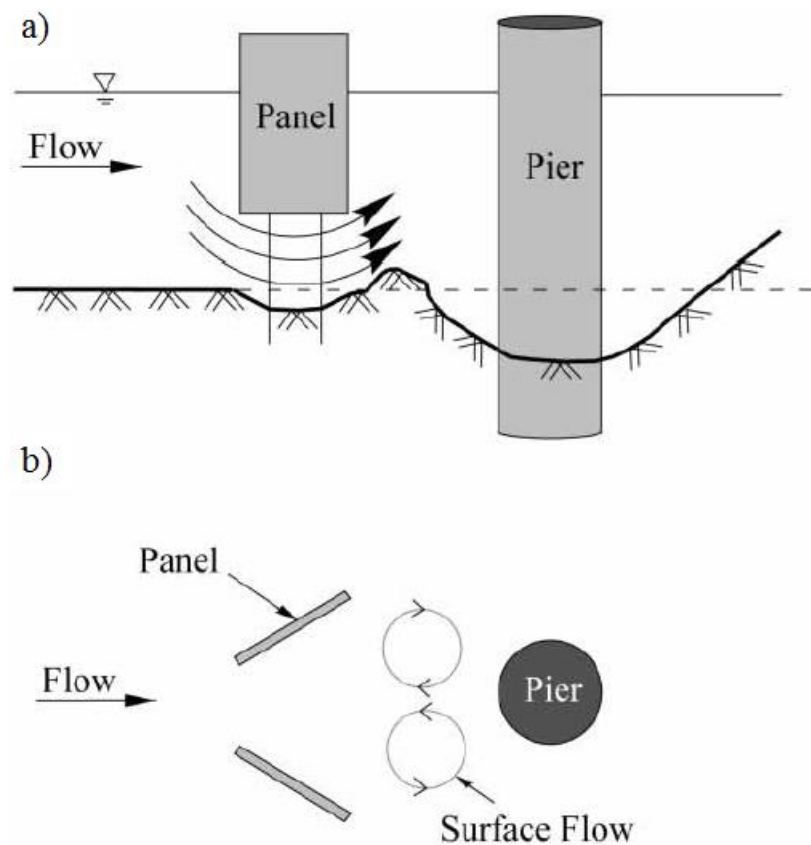


Figure 2.17. Surface guide panel; a) side view; b) plan view (modified from Huang et al., 2005)

- **Threaded Pier**

Dey et al. (2006) found that a threaded pile (helical wires or cables wrapped spirally on the pile to form threads) as shown in Figure 2.18 can reduce the local scour depth around a bridge pier. They stated that cables wrapped spirally on the pier help to diminish the strengths of the down-flow and horseshoe vortex. The results of their experiments showed that the depth of local scour decreased with increases in cable diameter and number of threads, and with a decrease in thread angle (α).

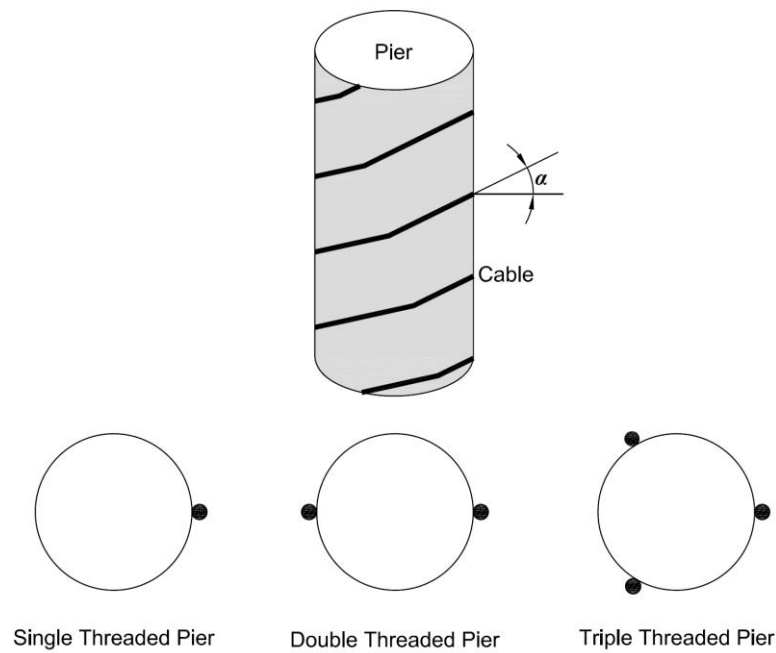


Figure 2.18. Threaded pier - helical wires or cables wrapped spirally on the pile to form thread (modified from Dey et al., 2006)

- **Bed Sill**

As considered by Grimaldi et al. (2009a), a bed sill at the downstream of a pier can be used as a countermeasure against local scour around the pier. They declared that the bed sill seems to be not effective at the beginning of the test and when the scour hole develops sufficiently and interacts with the countermeasure, the bed sill is more effective. They stated that a bed sill seems to act on the lower portion of the wake vortices. The results of their experiments showed that the effectiveness of this countermeasure increased when the distance between the pier and the bed sill decreased. When this distance is zero, bed sill excludes the wake vortices from the scour hole.

- **Subsidiary Triangular Pillar**

Fouli & Elsebaie (2016) proposed a subsidiary triangular pillar as a flow altering device. They considered a width for this subsidiary pillar equal to the pier diameter. It was also full depth. Three apex angles (60° , 90° , and 120°), and six spacing among the pier and the pillar (0, 0.5D, 1D, 1.5D, 2D, and 3D) were tested under clear water scour conditions. They concluded that this pillar can reduce the maximum scour depth by

28% when the apex angle is 90° , and the distance between the pillar and the pier is equal to $3D$. However, Fouli & Elsebaie (2016) did not report changes in flow field arising from implementation of the subsidiary triangular pillar. The absence of this data renders interpretation of the outcomes difficult.

In addition, the dimensions of the subsidiary triangular pillar are similar to those found in upstream piers. There is a question therefore whether the scour reduction arising from the subsidiary triangular pillar should be considered in the category of tandem piers rather than as a flow altering device.

- **Roughened Bridge Piers**

Abdelhaleem (2019) investigated the effects of the pier surface roughness as a local scour countermeasure. As stated by Abdelhaleem (2019), the mechanism of this countermeasure is creating turbulence and producing kinetic energy upstream of the pier. These changes delay flow separation and move the stagnation point toward the downstream of the pier. Accordingly, the strengths of the down-flow and horseshoe vortex become weaker. He concluded that the roughened piers can reduce the scour depth and volume, but extend the length of the scour hole at the upstream of the bridge piers.

Tafarojnoruz et al. (2010) carried out a broad literature review on flow-altering countermeasures. Based on the shape and performance of these devices, they classified them into four categories, including (i) openings through piers such as slot, and pier group; (ii) pier attachments such as collar, delta wing, and threaded pier; (iii) bed attachments such as sacrificial piles, Iowa vanes, permeable sheet pile, and bed sill; and (iv) other devices such as modifying pier shape. Based on this classification the following conclusion can be drawn.

Opening through pier countermeasures such as pier group or pier slot may reduce the scour depth by passing a part of the flow via the inner openings of a pier or between smaller piers, and consequently decreasing the strength of the down-flow and the horseshoe vortex. However, debris and floating materials during floods may also reduce the efficiency of these methods due to the blocking the slot or the gaps between the piers as stated by Vittal et al. (1994), Chiew (1992), Tafarojnoruz et al. (2010), Beg &

Beg (2013). Additionally, the opening through piers may not be applicable for existing pier because of reducing the strength of the pier structure.

Pier attachments such as the collar, delta wing, and threaded pier should be attached to the pier. These devices may reduce the pier-scour at the beginning of the scour process. However, it seems that when the scour-hole develops, they cannot protect the pier due to their connection to the pier.

Bed attachments such as sacrificial piles, Iowa vanes, permeable sheet pile, and bed sill are independent structures that should be installed at the upstream or downstream of the pier. These devices can be applied to both the existing and new waterway bridges. However, the scour around these structures is an important issue which affects the performance of this type of scour countermeasure. In addition, their size is another concern because making the size larger may produce a contraction to the flow and increase the potential of scour.

The fourth category of flow-altering countermeasures such as modifying pier shape, may not be appropriate for an already existing bridge. Although the pier shape is an effective factor in the amount of pier-scour, it cannot protect the pier when the scour-hole develops.

A comparison between some of the proposed flow-altering devices is summarised in Table 2.4. It is worthwhile to mention that the maximum scour depth reductions, which are observed in Table 2.4, achieved in different experimental conditions. In other words, the flow characteristics, sediment properties, pier geometries and time were not similar in different conducted researches. Therefore, some dissimilar results were reported. For example, four unlike values were reported as the maximum reduction of local scour by collar from 27% (Mashahir et al. 2004) to 100% (Moncada-M et al. 2009). In addition, the efficiency of the most previous flow altering devices was reported only based on the maximum scour depth reduction rather than the reduction of the scour hole volume. Although the maximum scour depth is an important factor, it happens at a specific point and finding this point and then measuring its depth might not be very accurate by using a point gage as reported in the most of those studies. Therefore, the comparison between different devices based on the maximum scour depth reduction may not be completely meaningful. Furthermore, the size and the installation location of the previously

proposed flow altering devices were not fully discussed, and the results were described based on some limited experimental work. In addition, as given in Table 2.5 the disadvantages of flow altering devices such as slot, internal connecting tubes, and pier group greatly outweigh their benefit and are not applicable for already existing bridges.

Table 2.5. Summary of different flow-altering devices as a pier scour countermeasure

Methods	Maximum scour depth reduction %	Advantages	Disadvantages
Collar	<ul style="list-style-type: none"> • 50% (Chiew 1992) • 30% (Richardson & York 1999) • 27% (Mashahir et al. 2004) • 100% (Moncada-M et al. 2009) 	<ul style="list-style-type: none"> • Applicable for both new and existing bridges 	<ul style="list-style-type: none"> • When general sediment transport occurs, the trough of a migrating bed form may expose the pier beneath the collar. Under such a condition, it loses its effectiveness. • Acts as an armouring devices and failure mechanisms of armouring device may happen for collar
Slot	<ul style="list-style-type: none"> • 30% (Chiew 1992) • 88% (Moncada-M et al. 2009) • 38% (Hajikandi & Golnabi 2017) 	-	<ul style="list-style-type: none"> • Ineffective if the approach flow and the slot are not aligned. • Debris and floating materials block the slot • Reduction of the strength of pier structure • May not applicable for existing bridge
Internal openings through the pier	<ul style="list-style-type: none"> • 39% (El-Razek et al. 2003) 	-	<ul style="list-style-type: none"> • May not applicable for existing bridge
Pier group	<ul style="list-style-type: none"> • 39% (Vittal et al. 1994) 	-	<ul style="list-style-type: none"> • Not applicable for existing bridge • Debris and floating materials block the slot
Threaded pier	<ul style="list-style-type: none"> • 46.3% (Dey et al. 2006) 	<ul style="list-style-type: none"> • Applicable for both new and existing bridges 	<ul style="list-style-type: none"> • When the scour hole developed, cannot protect the pier due to its connection to the pier
Delta wing	<ul style="list-style-type: none"> • 67% (Gupta & Gangadharaiah 1992) 	<ul style="list-style-type: none"> • Applicable for both new and existing bridges 	<ul style="list-style-type: none"> • When the scour hole developed, cannot protect the pier due to its connection to the pier
Roughened bridge piers	<ul style="list-style-type: none"> • 29% (Abdelhaleem 2019) 	<ul style="list-style-type: none"> • Applicable for both new and existing bridges • 	<ul style="list-style-type: none"> • When the scour hole developed, cannot protect the pier due to its connection to the pier

Table2.5. (cont.) Summary of different flow-altering devices as a pier scour countermeasure

Methods	Maximum scour depth reduction %	Advantages	Disadvantages
Sacrificial piles	<ul style="list-style-type: none"> • 56% (Melville & Hadfield 1999) 	<ul style="list-style-type: none"> • Applicable for both new and existing bridges 	<ul style="list-style-type: none"> • Ineffective for flow skewness more than 20° • Unsuccessful for high flow intensity • Accumulation of debris and floating materials around the unsubmerged sacrificial pile • High degree of contraction to the flow cross section • Chance of the collision with the boats and ships for the rivers with navigation for full-depth piles
Iowa vanes	<ul style="list-style-type: none"> • 50% (Lauchlan 1999) 	<ul style="list-style-type: none"> • Applicable for both new and existing bridges 	<ul style="list-style-type: none"> • Accumulation of debris and floating materials around this device • High degree of contraction to the flow cross section • Chance of the collision with the boats and ships for the rivers with navigation for full-depth piles
Permeable sheet pile	<ul style="list-style-type: none"> • 47% (Parker et al. 1998) 	<ul style="list-style-type: none"> • Applicable for both new and existing bridges 	<ul style="list-style-type: none"> • Accumulation of debris and floating materials around this device • Chance of the collision with the boats and ships for the rivers with navigation for full-depth piles
Surface guide panels	<ul style="list-style-type: none"> • 90% (Huang et al. 2005) 	<ul style="list-style-type: none"> • Applicable for both new and existing bridges 	<ul style="list-style-type: none"> • Accumulation of debris and floating materials around this device • High degree of contraction to the flow cross section • Chance of the collision with the boats and ships for the rivers with navigation for full-depth piles
Subsidiary triangular pillar	<ul style="list-style-type: none"> • 28% (Fouli & Elsebaie (2016) 	<ul style="list-style-type: none"> • Applicable for both new and existing bridges 	<ul style="list-style-type: none"> • Accumulation of debris and floating materials around this device • Chance of the collision with the boats and ships for the rivers with navigation for full-depth piles • High degree of contraction to the flow cross section due to its size
Bed sill	<ul style="list-style-type: none"> • 26% (Grimaldi et al. 2009a) 	<ul style="list-style-type: none"> • Applicable for both new and existing bridges 	<ul style="list-style-type: none"> • Bed sill is not effective at the beginning of the scour process, when there is the maximum rate of local scour • potential of increasing scour at downstream of the bed sill

2.7. Summary

According to the analysis of the outcomes of previously published studies in the literature, it can be concluded that the vast majority of investigations in the field of local scour have focused on the mechanism of this phenomenon. Therefore, it may be claimed that the mechanism of local scour related to the flow field around the bridge piers is well known to the researchers. However, the number of studies in the field of local scour countermeasures is limited compared to other aspects of the local scour.

Review of the previously published studies on the local scour countermeasures indicates that the main idea is to armour bed sediment as a countermeasure, while only a small number of studies has been conducted on changing the flow field around bridge piers as a means of controlling and reducing the local scour. Commonly used armouring devices may fail to protect bridge piers from local scour. This outcome arises from the different potential failure mechanisms including shear, winnowing, edge and bed-form undermining. Every year, several bridge failures are reported that were protected by armouring devices. Alternatively, the specific types of flow altering devices can have the potential to protect pier and as reported by Beg & Beg (2013) are more economical. The better economics of flow altering devices is especially the case when riprap or other material is not available near the bridge site or is costly.

Flow altering devices such as collar, slot, delta wing, threaded pier, and roughened bridge piers should be placed around or in a bridge pier. These devices may reduce the local scour around a pier at the beginning of the scour process. However, it seems that when the scour hole develops, they cannot protect the pier due to their connection to the pier. On the other hand, bed attachment flow-altering devices, which are independent structures and should be placed at the upstream or the downstream of the pier, have more potential to protect the bridge piers from the local scour failure. However, as explained in the earlier sections, the previously proposed bed attachments such as sacrificial piles, Iowa vanes, permeable sheet pile, surface guide panels, and bed sills have some major disadvantages that make them not completely successful.

According to the results of the previous studies, the significant factors including the shape, size, and place of installation affect the efficiency of this type of independent flow-altering devices. However, these important factors were not completely studied in

the previously proposed bed-attachments. It is noteworthy to state that the disadvantages of those bed-attachments are mainly related to overlooking of these important factors.

The analysis of the published literature outlined above has indicated that flow altering devices had the potential to modify flow field in a manner that mitigates local scour. However, the implementation of these devices is hampered by the lack of guidance on shape, size and location. Furthermore, the shear stress causing the local scour is maximised at the bed. This poses a question of what height of device within the water column is required to mitigate local scour without influencing other users such as **bridge** structure and river channels. Further investigations are required to fill this void of information.

In this study, a triangular prism refer to flow diversion structure (FDS) is proposed as an upstream bed attachment with the intention to divert the streamlines from the pier, thus reducing the potential of waterway bridge failure due to local scour around piers. The shape, size, and installation location of this new countermeasure are fully considered in the stepwise comprehensive experimental studies. In addition, the effects of this new countermeasure on the flow field around a circular pier are studied experimentally. All the experimental studies are presented in the next three chapters.

CHAPTER 3

Preliminary Experimental Investigation of Flow Diversion Structure as a Pier Scour Countermeasure



3.1. Introduction

In the preceding chapter, a comprehensive literature review was presented on the mechanism of local scour around bridge piers and countermeasures against this problem. As discussed therein, the complicated flow field around bridge piers causes local scour and represents the most important cause of waterway bridge failure. Therefore, a solution to mitigate local scour would be to change the flow field around bridge piers.

In this chapter, a new triangular flow altering device, referred to as “flow diversion structure” (FDS) is introduced. In assessing this FDS, a two-stage experimental study was employed. The first stage described in this chapter is a proof of concept; in other words, will the proposed FDS produce desirable outcomes. The second stage will be presented in the next chapter. For these proof of concept experiments, only a single set of dimensions for the FDS were considered. Consideration of alternative dimensions and their influence on local scour is the focal point of the next chapter

The proposed FDS has a triangular prismatic shape with dimensions much smaller than the pier and should be installed upstream of the pier. The main principles for selecting the shape of the FDS are presented in this Chapter.

Experimental studies on both local scour and flow field were conducted to examine the performance of the FDS for reducing local scour and changing the flow field around a circular pier. The procedures and the results of these experiments are also presented in this Chapter.

3.2. Selection the Shape of Flow Diversion Structure

The main hypothesis of this research study is use of a triangular FDS would mitigate the local scour around a bridge pier. The FDS achieves this by diverting the streamlines and changing the flow field in the vicinity of the pier. As discussed in Chapter 2, the shape of this structure is an important factor. To select an appropriate shape, the following principles have been considered.

Firstly, this structure should be able to divert the streamlines in the vicinity of the pier.

Secondly, the created wake behind the structure should be sufficiently wide that incorporates the pier. As concluded by Roshko (1954) for aeronautic purposes, the wake widths behind a normal plate, a triangular, and a circular shape are from broadest to narrowest, respectively (Figure 3.1). In Figure 3.1, U_∞ is the approach flow velocity, U_s is the velocity at separation point, d is the width of the structure, and d' is the wake width behind the structure.

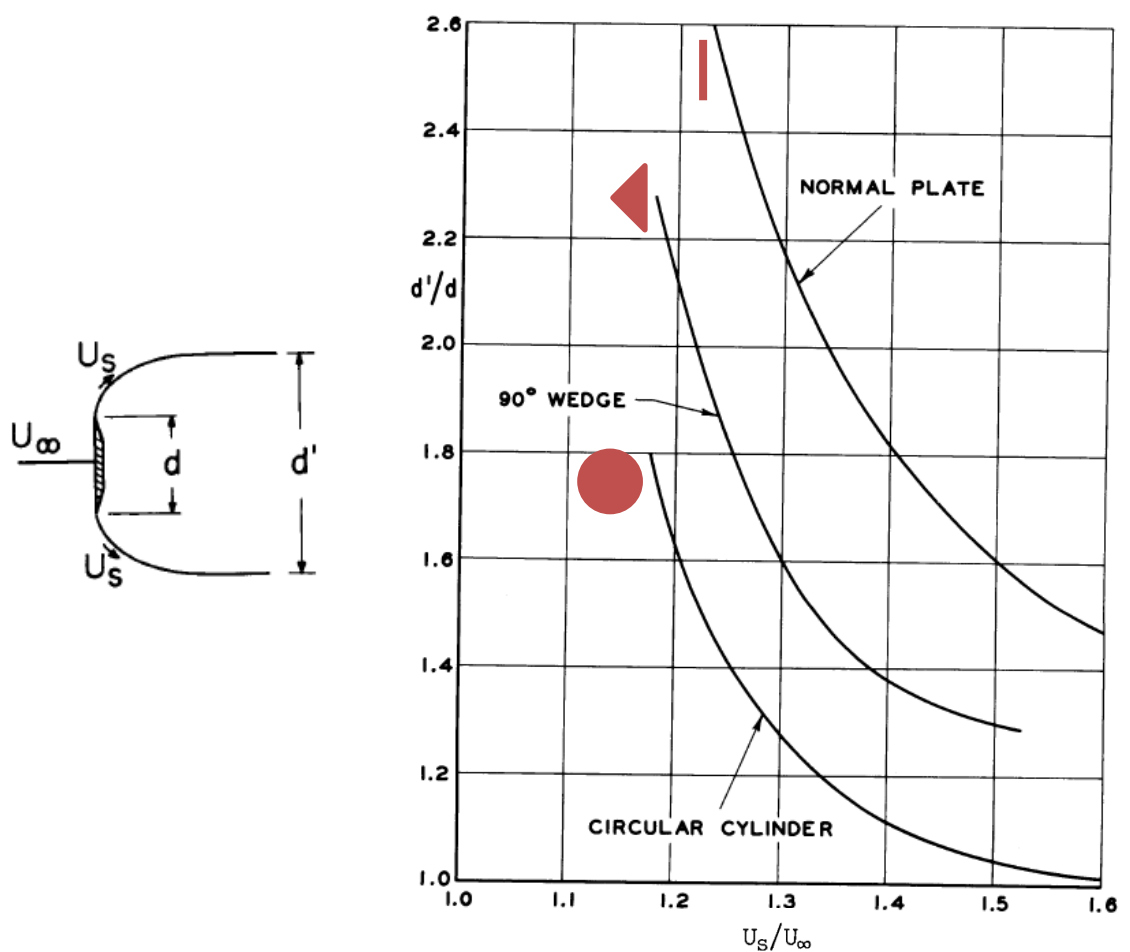


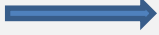

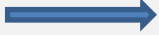

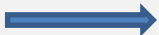



Figure 3.1. Wake width behind different structures (Roshko 1954)

Thirdly, the local scour around the structure should have a low amount. As discussed by several investigators, such as Melville & Coleman (2000), Richardson & Davis (2001), Ettema et al. (2011), and Al-Shukur & Obeid (2016) the pier shape affects the amount of local scour. Based on Melville & Coleman (2000), the effect of pier shape on local

scour can be considered by a shape factor. They defined this factor as the ratio of the scour depth for a specific shape to that for the standard shape, namely circular pier. Their recommended shape factors for different pier shapes are given in Table 3.1. Similar values for shape factors have been presented by Richardson & Davis (2001) and Al-Shukur & Obeid (2016).

Table 3.1. Shape factors for different pier shapes (modified from Melville & Coleman 2000)

Pier Shape		Shape Factor
Circular	Flow direction 	 1
Round Nosed	Flow direction 	 1
Square Nosed	Flow direction 	 1.1
Triangular Nosed	Flow direction 	 0.9

It should be mentioned that based on Melville & Sutherland (1988), the maximum possible scour depth (d_{se}) that can occur at a circular pier is estimated as 2.4 times the diameter of the pier. With consideration of the shape factors, the maximum possible scour depth for square and triangular nosed piers can be estimated as 2.64D ($1.1 \times 2.4D$) and 2.16D ($0.9 \times 2.4D$), respectively. In other words, local scour for square nosed pier is 22% more than triangular nosed and 10% more than circular and round nosed piers.

Having considered the above principles, it can be resulted that all of the above shapes can divert the streamlines in the vicinity of the pier. Regarding the wake width and scour depth, performance of the square nosed shape and normal plate are almost similar. These two shapes produce broadest wake width but more scour occurs around them. Therefore, normal plate and square nosed pier cannot be considered as the proper shapes. On the other hand, comparison between triangular nosed and circular shapes shows that triangular nosed shape produces wider wake and lower scour than circular

pier. Furthermore, triangular structure can divert the streamlines more smoothly than the other shapes, because this shape is more similar to streamlined body than the other shapes. Therefore, a triangular prism has been selected as an effective shape for the proposed structure and named flow diversion structure (FDS). Fouli & Elsebaie (2016) independently proposed the use of an upstream triangular pier to mitigate scour. These independent proposals for an upstream triangular shape structure confirm the suitability of this shape. Hence an FDS with a triangular shape was used in these proof of concept experiments.

An experimental study is designed here to examine the above hypothesis including the performance and effectiveness of this new countermeasure for changing flow field and subsequently its effect on pier scour. The experimental program is explained in the following sections and the results were compared with the results of circular FDS.

3.3. Experimental Setup and Procedure

3.3.1. Laboratory Flume

A rectangular glass-sided flume with the length of 15 m, width of 0.70 m, depth of 0.60 m and with the longitudinal slope equal to 0.0004 was used for the first set of experiments. The discharge was supplied from a constant head tank and measured using a Danfos electromagnetic flow-meter with an accuracy of $\pm 1\%$. This flume was also equipped with a digital point gauge of 0.1 mm accuracy to measure the scour-hole topography, an ADV to measure the flow velocity component, and a downstream sluice gate to regulate the water depth. The working section in the flume comprised a sediment recess, which had 3.0 m length and 0.12 m depth, and was placed at 9.0 m downstream from the inlet to achieve a fully developed flow.

3.3.2. Design of Experiment Conditions

The design of the experimental conditions is an important component of the experiment. To maximise the utility of the experiments, the literature pertaining to laboratory tests to estimate scour was reviewed. Constraints as experimental conditions identified in this review are outlined below.

The pier diameter was chosen to minimise the effect of contraction on the scour depth. Based on Melville & Coleman (2000), the ratio of the flume width to the pier diameter should be more than ten to avoid a contraction effect. In these experimental tests, a pier with a diameter of 50 mm was adopted; and the ratio of the flume width to the pier diameter (W/D) was 14, thereby satisfying the constraint of Melville & Coleman (2000).

Melville & Sutherland (1988) reported that the maximum possible local scour depth for an aligned¹ circular pier is equal to $2.4D$. In addition, the scour depth is not affected by the grain size when the ratio of the pier diameter to median size of bed sediment is more than 50 (Ettema 1976). Therefore, the experimental tests were conducted using 120 mm thick uniformly graded sand with a median grain size of $d_{50} = 0.8$ mm to satisfy these two criteria.

Based on Melville & Coleman (2000), the pier diameter to the water depth (y) ratio should be less than 0.7 to avoid water depth effects on the local scour depth. Hence, the water depth used in the experiments was set to be 100 mm to satisfy this requirement.

The maximum local scour depth in uniform sediment occurs when the cross-sectional averaged velocity (V) is equal to the critical mean flow velocity for sediment entrainment (V_c) as discussed by Melville & Coleman (2000). They proposed some relationships (Equations 4.4 and 4.5) to estimate V_c as a function of the water depth and the median grain size. In this preliminary laboratory test, the critical mean flow velocity was obtained as 0.312 m/s. The mean flow velocity was considered 0.3 m/s close to the critical mean flow velocity for sediment entrainment. Therefore, the flow rate ($Q = V \times y \times W$) was calculated to be equal to 21 L/s.

¹ - pier located in a straight section of a river

The flow diversion structure, employed in this study, was prismatic in shape with an isosceles triangle cross section. The lateral base was 10 mm, the longitudinal base was 25 mm, the height was full-depth, and located at 6 different spacings from the pier (i.e., $d/D = 0.5, 1, 1.5, 2, 2.5$ and 3.5 where d is the clear distance between the pier and FDS). Figure 3.2 schematically shows the preliminary experimental test set up.

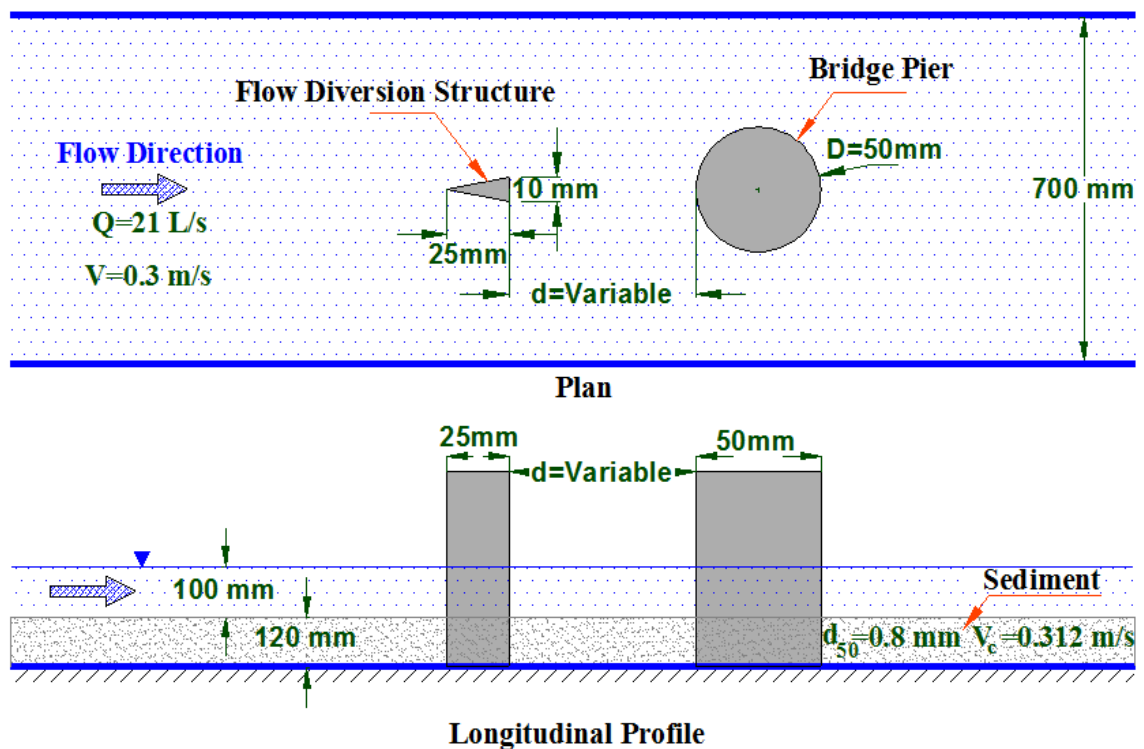


Figure 3.2. Schematic diagram of the preliminary experimental setup

3.3.3. Experimental Procedure

Firstly, the pier and the flow diversion structure were mounted at the centreline of the flume. After that the bed material was placed and levelled in the sand recess. Then, the water began flowing in the flume from downstream using a very low flow rate to maintain the levelled sand bed. The water depth was adjusted to the designed depth (0.1 m), and then the flow rate was slowly increased to the target rate ($Q=21$ L/s). The

tailgate was utilised to maintain the designed water depth. After 24 hours, the pump was turned off, and the flume was drained. The final bed topography was measured by a digital point gauge. The experimental tests were repeated with different distances between the pier and the flow diversion structure. Additionally, to recognise the effects of this structure on the amount of local scour, a control test was conducted without the flow diversion structure.

To find out the effects of FDS on the flow field, the flow velocity components were measured in the control test and the tests with $d/D = 1.5$ with fixed bed (no sediment). Three components of flow velocity were measured using a Micro-ADV or Acoustic Doppler Velocimetry (ADV) with a frequency of 50 samples per second. The Micro-ADV is a doppler velocity meter designed for laboratory with simple operation and no need for periodic recalibration (Sontek 1997). The ADV measures the velocity based on the change in frequency of the Doppler shift. The acoustic probe consists of three receivers and one transmitter. Ambient particles reflect the sound in three dimensions and some portions of this reflected signal are detected by the receivers. Since the sampling volume is located at 50 mm below the acoustic transmitter, there is no disturbance due to the probe. The velocity was measured in a grid of 35 nodal points (P1:P35) between the pier and flow diversion structure as shown in Figure 3.3. The measuring points were selected based on the capability of the ADV to measure the velocity. When the ADV probe is located near an object such as a pier model the accuracy of data may significantly reduce. It should be mentioned that the available ADV (Velocimeter) must be located in the water column for viable measurement. As the sample water must be 50 mm below the probes, only the bottom 50 mm velocity can be sampled. As it is the near-bed velocity that is the most significant, this limitation was not considered significant. More detailed analysis of the flow field was also undertaken using PIV technologies capable of measuring the boundary layer around the pier. These results have been presented in Chapter 5.

The measurement was made at the flume centreline. To control the accuracy of velocity data, two key parameters, namely, the signal to noise ratio (SNR) and the correlation coefficient (COR), should be checked. The best range of SNR and the COR for reporting reliable velocity data are higher than 15 dB and 70%, respectively (Sontek 1997). In the present experiments, all reported SNR and correlation coefficients were

checked at the beginning of each experiment to be within the acceptable ranges. Figure 3.4 illustrates the measuring velocity components by ADV.

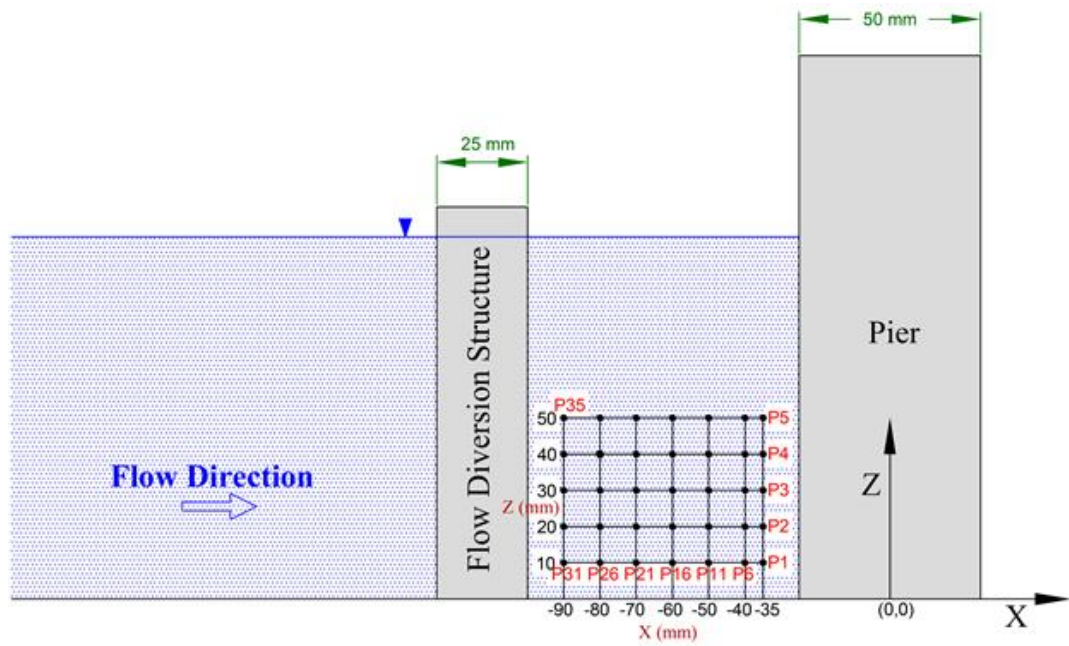


Figure 3.3. Schematic diagram of grid points positions for measuring velocity components (longitudinal view)

a)



b)



Figure 3.4. Photographs of measuring velocity components by ADV; a) control test; b) test with $d/D=1.5$

3.4. Results and Discussion

A flow diversion structure (FDS) to be used as a new countermeasure against local scour around a bridge pier has been tested experimentally. This experimental study was conducted to investigate the effects of the FDS on local scour and flow field around a circular pier.

A total of seven tests were conducted for situations of test with single pier without the FDS and six tests with single pier plus the FDS. The FDS was installed at six alternative locations upstream of the pier (namely $d/D = 0.5, 1, 1.5, 2, 2.5$ and 3.5). The duration of each experiment (T) was 24 hours because after this time no sediment movement around piers was noticed. All tests were conducted under clear water scour conditions. The hydraulic conditions for the above experimental tests are presented in Table 3.2. According to the Froude number, which is defined as the ratio of the velocity and wave speed, all tests were performed under the subcritical flow condition.

Table 3.2. Characteristics of the preliminary tests

Test No.	d/D	T (hour)	Q (L/s)	y (m)	V (m/s)	V/V _c	Froude number (Fr)
1	0 (Control test, no FDS)	24	21	0.1	0.3	0.96	0.3
2	0.5	24	21	0.1	0.3	0.96	0.3
3	1.0	24	21	0.1	0.3	0.96	0.3
4	1.5	24	21	0.1	0.3	0.96	0.3
5	2.0	24	21	0.1	0.3	0.96	0.3
6	2.5	24	21	0.1	0.3	0.96	0.3
7	3.5	24	21	0.1	0.3	0.96	0.3

3.4.1. Determination of the Maximum Scour Depth

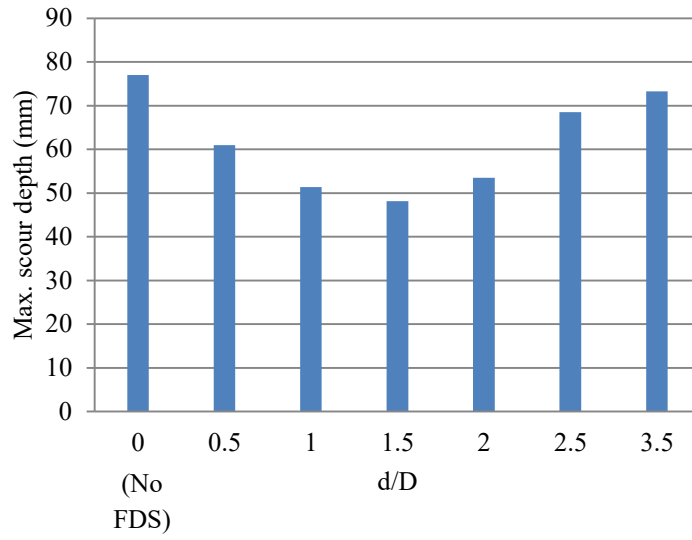
- **Triangular Prism FDS**

Data shown in Table 3.3 are the maximum scour depth for each test. An analysis was made to determine the reduction of scour depth when comparing to the maximum scour depth for the control test (Test 1 in Table 3.2). This comparison is presented in Figure 3.5. Referring to Table 3.3 and Figure 3.5, it can be inferred that the maximum scour depth occurs in the single pier case, and then scour depth decreased when a flow diversion structure was installed at upstream. As it can be seen in Figure 3.5b, reduction of the scour depth increases with an increase in the distance between the pier and the FDS up to 1.5D; after this point, the scour depth reduction decreases with an increase in d/D . The maximum reduction in scour depth was 38% when $d/D=1.5$. Furthermore, for $d/D>2.5$, less changes in the reduction of the maximum local scour depth was found.

Table 3.3. Tests conditions and scour depth characteristics

Test No.	d/D	Maximum scour depth (mm)	Maximum scour depth reduction with comparison to Test 1 (%)
1	0 (Control test, no FDS)	77	0
2	0.5	61	21
3	1.0	51	33
4	1.5	48	38
5	2.0	54	31
6	2.5	68	11
7	3.5	73	5

a)



b)

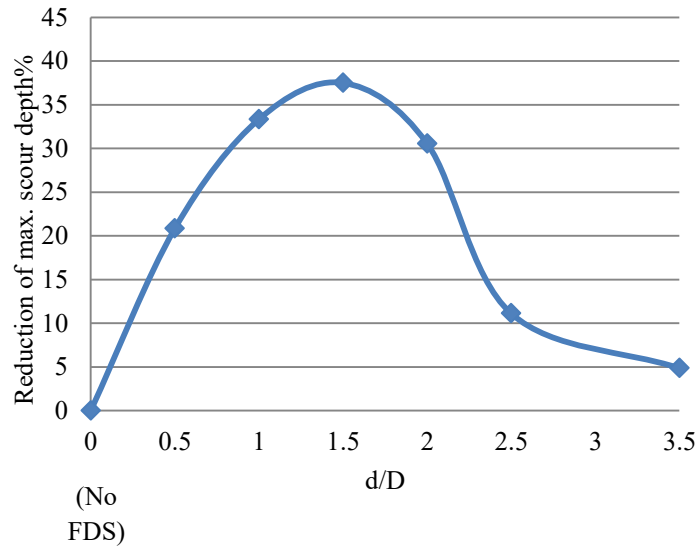


Figure 3.5. Scour depth vs. normalised distance to the pier; a) maximum scour depth; b) trend of maximum scour depth reduction

- **Circular FDS**

In order to compare the results with a circular flow diversion structure, the data of the current study was compared with the data reported by Keshavarzi et al. (2018); this data is available for the current study as the candidate participated in the study reported by Keshavarzi et al. (2018). They experimentally investigated the effects on the local scour depth for two in-line piers with different spacings aligned in the flow direction. Their experiments were conducted under three clear water scour conditions with $V/V_c = 0.74, 0.91$ and 0.93 . In addition, uniform sand with $d_{50} = 0.85$ mm was used. To enable a comparison between the experimental results obtained in the experiments reported herein and those of Keshavarzi et al. (2018), it was assumed that the front pier performed as a circular flow diversion structure for the rear pier. The results of Keshavarzi et al. (2018) including the maximum scour depth, and the percentage reduction of the maximum scour depth for the different spacings between the two in-line piers, and three flow conditions are tabulated in Table 3.4. This data has been used in Figures 3.6 to illustrate the outcomes of Keshavarzi et al. (2018). Referring to Table 3.4 and Figure 3.6, it can be seen that the maximum reduction in the scour depth at the rear pier occurred when $1 < d/D < 2$ depending on the value of V/V_c . Furthermore, regardless of the value of V/V_c , the maximum percentage of scour depth reduction was 16%.

- **Comparing of results**

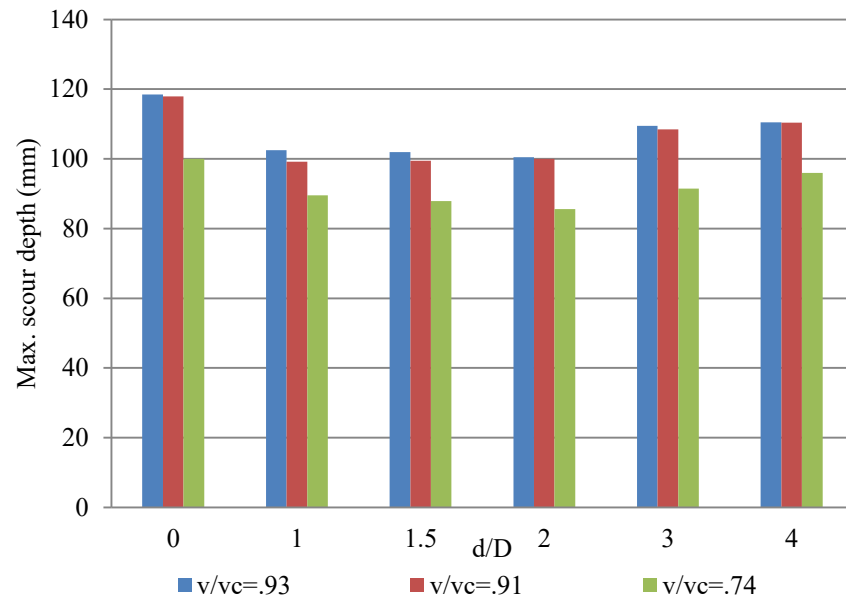
The triangular and circular FDS have been compared based on normalised data from this study and those reported by Keshavarzi et al. (2018). It is of interest to note that the triangular prism FDS proposed in this study with dimensions much smaller than the pier reduces the maximum scour depth by 38%. On the other hand, the scour depth reduces by just 16% at the rear pier in the case of two in-line piers. Although triangular FDS was tested in more critical condition than circular FDS, it was more efficient than circular FDS. Therefore, it can be concluded that the shape of the flow diversion structure is an effective factor for reducing the scour depth around piers. Accordingly, a triangular prism FDS is introduced as a new countermeasure against local scour around

bridge piers. The effectiveness of this shape was confirmed theoretically and experimentally.

Table 3.4. Scour depth characteristics at rear pier in tandem arrangement (after Keshavarzi et al., 2018)

Test No.	d/D	V/V _c	Maximum scour depth (mm)	Maximum scour depth reduction with comparison to single pier case (%)
1	0 (single pier)	0.74	100	0
2	1	0.74	89.5	11
3	1.5	0.74	87.9	12
4	2	0.74	85.6	14
5	3	0.74	91.5	9
6	4	0.74	96	4
7	0 (single pier)	0.91	117.9	0
8	1	0.91	99.2	16
9	1.5	0.91	99.5	16
10	2	0.91	100	15
11	3	0.91	108.5	8
12	4	0.91	110.4	6
13	0 (single pier)	0.93	118.5	0
14	1	0.93	102.5	14
15	1.5	0.93	101.9	14
16	2	0.93	100.5	15
17	3	0.93	109.5	8
18	4	0.93	110.5	7

a)



b)

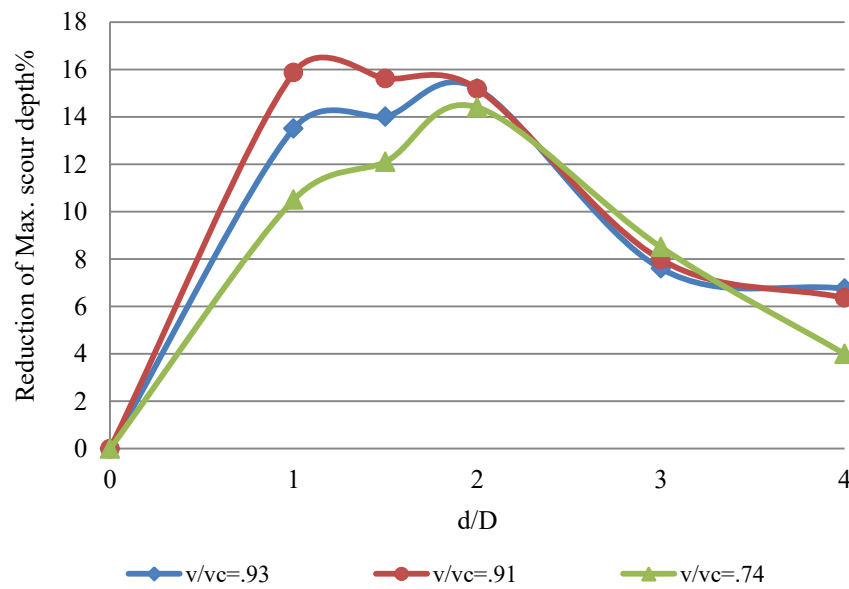


Figure 3.6. Maximum scour depth vs. normalised distance a) maximum scour depth at rear pier and b) maximum scour depth reduction at rear pier for the two in-line piers case

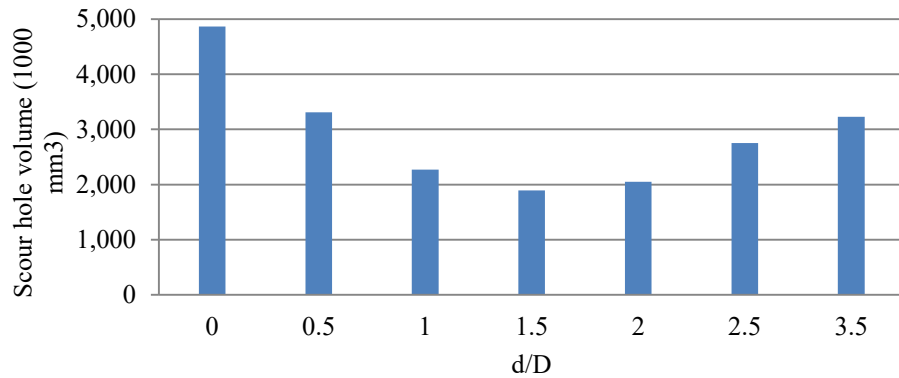
3.4.2. Determination of the Scour Hole Volume

In this study, after achieving an equilibrium condition, scour hole profiles were determined using a digital point gauge. This data was used to calculate the volume of the scour hole using Surfer software, version 15. Table 3.5 summarises the scour hole volume characteristics for seven preliminary laboratory tests. Figure 3.7 shows the scour hole volume and the percentage reduction of the scour hole volume after installation of the triangular flow diversion structure. As shown in Figure 3.7, usage of a flow diversion structure reduces the scour hole volume. In addition, the distance between this structure and the pier is a key factor, influencing the effectiveness of the flow diversion structure. As can be seen in Figure 3.7b, when d/D is equal to 0.5, the scour hole volume reduction is 32%. When d/D increases up to 1.5, the reduction in the scour hole volume increases to 61%. The maximum reduction in the scour hole volume was 61% when $d/D = 1.5$; after that point, an increase in d/D results in an increase in a scour hole volume. Hence, for the dimensions of the proposed flow diversion structure and the pier, the optimum clear distance to achieve the maximum reduction in scour volume, was 1.5 times of the pier diameter. These results are aligned with the results presented in previous section.

Table 3.5. Scour hole volume characteristics

Test No.	d/D	Scour hole volume (1000mm ³)	Scour hole volume reduction in comparison with Test 1 (%)
1	0 (No FDS)	4,867	0
2	0.5	3,311	32
3	1.0	2,272	53
4	1.5	1,896	61
5	2.0	2,051	58
6	2.5	2,751	43
7	3.5	3,230	34

a)



b)

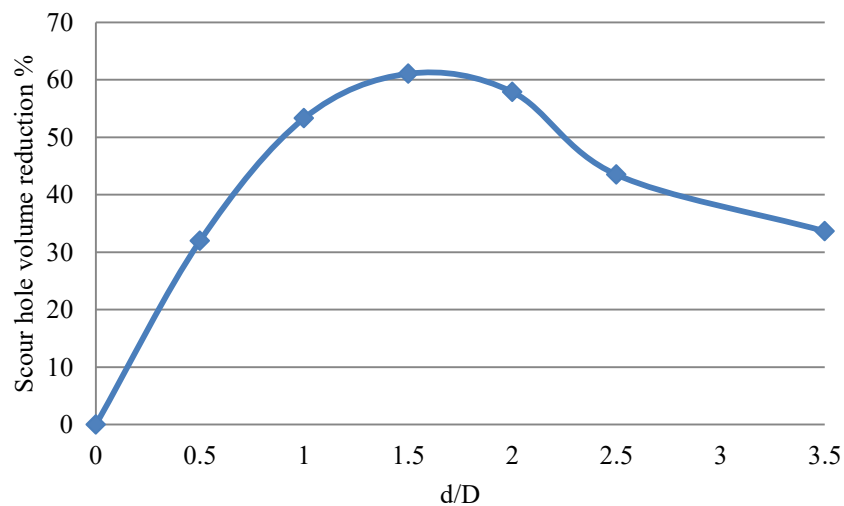


Figure 3.7. Scour hole volume against normalised distance; a) scour hole volume; b) scour hole volume reduction

3.4.3. Flow Field Analysis

Flow field around circular cylinders and their effects on bed scour have been investigated in previous studies. The problem of local scour is also very sensitive to many flow structural considerations, pier dimensions, and bed mobility parameters. The key parameters are the pier size, the pier shape, the Reynolds number, the sediment

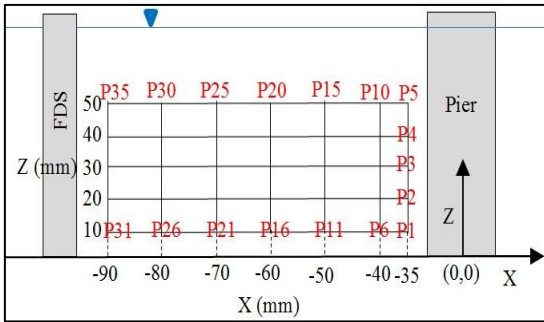
sizes and shapes as stated by Zdravkovich (1977) and Martinuzzi & Tropea (1993). In the studies carried out by Melville & Raudkivi (1977), Ettema (1980), and Dargahi (1989) it was shown that scour around a pier commences firstly at the sides of the pier and at the downstream wake and then bed scour by the dynamics of a horseshoe vortex located upstream of the pier becomes dominant. This phenomenon was also observed during the experimental tests in this study. However, no specific data were recorded. As the focus of the study was not the scour mechanism but rather scour mitigation using an FDS. The dynamics of the horseshoe vortex upstream of the pier consist of some vortices developing in a series of horseshoe vortex structure enlargement (Baker 1980).

The focus of this section is on the flow field upstream of a pier following installation of a triangular prism FDS at a distance upstream of the pier. The main purpose of these preliminary tests is to find out how triangular prism changes the flow field, and consequently local scour around a circular bridge pier.

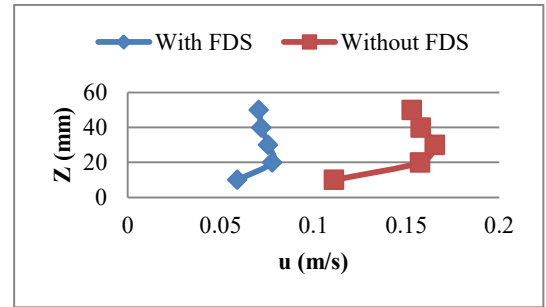
In order to find out how the proposed triangular prism affects the flow field at the upstream of a pier and, hence, produce a reduction in local bed scour around a bridge pier, velocity components of flow were measured by a Micro-ADV. The streamwise velocity component (u) and the vertical velocity component (w) at 35 grid points (Figure 3.3) in Test 1 (control test) and Test 4 (best performing test regarding the local scour reduction) were measured.

Figure 3.8 shows a comparison of the streamwise velocity component (u) in Tests 1 and 4. The positions of the 35 velocity measurement points (P1:P35), previously illustrated in Figure 3.3, once again are presented in Figure 3.8a to allow easy comparison. According to this figure, the streamwise velocities at all grid points in Test 4 were less than those of Test 1. The averages of streamwise velocity components at these 35 grid points in Test 1 and 4 were 0.23 and 0.07 m/s, respectively. It can be noted that the flow diversion structure reduced the average of streamwise velocity component at upstream of the pier up to 70%. The strength of down-flow and horseshoe vortex are dependent on the magnitude of the streamwise velocity (u) at upstream face of the pier, therefore, it can be concluded that these parameters may be reduced by installing the flow diversion structure at a specific distance from the upstream of the pier.

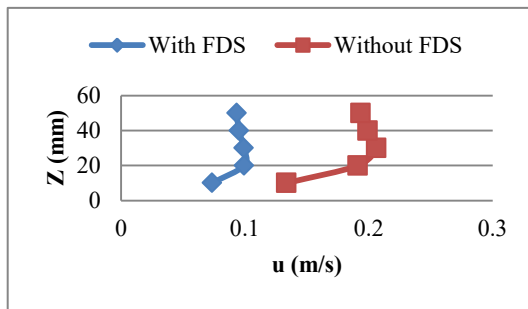
a) positions of 35 velocity measurement points (p1:p35)



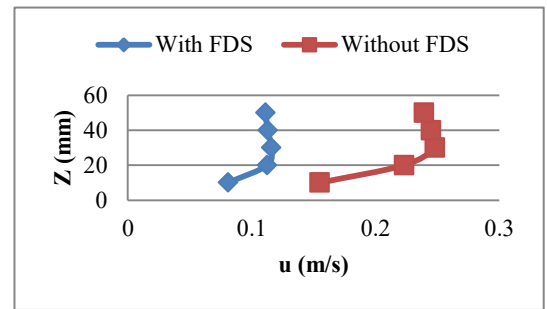
b) u along P1:P5



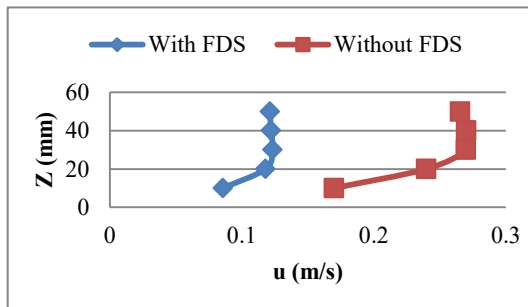
c) u along P6:P10



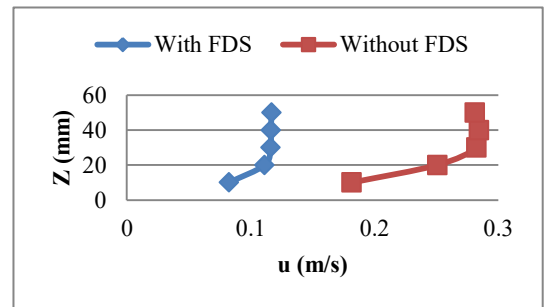
d) u along P11:P15



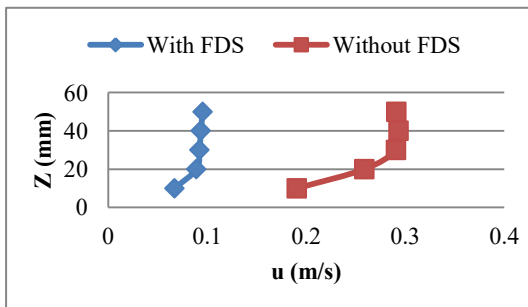
e) u along P16:P20



f) u along P21:P25



g) u along P26:P30



h) u along P31:P35

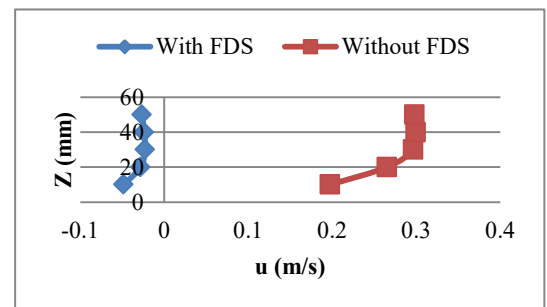


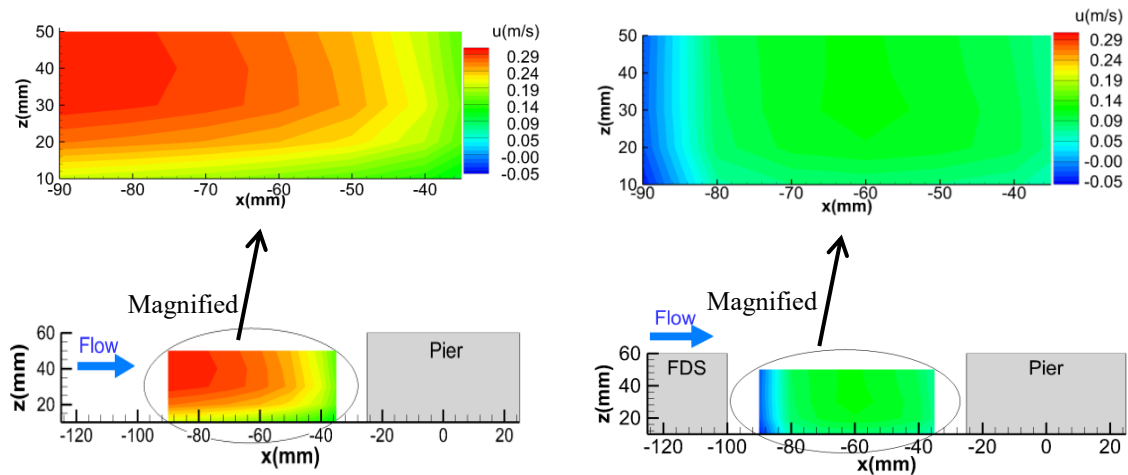
Figure 3.8. Comparison plot of streamwise velocity component (u) in Test 1 (without FDS) and Test 4 (FDS with $d/D=1.5$)

The velocity distributions for the case with triangular prism FDS and without triangular prism FDS were compared, and the results are shown in Figure 3.9. This figure depicts the contours of streamwise velocity (u) in Tests 1 and 4.

According to the results (Figures 3.8 and 3.9), a reduction in the streamwise velocity at upstream of the pier was observed after installing the flow diversion structure. The reduction of the streamwise velocity drops the gradient of the pressure at upstream surface of the pier. Consequently, the down-flow at the pier will decrease. Down-flow is one of the significant reasons of the local scour, and its reduction can reduce the local scour. In addition, the down-flow interacts with the horizontal layer near to the river bed and forms the horseshoe vortex. As the velocity of the down-flow and horizontal layer decreased due to installing the flow diversion structure, the horseshoe vortex also became weaker. Therefore, it can be concluded, for the scenarios tested, that flow diversion structure reduces the strength of down-flow and horseshoe vortex and subsequently reduces the local scour around a pier.

a) No FDS

b) pier and FDS with $d/D=1.5$



**Figure 3.9. Contour plots of time-averaged streamwise velocity component; a) Test 1;
b) Test 4**

Similar results can be found in Figure 3.10, illustrating the depth-averaged of streamwise velocity in Tests 1 and 4. Referring to Figure 3.10, the depth-averaged streamwise velocity at all sections in Test 4 were less than those of Test 1.

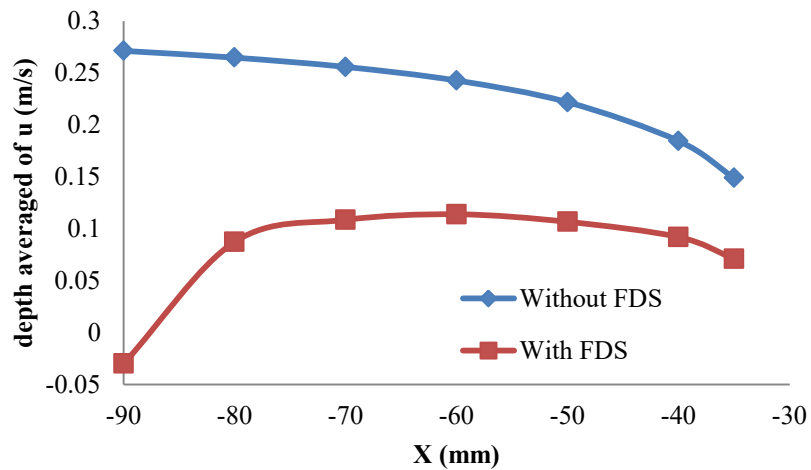


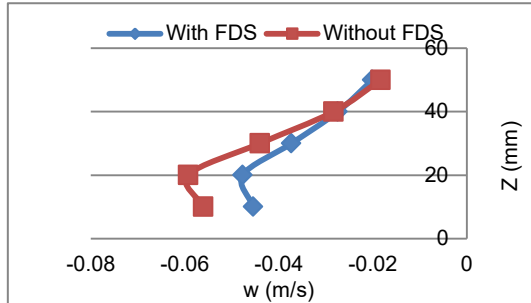
Figure 3.10. Comparison of the depth-averaged of u in Test 1 and Test 4

A similar analysis was carried out for the vertical velocity component (w). Figure 3.11 plots the vertical velocity component (w) in Test 1 and Test 4. The positive value of w indicates that the down-flow was reduced by installing the flow diversion structure. The averages of vertical velocity component in Tests 1 and 4 were -0.015 and -0.006 m/s, respectively, and could be resulted that the intensity of down-flow in Test 4 reduced up to 60% in comparison to Test 1.

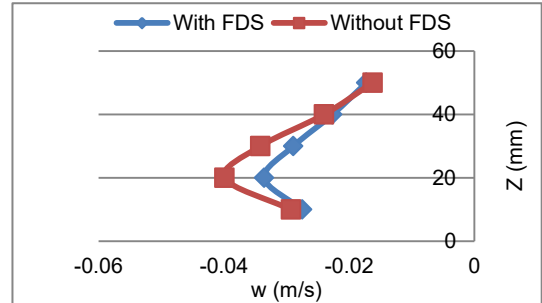
Figure 3.12 compares the contours of vertical velocity (w) in Tests 1 and 4. As can be seen from Figure 3.12, the velocity of down-flow at upstream of the pier reduced after installing flow diversion structure. For a better demonstration, the depth-averaged of w is shown in Figure 3.13. As can be observed in Figure 3.13, the negative values of depth-averaged of w prove the existence of downward flow at all sections upstream of the pier before installing the flow diversion structure. However, when the suggested structure was employed some upward flow occurred at the wake region of the structure, where the values of depth-averaged of w are positive, and the down-flow velocity

decreased at the upstream of the pier. These changes at the flow field lead to a reduction of the local scour around a pier.

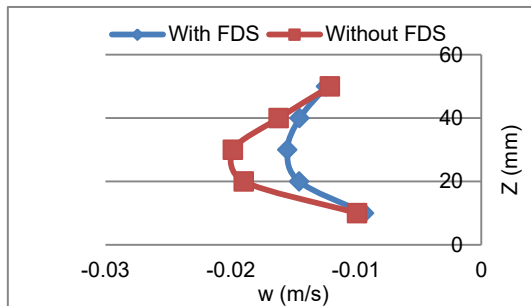
a) P1:P5



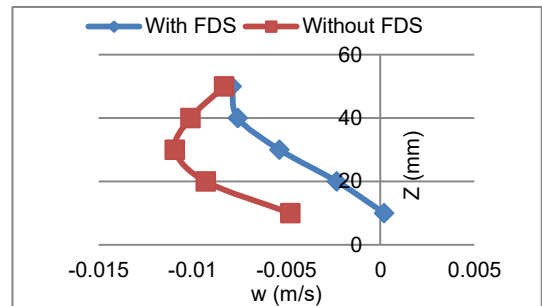
b) P6:P10



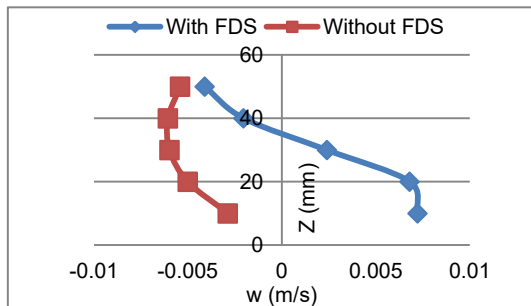
c) P11:P15



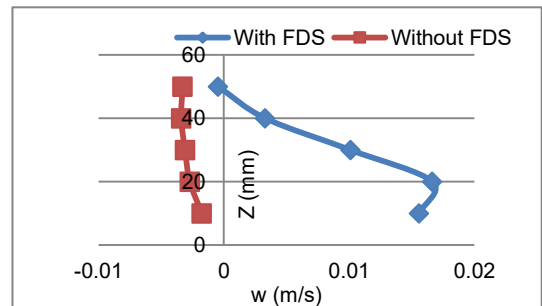
d) P16:P20



e) P21:P25



f) P26:P30



g) P31:P35

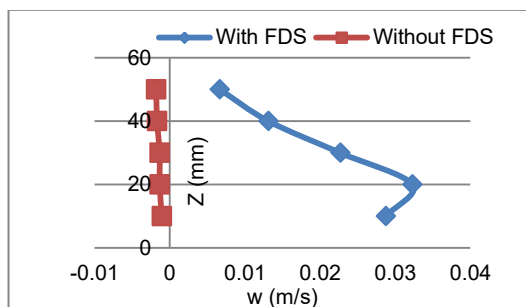


Figure 3.11. Comparison plot of vertical velocity component (w) in Test 1 (without FDS) and Test 4 (with FDS)

a) No FDS

b) pier and FDS with $d/D=1.5$

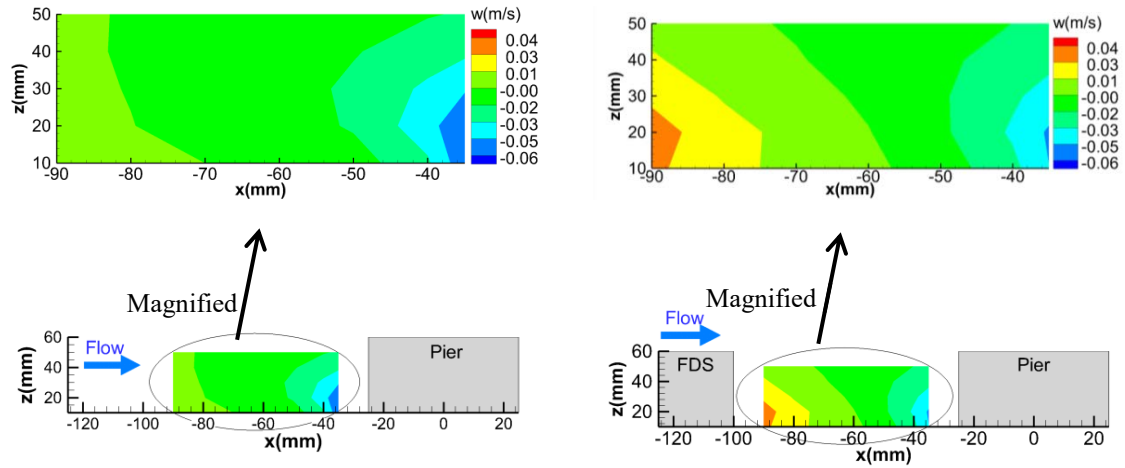


Figure 3.12. Contour plots of time-averaged vertical velocity component; a) Test 1; b) Test 4

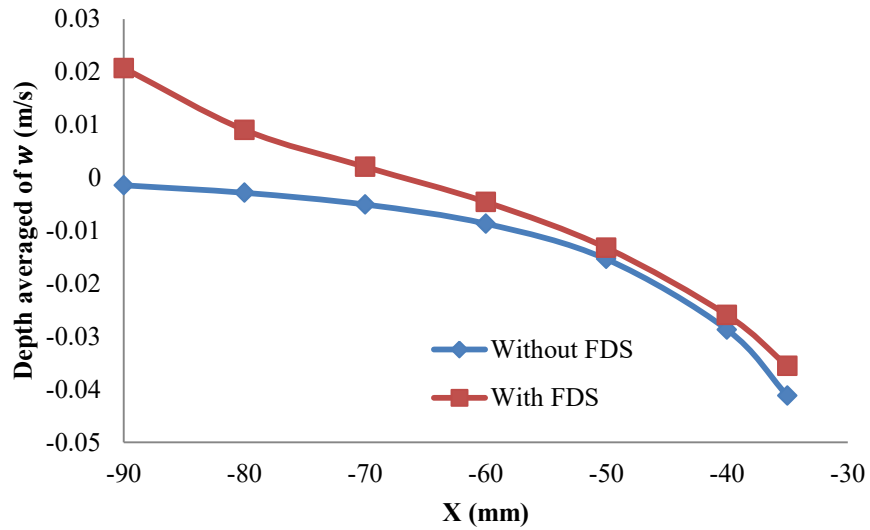


Figure 3.13. Comparison of the depth-averaged of w in Tests 1 and 4

Accordingly, it can be concluded that the proposed flow diversion structure may reduce the magnitudes of mean approach velocity (\bar{V}) due to the reduction of velocity components and change the direction of streamlines at the upstream of the pier as shown in Figure 3.14. This figure reveals that the flow diversion structure forms a

recirculation zone behind itself to a distance approximately three times of the triangular base. The above results are consistent with the results reported by Emerson et al. (2013).

a) No FDS

b) pier and FDS with $d/D=1.5$

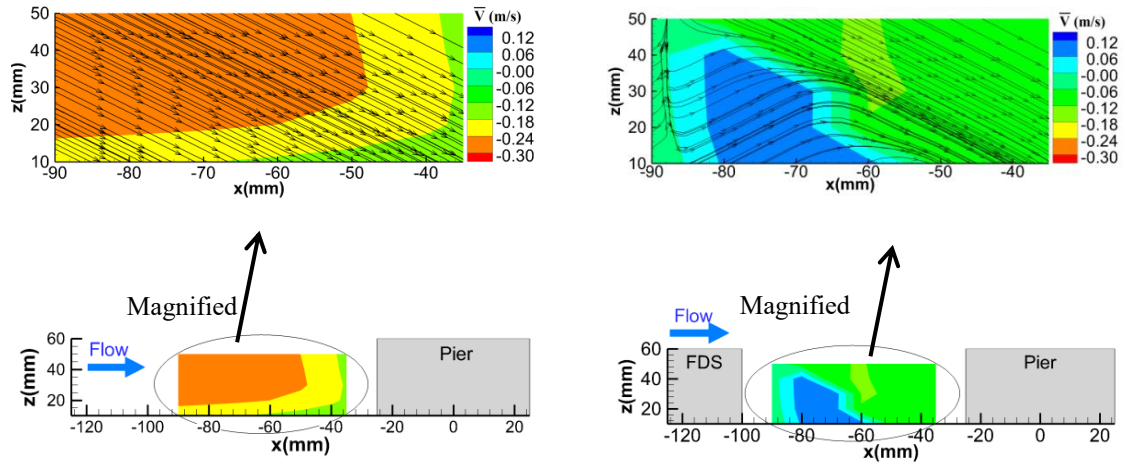


Figure 3.14. Contour plots of mean flow velocity and streamlines; a) Test 1; b) Test 4

3.4.4. Performance of the Proposed Flow Diversion Structure

Many parameters can influence the local scour around bridge piers. These parameters can be categorized into four groups, namely flow characteristics, sediment properties, pier geometry and time. Both sediment properties and time are uncontrollable factors in the real situations. On the other hand, the pier geometry is an important factor that should be considered during the design and construction of bridges. The flow characteristics comprising water depth, the flow velocity, and the flow direction are key parameters affecting the local scour. Use of a flow diversion structure, as proposed in this Chapter, may change both the flow direction and the flow velocity upstream of the pier. Figure 3.15 demonstrates the performance of the proposed structure to divert the streamlines at the upstream of the pier.

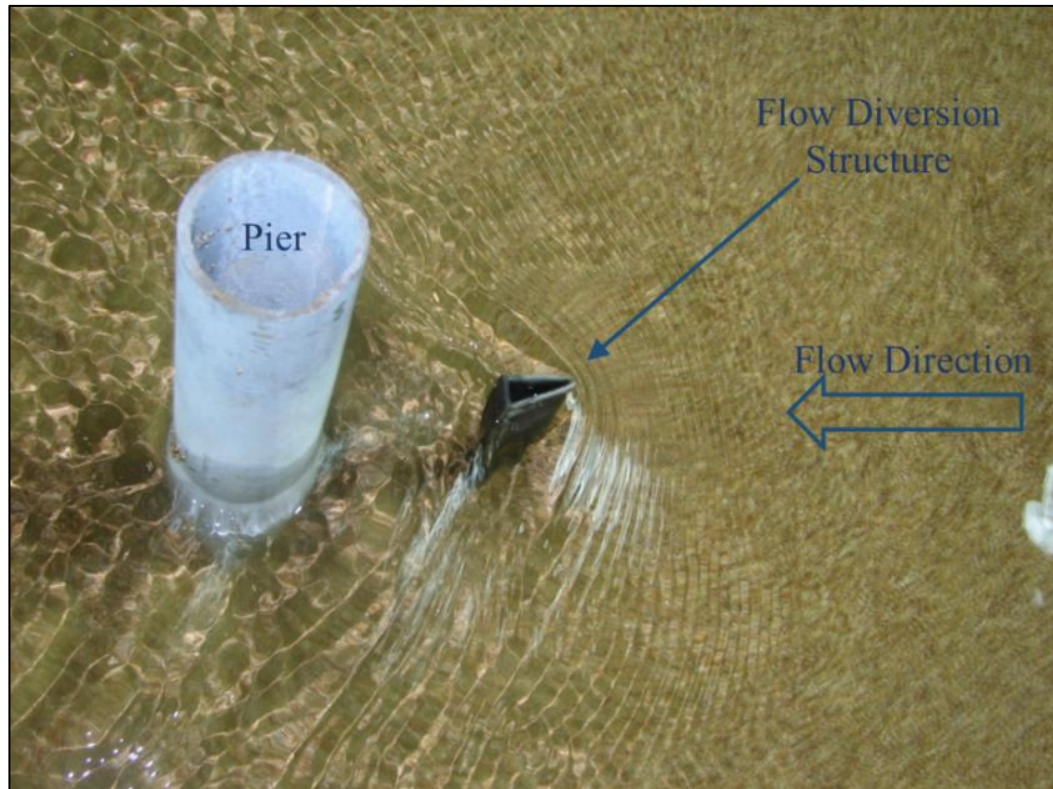


Figure 3.15. Streamlines diversion by triangular flow diversion structure

3.5. Summary

A triangular flow diversion structure (FDS) is presented as a new countermeasure against local scour around a circular bridge pier. A set of proof of concept laboratory tests were completed to test the effects of a triangular FDS on local scour around a circular pier and flow field upstream of the pier. From consideration of the outcomes and in particular the changes in velocity, it can be inferred that the proposed triangular FDS affects the flow field significantly, reducing the strength of down-flow and horseshoe vortex and diverts streamlines from the upstream of the pier, and consequently reduces the local scour around the pier. In addition, the clear distance between this FDS and the pier considerably affects the reduction percentage of the local scour depth and the scour hole volume. For the dimensions of the FDS and the pier used in this study, the optimum distance between them to achieve the maximum reduction in local scour, is approximately 1.5 times of the pier diameter. In this situation, the scour depth and the volume of scour hole around the pier reduced by 38% and 61%, respectively. These findings can be compared to the 16% reduction in the scour depth

for the case of two in-line piers as studied by Keshavarzi et al. (2018), with the assumption that the front pier performed as a circular flow diversion structure for the rear pier. Therefore, it can be claimed that the shape of FDS significantly affects the flow field and local scour around a bridge pier. Furthermore, the triangular shape of FDS, which was proposed and tested in this study, is an appropriate shape for further investigation as a protective measure against local scour.

CHAPTER 4

Experimental Optimisation of Hydrodynamic Performance of Flow Diversion Structure to Reduce Local Scour



4.1. Introduction

As explained in Chapter 3, a full-depth (unsubmerged) triangular prismatic shaped flow diversion structure (FDS) has been introduced as a new countermeasure against local scour around a bridge pier. This proposed FDS was examined via proof of concept laboratory experiments. The results confirmed that the proposed FDS in front of a pier could protect the pier against local scour by changing the flow field around the pier. It was inferred that the FDS reduced the strength of both the down-flow and the horseshoe vortices, and diverted the streamlines from upstream of the pier, consequently decreased the local scour. Furthermore, it was concluded that implementation of the FDS warranted investigation and in particular investigation into suitable dimensions and locations.

The main objective of this chapter is to achieve an efficient hydrodynamic performance of FDS by optimising its dimensions and location to produce the maximum reduction of local scour around a circular pier (depth and volume). Accordingly, a comprehensive experimental study of local scour around a circular pier with different upstream FDS has been conducted. Different FDS dimensions, locations, and submergence ratios were examined experimentally. Taguchi's method was employed to determine the specific parameter combinations to minimise the number of alternative tests. As a result, 28 tests were necessary to find the optimal FDS dimensions and location.

In this chapter the results from these tests are presented and analysed. These results included the outcomes from an experimental test of the optimal dimensions and location for the FDS. Flow field analyses of the FDS presented in Chapter 5 is based on these optimal dimensions and location.

4.2. Review of Bridge Pier Protection against Local Scour

A comprehensive literature review for protecting bridge piers against local scour was conducted and discussed in chapter 2. As mentioned, different techniques of pier-scour countermeasures can be classified into two distinct categories. The first category is armouring devices, which is a traditional solution to decrease local scour around bridge piers. However, this technique may not be considered as an appropriate solution due to

its cost and also different failure mechanisms as presented in Chapter 2. The second category is flow-altering devices. The basis of flow altering device is a change in the flow field around a bridge pier that reduces the local scour.

In a comprehensive review by Tafarjnoruz et al. (2010), the flow-altering countermeasures were classified into four categories, namely (1) openings through piers, (2) pier attachments, (3) bed attachments and (4) other devices. Of these classifications, the proposed FDS can be categorised as a bed attachment. Therefore, a brief review of bed-attachments is presented in the following paragraphs.

Bed attachments are independent structures that should be installed at upstream or at downstream of a pier. Few studies have been conducted on bed attachments; these include sacrificial piles (Melville & Hadfield 1999), vanes and sills (Lauchlan 1999; Odgaard & Wang 1987), surface guide panels (Huang et al. 2005), and sleeve and collared sleeve (Garg et al. 2008; Singh et al. 2001). Melville & Hadfield (1999) investigated some circular sacrificial piles as a scour countermeasure when the flow remains aligned and flow intensity is relatively small. However, the size and shape of the sacrificial piles remained unclear. In addition, the installation location, number of piles, their configurations and degree of submergence needs further investigation including consideration of the potential of a group of sacrificial piles to trap debris during flood events. Lauchlan (1999) investigated the use of Iowa vanes for pier scour reduction under live-bed condition. He concluded that although the maximum scour depth reduction was significant in some tests (30% to 50%), no significant trends were evident in the data. A sleeve is a larger diameter cylinder surrounding the pier and produces scour inside and outside of the sleeve. In order to reduce scour at outside, another countermeasure should also be applied. Consideration of the above studies suggests that the shape, size, and installation location affects the performance of these devices.

The major drawback of the proposed upstream bed-attachments countermeasures is associated with the size of the proposed methods, which induces a significant contraction in the flow cross-section. Regarding their height, some of them are full-depth (unsubmerged); therefore, there is a chance of collision with the boats and ships in the rivers with navigation system. Additionally, there is a risk of trapping floating debris by full-depth bed attachments, which reduces their performance dramatically.

One approach to mitigate these perceived disadvantages in bed attachments would be to ensure they were not full-depth structures; rather being smaller than the pier height to produce the minimum risk of collision, debris trap, and contraction to the flow. This approach was adopted in this study to optimise the proposed flow diversion structure.

As discussed earlier, the size and shape of the sacrificial piles, location, number of piles, their configurations, and the degree of submergence are very important influencing factors on local scour and still their values are unclear; therefore, further investigations are required. Regarding the shape, a triangular prism was shown to be an effective shape (Chapter 3). To resolve the problem of dimensions, submergence ratio, and location, these parameters (see Figure 4.1) have been optimised for the proposed flow diversion structure (FDS). The procedure of optimisation and the results are presented in this chapter.

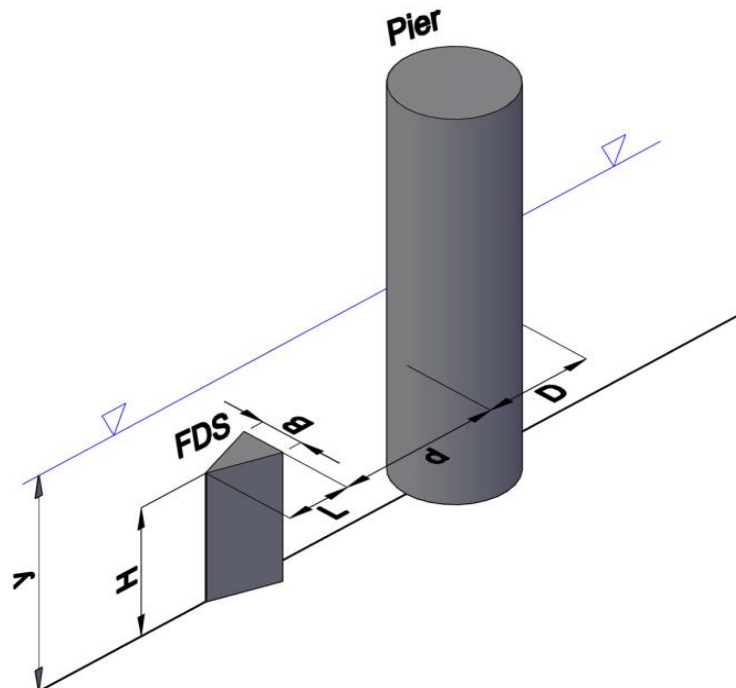


Figure 4.1. Schematic diagram of the pier and the flow diversion structure (FDS)

4.3. Materials and Methods

4.3.1. Dimensional Analysis and Definition of Dimensionless Variables

The effects of different factors on local scour have been investigated by several studies, (e.g. Melville & Coleman 2000; Ataie-Ashtiani & Beheshti (2006); Arneson et al. 2012; Keshavarzi et al. 2018). Arising from consideration of these studies, the factors influencing local scour can be categorised as flow characteristics, sediment properties, pier geometries and time. An outcome of the aforementioned studies is that alternative equations have been proposed for calculation of the equilibrium scour depth (d_{se}) at a pier. If a flow altering device is used to reduce local bed scour, the effects of this device should be added to the above factors. Therefore, the factors influencing the depth of scour at a pier in the presence of a flow altering device (d_s) can be presented in a functional form as:

$$\frac{d_s}{d_{se}} = k(\text{flow, sediment, pier, time, flow altering device}) \quad (4.1)$$

where, flow represents all flow characteristics influencing scour, etc. As previously mentioned the effects of the first four groups in Equation 4.1 on d_{se} have been studied for the case of no flow altering device and reported in the literature. Referring to the effects of a flow altering device, the parameters such as its shape, size and location affect the pier scour.

As concluded in the previous chapter, an unsubmerged triangular flow diversion structure (FDS) can be employed as an effective flow altering device. The purpose of this chapter is to determine the optimum location and dimensions for an FDS prior to a circular pier. To achieve this aim, the characteristics of the FDS considered were the lateral base (B), longitudinal base (L), height (H), and the upstream clear distance (d). These characteristics are illustrated in Figure 4.1.

The FDS affects the flow field near a pier; hence it is also needed to consider the water depth (y), flow velocity (V), and pier diameter (D). Consideration of the results from Melville & Coleman (2000) indicates that the greatest scour occurs when the cross-sectional average velocity (V) equals the critical flow velocity for particles entrainment (V_c). The cross-sectional average velocity for the experiments reported herein was maintained near the critical flow velocity for sediment entrainment. In addition, sediment properties and time were chosen regarding the criteria proposed in the literature and kept constant in all tests which are explained in the experimental setup and procedure section. These enabled the deletion of the flow velocity, sediment properties and time as the variable parameters for the experiments. Therefore, Equation 4.1 under these conditions can be rewritten as:

$$\frac{d_s}{d_{se}} = k(L, B, H, d, y, D) \quad (4.2)$$

Considering pier diameter as a horizontal scale parameter and water depth as a vertical scale parameter, Equation 4.2 can be rewritten by the dimensionless function Φ :

$$\frac{d_s}{d_{se}} = \Phi\left(\frac{B}{D}, \frac{L}{D}, \frac{d}{D}, \frac{H}{y}\right) \quad (4.3)$$

In order to find the best values of the parameters in Equation 4.3 for achieving the maximum reduction of pier-scour, different FDS dimensions, locations, and submergence ratios should be examined. The following procedure and criteria were made to select different values for the parameters mentioned above.

As this structure should be smaller than the pier, five values were considered for B/D and L/D from 0.2 to 1 with 0.2 increments. Similarly, five values of H/y were tested

(i.e., $H/y=0.25, 0.5, 0.75, 1$ and >1), so that the first four values were a fully submerged structure and the last one was an unsubmerged structure. With the intention of selecting the values for d/D the results of the preliminary tests presented in Chapter 3 and the published results by Keshavarzi et al. (2018) were used. The full-depth FDS employed in the preliminary tests was a triangular prism with $B/D=0.2$ and $L/D=0.5$. This structure was located at 6 different spacings from the pier (i.e. $d/D = 0.5, 1, 1.5, 2, 2.5$ and 3.5). Considering the outcomes of the experimental tests in Chapter 3 indicated that the optimum clear distance between the pier and the flow diversion structure was $1.5D$. Furthermore, the published results of an experimental study carried out by Keshavarzi et al. (2018) on local scour for two in-line piers with different spacings and under different flow conditions were considered; with this assumption that the front pier performed as a flow diversion structure for the rear pier. The outcomes of this case also showed that the minimum local scour occurred around the rear pier, when the clear distance between two in-line piers was in the ranges of 1 to 2 times of the pier diameter. These outcomes are displayed in Figure 4.2. As a result and for attaining further evidence, five values were considered for d/D from 0.5 to 2.5 (i.e. $d/D = 0.5, 1, 1.5, 2$ and 2.5).

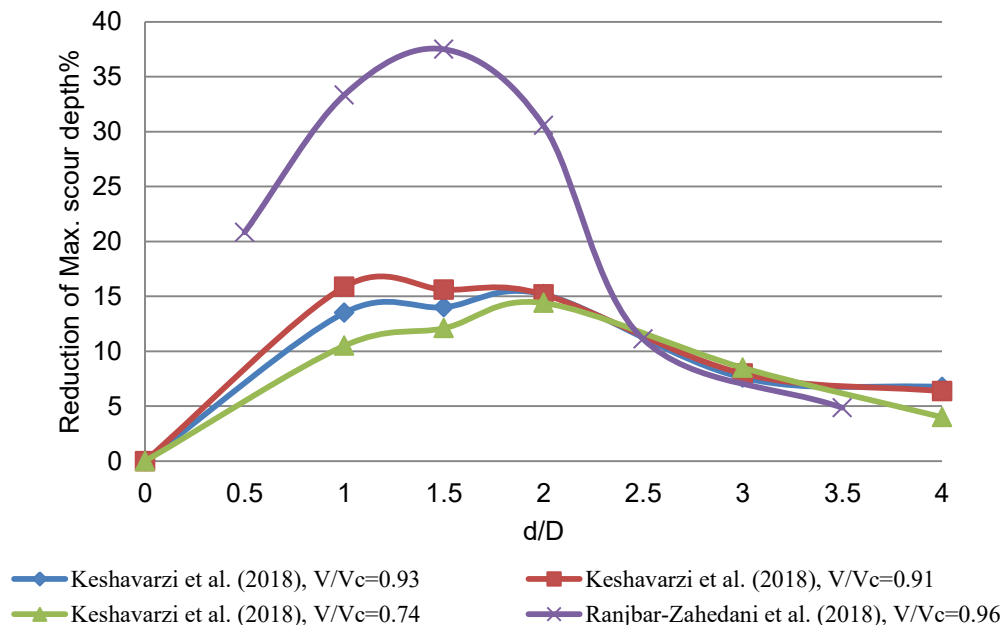


Figure 4.2. The effect of clear distance between the pier and FDS or between two in-line piers on local scour reduction around the rear pier

Table 4.1 illustrates all the variables and their values, which have been considered in this study. It should be noted that a number from 1 to 5 was assigned as the variable level for each value, as shown in Table 4.1.

Table 4.1. Experimental variables and their values and levels

Variables	Values of the variables (variables' levels)					Number of levels
B/D	0.20 (1)	0.40 (2)	0.60 (3)	0.80 (4)	1.00 (5)	5
L/D	0.20 (1)	0.40 (2)	0.60 (3)	0.80 (4)	1.00 (5)	5
H/y	0.25 (1)	0.50 (2)	0.75 (3)	1.00 (4)	>1.00 (5)	5
d/D	0.50 (1)	1.00 (2)	1.50 (3)	2.00 (4)	2.50 (5)	5

If Table 4.1 was considered, testing of all possible combinations of experimental variables would require 625 individual experimental tests. This number of experiments was not feasible. Hence, experimental design using Taguchi's method was undertaken.

4.3.2. Experimental Design Using Taguchi's Method

Taguchi's technique is a statistical methodology to optimise the setting of parameters to refine the result (Menon et al. 2012; Phadke 1995; Wu & Zhou 2011). The above technique can be used to define the impact of numerous factors, which influence the result of a particular laboratory test (Doddamani & Kulkarni 2011). Fundamentally, this technique is founded on factorial experimental design (Box et al. 1978). As such, the standard experimental table, based on an orthogonal array, discussed by Phadke (1995),

is used. This array reveals the influence of variables by performing a smaller amount of the tests. For the arrangement of data, the columns are equally orthogonal, for example for pair of columns, arrangement of all elements occurs in identical quantity of epochs (Sii et al. 2001). An appropriate arrangement can carefully be chosen on the total number of factors (Gunes et al. 2011). These standard arrays can give full information about all variables that affect the performance factor. The selection of orthogonal array is based on the number of independent variables and the number of levels for each independent variable. The basic principles of this technique are explained by (Bagchi 1993; Mori 2011; Roy 2010).

In this study, the number of independent variables is four; and five levels have been considered for each of them, as summarised in Table 4.1. Based on Taguchi's method, at least 25 tests should be conducted to find the optimum value for each variable. Beyond these tests, a control and an optimum test were necessary for comparison and confirmation the results. The configurations of the required tests are presented in Table 4.2. The orthogonal arrays shown in Table 4.2 have the following properties that can minimise the number of required tests:

- Firstly, the orthogonal arrays have the balancing property. It means that all variables' levels are repeated equally. In this study, the repetition for each variable's level is equal to 5, for example, $B/D = 0.2$ (i.e. level one of B/D) is repeated five times in Table 4.2, as like as all other variables' levels.
- Secondly, every two columns under each variable are mutually orthogonal. It means that if a weighing factor between -1 and 1 is normatively allocated to the levels of each variable, then the inner product summation of weighing factors for any two variables is equal to zero. In this study, the weighing factors -1, -0.5, 0, 0.5, and 1 are allocated to levels 1 to 5 for each variable. The inner products for every two variables are calculated and presented in Table 4.3 that confirms each variable are mutually orthogonal. According to the orthogonality, the experimental runs must be conducted as it designed. For instance, Run 1 in Table 4.2 cannot be conducted with any other value of B/D except $B/D=0.2$.

Table 4.2. Experimental design based on Taguchi's method

Run No	B/D	L/D	H/y	d/D
1	0.2	0.2	0.25	0.5
2	0.2	1	1	1.5
3	0.2	0.8	0.5	2.5
4	0.2	0.6	>1.00	1
5	0.2	0.4	0.75	2
6	0.4	1	0.75	1
7	0.4	0.4	0.5	1.5
8	0.4	0.6	1	0.5
9	0.4	0.2	>1.00	2.5
10	0.4	0.8	0.25	2
11	0.6	0.4	0.25	1
12	0.6	0.8	>1.00	1.5
13	0.6	0.2	1	2
14	0.6	0.6	0.75	2.5
15	0.6	1	0.5	0.5
16	0.8	0.6	0.5	2
17	0.8	0.8	1	1
18	0.8	1	0.25	2.5
19	0.8	0.2	0.75	1.5
20	0.8	0.4	>1.00	0.5
21	1	0.4	1	2.5
22	1	1	>1.00	2
23	1	0.6	0.25	1.5
24	1	0.8	0.75	0.5
25	1	0.2	0.5	1
26	Control test (single pier without a flow diversion structure)			
27	Optimum test (based on the acquired optimal conditions)			

Table 4.3. Mutually orthogonal of any two variables' weighing factors

Run No	Variables' weighing factor				Inner product of weighing factors of variables					
	B/D	L/D	H/y	d/D	(B/D) . (L/D)	(B/D) . (H/y)	(B/D) . (d/D)	(L/D) . (H/y)	(L/D) . (d/D)	(H/y) . (d/D)
1	-1	-1	-1	-1	1	1	1	1	1	1
2	-1	1	0.5	0	-1	-0.5	0	0.5	0	0
3	-1	0.5	-0.5	1	-0.5	0.5	-1	-0.25	0.5	-0.5
4	-1	0	1	-0.5	0	-1	0.5	0	0	-0.5
5	-1	-0.5	0	0.5	0.5	0	-0.5	0	-0.25	0
6	-0.5	1	0	-0.5	-0.5	0	0.25	0	-0.5	0
7	-0.5	-0.5	-0.5	0	0.25	0.25	0	0.25	0	0
8	-0.5	0	0.5	-1	0	-0.25	0.5	0	0	-0.5
9	-0.5	-1	1	1	0.5	-0.5	-0.5	-1	-1	1
10	-0.5	0.5	-1	0.5	-0.25	0.5	-0.25	-0.5	0.25	-0.5
11	0	-0.5	-1	-0.5	0	0	0	0.5	0.25	0.5
12	0	0.5	1	0	0	0	0	0.5	0	0
13	0	-1	0.5	0.5	0	0	0	-0.5	-0.5	0.25
14	0	0	0	1	0	0	0	0	0	0
15	0	1	-0.5	-1	0	0	0	-0.5	-1	0.5
16	0.5	0	-0.5	0.5	0	-0.25	0.25	0	0	-0.25
17	0.5	0.5	0.5	-0.5	0.25	0.25	-0.25	0.25	-0.25	-0.25
18	0.5	1	-1	1	0.5	-0.5	0.5	-1	1	-1
19	0.5	-1	0	0	-0.5	0	0	0	0	0
20	0.5	-0.5	1	-1	-0.25	0.5	-0.5	-0.5	0.5	-1
21	1	-0.5	0.5	1	-0.5	0.5	1	-0.25	-0.5	0.5
22	1	1	1	0.5	1	1	0.5	1	0.5	0.5
23	1	0	-1	0	0	-1	0	0	0	0
24	1	0.5	0	-1	0.5	0	-1	0	-0.5	0
25	1	-1	-0.5	-0.5	-1	-0.5	-0.5	0.5	0.5	0.25
Sum					0	0	0	0	0	0

As discussed by Bagchi (1993), the orthogonality causes that the effect of each variable at each level on output response can be estimated by averaging all output responses include that variable at that level. For example, the average of output responses in Run 1 to 5 in Table 4.2 only shows the effects of $B/D = 0.2$ on the output response. This important matter is used in this study to analyse the results.

4.4. Experimental Setup and Procedure

4.4.1. Flume and Its Components

These comprehensive experiments on local scour around a circular bridge pier with different upstream FDSs were conducted in a different flume as mentioned in Chapter 3.

Experiments were carried out in a rectangular Plexiglas-sided flume. The length, width and depth of this flume were 8 m, 0.45 m, and 0.30 m, respectively. The flume had a longitudinal slope of 0.0006 (m/m). The discharge was supplied from a tank with a recirculating electro-pump system. A variable speed drive has been provided to control the electromotor speed and consequently adjust the flow rate. The flume was equipped with a turbine insertion flow-meter to measure the flow rate with an accuracy of 0.5%. A rectangular flap gate was designed, built and installed at the downstream end to regulate the water depth along the flume. The inlet and outlet tanks were provided at the upstream and downstream of the flume, respectively. Figure 4.3 shows a schematic diagram of the laboratory flume.

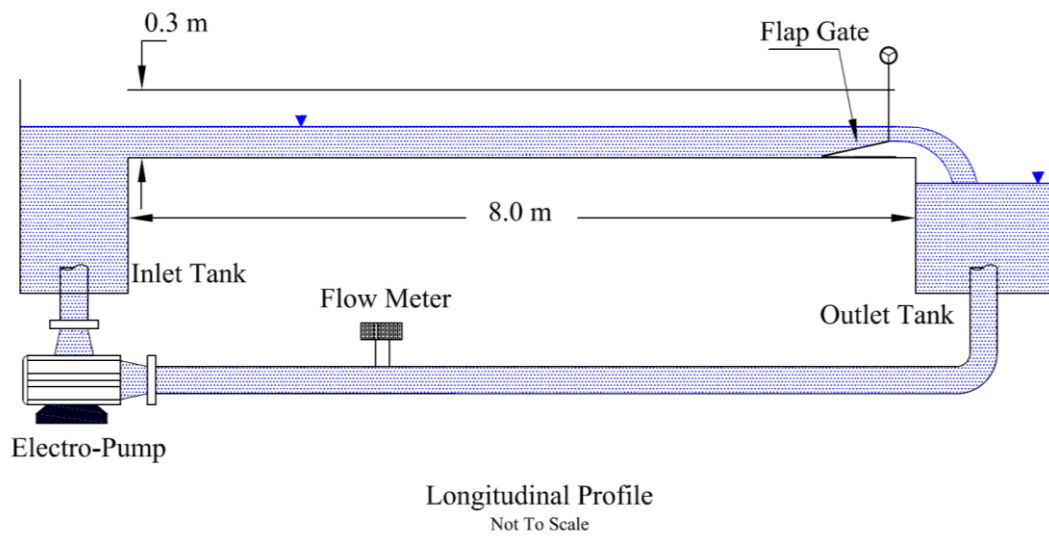


Figure 4.3. Schematic diagram of the laboratory flume

4.4.2. Designing Experiment Conditions

In this study, all parameters such as pier size, sediment characteristics, time, and hydraulic conditions were chosen regarding the criteria proposed in the literature and kept constant in all tests, which are explained in the following paragraphs.

- **Pier Diameter (D)**

The pier diameter (D) was selected to minimise any contraction effects on the scour depth. As stated by Melville & Coleman (2000), to minimise the effects of contraction, the ratio of the flume width (W) to the pier diameter (D) should be greater than ten. In this study, a 40 mm pier diameter was used. The resultant ratio (W/D) was 11.25 and therefore satisfied the criterion of Melville & Coleman (2000).

- **Bed Sediment Layer Thickness (S_t)**

According to Melville & Sutherland (1988), the maximum possible scour depth (d_{se}) that can occur at a cylindrical pier is estimated as 2.4 times the diameter of the pier.

Hence the thickness of the bed sediment layer was taken in such a way that it was sufficient to fulfil the above condition. For 40 mm diameter bridge pier, $2.4D = 2.4 \times 40 = 96$ mm. Hence depth of bed sediment layer must be greater than 96 mm. This parameter was opted equal to 120 mm, which was sufficient to satisfy the above condition.

- **Median Size of Bed Sediment (d_{50})**

Based on Ettema (1976), the scour depth is not affected by the grain size if the ratio of the pier diameter to the particle size (D/d_{50}) goes above 50. In addition, Melville (2008) mentioned that for d_{50} below about 0.7 mm a bed may form ripples can affect scour at a pier. Therefore, in this study, the median size of bed sediment should be between 0.7 and 0.8 mm. The median sediment size used in this study was 0.78 mm which is in the above limit (see Figure 4.4).

- **Sediment Uniformity (σ_g)**

Grading of sediment gives the sediment non-uniformity which is usually considered by the geometric standard deviation of the sediment size, $\sigma_g = (d_{84}/d_{16})^{0.5}$. Melville & Coleman (2000) stated that σ_g should be less than 1.3 for uniform sand. For σ_g greater than 1.3, non-uniform sediments armouring would be expected to occur on the channel bed and in the scour hole. Armour layer formation within the scour hole reduces the local scour depth. In this study in order to avoid the effects of armour layer on the local scour depth, non-cohesive uniform sand with $\sigma_g=1.24$ was used. The sieve analysis of the sand used in the experiments is shown in Figure 4.4.

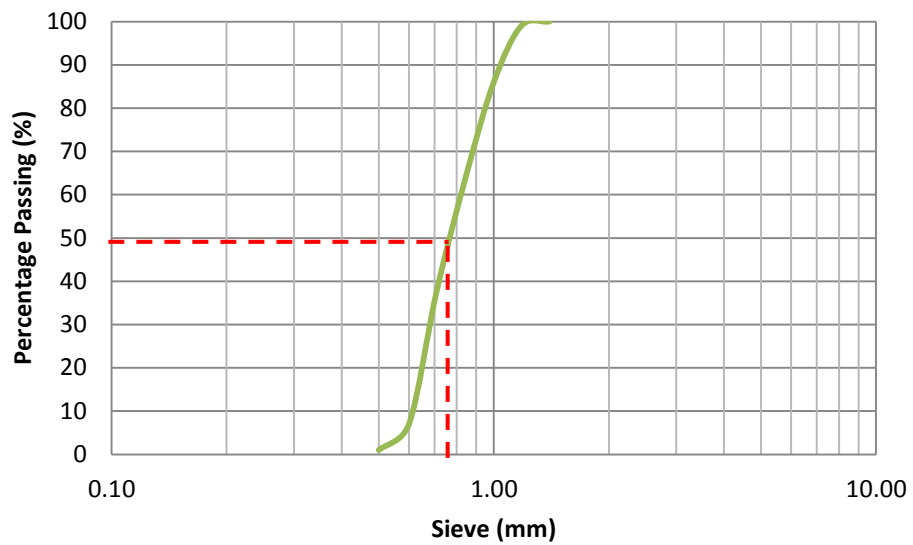


Figure 4.4. Sieve analysis of the sand used

- **Water Depth (y)**

To avoid the effects of water depth on the local scour depth, Melville & Coleman (2000) recommended that D/y should be less than 0.7. Referring to the selected pier diameter ($D=40$ mm), water depth for this experimental design must be greater than 57.14 mm. Hence, in this study water depth is selected to be 100 mm.

- **Flow Intensity**

According to Melville & Chiew (1999), the flow intensity is a dimensionless parameter, which is defined as the ratio of the cross-sectional average velocity (V) to the critical mean flow velocity for sediment entrainment (V_c). Melville & Coleman (2000) pointed out that the scour depth in uniform bed material increases in a linear manner with flow intensity to a maximum depth at the threshold velocity under clear-water conditions.

Melville and Coleman (2000) suggested the following relationships with respect to the flow intensity:

- *For clear water scour conditions:*

$(V/V_c) < 1;$ *for uniform sediments*

$[V-(V_a-V_c)]/V_c < 1;$ *for non-uniform sediments*

➤ **For live bed scour conditions:**

$(V/V_c) > 1;$ *for uniform sediments*

$(V/V_a) > 1;$ *for non-uniform sediments*

Where V_a (for non-uniform sediments) is the mean flow velocity at the armour peak ($\equiv V_c$ for uniform sediments).

Figure 4.5 shows the changes in the maximum pier scour depth as a function of flow intensity (Melville & Coleman 2000).

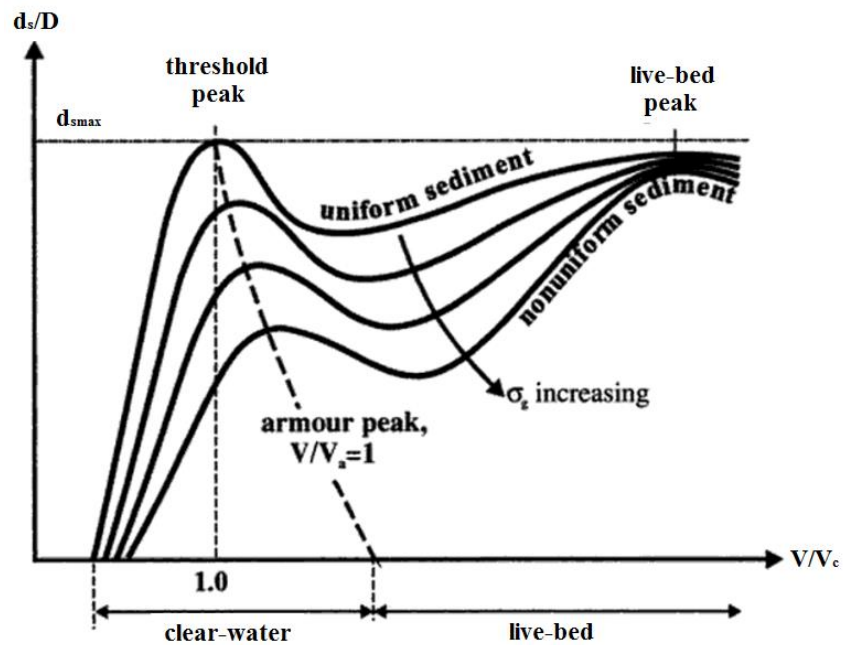


Figure 4.5. Local scour depth variation with flow intensity (after Melville & Coleman, 2000)

Referring to Figure 4.5 the maximum local scour depth occurs in uniform sediment and at the threshold peak ($V/V_c \approx 1$). The critical mean flow velocity for uniform sediment entrainment can be determined by the following equations that have been proposed by Melville & Coleman (2000).

$$u_{*c} = 0.0115 + 0.0125d_{50}^{1.4} \quad 0.1mm < d_{50} < 1mm \quad (4.4a)$$

$$u_{*c} = 0.0305d_{50}^{0.5} - 0.0065d_{50}^{-1} \quad 1mm < d_{50} < 100mm \quad (4.4b)$$

$$\frac{V_c}{u_{*c}} = 5.75 \log \left(5.53 \frac{y}{d_{50}} \right) \quad (4.5)$$

where, u_{*c} is the critical shear velocity. The unit of d_{50} in Equations 4.4a and 4.4b is mm while in Equation 4.5 is m.

Using the selected water depth ($y=100$ mm) and median sediment size ($d_{50}=0.78$ mm), the critical mean flow velocity was obtained as 0.327 m/s. Subsequently, the mean flow velocity was considered 0.32 m/s around the threshold condition. Therefore, in this study, the flow intensity was set to 0.98, which was very close to the threshold peak.

- **Time**

The duration of the experiments need to be sufficiently long for equilibrium, or near equilibrium, conditions to be obtained. The proportion of the equilibrium local scour depth achieved at time t is the time factor K_t . Melville & Coleman (2000) presented an equation for K_t , namely:

$$K_t = \exp \left\{ -0.03 \left| \frac{V_c}{V} \ln \left(\frac{t}{t_e} \right) \right|^{1.6} \right\} \quad (4.6)$$

where, t_e is given as:

$$t_e \text{ (days)} = 48.26 \frac{D}{V} \left(\frac{V}{V_c} - 0.4 \right) \quad \text{for} \quad \frac{y}{D} > 6, \quad \frac{V}{V_c} > 0.4 \quad (4.7a)$$

$$t_e \text{ (days)} = 30.89 \frac{D}{V} \left(\frac{V}{V_c} - 0.4 \right) \left(\frac{y}{D} \right)^{0.25} \quad \text{for} \quad \frac{y}{D} \leq 6, \quad \frac{V}{V_c} > 0.4 \quad (4.7b)$$

Here, y/D is less than 6, therefore Equation 4.7b can be applied. For this study, the time was taken to be 24 hours, and the time factor K_t calculated as 0.97, which means 97% of the equilibrium scour depth was achieved after 1 day.

- **Design and Architecting of Flow Diversion Structure**

Referring to Table 4.2 and considering the pier diameter (40 mm) and water depth (100 mm), 25 triangular prism FDS have been designed and built. The FDS dimensions are an assortment of B/D , L/D and H/y variables i.e. Models 1-5 have a B/D ratio of 0.2, meaning that the base of these 5 models is always $0.2 \times 40 = 8\text{mm}$ wide. The lengths of Models 1-5 vary from $0.2 - 1.0 \times 40\text{mm}$ (i.e. 8, 16, 24, 32 and 40 mm) long. Also, the height of Models 1-5 vary from $0.25 - 1.25 \times 100\text{ mm}$ (i.e. 25, 50, 75, 100, 125 mm). Similar explanation can be expanded for other Models. In this study, an advanced technology of 3D printer was employed to build the physical Models of the pier and the flow diversion structures accurately. Figure 4.6 schematically shows the FDSs employed in this study.

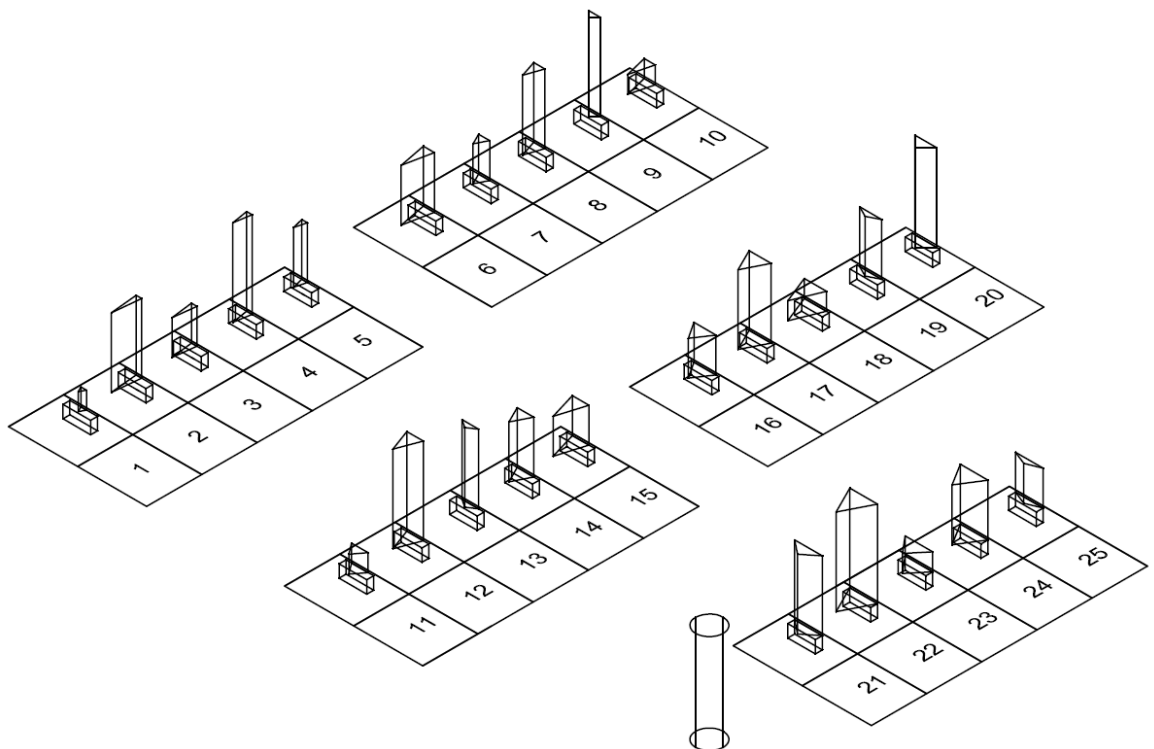


Figure 4.6. Schematic diagram of pier and FDSs used in this experimental study

4.4.3. Procedure of Local Scour Experiments

The first step of each test was to carefully install the pier and one of the flow diversion structures at the centreline of the flume. To achieve the fully developed flow, the distance between the flume inlet and nearest FDS was considered equal to 4.1 m.

To simply and accurately install the physical models of the pier and FDS in the flume, three plexiglass sheets with a thickness of 6 mm, the width equal to the flume width, and 300 mm in length were laid over each other on the flume bed. On each plexiglass sheet, a circular and five rectangular holes were embedded on the installation positions of the pier and FDSs for mounting them. The model of the pier was placed on its location into the circular hole. All models of the FDS had a cubic base, which was fitted into the rectangular hole. In other words, the pier and FDSs models had 18 mm bases which were fitted into their right positions on the plexiglass sheets. Figure 4.7 demonstrates an FDS, and the pier which was installed on its position in the plexiglass sheets.

a)



FDS base

*Five embedded holes
for installing FDS*

b)

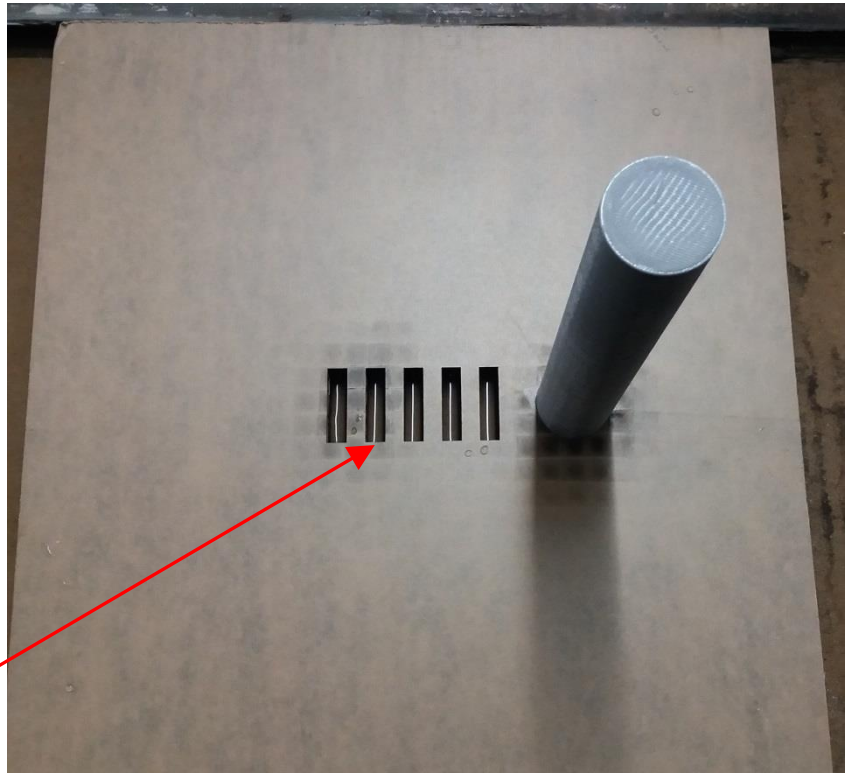


Figure 4.7. a) A photograph of an FDS; b) a photograph of pier on its position in the plexiglass sheets

A sand recess was formed at the working section of the flume, by installing false benches before and after the working section. Three false benches with 1 m length, 450 mm width (equals to the flume width) and 120 mm height were placed from the inlet of the flume to the beginning of working section, and similarly, a false bench was placed after the working section. The length of working section was considered to be 1.8 m. Hence, a sand recess with 1.8 m long and 120 mm deep was formed, which started at 3.0 m from the inlet of the flume. The sand recess was filled by the selected sand. Figure 4.8 demonstrates a typical photograph of the installed pier and FDS at the bed of test section.



Figure 4.8. A typical photograph of the test preparation (Test 10)

After installing the pier and an FDS, the bed materials were placed and levelled in the sand recess as shown in Figure 4.8. Then the flume was filled with water from downstream in a manner that ensured the levelled sand was not disordered. As the water depth increased to the target depth of 0.1 m, the rate of flow was slowly increased to the design rate of 14.4 L/s. The tailgate was utilised to maintain the required water depth.

After 24 hours, the flow was stopped, and the flume was drained. Finally, the measuring of the final bed topography was undertaken. The experimental tests were repeated for all the different configurations listed in Table 4.2.

A 3D scanner was utilised for measuring the final bed topography very quickly and precisely. The Artec Eva 3D scanner (Figure 4.9) with 3D point accuracy up to 0.1 mm was used. In each test, a 3D model of the scour hole was captured using software called Artec Studio, version 12. This software was capable to export the coordinates of all captured points. These exported points were utilised to calculate the volume of the scour hole using Surfer software, version 15. The 3D models of the scour holes are presented in Appendix A.



Figure 4.9. Photographs of Artec Eva 3D scanner

4.5. Results and Discussion

According to Taguchi's method (see Section 4.3.2.), at least 25 tests must be carried out to optimise the dimensions and the installation location of the proposed flow diversion structure as an effective pier-scour countermeasure. In addition, a test under optimum conditions was necessary to confirm the results of optimisation. To compare the experimental results and to assess the effectiveness of the FDS, a control test was performed with only a single pier without the FDS. Therefore, 27 tests were conducted. After achieving equilibrium condition, a 3D model of the bed profile was captured using a 3D scanner. The maximum depth and the volume of the scour-hole were extracted from the 3D model for each experimental test and are presented in Table 4.4.

Table 4.4. The results of local scour tests

Run No	B/D	L/D	H/y	d/D	Max scour depth around the pier (mm)	Scour volume (1000mm ³)
1	0.2	0.2	0.25	0.5	67.45	2457
2	0.2	1	1	1.5	72.62	2643
3	0.2	0.8	0.5	2.5	73.87	3123
4	0.2	0.6	>1.00	1	61.44	2221
5	0.2	0.4	0.75	2	70.83	2856
6	0.4	1	0.75	1	57.9	2142
7	0.4	0.4	0.5	1.5	55.16	2022
8	0.4	0.6	1	0.5	65.41	2647
9	0.4	0.2	>1.00	2.5	68.11	2756
10	0.4	0.8	0.25	2	60.78	2111
11	0.6	0.4	0.25	1	58.53	1913
12	0.6	0.8	>1.00	1.5	65.89	2574
13	0.6	0.2	1	2	66.89	2812
14	0.6	0.6	0.75	2.5	65.01	2720
15	0.6	1	0.5	0.5	65.83	2754
16	0.8	0.6	0.5	2	53.8	2051
17	0.8	0.8	1	1	65.83	2909
18	0.8	1	0.25	2.5	55.02	2080
19	0.8	0.2	0.75	1.5	66.53	3293
20	0.8	0.4	>1.00	0.5	72.91	3718
21	1	0.4	1	2.5	70.41	3591
22	1	1	>1.00	2	70.46	3760
23	1	0.6	0.25	1.5	51.9	2023
24	1	0.8	0.75	0.5	75.93	4099
25	1	0.2	0.5	1	68.05	3646
26	Control test (single pier without a flow diversion structure)				81.9	4242
27	Optimum test (based on the acquired optimal conditions)				49.16	1697

4.5.1. Sensitivity Analysis of the Dimensionless Parameters

The output responses from the experimental tests recorded in Table 4.4 are the maximum scour depth around the pier and the volume of scour-hole. The average value of the output responses related to each variable at each level was calculated by averaging the values for the variable at that level. For example, the average of the maximum scour depth related to $B/D=0.2$ was calculated by averaging the maximum scour depth in test 1 to 5 in Table 4.4. The results for the variable level average of the maximum pier scour depth are illustrated in Table 4.5. Furthermore, the main-effect plots are depicted in Figure 4.10.

Table 4.5. Variable level averages for the maximum pier scour depth (mm)

Variable Level	B/D	L/D	H/y	d/D
1	69.24*	67.41*	58.73	69.51
2	61.47	65.57	63.34	62.35
3	64.43	59.51	67.24	62.42
4	62.81	68.46	68.23	64.55
5	67.35	64.36	67.76	66.48
Max.	69.24	68.46	68.23	69.51
Min.	61.47	59.51	58.73	62.35
Delta (max-min)	7.77	8.95	9.50	7.16
Rank**	3	2	1	4

*All numbers are the average of the maximum scour depth related to the variables and their levels. For example, 69.24 is the average of the maximum scour depth of Run 1 to 5 which all $B/D=0.2$ and its level is 1, or 67.41 is the average of maximum scour depth for L/D ratios of 0.2 (Tests 1, 9, 13, 19, 25).

** Rank is related to the Delta values (the greatest delta has the first rank)

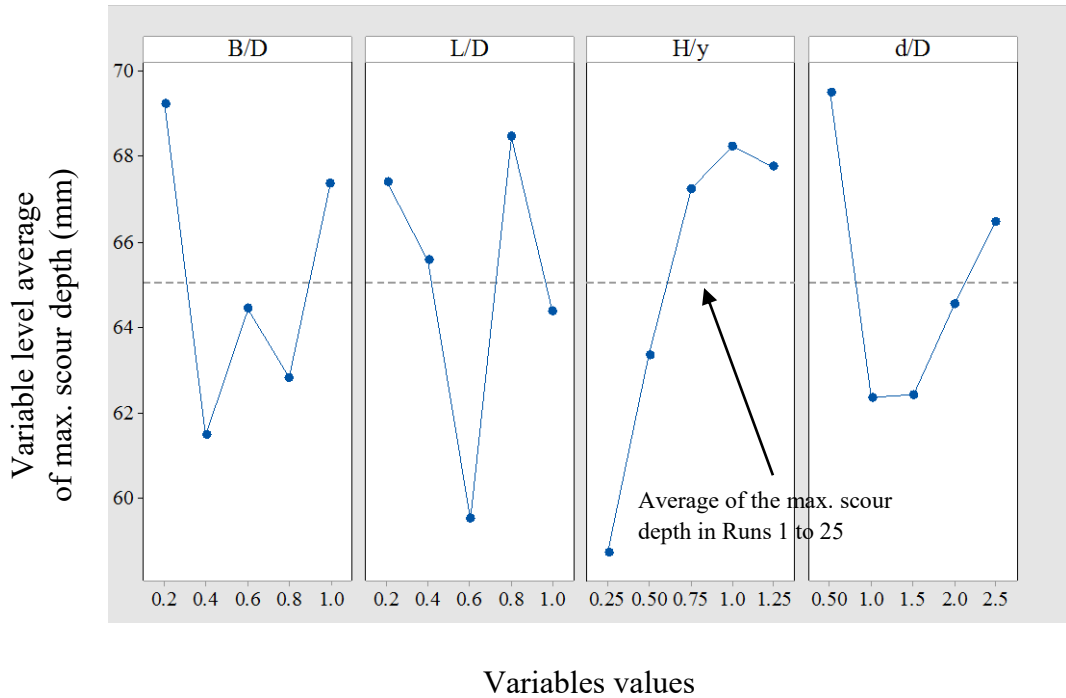


Figure 4.10. Main-effect plots of the maximum pier scour depth

Considering Table 4.5 and Figure 4.10, the height of the FDS has the greatest influence on the effectiveness of the FDS for reducing the maximum pier-scour depth. Moreover, it can be inferred that the sequence of the impact of all other parameters on the maximum pier-scour depth reduction can be expressed as $L/D > B/D > d/D$, as shown in Table 4.5. The best values of each variable should be chosen where the least scour depth has occurred. According to Figure 4.10, the best level for the width and the length of FDS are equal to 40% and 60% of the pier diameter, respectively.

The trend of clear distance between the pier and the FDS shows that, when this variable is between 1 to 1.5 times of pier diameters, the maximum reduction of the scour depth was achieved. Although in this study the effect of the flow velocity on optimum clear distance was not investigated, the results are consistent with previously published results (see Table 4.6). As summarised in Table 4.6, the minimum local scour at a pier with upstream FDS or at a rear pier for the case of two-inline piers, was reported when d/D was between $1D$ and $2D$. Similar results presented in Table 4.6 were achieved under different flow conditions. From consideration of these results, it can be suggested that the flow velocity does not significantly affect the best installation location of FDS

for the conditions considered. Accordingly, it can be concluded that the best installation location for the FDS is upstream of the pier with a clear distance of 1-1.5D.

Table 4.6. Comparison of the best d/D for different cases and hydraulic conditions

Data set	Case	Q (L/s)	Flume width (m)	Water depth (m)	V (m/s)	Fr	Re	Clear distance to have min scour at rear pier
Hannah (1978)	Two in-line unsubmerged circular piers	24.4	0.612	0.140	0.285	0.243	39900	1-2D
Melville & Hadfield (1999)	Group of submerged and unsubmerged sacrificial piles at the upstream	190	1.52	0.6	0.30	0.12	180000	0.5D for nearest piles and 2.5D for farthest pile
		260			0.39			
Ataie-Ashtiani & Beheshti (2006)	Two unsubmerged in-line circular piers	Not reported	0.41	Not reported	0.26 0.24 0.18	Not reported	Not reported	1-2D
Hooshmand (2010)	Unsubmerged approach flow guide at the upstream of circular and square pier	19.6	0.7	0.08	0.35	0.395	28000	1.5D
Keshavarzi et al. (2018)	Two unsubmerged in-line circular piers	18.5	0.61	0.115	0.264	0.249	30360	2D
		33.0	0.61	0.160	0.338	0.270	54080	1-2D
		31.5	0.61	0.150	0.344	0.284	51600	1-2D
Ranjbar-Zahedani et al. (2018)	Unsubmerged single FDS at the upstream	21.0	0.70	0.1	0.30	0.30	30000	1.5D
This study	Different size of FDS at the upstream	14.4	0.45	0.1	0.32	0.323	32000	1-1.5D

As illustrated in Figure 4.10, the optimum value for the height of FDS is equal to 25% of the water depth. Increasing this variable may reduce the effectiveness of this structure. However, there is still a question regarding the efficiency of FDS when its

height is lower than 25% of water depth. In order to answer this question, one more test was conducted with $H=0.15y$ under optimum values of other variables (i.e., $B=0.4D$, $L=0.6D$, $d=1.5D$). The result of this test was added to the previous findings of the maximum scour depth regarding the level average of the height of FDS and illustrated in Figure 4.11. As can be seen in Figure 4.11, any further reduction in the FDS height from 25% of the water depth reduces the performance of the FDS. Therefore, the best level for the height of FDS is around 25% of the water depth. Melville and Hadfield (1999) concluded that submerged and full-depth sacrificial piles give similar reductions in scour depth. However, the results of our comprehensive tests reveal that the degree of submergence highly affects the performance of FDS.

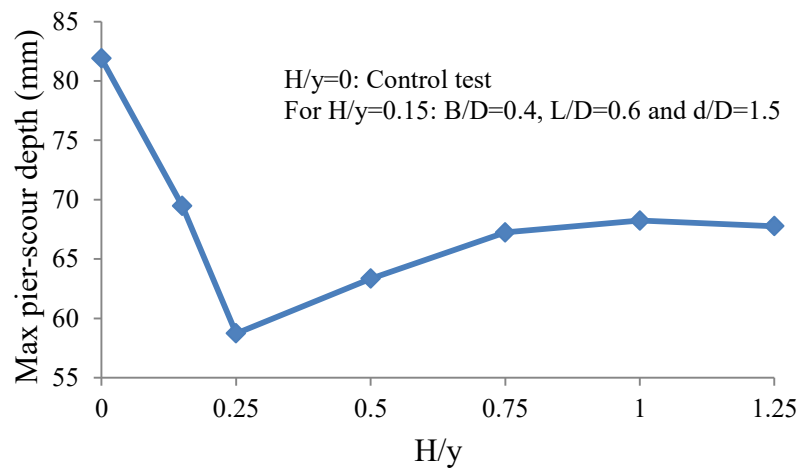


Figure 4.11. Effects of the height of FDS on the maximum pier scour depth

4.5.2. Analysis of Variance (ANOVA) for Maximum Scour Depth

The selected set of experiments based on Taguchi's method is a part of the full factorial combinations of experiments. Therefore, the analysis of the partial experiment must include an analysis of confidence to qualify the results (Roy 2010). Analysis of variance (ANOVA) is a standard statistical technique routinely used to provide a measure of confidence. In this technique, various quantities such as degrees of freedom (f), sums of squares (SS), mean square (MS), and the variance ratio (F) are computed and organized

in a standard tabular format. The degree of freedom of each variable is equal to the number of variable's levels minus one. The total degree of freedom is equal to the number of tests minus one, and the error degree of freedom is defined as the difference between the total degree of freedom and the sum of degrees of freedom for each variable.

The total sum of square (SS_T) is calculated by Equation 4.8.

$$SS_T = \sum_{i=1}^n Y_i^2 - \frac{G^2}{n} \quad (4.8)$$

where, n is the total number of tests, Y_i is the response factor of test i , and G is the sum of all output responses. Equation 4.9 can be employed to determine the sum of square for each variable (SS_A).

$$SS_A = \sum_{j=1}^m \left(\frac{SY_j^2}{m} \right) - \frac{G^2}{n} \quad (4.9)$$

where, A represents one of the tested variables, j and m are the level number and the total number of levels of this variable respectively, SY_j is the sum of all output responses involving the variable A at level j . The residual error is estimated as the difference between the total sum of square and the sum of squares for each variable.

The mean square is defined as the ratio of the sum of square to the degree of freedom. Finally, the variance ratio, commonly called the F statistic, is the ratio of the mean square to the mean square of the error. This ratio is used to measure the significance of the variable. The F value obtained in the analysis should be compared with the critical F

value from standard F-tables (as shown in Appendix C) for a given statistical level of significance. The F value of each variable which is greater than the critical F value shows this variable has a significant effect on the output response.

In this study, the analysis of variance for the maximum scour depth was undertaken, and the results are depicted in Table 4.7. The critical F values for 95% and 90% confidence intervals are 3.84 and 2.81 respectively (see Appendix C). Accordingly, it can be claimed that the size of FDS including width, length and height have significant effects on reduction of the local scour around a pier; the F values of these variables exceed the 95% confidence interval. In addition, it can be noted that the installation location of FDS has a significant effect on the local scour reduction only at the 90% confidence interval.

Table 4.7. Analyses of variance for the maximum scour depth

Source	f	SS	MS	F
B/D	4	205.20	51.31	3.87
L/D	4	242.90	60.74	4.58
H/y	4	325.50	81.39	6.14
d/D	4	181.80	45.44	3.43
Residual Error	8	106.10	13.26	
Total	24	1061.60		

4.5.3. Analysis of Scour-Hole Volume

Similar analyses, described in Sections 4.5.1 and 4.5.2, were performed for the volume of the scour-hole. The results for the variable level average of the scour-hole volume are illustrated in Table 4.8, while the main-effect plots depicted in Figure 4.12.

Table 4.8. Variable level averages for the scour-hole volume (1000 mm³)

Variable Level	B/D	L/D	H/y	d/D
1	2660*	2993	2117	3135
2	2336	2820	2719	2566
3	2555	2333	3022	2511
4	2810	2963	2920	2718
5	3424	2676	3006	2854
Max.	3424	2993	3022	3135
Min.	2336	2333	2117	2511
Delta (Max-Min)	1088	660	905	624
Rank**	1	3	2	4

*All numbers are the average of scour-hole volume related to the variables and their levels. For example 2660 is the average of the scour-hole volume of Run 1 to 5 which all B/D=0.2 and its level is 1.

** Rank is related to the Delta values (the greatest delta has the first rank)

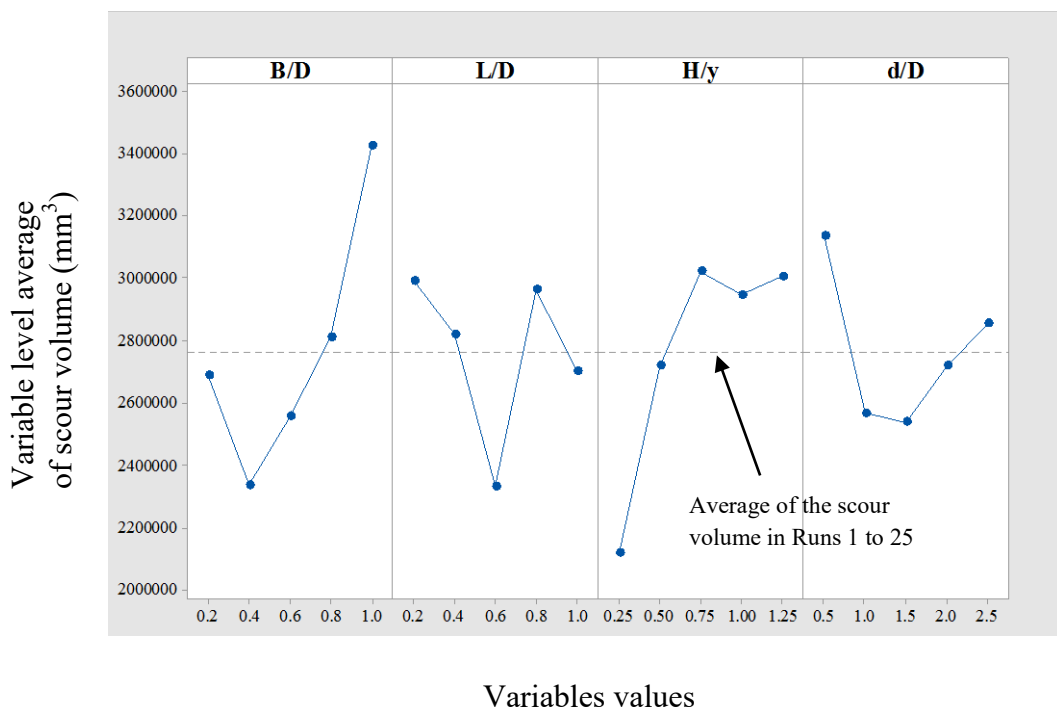


Figure 4.12. Main-effect plots of the scour-hole volume

As indicated in Table 4.8, the width of the FDS is placed in the first rank for reducing the scour-hole volume. Other variables including the height and length of the FDS and the clear distance between the pier and FDS are in the next ranks, respectively. Although the comparison of the results presented in Tables 4.8 and 4.5 show different ranks of each variable, Figures 4.10 and 4.12 portray the same optimum value for each variable. Hence, the best dimensions of FDS to achieve the maximum reduction of the score-hole volume are equal to $B=0.4D$, $L=0.6D$, and $H=0.25y$. This structure should be installed upstream of the pier with a clear distance between the pier and the FDS of 1 to 1.5D.

Results of the ANOVA analysis for the scour-hole volume are presented in Table 4.9. As expected, the dimensions of FDS (B, L, and H) and its installation location significantly affect the scour-hole volume around a pier at 95% and 90% confidence intervals, respectively.

Table 4.9. Analyses of variance for the scour-hole volume

Source	f	SS	MS	F
B/D	4	3377110	844276	9.27
L/D	4	1444250	361062	3.97
H/y	4	2851050	712763	7.83
d/D	4	1253500	313374	3.44
Residual Error	8	728454	91057	
Total	24	9654350		

4.5.4. Confirmation Test

Based on Taguchi's design approach a confirmation test should be run under optimum conditions to verify the experimental results. In this study, a confirmation test was conducted by utilizing the best levels of the variables (i.e., $B=0.4D$, $L=0.6D$, $H=0.25y$, and $d=1.5D$). Figures 4.13(a) and 4.13(b) illustrate the photographs of the scour-hole in the control and optimum tests while Figures 4.14(a) and 4.14(b) show the 3D models of scour-hole in the control and optimum tests, respectively.

In this study, when the optimised FDS was implemented, the maximum pier-scour depth and the volume of scour-hole were measured to be equal to 49.16 mm and $1.697 \times 10^6 \text{ mm}^3$, respectively. These values are the minimum of the local scour depth and the minimum volume of the scour-hole among all the conducted tests. After a comparison of the control test with the optimum test, it was found that the optimised FDS can reduce the maximum depth and the volume of the scour-hole by 40% and 60%, respectively.

a)



b)

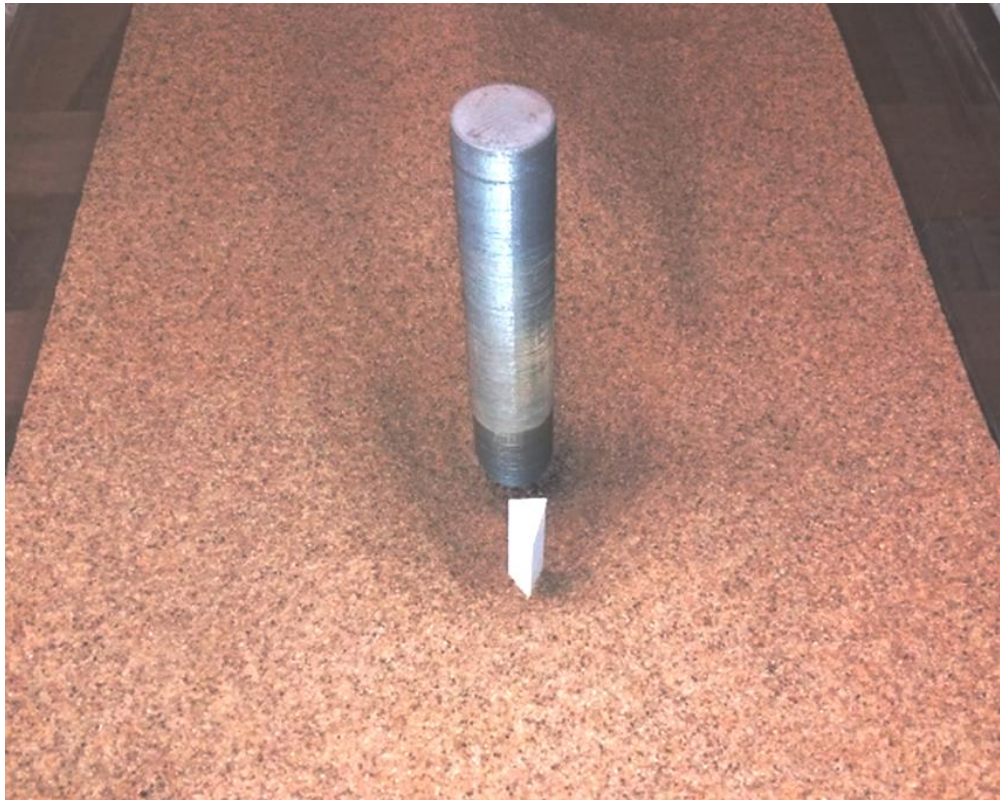
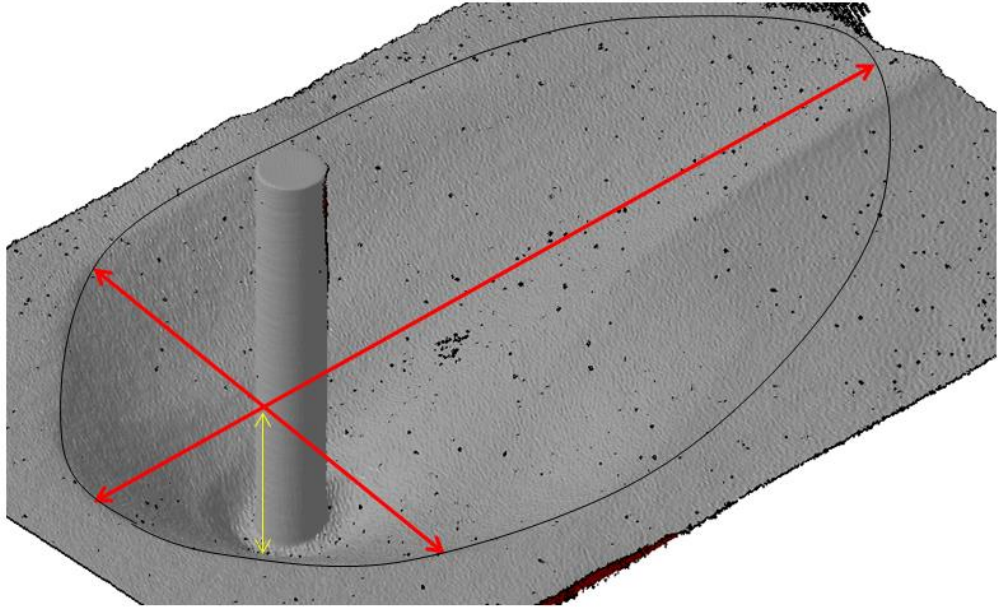


Figure 4.13. Photographs of scour-hole; a) control test; b) optimum test

a)



b)

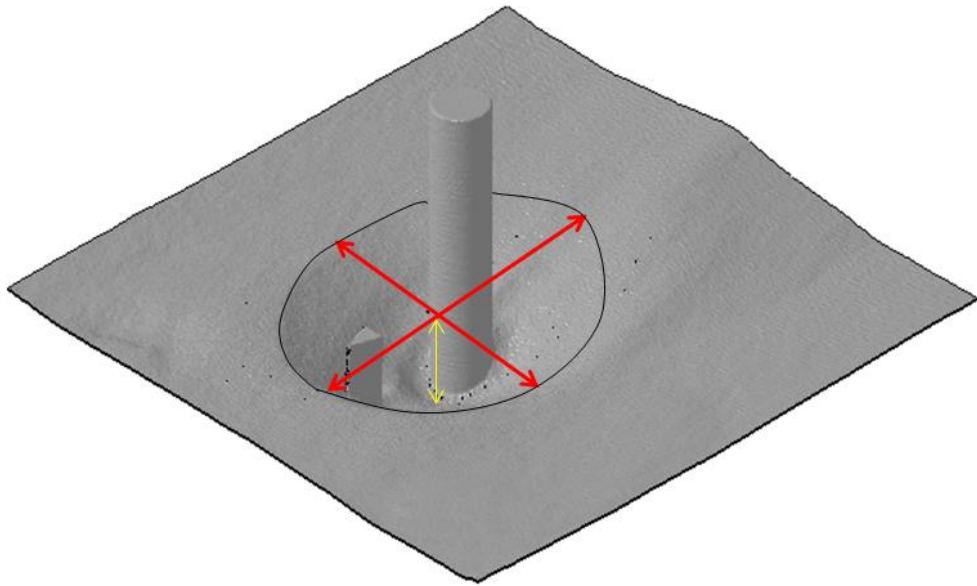


Figure 4.14. 3D models of scour-hole; a) control test; b) optimum test

4.6. Conceptual Field Application of FDS

As presented in the previous section, the confirmation test shows that the optimisation procedure was correct. Accordingly, it can be stated that these dimensionless parameters of $B/D = 0.4$, $L/D = 0.6$, $H/y = 0.25$, and $d/D = 1.5$ have the potential to be used to extrapolate the results to prototype scale with considering the similarity. According to Link et al. (2019), the similarity in the scour can be achieved when both model and prototype have the same sediment transport conditions; and thus V/V_c should be in similar ranges. It means that the results of this study have the potential to be used for real cases when V/V_c is in a similar range to this study ($V/V_c < 1$, clear-water scour).

In this section the architecting design method of the FDS is applied to a real case. The salient information of this real bridge was reported by Melville & Coleman (2000), as follows:

- Local scour at circular pier
- Pier diameters: 2 m
- Design flow rate: 1250 m³/s
- River width: 200 m
- Flow depth (y): 3m
- Flow velocity (V): 2.08 m/s
- Median size of bed sediment (d_{50}): 20 mm
- Critical mean flow velocity for sediment entrainment (V_c): 2.5 m/s
- Flow Intensity (I): $0.83 < 1$ (clear-water scour)

As the flow intensity is less than one, the clear water scour occurs around the circular piers of this bridge. Therefore an FDS can be designed for this bridge. The following is the architecture design of the FDS:

Width of the FDS: $B = 0.4D$  $B = 0.4 \times 2 = 0.8 \text{ m}$

Length of the FDS: $L = 0.6D$  $L = 0.6 \times 2 = 1.2 \text{ m}$

Height of the FDS: $H = 0.25y$  $H = 0.25 \times 3 = 0.75 \text{ m}$

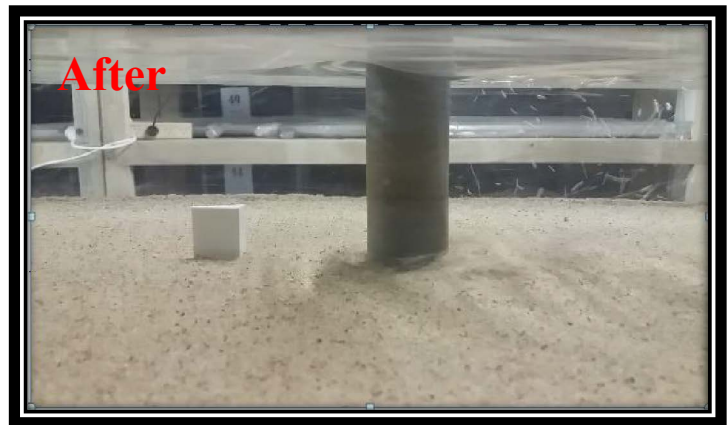
Distance from the pier: $d = 1.5D$  $d = 1.5 \times 2 = 3 \text{ m}$

4.7. Conclusions

In this chapter, the efficient countermeasure against pier-scour named triangular flow diversion structure (FDS), introduced in Chapter 3, has been optimised. Taguchi's method, which is a statistical approach for the design of experiments, was applied to find the optimal size and the best place for installing FDS to achieve the maximum reduction of the pier-scour. According to Taguchi's method, 27 FDSs were tested to find and to confirm the optimal size and installation location of the FDS. The outcomes demonstrated that the best width, length, and height of FDS are equals to $0.4D$, $0.6D$, and $0.25y$, respectively. Furthermore, the best clear distance between FDS and the pier is approximately between 1 and 1.5 times of the pier diameter. In the optimal situation, the maximum depth and the volume of the scour hole around the pier reduced by 40% and 60%, respectively.

CHAPTER 5

Flow Field around a Circular Pier with Optimised Flow Diversion Structure at Upstream



5.1. Introduction

The comprehensive experimental study of local scour around a circular bridge pier with the upstream flow diversion structures (FDS) has been described in Chapter 4. The primary objectives of those experimental tests were to find the optimum size and the best installation location of FDS to achieve the maximum reduction of local pier-scour. Consideration of experimental results reveals that the best width, length and height of FDS were equal to $0.4D$, $0.6D$, and $0.25y$, respectively. It can be noted that D represents the pier diameter and y denotes the height of water. Furthermore, the best clear distance between FDS and the pier was approximately between 1 and 1.5 times of the pier diameter. In the optimum situation, the scour depth and the volume of the scour hole around a circular pier reduced by 40% and 60%, respectively.

As noted earlier in Chapter 2, it is the interaction of three-dimensional flow field with the bridge piers that results in bed erosion around the piers. The focus of this Chapter is to investigate how the optimised FDS alters the flow field around the pier and accordingly reduces the local scour. This experimental study of flow field was conducted using Particle Image Velocimetry (PIV).

5.2. Review of Flow Structures near Bridge Piers

As reported in Chapter 2, many researches have been performed in the area of local scour mechanism. A brief overview to highlight the key results of the local scour mechanism around a single pier is presented in this section.

Pier scour is caused by the interference of the pier with the flow and characterised by the formation of the scour hole immediately around the pier. To understand the mechanism of pier scour, several studies have been conducted such as those by Laursen & Toch (1956), Melville (1975), Melville & Raudkivi (1977), Ahmed & Rajaratnam (1997), Melville & Coleman (2000), Kirkil et al. (2008), Ettema et al. (2011), Keshavarzi et al. (2014), and Ettema et al. (2017). In these studies, it has been declared that a vortices system shaped around piers is the underlying mechanism of local scour. According to Melville & Coleman (2000), there are four major types of the flow field around a single bridge pier including down-flow, horseshoe vortices, surface rollers,

and wake vortices. As shown in Figure 5.1, down-flow and surface rollers occur upstream of a pier, while horseshoe and wake vortices are formed at the base and the downstream of the pier, respectively. The down-flow impinges on the bed materials. The horseshoe vortex increases the velocity near the bed, leads to a rise in the transport capability of the sediment particles. The wake vortex suspends the particles. It also actions like a vacuum cleaner while moving the sediment particles downstream. Therefore, a practical solution to control and reduce the pier-scour can be changing the complex flow field around the pier.

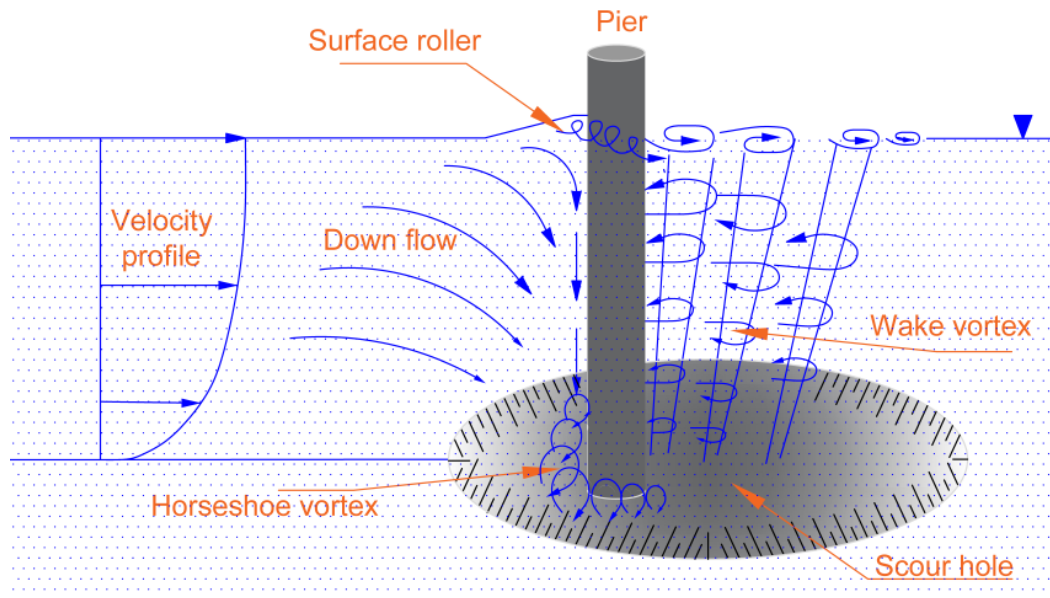


Figure 5.1. Flow field around a bridge pier

5.3. Experimental Setup and Procedure

5.3.1. Flume and Its Components

This part of the required experimental tests was conducted in a flume differed from those mentioned in Chapters 3 and 4; as the PIV was employed, OHS required the use of an alternative flume setup specifically for PIV measurement. The available flume was a rectangular glass-sided tilting flume with the stainless steel bed. The glass sidewalls allowed clear viewing of the flow patterns associated with the model or

accessory in use. The flume's length was 5 m, its width was 0.3 m, and its depth was 0.45 m. This flume included electrically operated jacking system for varying the slope of the channel bed. Inlet and outlet tanks were installed at the upstream and downstream of the flume, respectively. Discharge was supplied from a main reservoir with a centrifugal water pump. This pump was also equipped with a variable speed drive to control the electromotor speed and consequently adjust the flow rate. An electrical console controlled the electrical instruments such as electromotor and variable speed drive. Moreover, the flow rate was showed on a digital monitor, provided on the electrical console. This flume was also equipped with a downstream flap gate to regulate the water depth. Figure 5.2 shows a photograph of the flume and its components.



Figure 5.2. A photograph of the flume and its components

5.3.2. Physical Models of Bridge Pier and Flow Diversion Structures

As this part of the experimental tests was carried out in a different flume, new physical models were designed and built according to the size of this flume and the previous results of the pier-scour tests. All experiments were conducted in a fixed-bed flume with

no sediment layer. However, the criteria of local scour around the bridge piers were considered to select the geometric and hydraulic parameters of the experimental setup.

The pier diameter was carefully chosen according to Melville & Coleman (2000) criterion (explained in the previous chapter) to avoid contraction effect. In these tests, a pier with a diameter of 25 mm was adopted. The ratio of W/D was 12, satisfying the boundary condition criterion, recommended by Melville & Coleman (2000).

Referring to the results of the previous chapter, the optimum size and the best installation location of the flow diversion structures were achieved as a function of the pier diameter and water depth (i.e., $B/D=0.4$, $L/D=0.6$, $H/y=0.25$, and $d/D=1-1.5D$). Therefore, the width (B) and length (L) of FDS were considered equals to 10 and 15 mm, respectively. In addition, the gap between the pier and FDS was selected equal to the upper limit ($1.5D = 37.5$ mm) to have more space and consequently better visualisation of flow field in the gap region.

The optimum height of FDS is equal to one-fourth of the water depth and increasing the height of FDS decreases its performance. Due to the variations of the water depth in the real situation, the height of FDS should be designed regarding the highest water level. To understand the effects of submergence ratio on the performance of FDS, four levels of H/y were tested (i.e., $H/y=0.25$, 0.5 , 0.75 and > 1). The first three levels were a fully submerged structure, and the last one was an unsubmerged structure. In all tests, the water depth was kept constant, and four different heights of FDS were built and tested. The advanced 3D printing technology was employed to build the physical models of the pier and the FDSs accurately.

For the convenience of installing physical models on the flume, three plexiglass sheets with a thickness of 6 mm and the width and length equal to the flume width and length were laid over each other on the bed. On each plexiglass sheet, two circular and rectangular holes were embedded on the installation positions of the pier and FDS for mounting them. The model of the pier was placed on its location into the circular hole. All models of the FDS had a cubic base, which was fitted into the rectangular slot. In other words, the pier and FDS models had 18 mm bases, which were fitted into their right positions on the plexiglass sheets accurately. To minimise reflection effects during experiments, the model FDSs were painted matt black. The pier was treated in a similar

manner. Showing Figure 5.3 are the FDS models and their installation in the flume prior to painting.

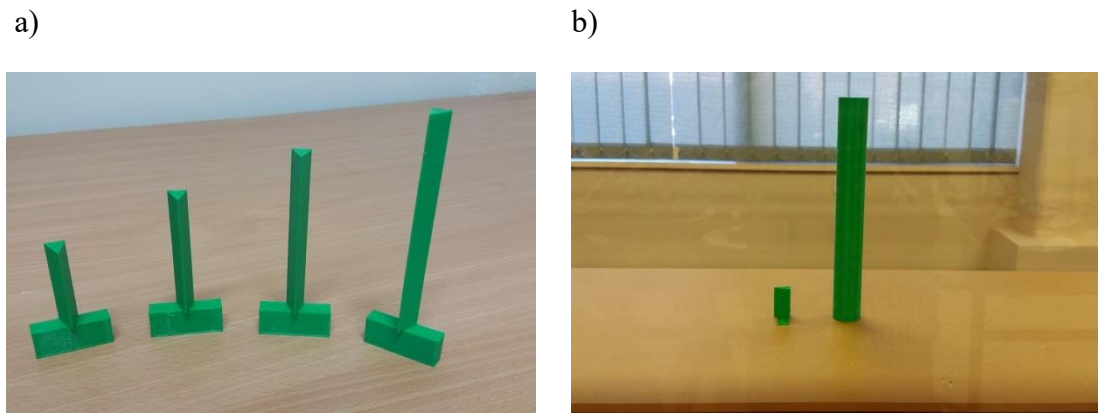


Figure 5.3. a) FDS models; b) installation of the models into the plexiglass sheets on the flume bed

5.3.3. Hydraulic Conditions

To avoid the water depth effects on the local scour depth, Melville & Coleman (2000) pointed out that the pier diameter to the water depth ratio (D/y) should be less than 0.7. Therefore, the water depth used in the experiments was set to 100 mm to satisfy this requirement. The maximum flow velocity, which could be measured by the available PIV system, was 0.1 m/s. Hence, the cross-sectional average velocity (V) was selected to be 0.1 m/s, and consequently, the flow rate supplied to the flume in all tests was 3 l/s. Table 5.1 summarises the hydraulic conditions of the experimental tests on flow field.

Table 5.1. Flow conditions for experimental tests on flow field

Flow rate (Q) (l/s)	Water depth (y) (mm)	Flow velocity (V) (m/s)	Froude number (Fr)
3	100	0.1	0.1

5.3.4. Particle Image Velocimetry (PIV)

To study the flow field around a bridge pier with an upstream FDS, Particle Image Velocimetry (PIV) technique was employed. For these tests PIV apparatus and VidPIV software version 4.6, manufactured and developed by ILA GbmH company was employed.

PIV system calculates the flow velocity based on the displacement of the tracer particles within the flow at a particular time. In this technique, the flow is seeded with small tracer particles, and a light sheet illuminates a cross-section of the flow. The displacement of the tracer particles in the illuminated cross-section is recorded in a pair of images by using a high-speed camera. Then, the flow velocity can be obtained by considering the displacement of the particles in a couple of images and the time interval between them. It is important to note that the characteristics of the tracer particles must be consistent with the properties of the fluid. Appropriate particles have a spherical shape, and their density is similar to the fluid density. In the experimental tests, polyamide 2070 was utilized as the seeding particles, which is spherical with 5 μm diameter, and 1.016 g/cm^3 density. Figure 5.4 schematically demonstrates the PIV system and its components.

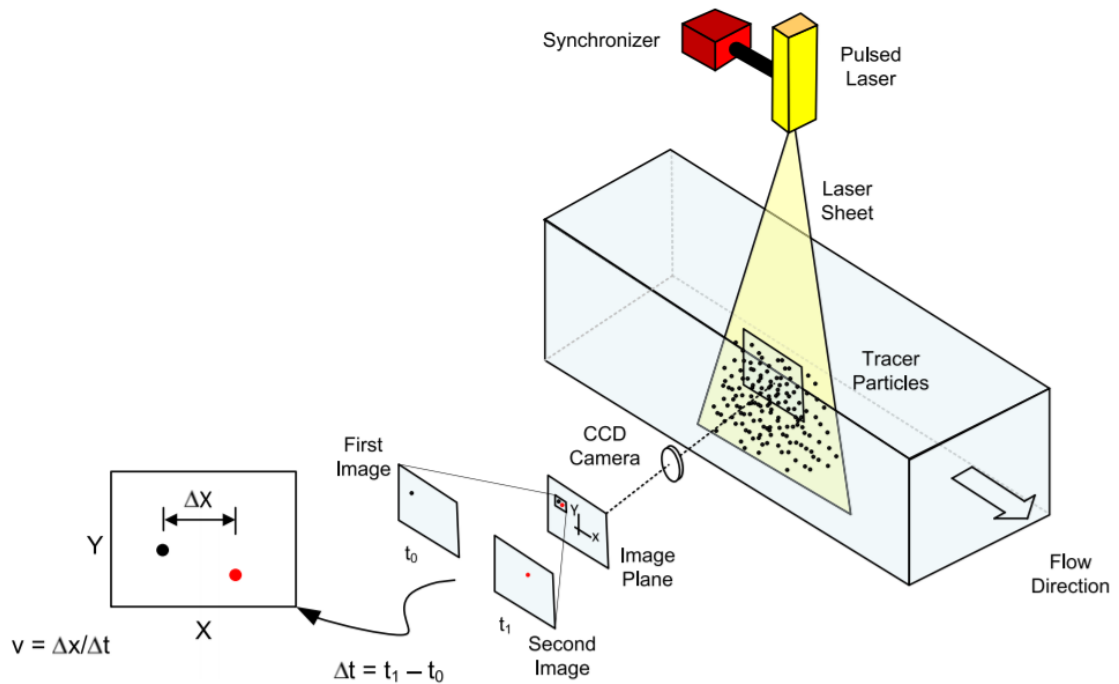


Figure 5.4. Schematic diagram of the PIV technique (Goharzade & Molki, 2014)

5.3.5. Procedure of Flow Field Experiments

Experimental tests were started with a single circular pier as a control test, then continued with the pier plus FDS at the upstream. A set of 25 numbers of experimental tests were conducted to find out how the FDS with different submergence ratio affects the flow field around the bridge pier (see Table 5.2).

In each test, the models of the pier and FDS were fixed at their locations in the flume. The FDS was located at a distance of 2.7 m from the inlet section of the flume to achieve a fully developed flow. The flow rate was adjusted to 3 l/s, and the water depth adjusted to 100 mm. Table 5.1 shows the details of hydraulic conditions. Furthermore, the PIV apparatus was set up for measuring the velocity components. The light arm was placed above of the flume to illuminate the objective measurement plane. The camera was fixed at the side of the flume perpendicular to the light sheet. After finishing the setup, polyamide seeding materials was added to the current. A high-resolution digital camera acquired the light scattered by seeded particles. The movements of the seeding particles among two successive pictures were used to measure the velocity. For each set of test, 20 pair images were captured. As presented in Figure 5.5, the measurements were repeated on different planes (these planes were at $Y/D = 0, 1, 2, 3$ and 4). A software package (VidPIV, version 4.6) was employed for images processing. This software extracts displacement information and calculates velocity components from the PIV recordings. The details of the test configurations are summarised in Table 5.2, while Figure 5.6 displays the experimental setup.

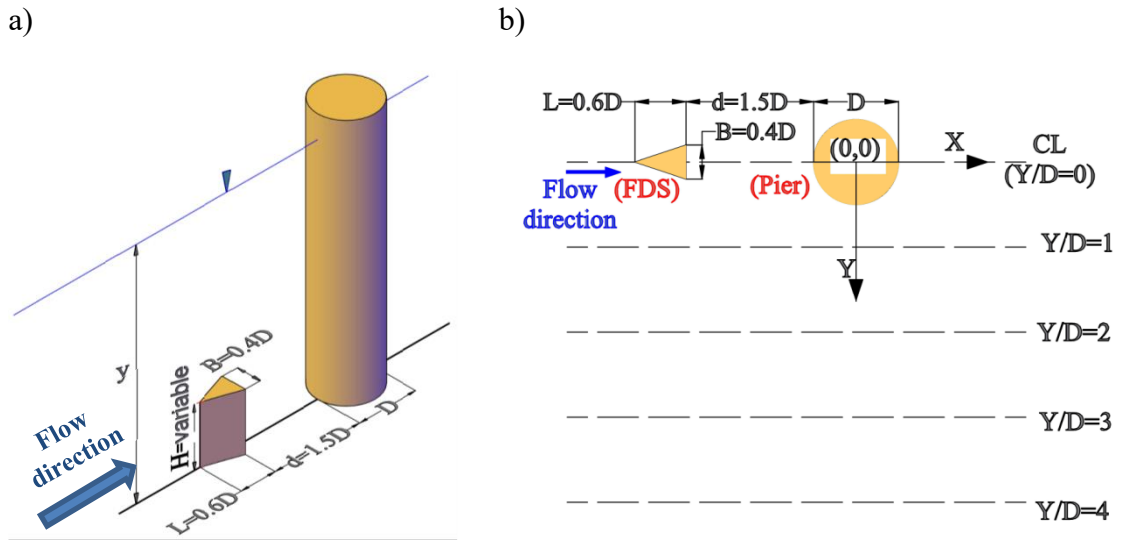


Figure 5.5. Experimental setup; a) a schematic diagram of the pier and FDS; b) different planes of PIV measurements (plan view)

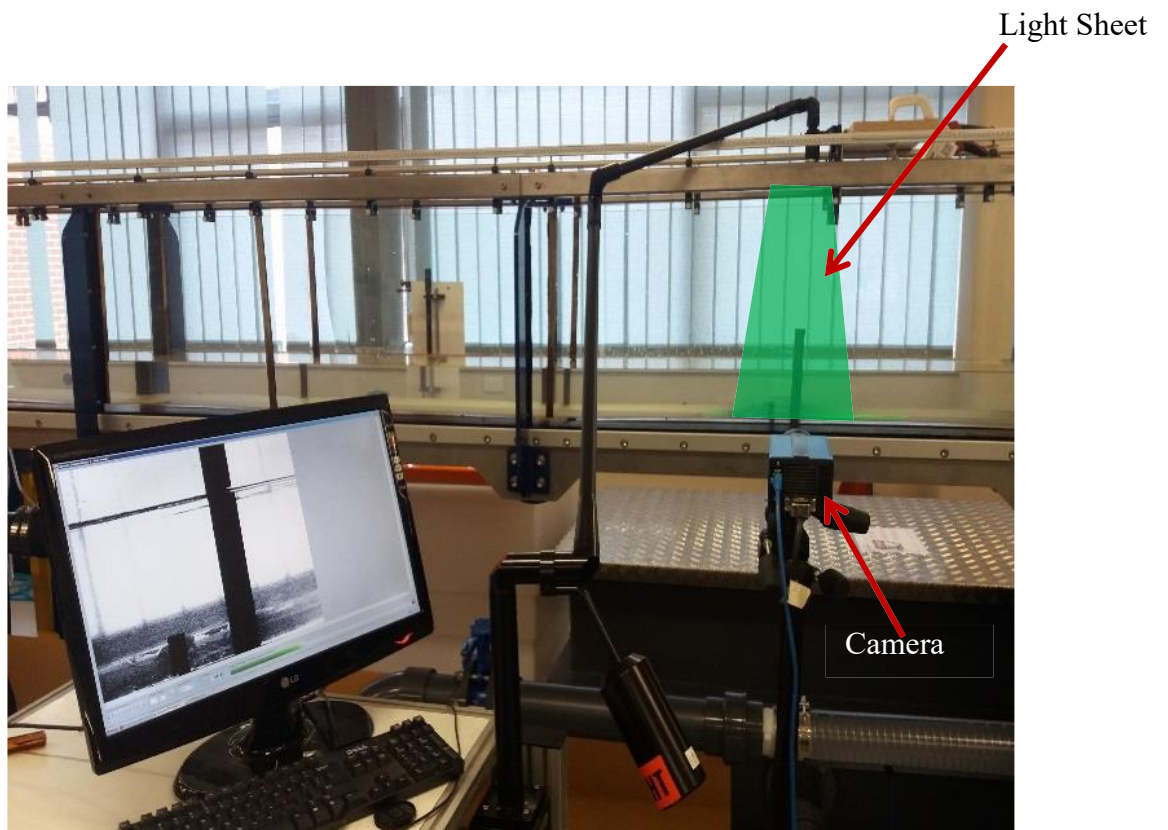


Figure 5.6. A photograph of experimental set up and PIV system in the laboratory

Table 5.2. The details of the flow field tests configurations

Run no.	D (mm)	y (mm)	V (m/s)	Y/D	B/D	L/D	H/y	d/D
1	25	100	0.1	0			single pier	
2	25	100	0.1	0	0.4	0.6	0.25	1.5
3	25	100	0.1	0	0.4	0.6	0.50	1.5
4	25	100	0.1	0	0.4	0.6	0.75	1.5
5	25	100	0.1	0	0.4	0.6	>1	1.5
6	25	100	0.1	1			single pier	
7	25	100	0.1	1	0.4	0.6	0.25	1.5
8	25	100	0.1	1	0.4	0.6	0.50	1.5
9	25	100	0.1	1	0.4	0.6	0.75	1.5
10	25	100	0.1	1	0.4	0.6	>1	1.5
11	25	100	0.1	2			single pier	
12	25	100	0.1	2	0.4	0.6	0.25	1.5
13	25	100	0.1	2	0.4	0.6	0.50	1.5
14	25	100	0.1	2	0.4	0.6	0.75	1.5
15	25	100	0.1	2	0.4	0.6	>1	1.5
16	25	100	0.1	3			single pier	
17	25	100	0.1	3	0.4	0.6	0.25	1.5
18	25	100	0.1	3	0.4	0.6	0.50	1.5
19	25	100	0.1	3	0.4	0.6	0.75	1.5
20	25	100	0.1	3	0.4	0.6	>1	1.5
21	25	100	0.1	4			single pier	
22	25	100	0.1	4	0.4	0.6	0.25	1.5
23	25	100	0.1	4	0.4	0.6	0.50	1.5
24	25	100	0.1	4	0.4	0.6	0.75	1.5
25	25	100	0.1	4	0.4	0.6	>1	1.5

5.3.6. Image Processing

The captured images by the camera were stored on the computer. The stored images and their corresponding time interval were processed using the VidPIV software package to extract the instantaneous velocity components. The software has different functions for processing the images and computing the velocity. Initially, the pixel unit should be converted to the real units by using the image mapping function. After that, annotations function is used to add other information such as flow boundary and obstacles. Then, the cross-correlation function can be used to determine the displacement of the particles between each pair of images. To increase the accuracy of the data, other particular functions, including adaptive cross-correlation, and filtering & interpolation can be applied and repeated. The velocity vectors can be achieved from the vector maps. This data can be extracted in a text format, which includes the position of the points and the corresponding velocity components.

Regarding the 20 image pairs, which were captured for each run, 20 text files of 2-D velocity components were achieved in each run. Each file consisted of velocity components for around 8000 points. For further analysis, a MATLAB program was developed.

5.3.7. MATLAB Programming for PIV Data Analysis

The instantaneous velocity components collected by the PIV system was used to calculate the turbulence characteristics of the flow. Due to the extensive amount of data, a program using MATLAB software was developed to estimate the flow turbulence characteristics. The outputs of VidPIV software were many text files including points' coordinates and corresponding streamwise instantaneous velocity components (u), vertical instantaneous velocity components (w), and absolute velocity ($V_a = (u^2 + w^2)^{0.5}$). In each test, the multiple text files gave similar data in different time steps.

The provided program calculates turbulent characteristics of flow in each point. In this program the root mean square values of velocity fluctuations were calculated as the turbulence intensity components TI_u , and TI_w and normalised by using cross-sectional average velocity (V), as follows:

$$TI_u = \frac{\sqrt{u'^2}}{V}; TI_w = \frac{\sqrt{w'^2}}{V}$$

Besides, this program calculates the TKE and RSS which were explained in chapter 2. This program enables to open, analyse, and close all test files that are located in a specific folder automatically. Finally, the results can be saved in text files. The developed code is presented in Appendix D.

The output of the developed program in MATLAB was given as an input to the Tecplot software so that the results were plotted graphically and eventually interpreted and compared. The achieved results are presented in the following sections.

5.4. Results and Discussion

Velocity components at a vicinity of a pier with the optimised flow diversion structure (FDS) under different submergence ratio were measured using the PIV technique. The collected data sets were analysed to find out how the optimised FDS affects the flow field and consequently reduces the local scour around a circular bridge pier.

PIV measurements were performed on four planes. As presented in Figure 5.5.b, these planes were located at non dimensional widths of 0, 1, 2, 3, and 4 pier diameter from the centreline. The measurements were made in each plane with a single pier case, and a single pier with the optimised FDS at the upstream with $H/y = 0.25, 0.5, 0.75,$ and >1 . The streamwise (u) and vertical (w) velocity components were determined from analysis of the PIV images collected during the individual experiments. Further analyses were carried out by a developed code in MATLAB and the results were plotted using Tecplot software. The outcomes for $u/V, w/V, TI_u/V, TI_w/V, TKE/V^2$ and $\overline{u'w'}/V^2$ have been displayed with contour plots. The results were compared for various arrangements comprising the single pier as a control test and the pier with the optimised FDS under different H/y ratios. In this Chapter, only the figures for $Y/D = 0$ are illustrated. The plots for other planes are depicted in Appendix B. The results and discussions of the flow field around a circular bridge pier with the optimised FDS are presented in the following sections. The data have been stored into UTS Stash system. This DOI <https://doi.org/10.26195/bf5n-0n94> can be used to access the data.

5.4.1. Time Average Velocity Components

The plots of the streamwise velocity (u) in the central vertical plane for Run 1 to 5 (see Table 5.2) are shown in Figures 5.7 to 5.11. In these figures, the streamwise velocity component (u) is normalised by the cross-sectional average velocity (V).

As expected and also shown in Figure 5.7, the values of u/V become smaller as the flow approaches the pier and finally reduce to zero at the upstream pier face. As described by Melville & Raudkivi (1977), the approach flow velocity at the upstream surface of a pier is reduced to zero which, in turn, increases the pressure. This increased pressure has the highest amount near the surface, where the greatest deceleration can be observed and decreases downwards. This difference in the pressure forms an adverse pressure gradient on the upstream face of the pier in the vertical direction as a result of the approaching boundary layer flow. If this pressure gradient is strong enough, it will be capable of causing a down-flow on the upstream face of the pier. Down-flow interacts with the horizontal layer close to the river bed, forming a horseshoe vortex. Both the down-flow and horseshoe vortex have a significant influence on pier-scour.

Figure 5.7 shows that, over the full flow depth, u/V upstream of the pier remains undisturbed for $X/D \geq 1.75$ measured from the pier centre. In other words, the pier affects the upstream flow field in a section between the pier and a distance of $1.25D$. This result is consistent with the results, stated by Keshavarzi et al. (2017).

Downstream of the pier, the values of u/V are negative as demonstrated in Figure 5.7. These negative values confirm the existence of reverse flow and the formation of a wake in this region. The wake region behind the pier keeps the sediment particles suspended and moves them further downstream. This plot also displays that the values of u/V increase further downstream of the pier and eventually return to normal conditions.

According to Figure 5.8, when the optimised FDS ($H/y=0.25$) is placed at the upstream of the pier, the u values decrease, and their direction became negative (from pier to the FDS) in the gap region between the pier and the FDS, and from bed up to the height of FDS. The negative values of u interact with the horizontal layer nearby the bed and

consequently can distract the formation of horseshoe vortices. Besides, a jet-flow is observed above the FDS which can affect the flow field at the gap region.

At the downstream of the pier, this optimised FDS significantly affects the magnitudes and direction of streamwise velocity component. In the case of the single pier (Figure 5.7), the high negative values of u indicate the strong wake vortices behind the pier which can washout the sediment particles and increase the scour depth and volume. However, Figure 5.8 reveals that the wake vortices behind the pier become weaker by using this optimised FDS. In addition, the length of this wake region is reduced and the flow comes to the normal flow condition by passing through a shorter distance. In this case, even the positive values of u are observed behind the pier near to the bed.

Figures 5.9 to 5.11 show, for the case of pier and FDS with $H/y=0.5, 0.75, >1$, plots of normalised streamwise velocity components. These figures illustrate that increasing the height of FDS significantly changes the streamwise velocity in the gap region between the pier and FDS. In this region, both the negative and positive values of u exist from the bed up to the height of FDS. However, by increasing the height of FDS, the area of negative values (blue colour) becomes more dominant especially when $H/y>0.5$. It means that the wake in the gap region may be extended with the increase of FDS height. This extension of wake in the gap region may increase the local scour around the FDS. Also, by elevating the height of FDS up to near the water surface, the velocity of jet-flow enlarges which can affect the turbulence characteristics of the flow in the gap region.

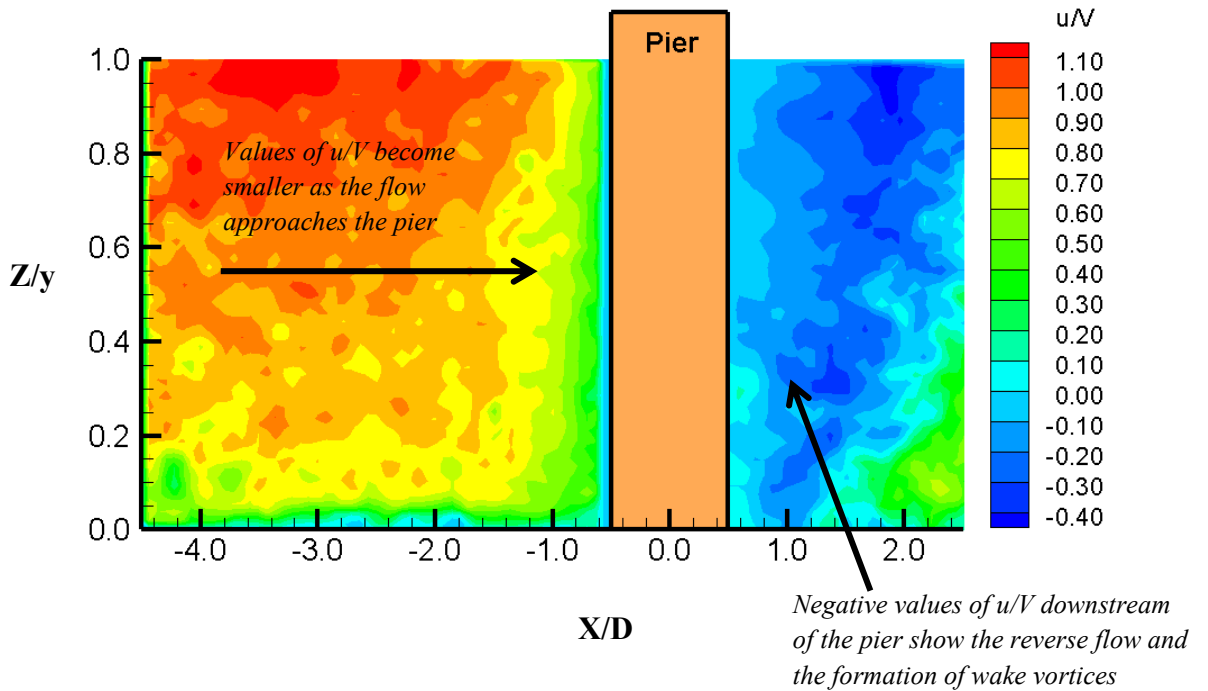


Figure 5.7. Normalised streamwise velocity for the single pier case at $Y/D = 0$

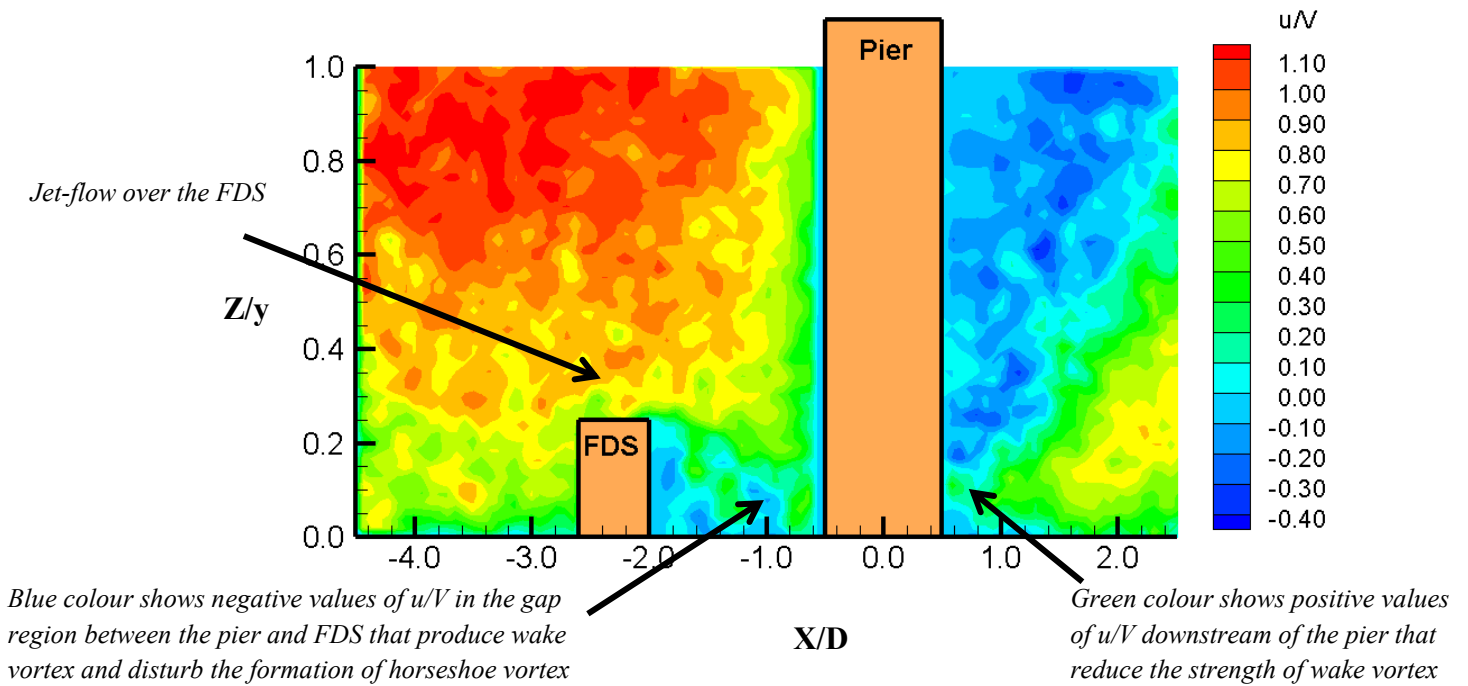
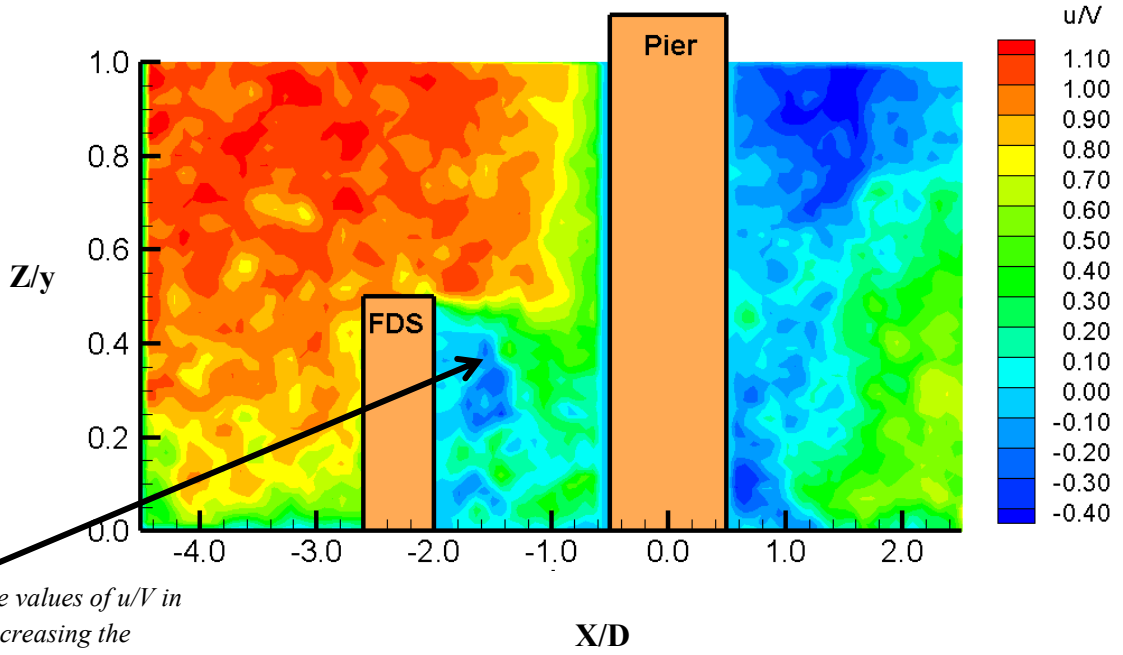


Figure 5.8. Normalised streamwise velocity for the single pier case and FDS with $H/y=0.25$ at $Y/D = 0$



Extending the negative values of u/V in the gap region with increasing the height of FDS

Figure 5.9. Normalised streamwise velocity for the single pier case and FDS with $H/y=0.50$ at $Y/D = 0$

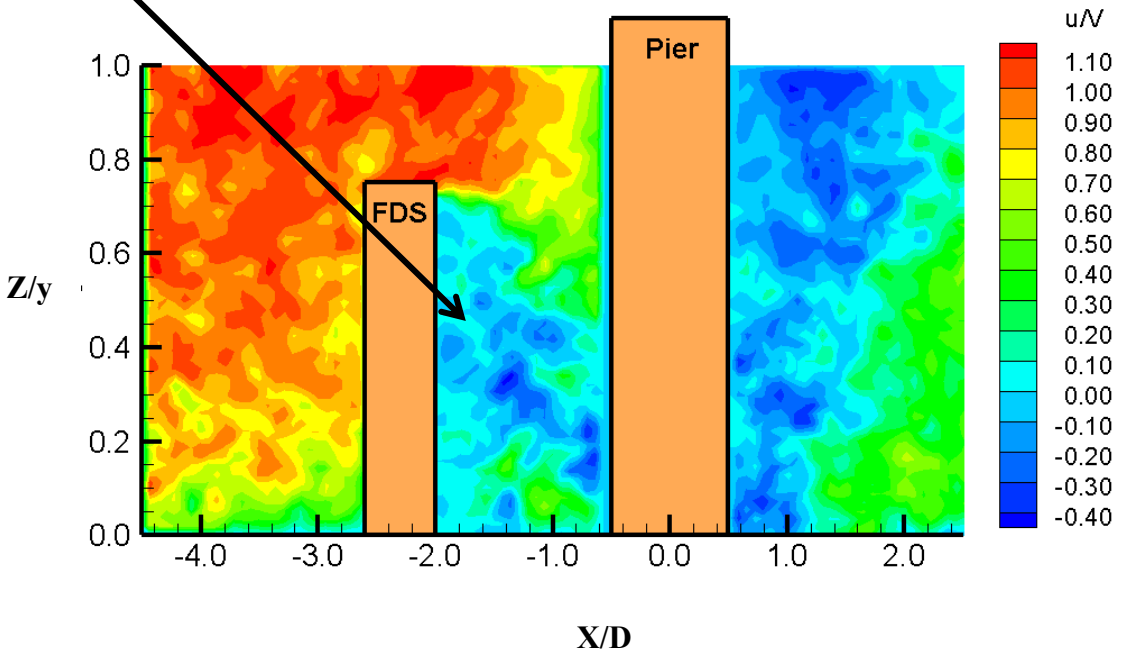


Figure 5.10. Normalised streamwise velocity for the single pier case and FDS with $H/y=0.75$ at $Y/D = 0$

Extending the negative values of u/V in gap region with increasing the height of FDS

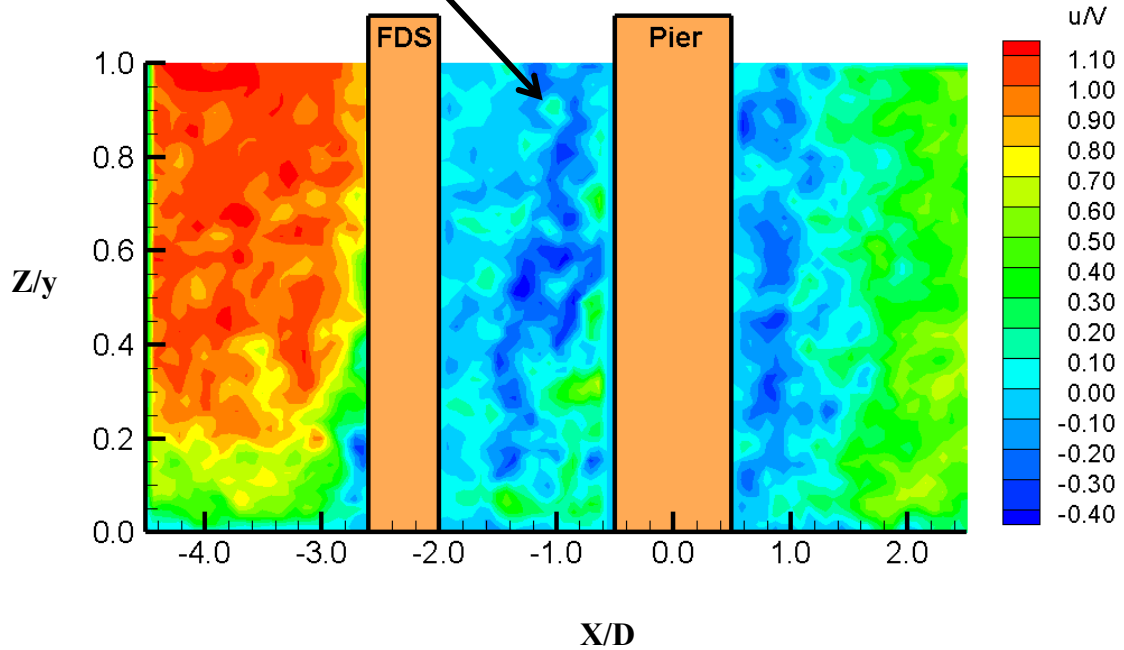


Figure 5.11. Normalised streamwise velocity for the single pier case and FDS with $H/y > 1$ at $Y/D = 0$

Contour plots of the normalised streamwise velocity component for different vertical planes positioned at $Y/D = 1, 2, 3,$ and 4 are presented in Appendix B. The general trend of the effect of FDS on the streamwise velocity component shows the reduction of velocity at the pier vicinity for all vertical planes. However, the acquired results indicate that the impact of FDS to reduce u becomes smaller by increasing the FDS height, and by increasing transverse distance from the central and finally, will be faded at around $Y/D=4$.

Figures 5.12 to 5.16 depict the plots of w/V for Runs 1 to 5 in the central vertical plane. Referring to Figure 5.12, it can be observed that the strong down-flows are formed upstream of the single pier case, nearby the bed. This system of down-flows impinges the bed and removes the sediments particle from the upstream of the pier. Figure 5.13 indicates that the optimised FDS changes the flow field and forms a system of upward flow ($w/V > 0$) at upstream of the pier near to the bed. This system of upward flow reduces the strength of down-flow at upstream of the pier and also can prevent the formation of horseshoe vortices. Therefore, it can be expected to have a smaller amount of scour around the pier.

When comparing the contour plots presented in Figures 5.13 to 5.16, it can be seen that increasing the height of FDS causes:

- formation of a stronger down-flow upstream of the FDS
- an increase in the magnitude and intensity of the upward flow in the gap between the pier and FDS.

Therefore, more scour around the FDS and upstream of the pier can be predicted.

For the cases of $H/y=0.25$, 0.50 , and 0.75 (Figures 5.13 to 5.15) a system of down-flow forms near the pier which starts from a depth nearby the FDS height but does not reach to the bed. This down-flow is due to the jet-flow above the FDS that falls in the gap region.

These results of the velocity components and the effects of FDS height on the flow field are consistent with previous results reported by Faheem Sadeque et al. (2009). In addition, the outcomes of the local scour experiments presented in the Chapter 4 confirm the above analysis.

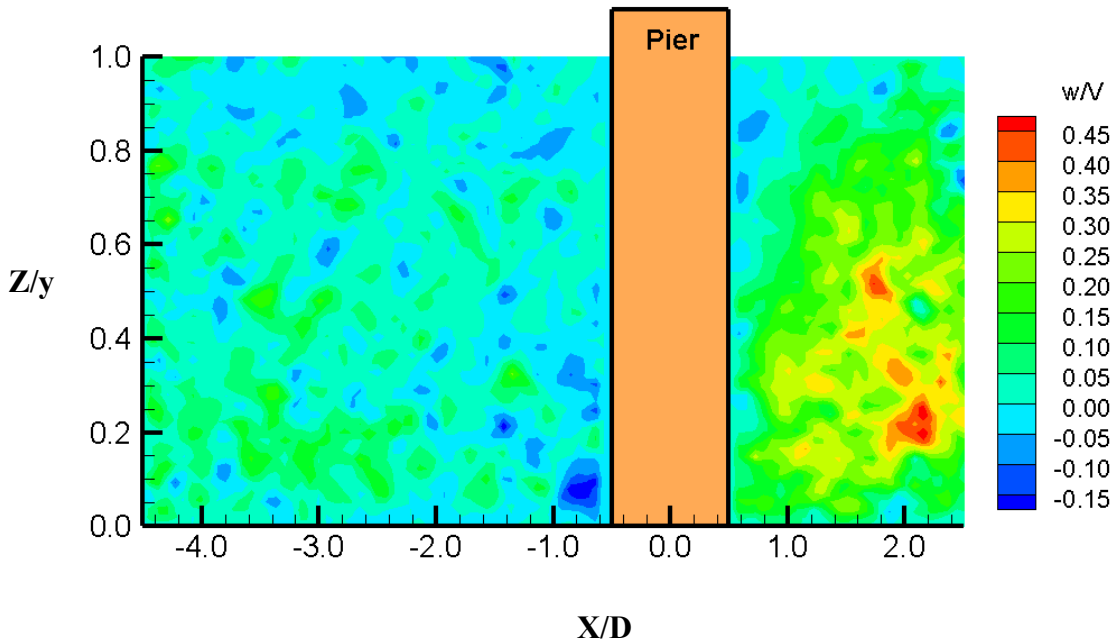


Figure 5.12. Normalised vertical velocity for the single pier case at $Y/D = 0$

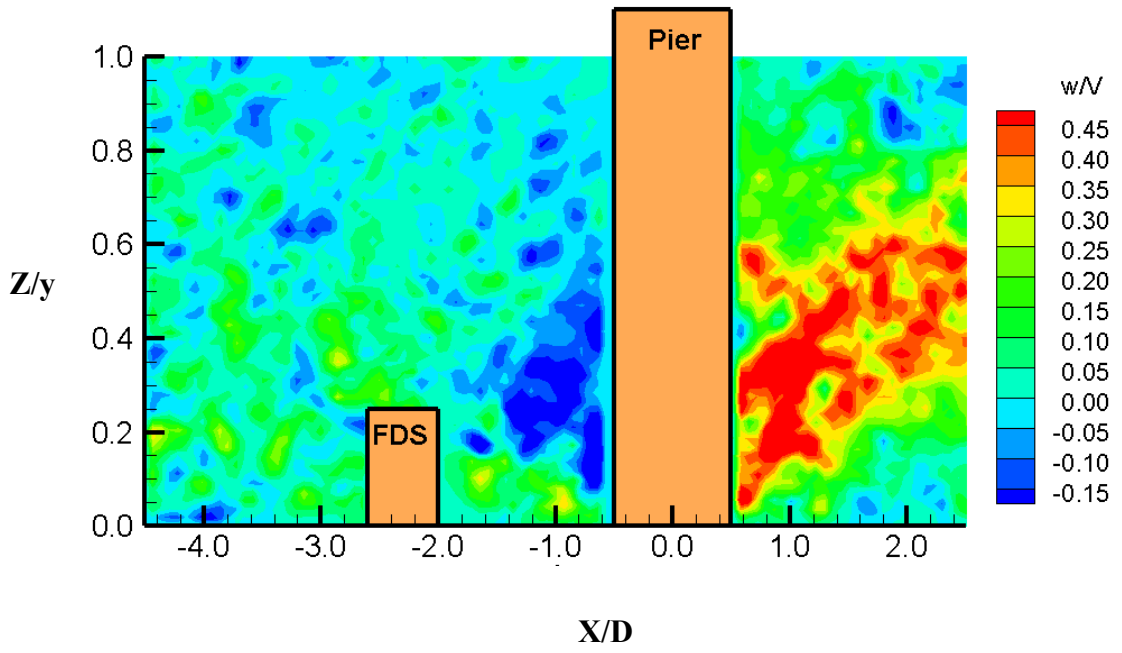


Figure 5.13. Normalised vertical velocity for the single pier case and FDS with $H/y=0.25$ at $Y/D = 0$

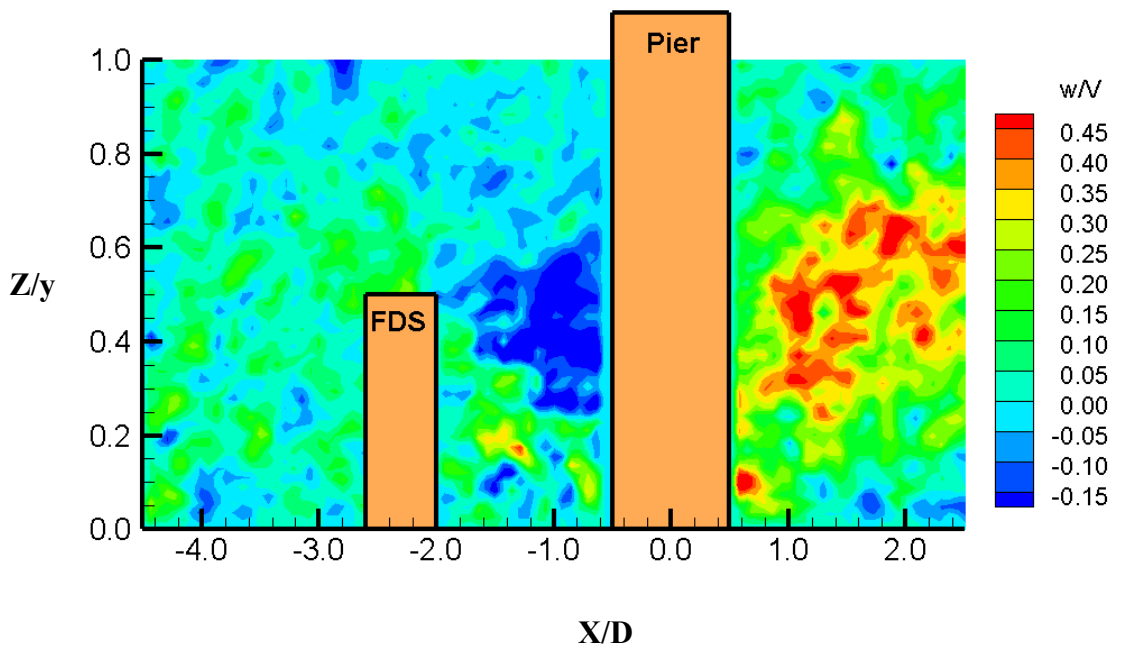


Figure 5.14. Normalised vertical velocity for the single pier case and FDS with $H/y=0.50$ at $Y/D = 0$

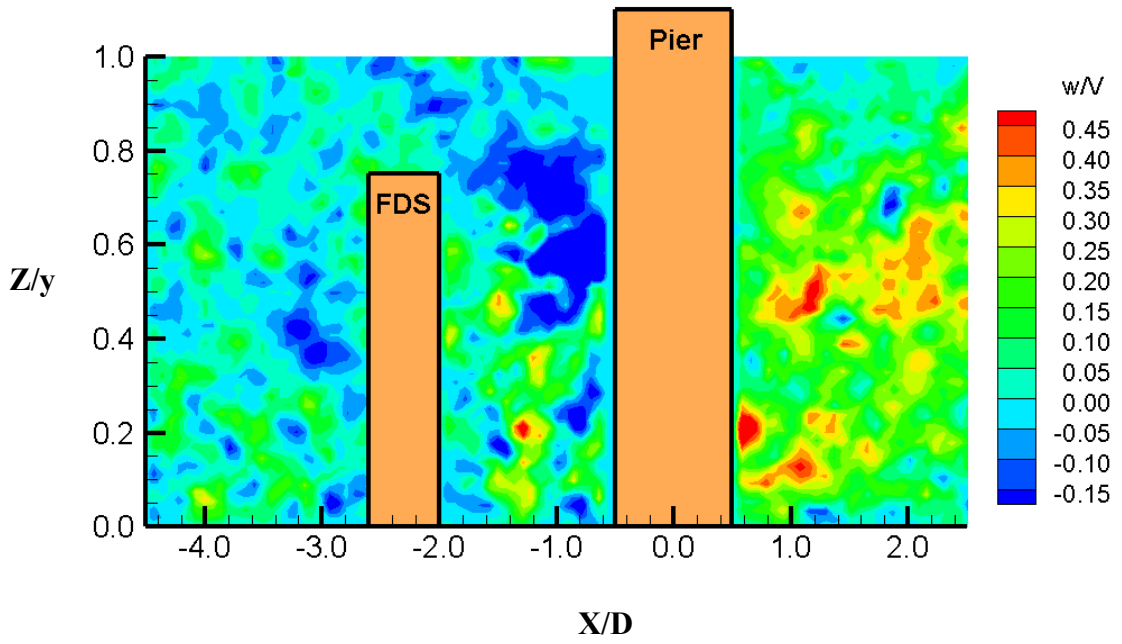


Figure 5.15. Normalised vertical velocity for the single pier case and FDS with $H/y=0.75$ at $Y/D = 0$

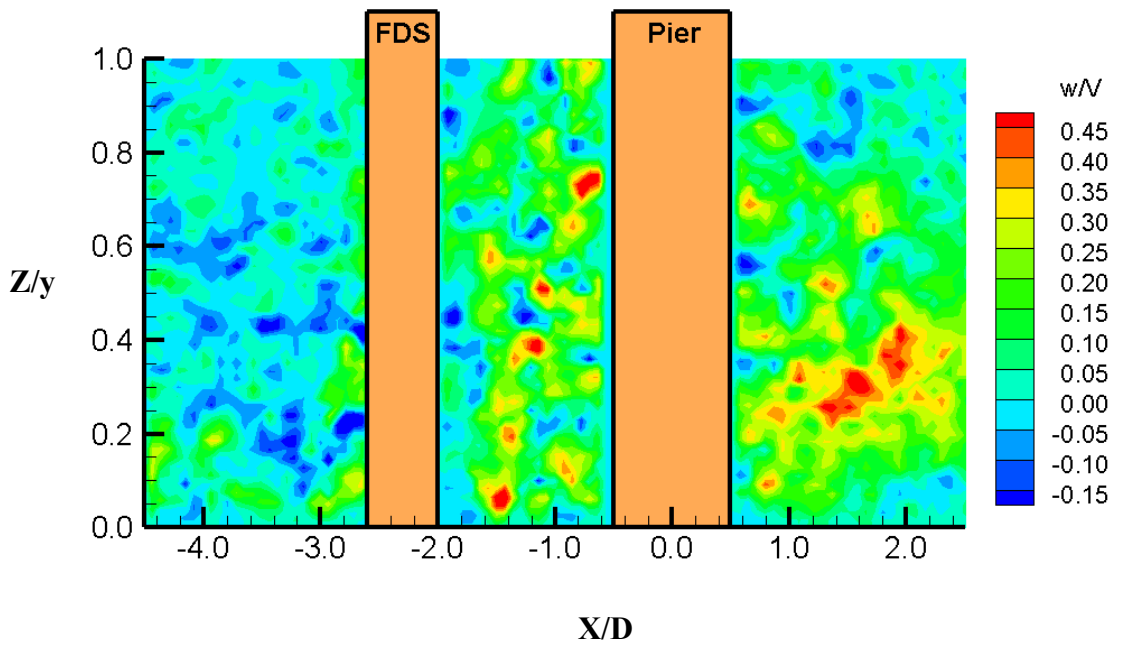


Figure 5.16. Normalised vertical velocity for the single pier case and FDS with $H/y>1$ at $Y/D = 0$

5.4.2. Flow Pattern

For better visualisation of the velocity components, the streamlines patterns shown in Figures 5.17 to 5.21 were developed. The background of these diagrams shows the contour plots of the normalised absolute flow velocity ($V_a = (u^2 + w^2)^{0.5}$).

As can be seen in these flow pattern figures, by installing the FDS at the upstream of a pier, the flow pattern significantly changes around the pier. Figure 5.17a demonstrates the streamlines impinge to the bed at the upstream of the single pier. Also, a wake region at downstream of the pier can be seen that extends around 2D behind the pier and over the entire depth. The length of this wake region can be simply recognised from the flow pattern diagram. These results are consistent with Shrestha (2015), and Keshavarzi et al. (2017) and hence with the earlier results stated by Sahin et al. (2007), Ataie-Ashtiani & Aslani-Kordkandi (2013). This wake region starts to diminish from a distance around 1.3D behind the pier, and near the bed.

A scientific camera Pco.1600 with a resolution of 1600×1200 pixels was used. Two different camera locations were employed, namely a wide frame (from upstream of the FDS to the downstream of the pier), and a tight frame (only the gap region between the pier and FDS). Clear definition of the vortices was not possible with the wide frame images; the presence of vortices was apparent but the resolution of images was insufficient to define them. The tight frame images clearly define vortices due to the resolution over a smaller sample space. To plot the vortexes, in two cases including a single pier with and without optimised FDS (with $H/y=0.25$) at $Y/D = 0$, a tight frame was selected, which only captured the gap region between the pier and FDS, but missed the jet-flow over the FDS, and wake at downstream of the pier. The streamlines from analyses of these two cases are presented in Figures 5.18. The formation of down-flow and horseshoe vortex at upstream of the single pier can be seen in Figure 5.18a.

As illustrated in Figures 5.17 to 5.21, the flow pattern changes around the pier when the FDS is placed at the upstream of the pier. Figure 5.17b reveals the existing of upward flow in the gap region between the pier and the optimised FDS up to its height. In fact, a wake region forms behind the FDS, and the pier locates in this region. These wake vortexes and upward flow reduce the strength of down-flow at the pier's upstream. In

addition, at the base of the pier, this wake disturbs the formation of horseshoe vortices. The wake region downstream of pier is influenced also by the FDS. The comparison between Figure 5.17a with Figure 5.17b shows that the optimised FDS reduces the length of the wake region behind the pier by around $0.6D$.

A system of down-flow is produced at the upstream of the FDS by elevating the height of FDS, especially when its crest is above the $0.5y$. Additionally, the wake vortices in the gap region between the pier and the FDS extend upward as much as the FDS height. However, the alterations of the wake region behind the pier are not very significant.

The flow pattern in other vertical planes ($Y/D=1, 2, 3,$ and 4), are presented in Appendix B. Comparing the flow pattern in all sets of experiments can be concluded that the FDS significantly affects the flow field around the pier. Due to its triangular shape, the FDS diverts the streamlines from the vicinity of the pier. The FDS produces a system of upward flow in the gap region between the FDS and the pier. This upward flow withstands the down-flow in this gap region. Moreover, the FDS disturbs the formation of the horseshoe vortices at the base and reduces the strength of wake vortices behind the pier. These changes in the flow field around the pier decrease the amount of local scour at the vicinity of the pier. It is noteworthy to state that by elevating the FDS height above $0.5y$ its effects may reduce due to the formation of the stronger down-flow and wake vortices at upstream and downstream of FDS, respectively. However, even the unsubmerged FDS can protect the pier from local scour due to its sheltering effect. Finally, the effects of FDS on flow field decrease by laterally getting away from the central and eventually will be faded at around $Y/D = 4$.

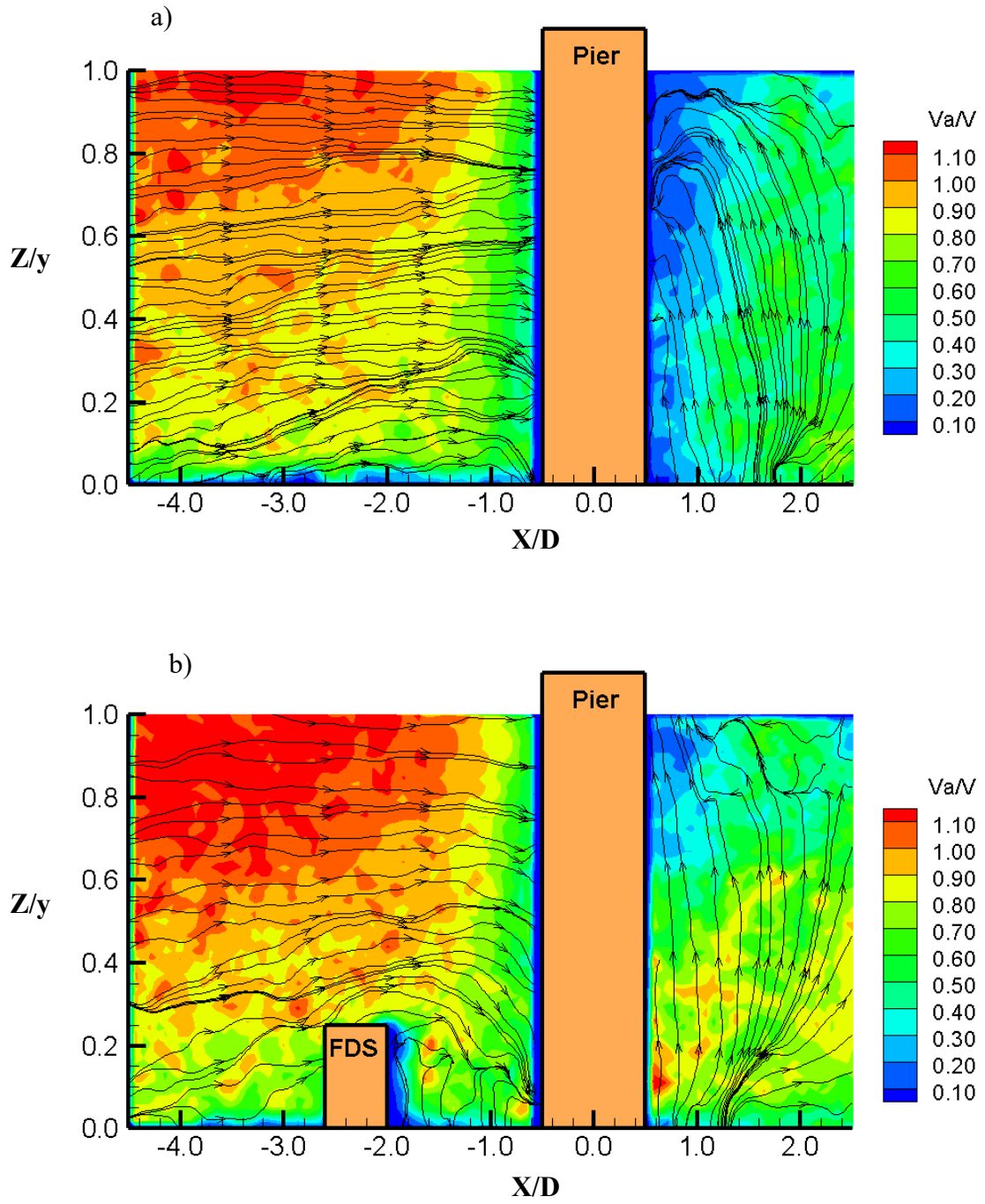


Figure 5.17. Normalised absolute flow velocity and Streamlines in wide frame at $Y/D = 0$; a) single pier case; b) single pier case and FDS with $H/y=0.25$

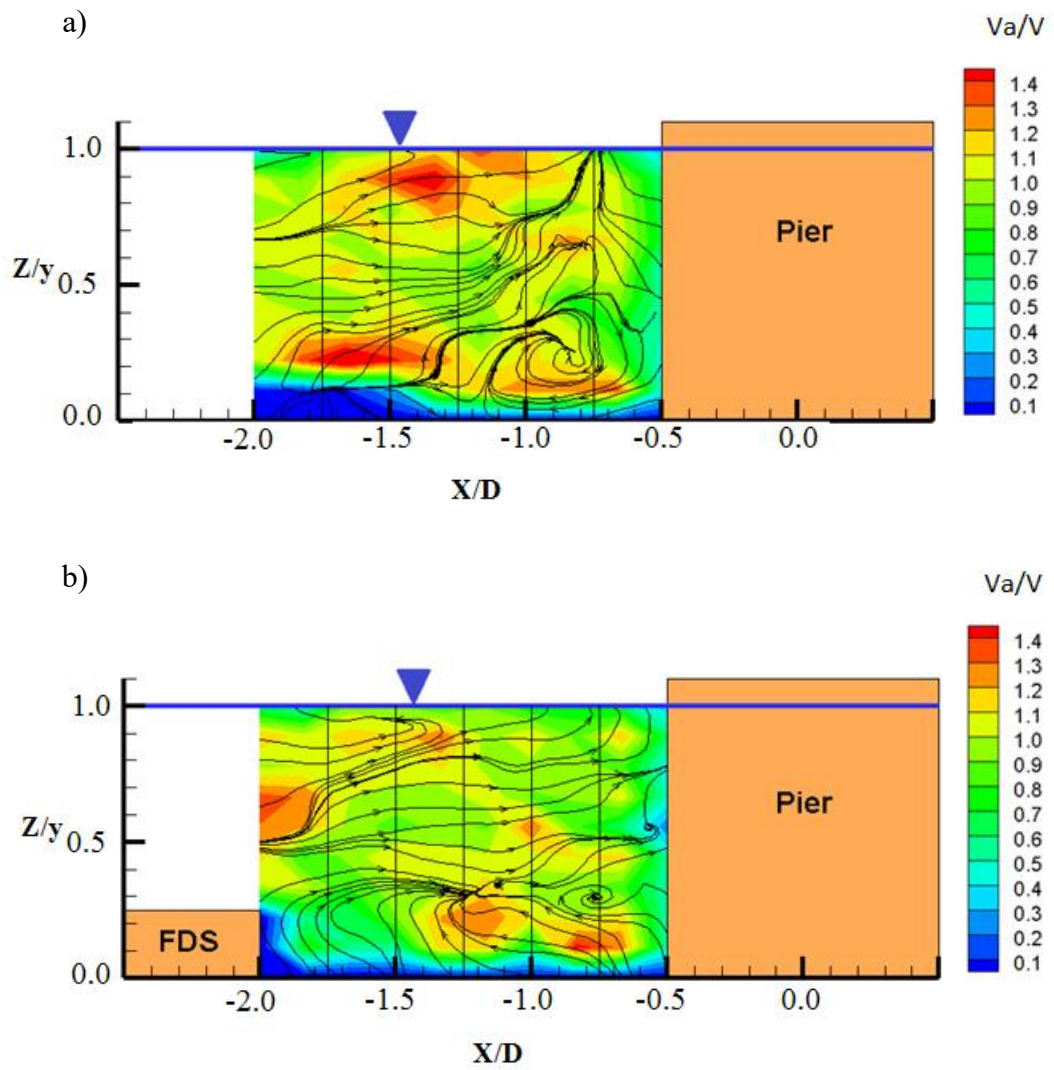


Figure 5.18. Normalised absolute flow velocity and Streamlines in tight frame at $Y/D = 0$; a) single pier case; b) single pier case and FDS with $H/y=0.25$

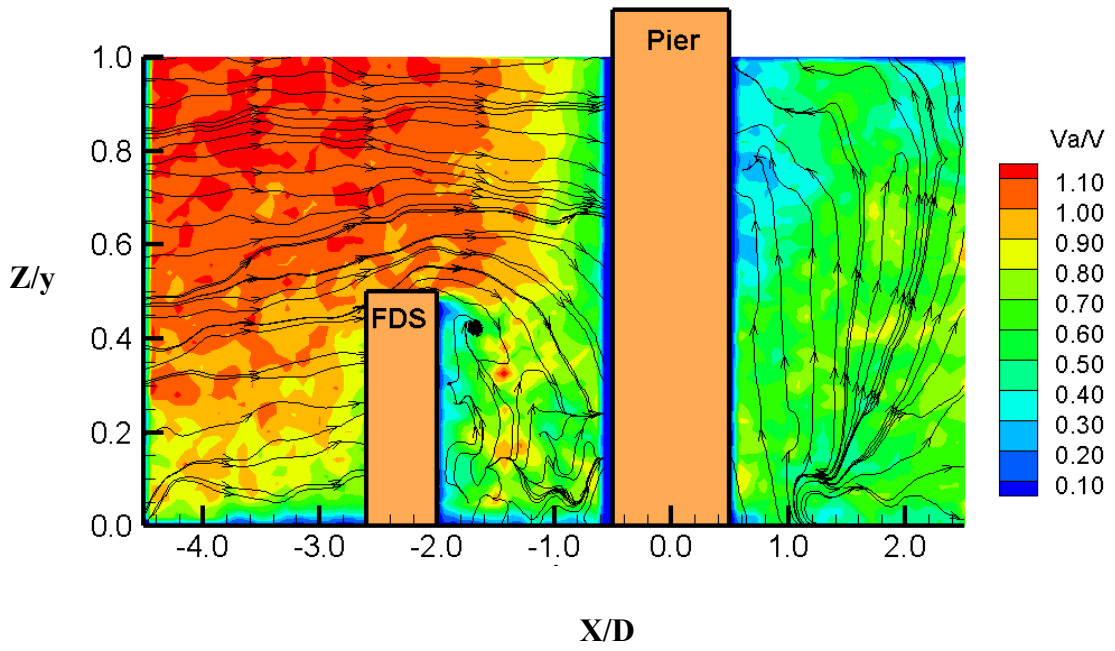


Figure 5.19. Normalised absolute flow velocity and Streamlines for the single pier case and FDS with $H/y=0.50$ at $Y/D = 0$

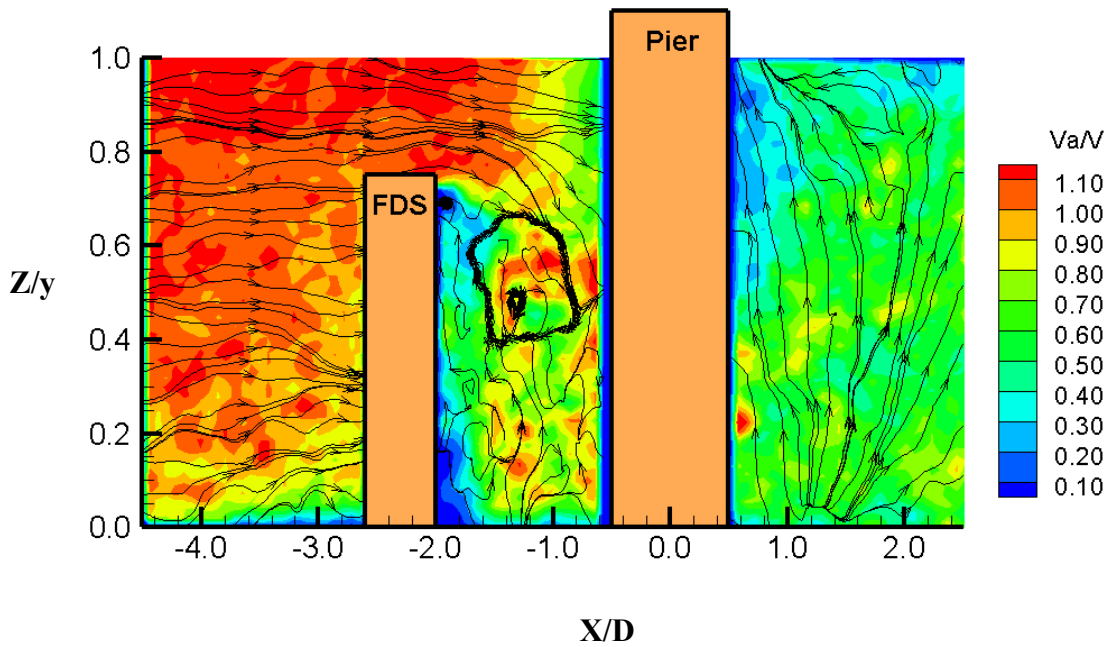


Figure 5.20. Normalised absolute flow velocity and Streamlines for the single pier case and FDS with $H/y=0.75$ at $Y/D = 0$

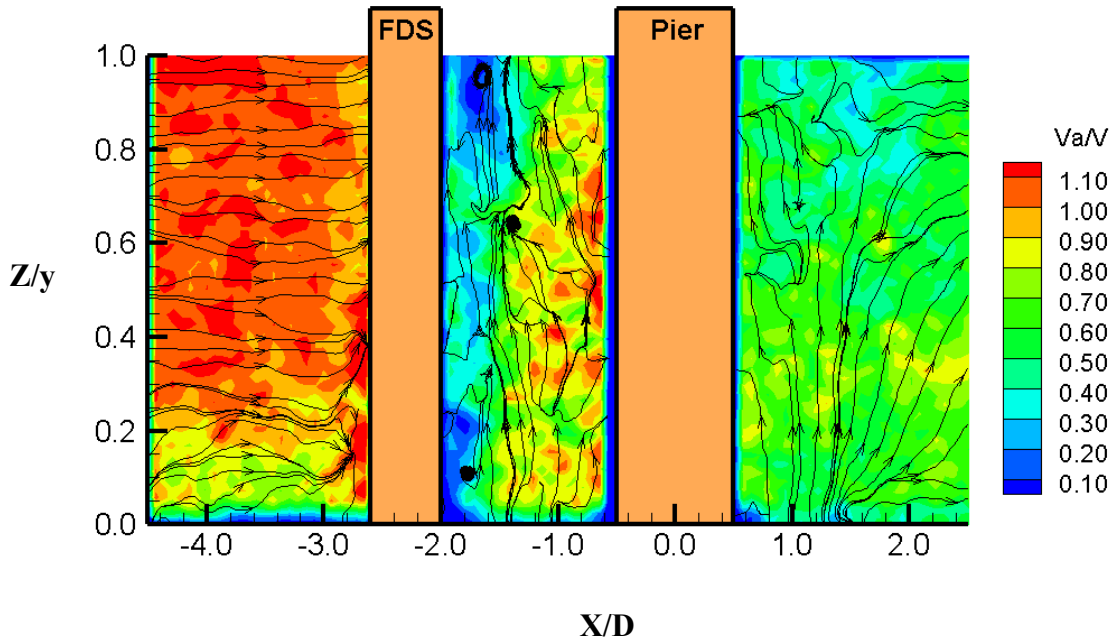


Figure 5.21. Normalised absolute flow velocity and Streamlines for the single pier case and FDS with $H/y > 1$ at $Y/D = 0$

5.4.3. Turbulence Intensity Components

In this study, the streamwise turbulence intensity (TI_u) and vertical turbulence intensity (TI_w) have been calculated from the velocity fluctuations components (u' and w'). The results for TI_u are depicted in the contour plots form in Figures 5.22 to 5.26. In these figures, the turbulence intensity components are normalised using the cross-sectional average velocity (V).

Figure 5.22 displays a relatively high value of TI_u/V at the upstream of the single pier close to the bed. At upstream, the values of this parameter reduce with increase in the space toward the free surface. Similar results have been stated by Beheshti & Ataie-Ashtiani (2010), Shrestha (2015), and Keshavarzi et al. (2017) for the case of a single circular pier. At the downstream of the pier, the variations of streamwise turbulence intensity are much higher immediately behind the pier and decrease with getting far from the pier. However, the maximum values of TI_u/V occur within a distance around

1-2D after the pier. These results are consistent with the results stated by Faheem Sadeque et al. (2009), and Shrestha (2015).

When the FDS is located at the upstream of the pier, the values of TI_u become higher in the vicinity of the pier as shown in Figures 5.23 to 5.26. This increasing of TI_u is due to the more interactions between the flow and two obstacles rather than the single pier case. For example, in the cases of completely submerged FDS, the overflow above the FDS impinges the wake in the gap region and increases the turbulence intensity. As the height of FDS elevates, TI_u also increases. This growth of the streamwise turbulence intensity is more significant in the upstream of the FDS and the gap region rather than behind the pier.

Comparing the contour plots of streamwise velocity with the turbulence intensity indicates an inverse trend between the magnitudes of velocity and turbulence intensity. This outcome is consistent with the outcome of Faheem Sadeque et al. (2009), who found the smaller mean velocity and high turbulence in the wake region behind the circular cylinders under different submergence ratios. Therefore, it can be argued that the higher turbulence intensity does not necessarily indicate more local scour. This claim can be confirmed by the results of local scour tests presented in the previous chapter.

The contour plots of normalised streamwise turbulence intensity in other vertical planes ($Y/D = 1, 2, 3,$ and 4) are shown in Appendix B. The general trend of TI_u in the planes of $Y/D = 1$ is similar to the central vertical plane, but the amount of variations are not significant as in the plane of $Y/D = 0$. The turbulence intensity in the plane of $Y/D = 2$ becomes smaller by FDS. However, there is no highlighted trend in the variations of this parameter in other planes due to the complexity of the flow field and the interactions between the flow, pier, FDS, bed, and side wall.

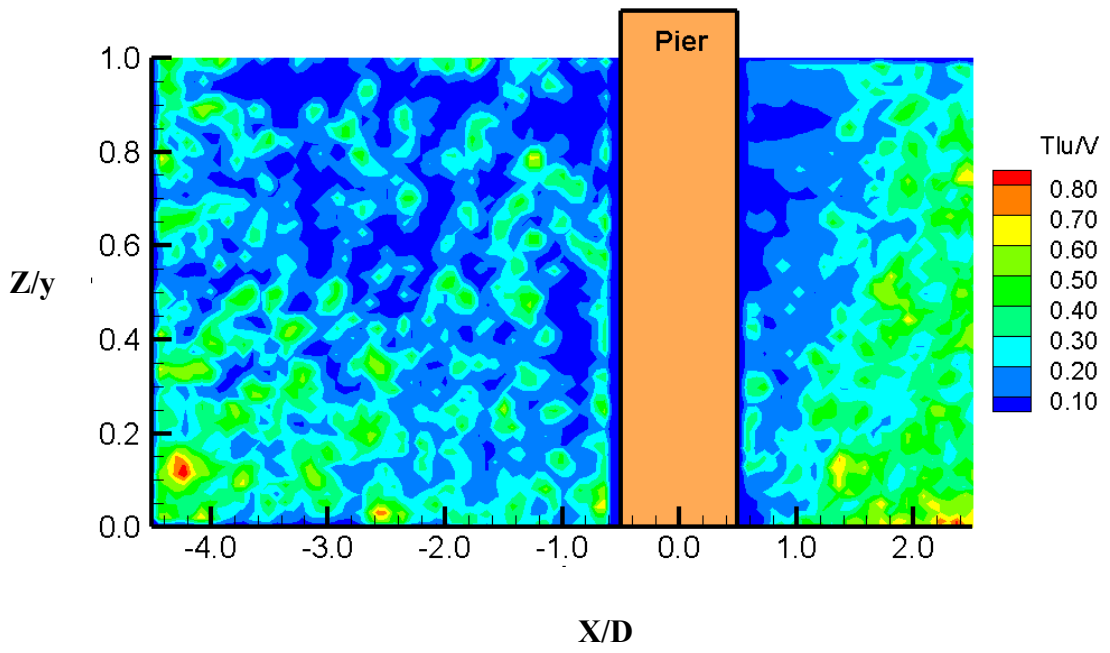


Figure 5.22. Normalised streamwise turbulence intensity for the single pier case at $Y/D = 0$

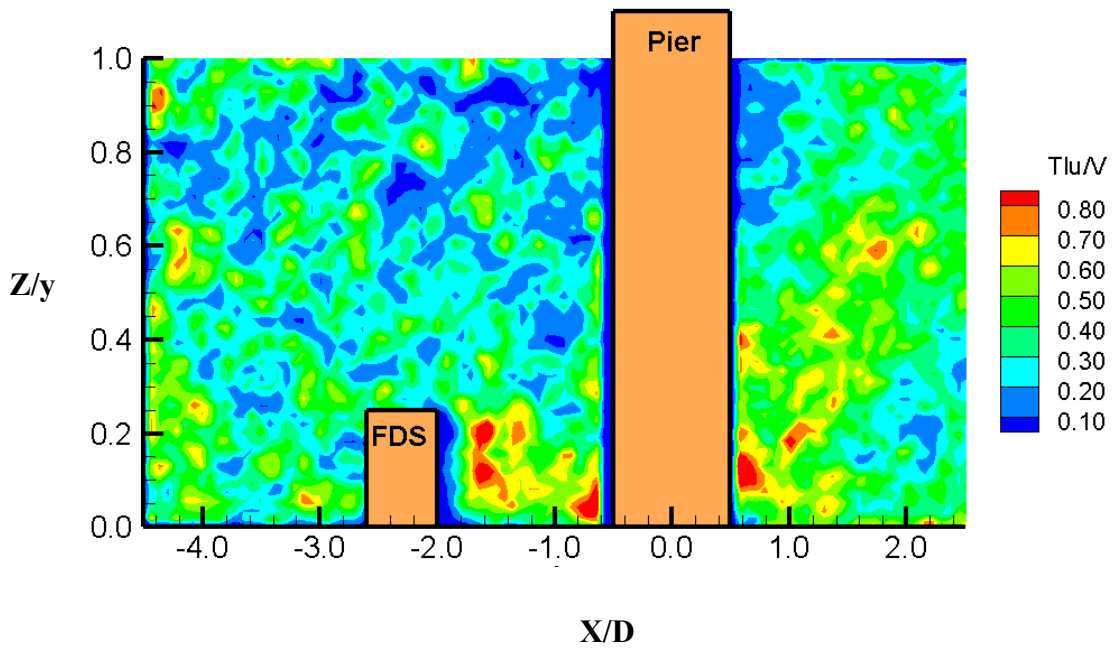


Figure 5.23. Normalised streamwise turbulence intensity for the single pier case and FDS with $H/y = 0.25$ at $Y/D = 0$

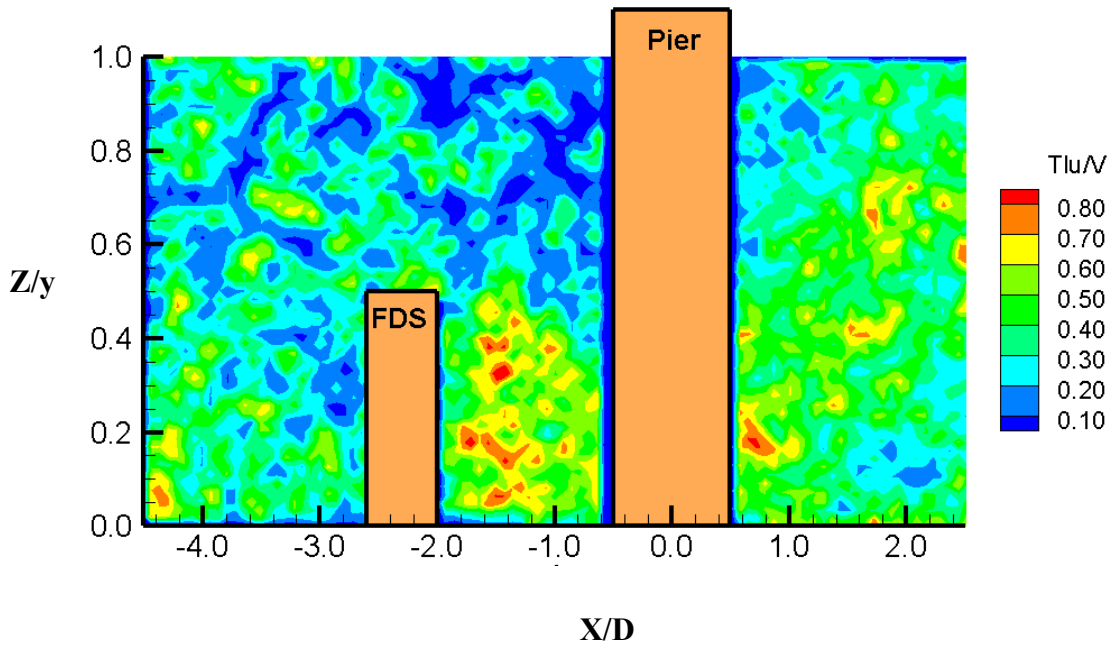


Figure 5.24. Normalised streamwise turbulence intensity for the single pier case and FDS with $H/y=0.50$ at $Y/D = 0$

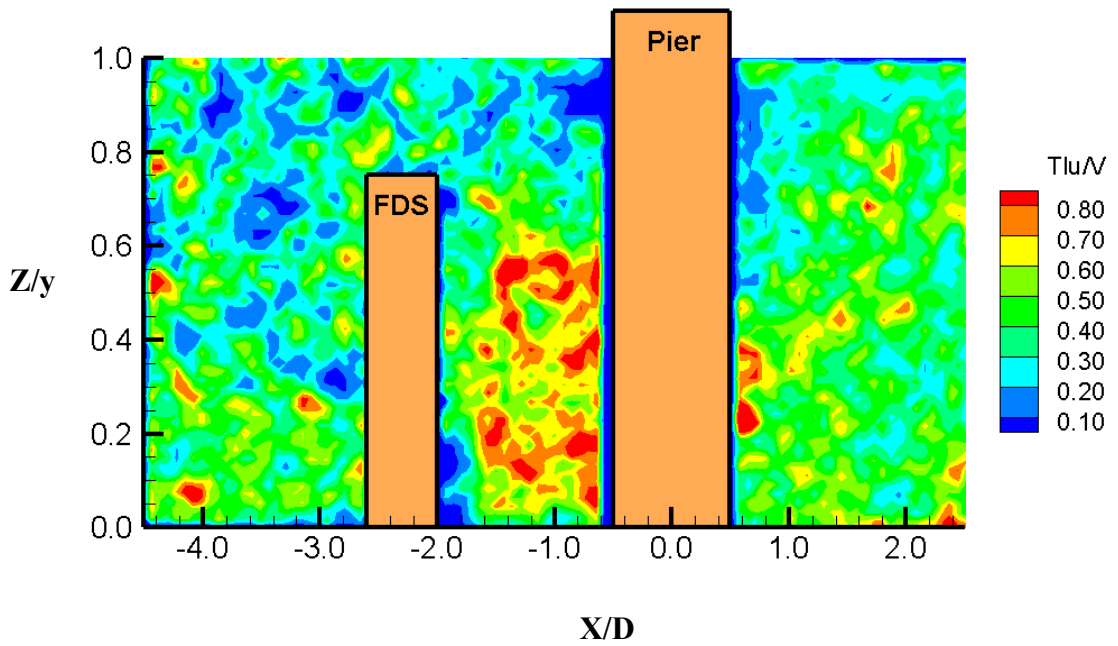


Figure 5.25. Normalised streamwise turbulence intensity for the single pier case and FDS with $H/y=0.75$ at $Y/D = 0$

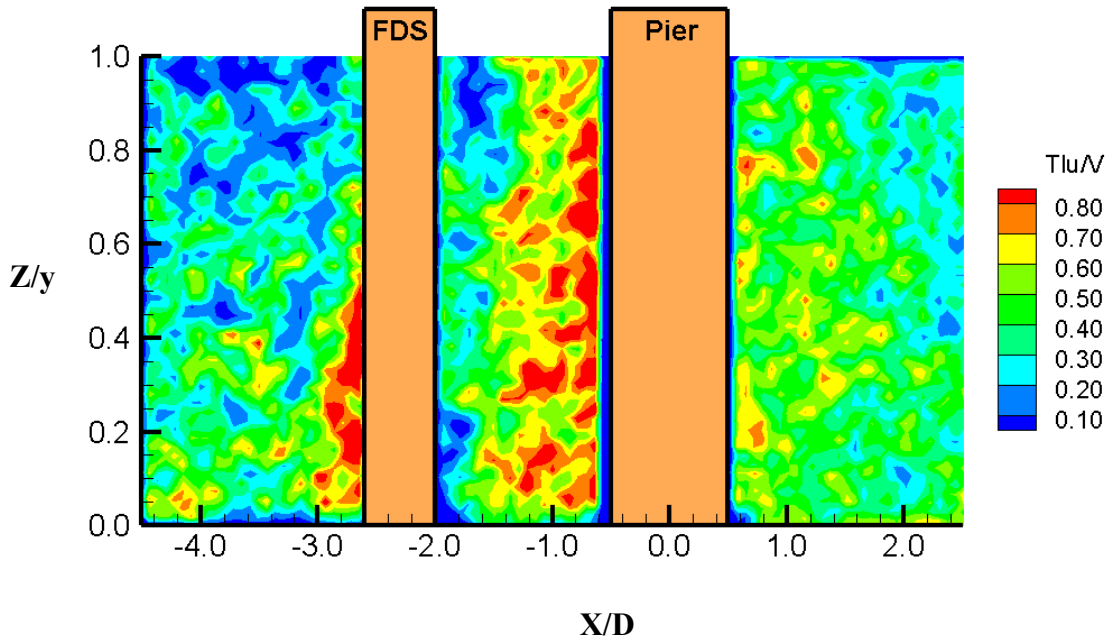


Figure 5.26. Normalised streamwise turbulence intensity for the single pier case and FDS with $H/y > 1$ at $Y/D = 0$

The plots of TI_w/V in the plane of symmetry for Runs 1 to 5 are given in Figures 5.27 to 5.31. These figures show the similar results to the TI_u . Installing the FDS at upstream of the pier raises the TI_w especially in the gap region between the pier and FDS. This upturn is due to the formation of wake vortices and upward flow behind the FDS. The interactions between the upward flow in the gap region and the down-flow in front of the pier increase the fluctuation part of the vertical velocity component and consequently increase the TI_w . Similar to the results of TI_u , in this case also the increasing of TI_w does not indicate more local scour around the pier. Besides, decreasing the submergence ratio (y/H) increases TI_w .

The plots of TI_w/V in the planes of $Y/D = 1, 2, 3,$ and 4 are accessible in Appendix B. For the case of $Y/D = 1$, the overall changes of TI_w at the vicinity of the pier due to FDS is like as the plane of $Y/D = 0$, but the amount of changes are much less in the plane of $Y/D = 1$. It means that the FDS has more effects on TI_w in the plane of $Y/D=0$ rather than $Y/D = 1$. The FDS reduces the TI_w in the plane of $Y/D = 2$. However, in the plane of $Y/D = 3,$ and 4 TI_w increases again. In all cases reducing the submergence ratio results in more TI_w . Finally, these various trends of TI_w in different vertical planes confirm the complicated flow field around the pier with the upstream FDS.

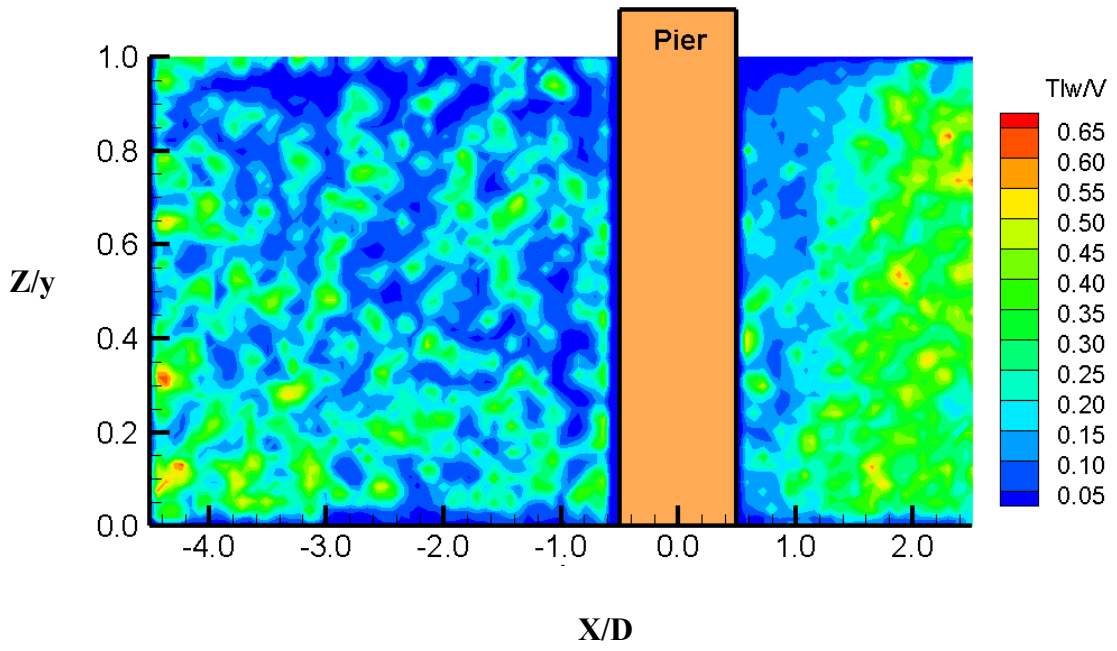


Figure 5.27. Normalised vertical turbulence intensity for the single pier case at $Y/D = 0$

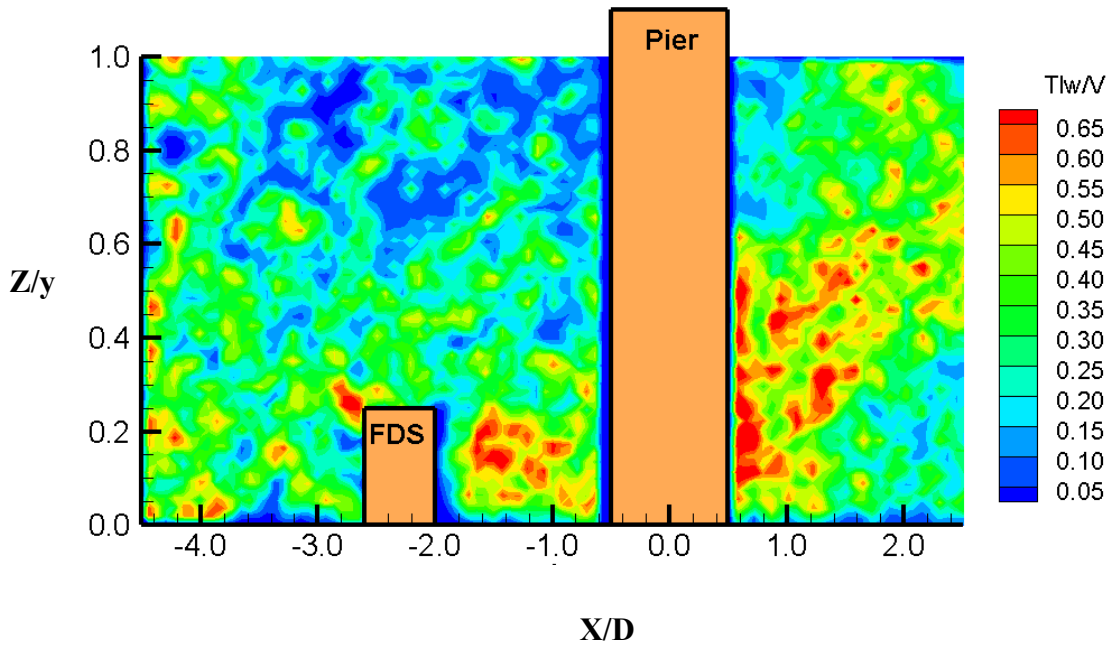


Figure 5.28. Normalised vertical turbulence intensity for the single pier case and FDS with $H/y = 0.25$ at $Y/D = 0$

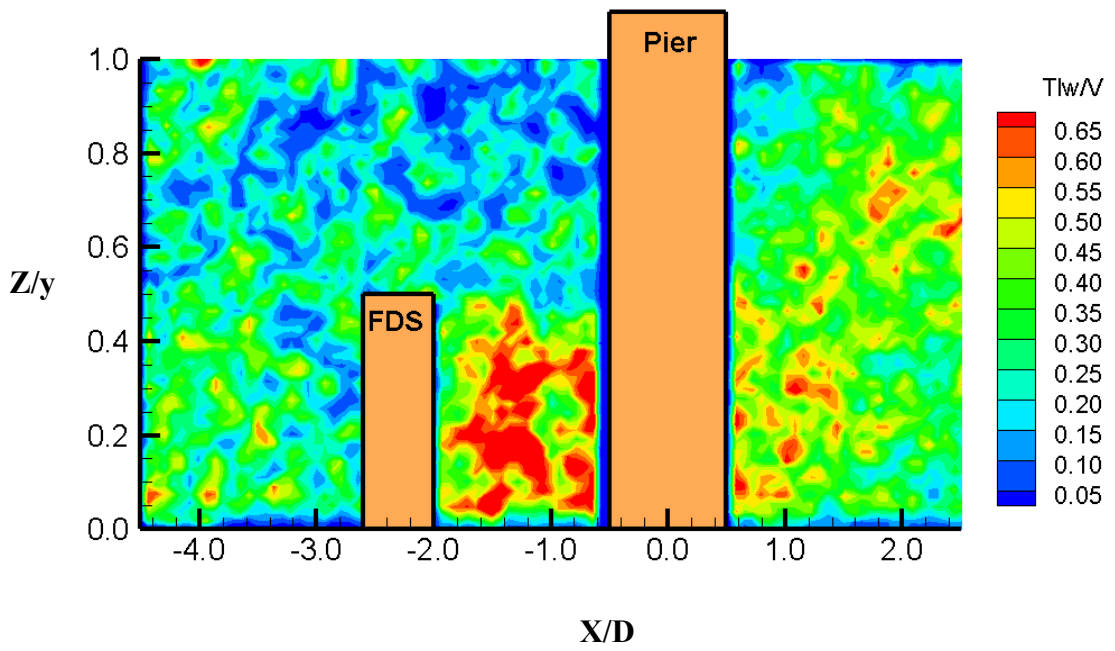


Figure 5.29. Normalised vertical turbulence intensity for the single pier case and FDS with $H/y=0.50$ at $Y/D = 0$

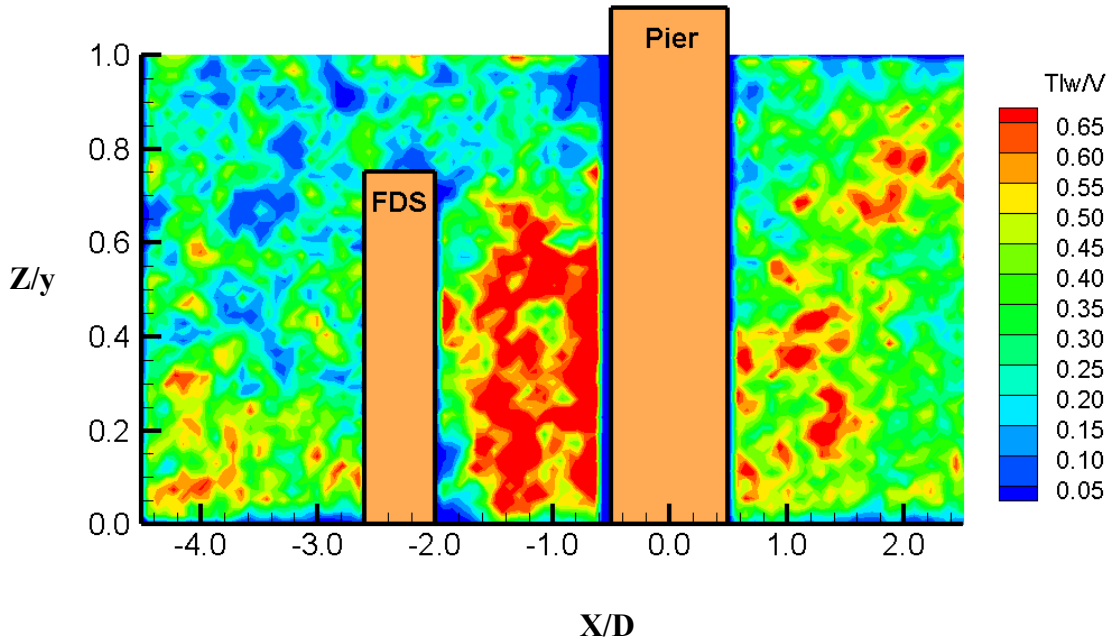


Figure 5.30. Normalised vertical turbulence intensity for the single pier case and FDS with $H/y=0.75$ at $Y/D = 0$

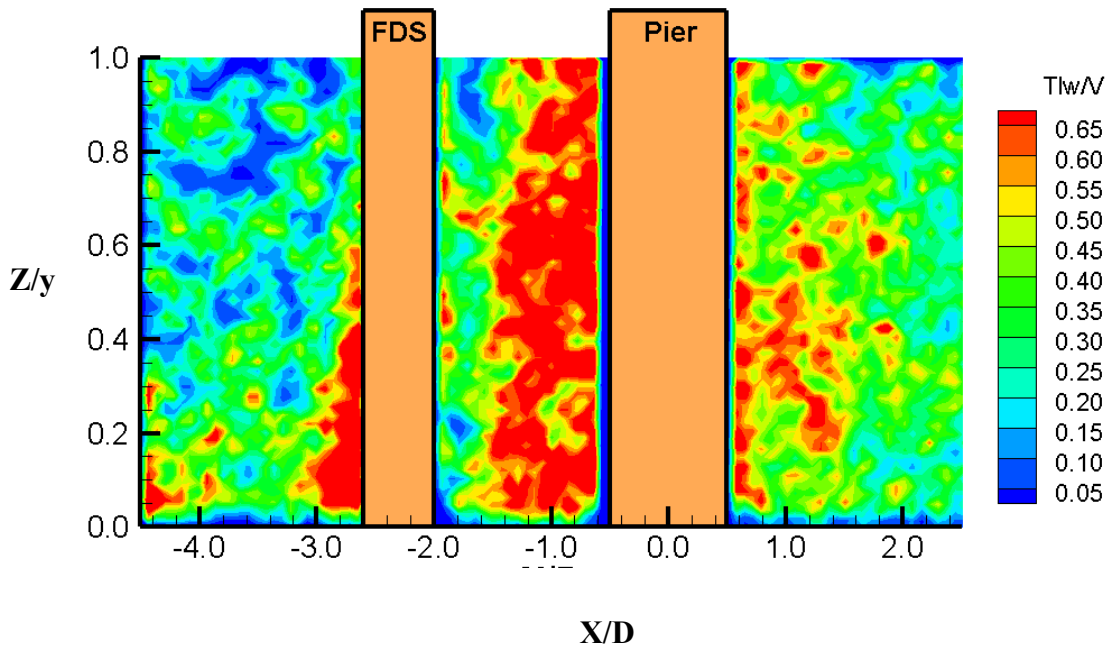


Figure 5.31. Normalised vertical turbulence intensity for the single pier case and FDS with $H/y > 1$ at $Y/D = 0$

5.4.4. Turbulent Kinetic Energy

2-D TKE has been estimated from the fluctuations of the streamwise and vertical velocity components, for all of the experimental tests. The contour plots of TKE for $Y/D = 0$ are provided in this section. In this study, TKE was normalised using the square of the cross-sectional average velocity (V^2).

Figure 5.32 illustrates TKE/V^2 for a single pier in a vertical plane of symmetry. The moderately higher values of TKE can be seen from Figure 5.32 in front of the pier near the bed and gradually decreases on the way to the water surface. TKE is minor at the immediate downstream of the pier. The maximum TKE at the downstream occurs around 1-2D from the pier. The values of TKE at downstream of the pier are higher than that of upstream. In general, the distribution of TKE and TI around the single pier is similar.

The distribution of TKE/V^2 for the case of the pier with FDS under different submergence ratios are plotted in Figures 5.33 to 5.36 for the vertical plane of

symmetry. These Figures reveal the significant effects of FDS on TKE around the pier. These effects are more dominant in that gap region due to the formation of a wake system behind the FDS. In addition, increasing the FDS height causes growth in the TKE upstream of FDS and in the gap region between FDS and pier.

The contour plots of TKE/V^2 for other vertical planes ($Y/D = 1, 2, 3,$ and 4) are illustrated in Appendix B. According to these figures, the trend of TKE in each vertical plane is alike to the trend of turbulence intensity in the corresponding plane.

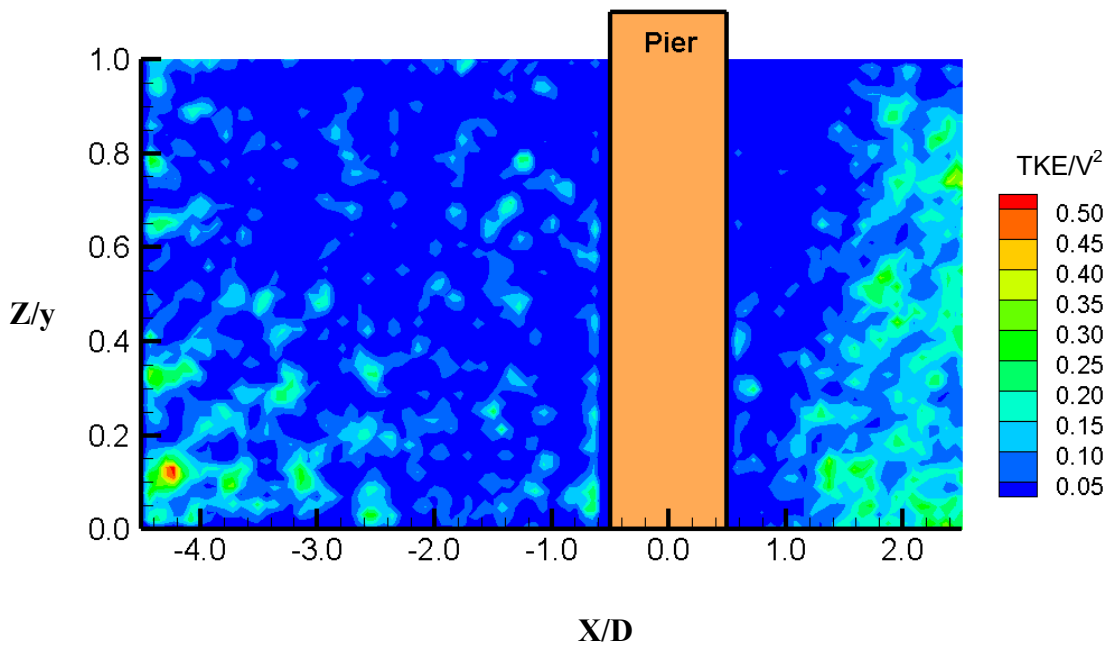


Figure 5.32. Normalised turbulent kinetic energy for the single pier case at $Y/D = 0$

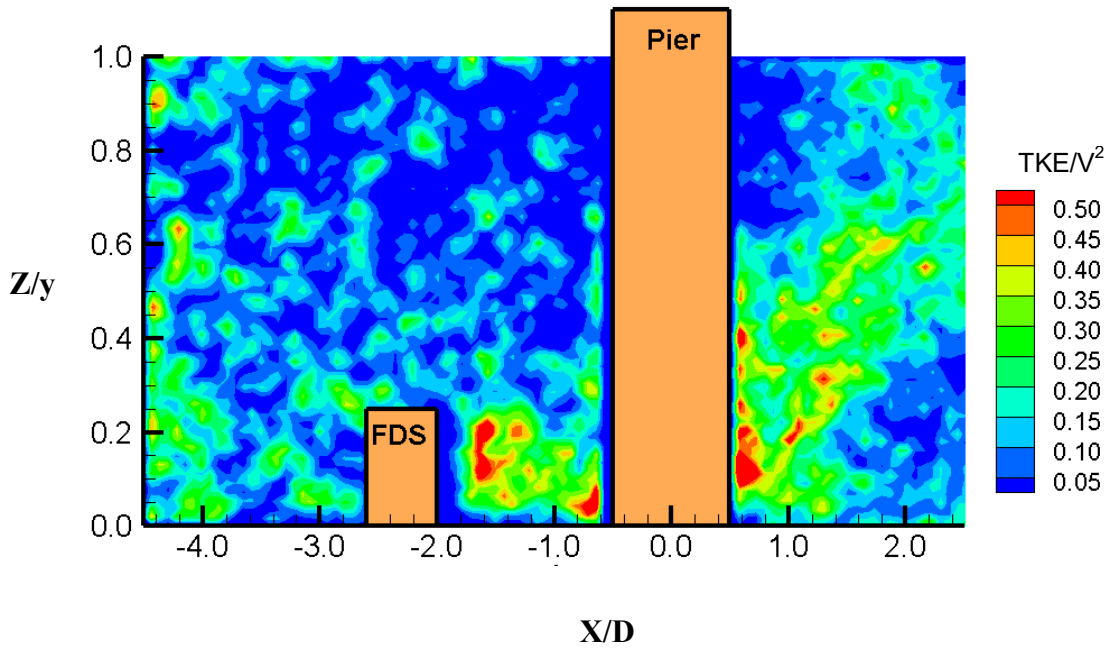


Figure 5.33. Normalised turbulent kinetic energy for the single pier case and FDS with $H/y=0.25$ at $Y/D = 0$

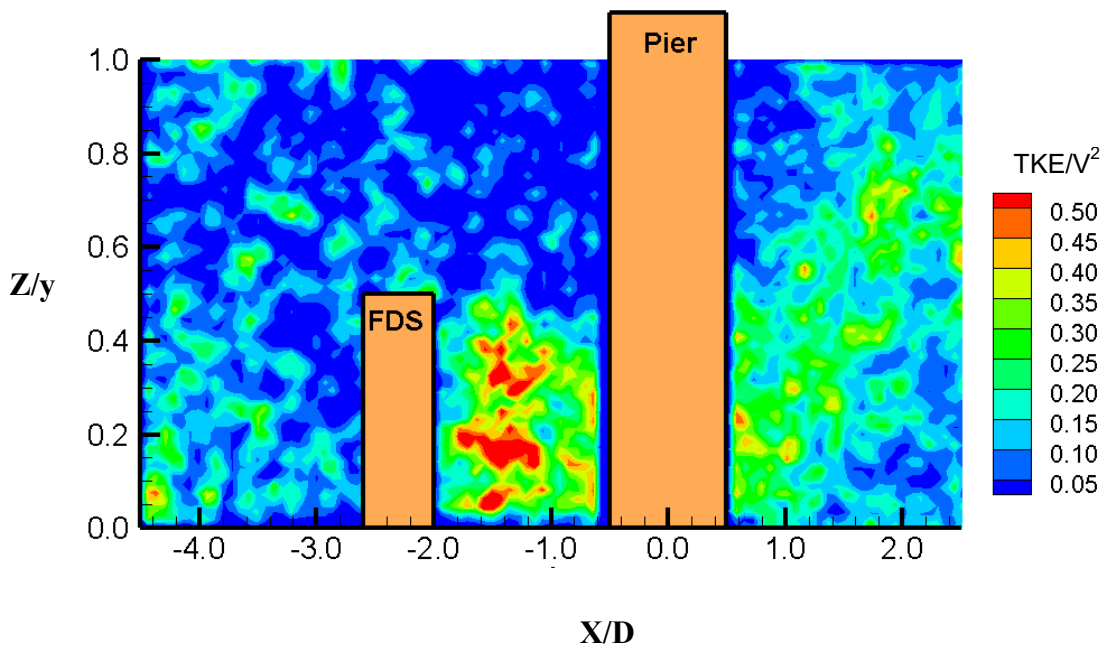


Figure 5.34. Normalised turbulent kinetic energy for the single pier case and FDS with $H/y=0.50$ at $Y/D = 0$

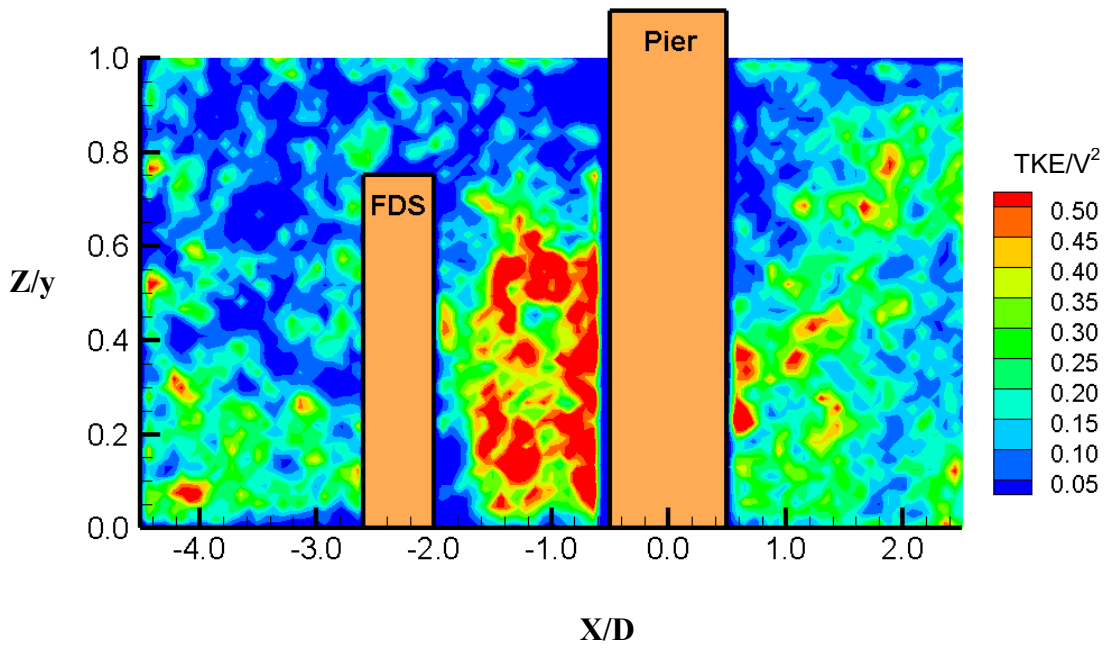


Figure 5.35. Normalised turbulent kinetic energy for the single pier case and FDS with $H/y=0.75$ at $Y/D = 0$

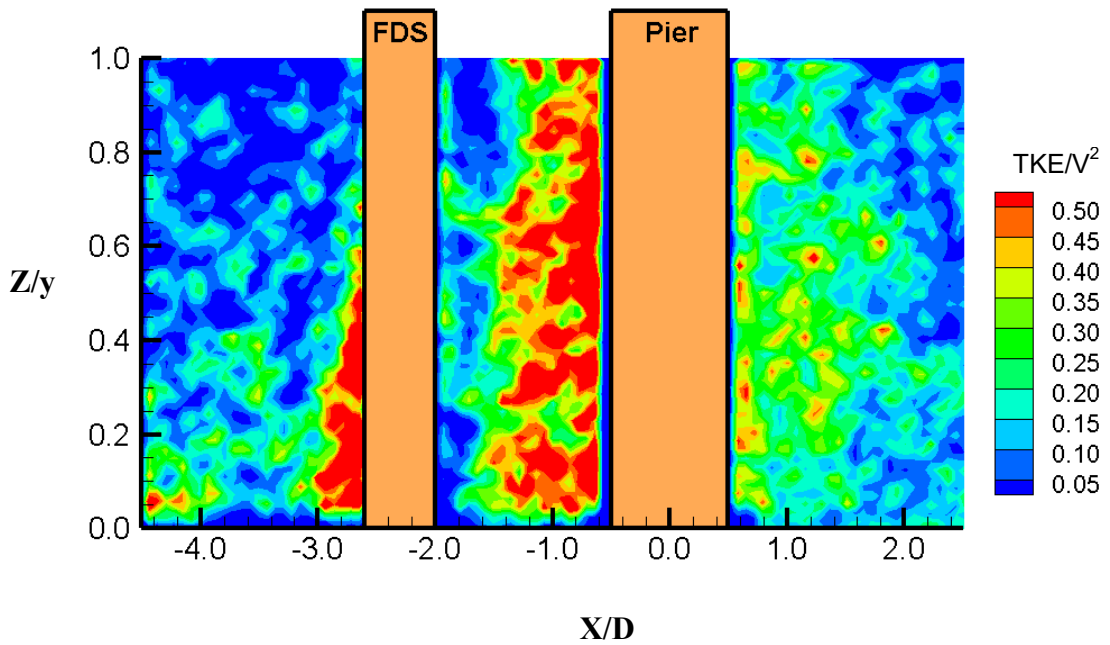


Figure 5.36. Normalised turbulent kinetic energy for the single pier case and FDS with $H/y > 1$ at $Y/D = 0$

5.4.5. Reynolds Shear Stress

The last turbulence characteristic, examined in this study, is associated with Reynolds Shear Stress (RSS). This parameter is a function of the velocity components fluctuations and the mass density of the fluid (ρ), and calculated by $RSS = -\rho\overline{u'w'}$. Here, the values of RSS are normalised by $-\rho V^2$.

The contour plots of normalised RSS for Runs 1 to 5 are illustrated in Figures 5.37 to 5.41. For the single pier case (Figure 5.37), the values of Reynolds Shear Stress at the upstream of the pier moderately increase as the flow approaches to the pier. Moreover, relatively higher values of shear stress can be seen in front of the pier near the bed. At downstream of the pier, pretty greater values of shear stress extend around two times of the pier diameter after the pier.

The distributions of Reynolds Shear Stress in the vertical plane of symmetry for Runs 2 to 5 are depicted in Figures 5.38 to 5.41. According to these plots, FDS increases the Reynolds Shear Stress in the vicinity of the pier. In all cases, the growth of RSS is more significant in the gap region and downstream of the pier rather than the upstream of the FDS. In addition, Reynolds Shear Stress increases by elevating the height of FDS.

The plots of RSS at the other vertical planes ($Y/D = 1, 2, 3,$ and 4) are presented in Appendix B. The results show that FDS increases RSS in all vertical planes except $Y/D = 2$. These results are similar to the attained results for the other turbulence characteristics. It may be due to the lateral diversion of the flow by FDS. It seems that the interactions between the flow and FDS, pier, bed and sidewall of the flume cause to increase the turbulence characteristics. However, there is a boundary at around $Y/D = 2$ where the turbulence characteristics of the flow reduced. To prove this claim, experimental study should be conducted for the horizontal plane that is beyond the objectives of this study.

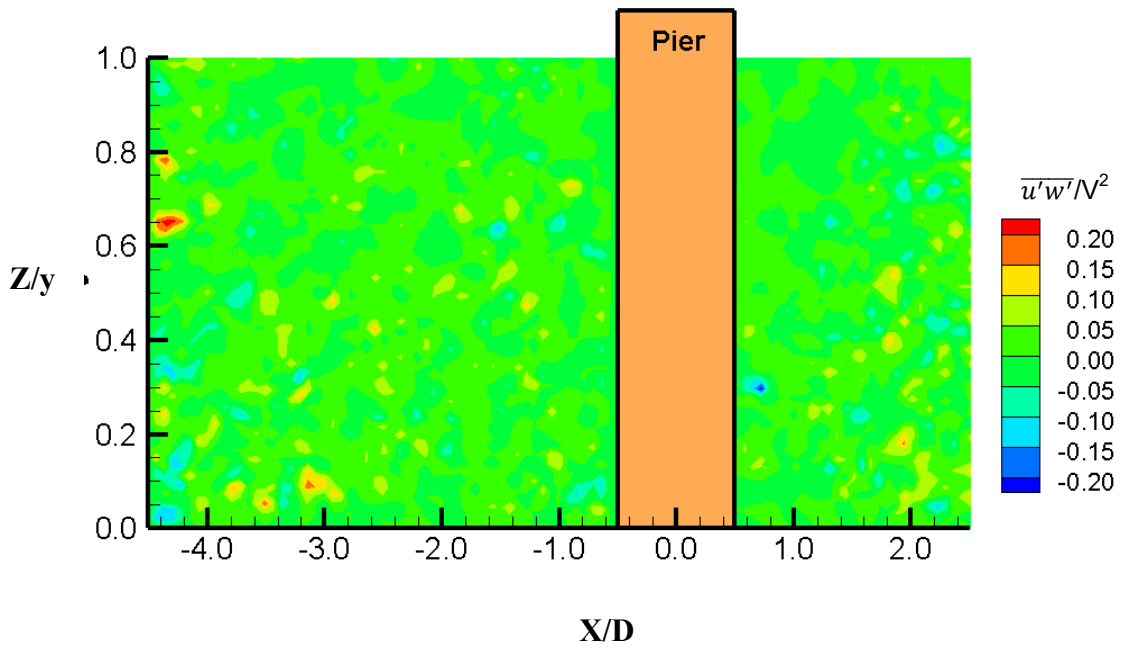


Figure 5.37. Normalised Reynolds Shear Stress for the single pier case at $Y/D = 0$

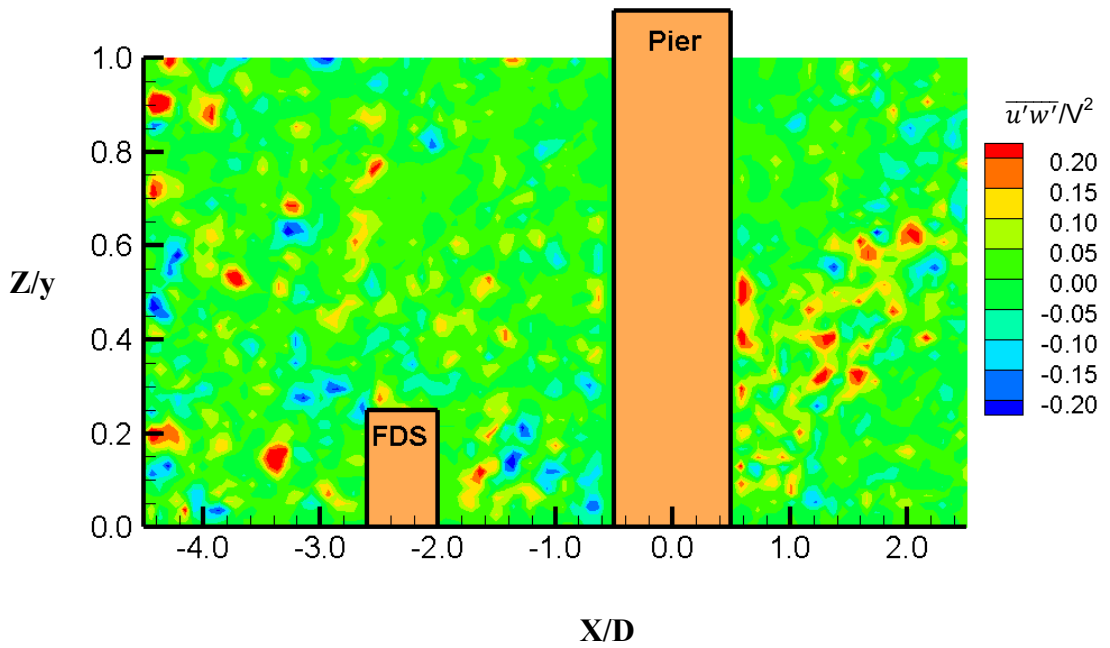


Figure 5.38. Normalised Reynolds Shear Stress for the single pier case and FDS with $H/y=0.25$ at $Y/D = 0$

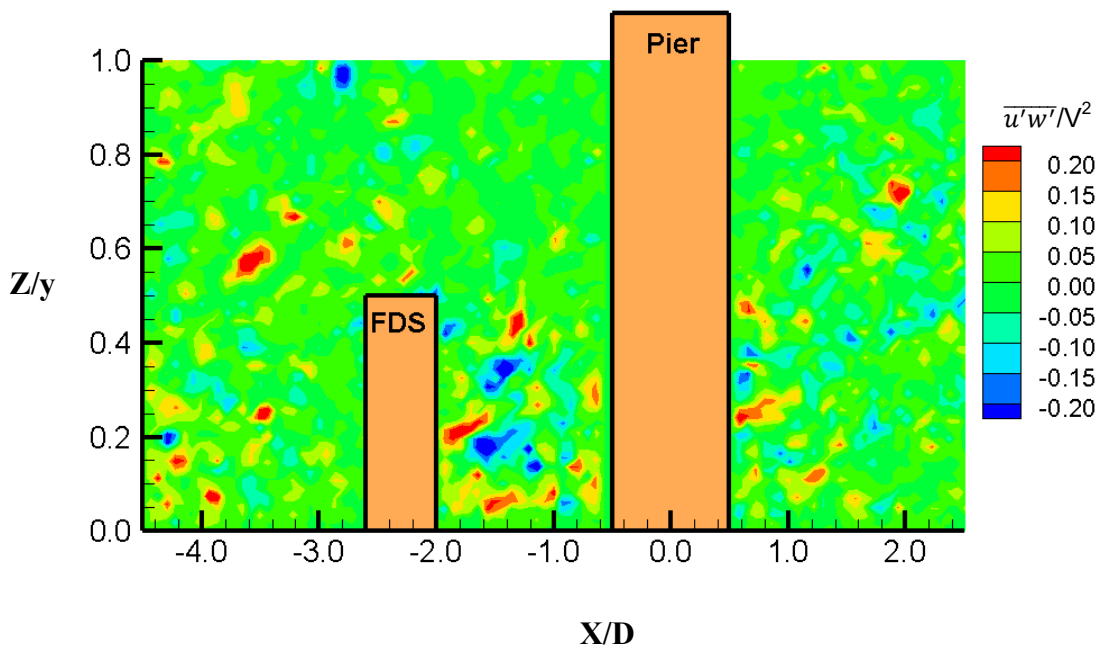


Figure 5.39. Normalised Reynolds Shear Stress for the single pier case and FDS with $H/y=0.50$ at $Y/D = 0$

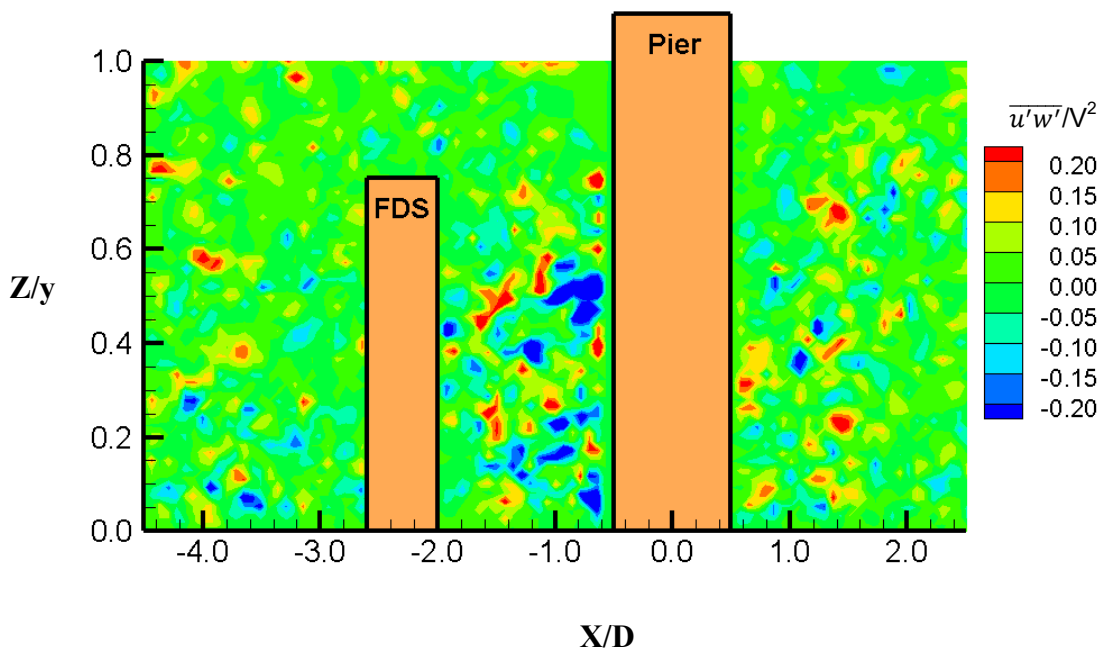


Figure 5.40. Normalised Reynolds Shear Stress for the single pier case and FDS with $H/y=0.75$ at $Y/D = 0$

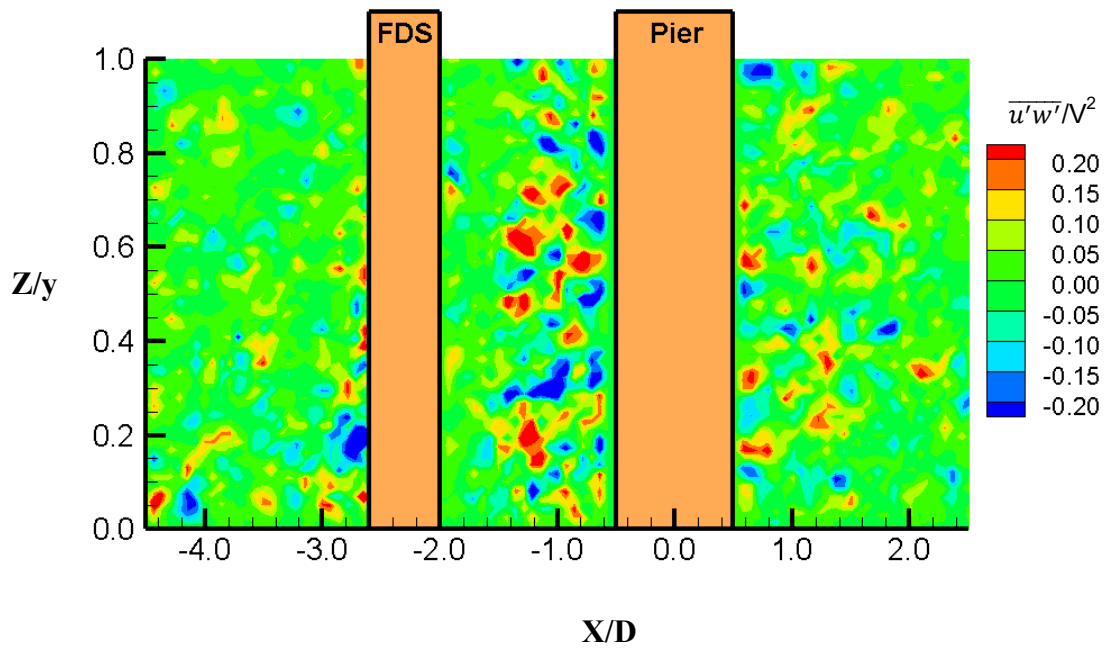


Figure 5.41. Normalised Reynolds Shear Stress for the single pier case and FDS with $H/y > 1$ at $Y/D = 0$

5.5. Conclusions

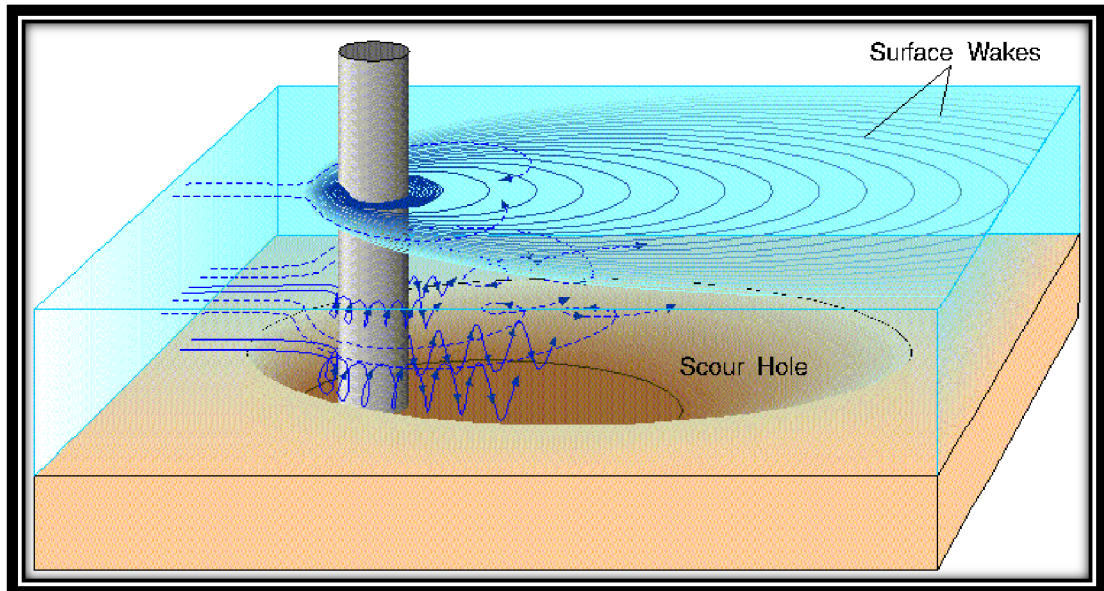
The PIV technique was used to study the effects of an optimised flow diversion structure (FDS) under different submergence ratio on the flow field around a circular bridge pier. The findings of this experimental study demonstrate that the optimised FDS significantly affects the flow field around the pier. This structure changes both the magnitude and direction of the velocity components and also diverts the streamlines at the vicinity of the pier. In fact, the bridge pier is located in a wake region, which is produced by the FDS. This wake withstands the down-flow in the gap region and also disturbs the formation of the horseshoe vortices at the pier base. Furthermore, this FDS reduces the strength of wake vortices behind the pier. All of these changes in flow field reduce the local scour around the pier. The turbulence characteristics of the flow around the pier may increase due to the formation of a wake system in the gap region between the FDS and the pier. The turbulence characteristics are the function of the fluctuating components of velocity. In addition, it may happen that the mean components of velocities decrease, but the fluctuating parts increase. Therefore, this increasing of turbulence does not necessarily increase the local scour.

The results of this study may have demonstrated that the height of FDS is an effective factor in the flow field around the pier. Referring to the results of Chapter 4, the best height for FDS to achieve the maximum reduction of local scour is about one-fourth of the water depth. Besides, the effectiveness of FDS decreases by increasing the FDS height. However, even an unsubmerged FDS can protect a pier from local scour due to the sheltering effect of FDS. These results are validated with the results of the flow field study. Elevating the FDS crest forms the stronger down-flow and wake vortices at the upstream and downstream of FDS respectively. Therefore, local scour may increase.

By and large, it can be stated that the FDS reduces the pier-scour by changing the complicated vortices systems including down-flow, horseshoe vortex and wake vortex near the pier.

CHAPTER 6

Conclusions



6.1. Summary

The results of previous studies have revealed that the bridge scour is the leading cause of waterway bridge failures. Around 60% of waterway bridge failures have occurred due to local scour and other related hydraulic issues. A bridge collapse directly affects the social and economic development of a nation and causes several problems such as injuries and fatalities, enormous financial losses, disruptions in the transportation system. Therefore, the investigation of bridge pier-scour mechanism and prediction of the amount of scour are essential. Besides, the study of the local scour countermeasure, which is the key target of this research, is more significant and crucial for reducing the risk of bridge failure.

Numerous studies have been conducted attempting to realize the mechanism of pier scour. Arising from consideration of those studies, the pier-scour is due to the formation of a complicated vortices system around the pier comprising down-flow, horseshoe vortex, and wake vortex. Therefore, an appropriate local scour countermeasure technique can be using a flow-altering device at the upstream of a pier to disturb these vortices in a manner that reduces the potential for erosion around the bridge pier.

A review of the previously published studies on upstream flow-altering devices indicates that only limited studies have been conducted in this field. Based on those studies, it can be concluded that the effectiveness of devices is a function of their shape, size, and installation location. However, the effects of these factors were not fully considered in the previous proposed upstream flow-altering devices; and still, their values are unclear. Due to the lack of information and design guidelines of these proposed devices, there is no report to use such a method in the field situation. Therefore, further investigations are required.

In this study, a new flow-altering device named flow diversion structure (FDS) has been introduced, examined, and optimised. This research has been conducted in three stages of the experimental studies in both local scour and flow field around a circular bridge pier with upstream FDS. The shape, size, and installation location of this new countermeasure against pier-scour have been thoroughly examined to address the problems mentioned earlier.

6.2. Conclusions

A comprehensive study of the effects of a proposed triangular prism flow diversion structure (FDS) on both local scour and flow field around a circular pier has been conducted as the main contribution of this research. The three stages of this research including proof of concept, optimisation of concept, and flow field are briefly presented and concluded in the following sections.

6.2.1. Proof of Concept

In the first stage, the main objective was to test a triangular FDS for local scour mitigation and to ascertain changes in the flow field arising from deployment of a triangular FDS. Three criteria have been considered to select the shape including diverting streamlines from the vicinity of pier, creating a relatively wide wake region behind the FDS, and having the lowest amount of local scour around the FDS. Based on these criteria and by reviewing the literature, a triangular prism was recognised as a proper shape.

A series of preliminary laboratory tests were conducted to evaluate the effects of this triangular prism FDS on local scour and flow field around a circular bridge pier. These tests were completed in a rectangular laboratory flume as presented in Chapter 3.

The flow diversion structure, employed in this stage, was built in a shape of prismatic of isosceles triangle with a lateral base of $0.2D$, longitudinal base of $0.5D$, and full-depth that was located at the six different spacing from the pier (i.e., $d/D = 0.5, 1, 1.5, 2, 2.5$ and 3.5 , where D is the pier diameter, and d is the clear distance between the pier and FDS). An additional test was carried out with a single pier only, as a control test. All of these tests were conducted under clear water scour condition. After achieving equilibrium condition, the bed profile was measured, and the volume of the scour-hole determined for each experimental test.

The results of local scour tests revealed that the clear distance between the proposed FDS and the pier significantly affects the reduction percentage of the local scour depth and the scour-hole volume. According to the dimension of the FDS and the pier in these

tests, the best clear distance between them to achieve the maximum yield was found to be approximately 1.5 times of the pier diameter. In this situation, the scour depth and the volume of scour-hole around the pier were reduced by 38% and 61%, respectively. In addition, the results of this study were compared to the results of a previous study using two in-line piers with the assumption that the front pier performed as a circular FDS for the rear pier. These findings are very favourable when compared with the 16% reduction in scour depth for the case of two in-line piers studied by Keshavarzi et al. (2018).

The flow field analysis was conducted in the control test, and the best performing test regarding the local scour reduction (i.e., $d/D = 1.5$). The results clearly revealed that the proposed triangular FDS affects the flow field significantly, reduces the strength of both the down-flow and horseshoe vortices and diverting the streamlines from upstream of the pier, and consequently decreases the local scour around the pier.

Based on the work conducted in this stage, this concept was proved that a triangular shape of FDS was suitable to reduce the local scour and change the flow field. In addition, the installation location of the FDS affected the performance of this countermeasure against local scour. However, the size of this triangular FDS was still unknown and needed further investigation. Therefore, the second stage of this research was completed to find out the optimum size and also the best installation location of the proposed FDS.

6.2.2. Optimisation of Concept

A comprehensive experimental study was conducted to understand the optimum size and the best installation location of the triangular prism FDS as an effective pier-scour countermeasure. In fact, the main objective of this stage was to find out the optimum value of the variables including the base (B), length (L), and height (H) of the triangular FDS, and also the best clear distance between the pier and FDS (d) as a function of pier diameter (D) and flow depth (y). Four dimensionless variables were defined (B/D, L/D, H/y, d/D) by considering pier diameter as a horizontal scale parameter, and water depth as a vertical scale parameter. Furthermore, five values were selected for each

dimensionless variable. Accordingly, 625 individual experiments were required for testing of all possible combinations of experimental variables. This number of experiments was not feasible. Hence, an efficient statistical approach to experimental design, called Taguchi's method, was employed to design the experimental program and to reduce the number of tests. This scientific method can be used to find the best values of the controllable variables with a minimum number of tests. According to Taguchi's method, 27 FDSs should be tested to find the optimum size and installation location of this structure. Besides, to compare the experimental results and to assess the effectiveness of FDS, a control test was required.

The experimental tests of this stage were conducted in a rectangular laboratory flume with dimensions as presented in section 4.4.1. The flume was equipped with a turbine insertion flow-meter to measure flow rate and a downstream rectangular flap gate to regulate the water depth. In this stage, a 3-D scanner was utilised for measuring the final bed topography very quickly and precisely, and an advanced technology of 3-D printer employed to build accurate physical models of the pier and FDSs.

Clear water scour condition was considered for all experimental runs. The parameters including hydraulic conditions, sediment properties, and pier geometries were chosen carefully regarding the presented criteria in the literature and kept constant in all tests.

At the end of all experimental tests, a sensitivity analysis of the dimensionless variables and analysis of variance have been performed with two sets of measured data including the maximum depth and the volume of scour-hole.

The outcomes demonstrated that the best width, length, and height of FDS were equals to $0.4D$, $0.6D$, and $0.25y$, respectively. Furthermore, the best clear distance between FDS and the pier was approximately between 1 and 1.5 times of the pier diameter. In the optimum situation, the maximum depth and the volume of the scour hole around the pier reduced by 40% and 60%, respectively. It is anticipated that the optimised FDS would not block debris and floating materials due to its short height. The optimum triangular FDS can be applied for both new and existing bridge piers to control and to reduce the depth and volume of local scour around them.

It may be highlighted that one of the interesting results of this stage was discovering the optimum size of FDS, which was much smaller than the pier size. In addition, the most remarkable outcome was related to the height of FDS, where the short height ($H = 0.25y$) had the best performance to reduce the pier-scour. However, the remaining question was that how this small and short FDS affects the flow field around a bridge pier? Accordingly, the third stage of this research was conducted to comprehend the answer to this critical question.

6.2.3. Flow Field

The focus of this stage was to investigate the flow field around a circular bridge pier with an optimised FDS at upstream. Therefore, an experimental study of flow field has been conducted using a Particle Image Velocimetry (PIV) system.

A rectangular flume which was used in this stage had 5 m length, 0.3 m width and 0.45 m depth. This equipped flume was connected to an electrical console that controlled the instruments such as electromotor and variable speed drive, and also displayed the flow rate which was measured by an electromagnetic flow-meter. Besides, a manual downstream flap gate was provided to regulate the water depth.

The experimental tests and the physical models (pier and FDS) were designed based on the criteria in the literature, and the obtained results from Stage two (optimisation of concept). All tests were conducted under fixed bed condition with no sediment. The optimised FDS was installed at the best location upstream of the pier ($d/D = 1.5$), and the velocity components were measured at the various planes (i.e., $Y/D = 0, 1, 2, 3$ and 4). A similar test was carried out with only a single pier without FDS as a control test.

As the water depth is an uncontrollable variable in the real condition in the field, therefore, the optimised FDS was tested in four different submergence ratios (i.e., $H/y = 0.25, 0.5, 0.75$, and >1). It should be mentioned that the water depth was kept constant in all the tests, and the height of FDS was changed.

The PIV images collected during the individual experiments were processed to determine the streamwise (u) and vertical (w) velocity components. A code was

developed using MATLAB to calculate various influencing flow characteristics including TI, TKE, and RSS, with the results plotted using Tecplot.

Analysis of the results indicated that the optimised FDS significantly affected the flow field at the upstream and downstream of the pier. This triangular prism FDS changed both the magnitude and direction of the velocity components and also diverted the streamlines at the vicinity of the pier.

In the gap region the FDS formed a wake with the bridge pier located within this wake. For the case of $H = 0.25y$, the optimum height of FDS, the wake resisted the down-flow in the gap region and disturbed the formation of horseshoe vortices around the pier. In addition, the FDS reduced the strength of the wake vortices formed by the pier and located downstream of the pier. These substantial changes in the flow field significantly reduced the pier scour. The performance of the FDS with $H = 0.5y$ was almost similar to the case of $H = 0.25y$.

By increasing the height of FDS more than $0.5y$, the strength of down-flow at the upstream of FDS, and wake vortices in the gap region between the pier and FDS increased. Accordingly, the effectiveness of the FDS for decreasing the local scour around the pier reduced. However, the local scour around a pier with even an unsubmerged FDS was less than the single pier case due to the sheltering effect of FDS.

The most exciting outcome of this stage was that the FDS might increase the turbulence characteristics around a pier, but the local scour would certainly decrease. It can be stated that the turbulence characteristics are the function of fluctuating components of the velocity. In other words, the mean components of velocities decrease, but the fluctuating parts increase. Therefore, increasing the turbulence characteristics does not necessarily induce an increase in the local scour depth.

As a final point, it can be concluded that the optimised FDS has a potential to be used as an effective countermeasure against local pier-scour for both new and already existing bridges. This innovative small structure reduces the pier-scour by changing the complicated vortices systems formed around the pier including down-flow, horseshoe vortex, and wake vortex. It is necessary to state that rivers located in the upland mountain region are high energy rivers. Those rivers in the riverine estuarine region are

low energy rivers. The current study has been conducted for low energy rivers where the majority of people reside.

6.3. Recommendations

In this research, a flow diversion structure (FDS) has been introduced for reducing the local scour around a bridge pier. Some series of the experimental studies were conducted to test, optimise, and understand the performance of this structure for reducing the local scour around a single circular pier. The results show that the optimised FDS is an effective countermeasure against pier-scour. According to the main outcomes of this research, the following recommendations are proposed to extend the application of this innovative method in the real situation.

- 1- In this research, the performance of the proposed FDS has been studied with only one single circular pier. However, in real situations, most bridges comprise multiple piers in tandem or side by side arrangements. Therefore, the study of the effects of the proposed FDS on local scour for the case of multiple piers is necessary, especially for two cases including two piers with the tandem or side by side arrangements.
- 2- Bridge piers are designed and constructed with different shapes. Hence, investigating the performance of the proposed flow diversion structure in reduction of the local scour around various shapes of bridge piers is recommended.
- 3- Due to the limitations of the available laboratory facilities, all the experimental tests in this research were conducted under clear water scour condition. Previous investigations have revealed that scour under clear water conditions is maximised near the threshold velocity and typically will be greater than live bed conditions. Nonetheless, it is recommended to carry out an array of tests to study the influence of FDS on the local scour reduction under live bed conditions to confirm previous outcomes remain valid for the situation considered here.
- 4- In most rivers, the flow is unidirectional, but in some situation, especially in the coastal area, the flow may be bidirectional due to the tidal condition. Therefore, the

study of the effects of FDS on local scour around a bridge pier under tidal flow condition may be useful.

- 5- From the economic point of view, the numerical modelling of the proposed FDS in different conditions is highly recommended. The valuable experimental data of this study can be used to validate the numerical outputs.
- 6- The best height of FDS is equal to 0.25 water depth. As the water depth in the real situation is a variable parameter, it can be recommended to build an intelligent FDS with an automatic adjustable height to have the maximum performance of FDS in all conditions.

References

- Abdelhaleem, F.S.F. 2019, 'Roughened bridge piers as a scour countermeasure under clear water conditions', *ISH Journal of Hydraulic Engineering*, vol. 25, no. 1, pp. 94-103.
- Ahmed, F. & Rajaratnam, N. 1997, 'The three-dimensional turbulent boundary layer flow around bridge piers', *Journal of Hydraulic Research*, vol. 35, no. 2, pp. 209-24.
- Al-Shukur, A.-H.K. & Obeid, Z.H. 2016, 'Experimental Study of Bridge Pier Shape to Minimize Local Scour', *International Journal of Civil Engineering and Technology*, vol. 7, no. 1, pp. 162-71.
- Arneson, L., Zevenbergen, L., Lagasse, P. & Clopper, P. 2012, *Evaluating scour at bridges, Fifth Edition*, Hydraulic Engineering Circular No. 18, Federal Highway Administration, Washington, DC.
- Ataie-Ashtiani, B. & Aslani-Kordkandi, A. 2013, 'Flow Field Around Single and Tandem Piers', *Flow, turbulence and combustion*, vol. 90, no. 3, pp. 471-90.
- Ataie-Ashtiani, B. & Beheshti, A. 2006, 'Experimental investigation of clear-water local scour at pile groups', *Journal of Hydraulic Engineering*, vol. 132, no. 10, pp. 1100-4.
- Bagchi, T.P. 1993, *Taguchi methods explained: Practical steps to robust design*, Prentice-Hall of India Private Limited, New Delhi, India.
- Baker, C. 1980, 'The turbulent horseshoe vortex', *Journal of Wind Engineering and Industrial Aerodynamics*, vol. 6, no. 1-2, pp. 9-23.
- Beg, M. & Beg, S. 2013, 'Scour reduction around bridge piers: A review', *International Journal of Engineering Inventions*, vol. 2, no. 7, pp. 7-15.
- Beheshti, A. & Ataie-Ashtiani, B. 2016, 'Scour hole influence on turbulent flow field around complex bridge piers', *Flow, Turbulence and Combustion*, vol. 97, no. 2, pp. 451-74.
- Beheshti, A.A. & Ataie-Ashtiani, B. 2010, 'Experimental study of Three-Dimensional Flow Field around a Complex Bridge Pier', *Journal of Engineering Mechanics, ASCE*, vol. 136, no. 2, pp. 143-54.
- Box, G.E., Hunter, W.G. & Hunter, J.S. 1978, *Statistics for experimenters*, John Wiley & Sons, Inc., New York, USA.

- Breusers, H., Nicollet, G. & Shen, H. 1977, 'Local scour around cylindrical piers', *Journal of Hydraulic Research*, vol. 15, no. 3, pp. 211-52.
- Breusers, H. & Raudkivi, A. 1991, *Scouring: Hydraulic Structures Design Manual Series*, CRC Press, Balkema Rotterdam, Netherlands.
- Brice, J.C. & Blodgett, J. 1978, *Countermeasures for Hydraulic Problems at Bridges: Analysis and assessment*, vol. 1, Office of Research and Development, Federal Highway Administration, USA.
- Chang, W.-Y., Constantinescu, G., Lien, H.-C., Tsai, W.-F., Lai, J.-S. & Loh, C.-H. 2013, 'Flow structure around bridge piers of varying geometrical complexity', *Journal of Hydraulic Engineering*, vol. 139, no. 8, pp. 812-26.
- Chiew, Y.-M. 1992, 'Scour protection at bridge piers', *Journal of Hydraulic Engineering*, vol. 118, no. 9, pp. 1260-9.
- Chiew, Y.-M. 1995, 'Mechanics of riprap failure at bridge piers', *Journal of Hydraulic Engineering*, vol. 121, no. 9, pp. 635-43.
- Chiew, Y.-M. 2004, 'Local scour and riprap stability at bridge piers in a degrading channel', *Journal of Hydraulic Engineering*, vol. 130, no. 3, pp. 218-26.
- Chiew, Y.-M. & Lim, F.-H. 2000, 'Failure behavior of riprap layer at bridge piers under live-bed conditions', *Journal of Hydraulic Engineering*, vol. 126, no. 1, pp. 43-55.
- Chiew, Y. 2002, 'Failure mechanisms of riprap layer around bridge piers', *First International Conference on Scour of Foundations*, Texas, USA.
- Chiew, Y. & Lim, S. 2003, 'Protection of bridge piers using a sacrificial sill', *Proceedings of the Institution of Civil Engineers-Water and Maritime Engineering*, vol. 156, Thomas Telford Ltd, pp. 53-62.
- Chiew, Y.M. 1984, 'Local scour at bridge piers', PhD Thesis, Department of Civil Engineering, University of Auckland, Auckland, New Zealand.
- Croad, R.N. 1997, *Protection from scour of bridge piers using riprap*, Transfund New Zealand research report, no. 82., Wellington, New Zealand.
- Dargahi, B. 1989, 'The turbulent flow field around a circular cylinder', *Experiments in Fluids*, vol. 8, no. 1, pp. 1-12.
- Dargahi, B. 1990, 'Controlling mechanism of local scouring', *Journal of Hydraulic Engineering*, vol. 116, no. 10, pp. 1197-214.

- David, F. 1994, *Waterway Design: A Guide to the Hydraulic Design of Bridges, Culverts and Floodways*, Austroads, Sydney, Australia.
- Debnath, K., Manik, M. & Mazumder, B. 2012, 'Turbulence statistics of flow over scoured cohesive sediment bed around circular cylinder', *Advances in water resources*, vol. 41, pp. 18-28.
- Dey, S. & Raikar, R.V. 2007, 'Characteristics of horseshoe vortex in developing scour holes at piers', *Journal of Hydraulic Engineering*, vol. 133, no. 4, pp. 399-413.
- Dey, S., Sumer, B.M. & Fredsøe, J. 2006, 'Control of scour at vertical circular piles under waves and current', *Journal of Hydraulic Engineering*, vol. 132, no. 3, pp. 270-9.
- Doddamani, M. & Kulkarni, S. 2011, 'Dynamic response of fly ash reinforced functionally graded rubber composite sandwiches-a Taguchi approach', *International Journal of Engineering, Science and Technology*, vol. 3, no. 1.
- El-Razek, M., El-Motaleb, M.A. & Bayoumy, M. 2003, 'Scour reduction around bridge piers using internal openings through the pier', *Alexandria Engineering Journal*, vol. 42, no. 2, pp. 241-8.
- Emerson, B., Mondragon, U., Acharya, V., Shin, D.-H., Brown, C., McDonell, V. & Lieuwen, T. 2013, 'Velocity and flame wrinkling characteristics of a transversely forced, bluff-body stabilized flame, part I: experiments and data analysis', *Combustion Science and Technology*, vol. 185, no. 7, pp. 1056-76.
- Ettema, R. 1976, 'Influence of bed material gradation on local scour', M.Eng Thesis, Department of Civil Engineering, University of Auckland, Auckland, New Zealand.
- Ettema, R. 1980, 'Scour at bridge piers', PhD Thesis, Department of Civil Engineering, University of Auckland, Auckland, New Zealand.
- Ettema, R., Constantinescu, G. & Melville, B. 2011, *Evaluation of bridge scour research: Pier scour processes and predictions*, NCHRP Report 175, Washington D.C, USA.
- Ettema, R., Constantinescu, G. & Melville, B.W. 2017, 'Flow-field complexity and design estimation of pier-scour depth: Sixty years since Laursen and Toch', *Journal of Hydraulic Engineering*, vol. 143, no. 9.

- Faheem Sadeque, M., Rajaratnam, N. & Loewen, M.R. 2009, 'Shallow turbulent wakes behind bed-mounted cylinders in open channels', *Journal of Hydraulic Research*, vol. 47, no. 6, pp. 727-43.
- Farraday, R. & Charlton, F. 1983, *Hydraulic factors in bridge design*, Hydraulics Research, Wallingford, UK.
- Fotherby, L.M. 1992, 'Footings, mats, grout bags, and tetrapods: Protection methods against local scour at bridge piers', Msc Thesis, Colorado State University, Fort Collins, CO, USA.
- Fouli, H. & Elsebaie, I.H. 2016, 'Reducing local scour at bridge piers using an upstream subsidiary triangular pillar', *Arabian Journal of Geosciences*, vol. 9, no. 12, pp. 598-606.
- Froehlich, D.C. 2013, 'Protecting bridge piers with loose rock riprap', *Journal of Applied Water Engineering and Research*, vol. 1, no. 1, pp. 39-57.
- Garg, V., Setia, B. & Verma, D. 2008, 'Prevention of scour by combination of scour protection devices around bridge piers', *Proc. River Flow*, pp. 1637-43.
- Gautam, P., Eldho, T., Mazumder, B. & Behera, M. 2019, 'Experimental study of flow and turbulence characteristics around simple and complex piers using PIV', *Experimental Thermal and Fluid Science*, vol. 100, pp. 193-206.
- Gogus, M. & Dogan, A.E. 2010, 'Effects of Collars on Scour Reduction at Bridge Abutments', *Scour and Erosion*, pp. 997-1007.
- Goharzadeh, A. & Molki, A., 2014. 'Measurement of fluid velocity development behind a circular cylinder using particle image velocimetry (PIV)', *European Journal of Physics*, 36(1), p.015001.
- Grimaldi, C., Gaudio, R., Calomino, F. & Cardoso, A.H. 2009a, 'Control of scour at bridge piers by a downstream bed sill', *Journal of Hydraulic Engineering*, vol. 135, no. 1, pp. 13-21.
- Grimaldi, C., Gaudio, R., Calomino, F. & Cardoso, A.H. 2009b, 'Countermeasures against local scouring at bridge piers: slot and combined system of slot and bed sill', *Journal of Hydraulic Engineering*, vol. 135, no. 5, pp. 425-31.
- Gu, Z. 1996, 'On interference between two circular cylinders at supercritical Reynolds number', *Journal of Wind Engineering and Industrial Aerodynamics*, vol. 62, no. 2-3, pp. 175-90.

- Gunes, S., Manay, E., Senyigit, E. & Ozceyhan, V. 2011, 'A Taguchi approach for optimization of design parameters in a tube with coiled wire inserts', *Applied Thermal Engineering*, vol. 31, no. 14-15, pp. 2568-77.
- Gupta, A. & Gangadharaiyah, T. 1992, 'Local scour reduction by a delta wing-like passive device', *Proceeding of 8th Congress of Asia & Pacific Reg*, Pune, India.
- Hajikandi, H. & Golnabi, M. 2017, 'Y-shaped and T-shaped slots in river bridge piers as scour countermeasures', *Proceedings of the Institution of Civil Engineers-Water Management*, vol. 171, Thomas Telford Ltd, pp. 253-63.
- Hamill, L. 1998, *Bridge hydraulics*, CRC Press, Boca Raton, Florida, USA.
- Haque, M.A., Rahman, M.M., Islam, G.T. & Hussain, M.A. 2007, 'Scour mitigation at bridge piers using sacrificial piles', *International Journal of Sediment Research*, vol. 22, no. 1, p. 49.
- Heidarpour, M. 2002, 'Control and reduction of local scour at bridge piers by using slot', *Proc. River Flow*, pp. 1069-72.
- Heidarpour, M., Khodarahmi, Z. & Mousavi, S. 2003, 'Control and reduction of local scour at bridge pier groups using slot', *Proceedings, XXX IAHR Congress, Thessaloniki, Greece, August*, pp. 24-9.
- Huang, C., Tang, C. & Kuo, T. 2005, 'Use of surface guide panels as pier scour countermeasures', *International Journal of Sediment Research*, vol. 20, no. 2, p. 117.
- ILA-GmbH 2004, *Introduction to VidPIV User Manual*, ILA GmbH, Juelich, Germany.
- Karimae Tabarestani, M. & Zarrati, A.R. 2015, 'Design of riprap stone around bridge piers using empirical and neural network method', *Civil Engineering Infrastructures Journal*, vol. 48, no. 1, pp. 175-88.
- Karimaei Tabarestani, M. & Zarrati, A.R. 2019, 'Reliability analysis of riprap stability around bridge piers', *Journal of Applied Water Engineering and Research*, vol. 7, no. 1, pp. 79-88.
- Keshavarzi, A., Melville, B. & Ball, J. 2014, 'Three-dimensional analysis of coherent turbulent flow structure around a single circular bridge pier', *Environmental Fluid Mechanics*, vol. 14, no. 4, pp. 821-47.
- Keshavarzi, A., Shrestha, C.K., Melville, B., Khabbaz, H., Ranjbar-Zahedani, M. & Ball, J. 2018, 'Estimation of maximum scour depths at upstream of front and rear

- piers for two in-line circular columns', *Environmental Fluid Mechanics*, vol. 18, no. 2, pp. 537-50.
- Keshavarzi, A., Shrestha, C.K., Zahedani, M.R., Ball, J. & Khabbaz, H. 2017, 'Experimental study of flow structure around two in-line bridge piers', *Proceedings of the Institution of Civil Engineers - Water Management*, pp. 1-17.
- Khodashenas, S.R., Shariati, H. & Esmaeeli, K. 2018, 'Comparison between the circular and square collar in reduction of local scouring around bridge piers', *E3S Web of Conferences*, vol. 40, EDP Sciences, p. 03002.
- Kirkil, G., Constantinescu, G. & Ettema, R. 2009, 'Detached eddy simulation investigation of turbulence at a circular pier with scour hole', *Journal of Hydraulic Engineering*, vol. 135, no. 11, pp. 888-901.
- Kirkil, G., Constantinescu, S. & Ettema, R. 2008, 'Coherent structures in the flow field around a circular cylinder with scour hole', *Journal of Hydraulic Engineering*, vol. 134, no. 5, pp. 572-87.
- Kumar, A. & Kothiyari, U.C. 2011, 'Three-dimensional flow characteristics within the scour hole around circular uniform and compound piers', *Journal of Hydraulic Engineering*, vol. 138, no. 5, pp. 420-9.
- Kumar, V., Raju, K.G.R. & Vittal, N. 1999, 'Reduction of local scour around bridge piers using slots and collars', *Journal of Hydraulic Engineering*, vol. 125, no. 12, pp. 1302-5.
- Kumcu, S.Y., Kokpinar, M.A. & Gogus, M. 2014, 'Scour protection around vertical-wall bridge abutments with collars', *KSCE Journal of Civil Engineering*, vol. 18, no. 6, pp. 1884-95.
- Lagasse, P.F., Clopper, P., Zevenbergen, L. & Ruff, J. 2006, *Riprap Design Criteria, Recommended Specifications, and Quality Control*, NCHRP Report 568, Transportation Research Board of the National Academies, Washington, DC, USA.
- Lagasse, P.F., Clopper, P., Zevenbergen, L. & Girard, L. 2007, *Countermeasures to Protect Bridge Piers from Scour*, NCHRP Report 593, Transportation Research Board of the National Academies, Washington, DC, USA.
- Lauchlan, C.S. 1999, 'Pier scour countermeasures', PhD Thesis, Civil and Resource Engineering, University of Auckland, Auckland, New Zealand.
- Lauchlan, C.S. & Melville, B.W. 2001, 'Riprap protection at bridge piers', *Journal of Hydraulic Engineering*, vol. 127, no. 5, pp. 412-8.

- Laursen, E.M. & Toch, A. 1956, *Scour around bridge piers and abutments*, Iowa Highway Research, Iowa, USA.
- Lee, G.C., Mohan, S., Huang, C. & Fard, B.N. 2013, *A study of US bridge failures (1980-2012)*, Technical Report MCEER-13-0008, U.S. Department of Transportation, Washington DC, USA.
- Lim, F.-H. & Chiew, Y.-M. 2001, 'Parametric study of riprap failure around bridge piers', *Journal of Hydraulic Research*, vol. 39, no. 1, pp. 61-72.
- Lin, J.-C., Yang, Y. & Rockwell, D. 2002, 'Flow past two cylinders in tandem: instantaneous and averaged flow structure', *Journal of Fluids and Structures*, vol. 16, no. 8, pp. 1059-71.
- Link, O., Henríquez, S. and Ettmer, B., 2019. 'Physical scale modelling of scour around bridge piers', *Journal of Hydraulic Research*, 57(2), pp.227-237.
- Martinuzzi, R. & Tropea, C. 1993, 'The flow around surface-mounted, prismatic obstacles placed in a fully developed channel flow', *Journal of Fluids Engineering*, vol. 115, pp. 85-.
- Mashahir, M.B., Zarrati, A.R. & Mokallaf, E. 2009, 'Application of riprap and collar to prevent scouring around rectangular bridge piers', *Journal of Hydraulic Engineering*, vol. 136, no. 3, pp. 183-7.
- Mashahir, M.B., Zarrati, A.R. & Rezayi, M. 2004, 'Time development of scouring around a bridge pier protected by collar', *Proceedings 2nd International Conference on Scour and Erosion (ICSE-2)*, Singapore.
- Max Sheppard, D. 2004, 'Overlooked local sediment scour mechanism', *Transportation Research Record: Journal of the Transportation Research Board*, no. 1890, pp. 107-11.
- Melville, B. 1992, 'Local scour at bridge abutments', *Journal of Hydraulic Engineering*, vol. 118, no. 4, pp. 615-31.
- Melville, B. 2008, 'The physics of local scour at bridge piers', *Fourth International Conference on Scour and Erosion*, pp. 28-38.
- Melville, B. & Sutherland, A. 1988, 'Design method for local scour at bridge piers', *Journal of Hydraulic Engineering*, vol. 114, no. 10, pp. 1210-26.
- Melville, B.W. 1975, 'Local scour at bridge sites', PhD Thesis, School of Engineering, University of Auckland, Auckland, New Zealand.

- Melville, B.W. & Chiew, Y.-M. 1999, 'Time scale for local scour at bridge piers', *Journal of Hydraulic Engineering*, vol. 125, no. 1, pp. 59-65.
- Melville, B.W. & Coleman, S.E. 2000, *Bridge scour*, Water Resources Publication, LLC, Colorado, USA.
- Melville, B.W. & Hadfield, A.C. 1999, 'Use of sacrificial piles as pier scour countermeasures', *Journal of Hydraulic Engineering*, vol. 125, no. 11, pp. 1221-4.
- Melville, B.W., Lauchlan, C.S. & Hadfield, A.C. 1997, 'Bridge Pier Scour Countermeasures', paper presented to the *Proceedings of the Conference on Management of Landscapes Disturbed by Channel Incision: Stabilization, Rehabilitation, Restoration*, Oxford Campus, University of Mississippi, USA.
- Melville, B.W. & Raudkivi, A.J. 1977, 'Flow characteristics in local scour at bridge piers', *Journal of Hydraulic Research*, vol. 15, no. 4, pp. 373-80.
- Meneghini, J., Saltara, F., Siqueira, C. & Ferrari, J. 2001, 'Numerical simulation of flow interference between two circular cylinders in tandem and side-by-side arrangements', *Journal of fluids and structures*, vol. 15, no. 2, pp. 327-50.
- Menon, P., Kandiah, K., Mandeep, J., Shaari, S. & Apte, P. 2012, 'Near field and far field effects in the Taguchi-optimized design of an InP/GaAs-based double wafer-fused MQW long-wavelength vertical-cavity surface-emitting laser', *Journal of Nonlinear Optical Physics & Materials*, vol. 21, no. 01, p. 1250006.
- Moncada-M, A., Aguirre-Pe, J., Bolivar, J. & Flores, E. 2009, 'Scour protection of circular bridge piers with collars and slots', *Journal of Hydraulic Research*, vol. 47, no. 1, pp. 119-26.
- Mori, T. 2011, *Taguchi methods: benefits, impacts, mathematics, statistics, and applications*, ASME Press, New York, USA.
- Muzzammil, M. & Gangadhariah, T. 2003, 'The mean characteristics of horseshoe vortex at a cylindrical pier', *Journal of Hydraulic Research*, vol. 41, no. 3, pp. 285-97.
- Neill, C.R. 1973, *Guide to bridge hydraulics*, University of Toronto Press, Toronto.
- Odgaard, A.J. & Wang, Y. 1987, 'Scour prevention at bridge piers', *Hydraulic Engineering*, ASCE, pp. 523-7.
- Odgaard, A.J. & Wang, Y. 1991, 'Sediment management with submerged vanes. I: Theory', *Journal of Hydraulic Engineering*, vol. 117, no. 3, pp. 267-.

- Parker, G., Toro-Escobar, C. & Voigt Jr, R.L. 1998, *Countermeasures to protect bridge piers from scour*, 433.2, vol. 2, Transportation Research Board, Washington DC, USA.
- Parola, A. 1993, 'Stability of riprap at bridge piers', *Journal of Hydraulic Engineering*, vol. 119, no. 10, pp. 1080-93.
- Parola, A. 1995, 'Boundary stress and stability of riprap at bridge piers', *River, Coastal, and Shoreline Protection. CR Thorne et al*, pp. 149-59.
- Parola, A., Jones, J. & Miller, A. 1989, 'Model Study on the Stability of Riprap Placed in Local Scour Holes at Bridge Piers', *Proceedings of the Bridge Scour Symposium*, Interagency Advisory Committee on Water Data, Virginia, USA.
- Phadke, M.S. 1995, *Quality engineering using robust design*, Prentice Hall PTR, New Jersey, USA.
- Pope, S.B. 2000, *Turbulent flows*, Cambridge University Press Cambridge, USA.
- Qadar, A. 1981, 'The vortex scour mechanism at bridge piers', *Proceedings of the Institution of Civil Engineers*, vol. 71, no. 3, pp. 739-57.
- Quazi, M. & Peterson, A. 1973, 'A method for bridge pier riprap design', *Proceedings of 1st Canadian Hydraulic Conference*, pp. 96-106.
- Rajagopalan, S. & Antonia, R. 2005, 'Flow around a circular cylinder—structure of the near wake shear layer', *Experiments in fluids*, vol. 38, no. 4, pp. 393-402.
- Ranjbar-Zahedani, M., Keshavarzi, A. & Khabbaz, H. 2017, 'Control of local scour at vicinity of bridge piers using flow diversion structure', *Proceedings of the 37th IAHR World Congress*, Kuala Lumpur, Malaysia.
- Ranjbar-Zahedani, M., Keshavarzi, A., Khabbaz, H. & Ball, J. 2018, 'Protecting bridge pier against local scour using flow diversion structure', *Proceedings of the Institution of Civil Engineers-Water Management*, pp. 1-26.
- Ranjbar-Zahedani, Khabbaz, H. & Ball, J. 2020, 'Flow field around a circular bridge pier with an upstream triangular prism using Particle Image Velocimetry', *Dataset*, UTS Stash. <https://doi.org/10.26195/bf5n-0n94>.
- Richardson, E. & Davis, S. 2001, 'Evaluating scour at bridges (HEC-18)', *US Department of Transportation, Federal Highway Administration, Colorado, 4th edn. FHWA NHI*, pp. 01-001.
- Richardson, E.V. & Davis, S.R. 1995, *Evaluating scour at bridges*, FHWA-IP 90-017, Federal Highway Administration, Washington DC, USA.

- Richardson, J. & York, K. 1999, 'Hydrodynamic countermeasures for local pier scour', *Transportation Research Record: Journal of the Transportation Research Board*, no. 1690, pp. 186-92.
- Richardson, J.E. & Panchang, V.G. 1998, 'Three-dimensional simulation of scour-inducing flow at bridge piers', *Journal of Hydraulic Engineering*, vol. 124, no. 5, pp. 530-40.
- Roshko, A. 1954, *On the drag and shedding frequency of two-dimensional bluff bodies*, Technical Note 3169, National Advisory Committee for Aeronautics, Washington, USA.
- Roulund, A., Sumer, B.M., Fredsøe, J. & Michelsen, J. 2005, 'Numerical and experimental investigation of flow and scour around a circular pile', *Journal of Fluid Mechanics*, vol. 534, pp. 351-401.
- Roy, R.K. 2010, *A primer on the Taguchi method*, Second edn, Society of Manufacturing Engineers, Dearborn, Michigan, USA.
- Sahin, B., Ozturk, N.A. & Akilli, H. 2007, 'Horseshoe vortex system in the vicinity of the vertical cylinder mounted on a flat plate', *Flow Measurement and Instrumentation*, vol. 18, no. 2, pp. 57-68.
- Salamatian, S.A. & Zarrati, A.R. 2019, 'Reliability study on uncertainty parameters and flood duration on scouring around unprotected and protected bridge piers', *ISH Journal of Hydraulic Engineering*, pp. 1-9.
- Sarkar, K., Chakraborty, C. & Mazumder, B. 2016, 'Variations of bed elevations due to turbulence around submerged cylinder in sand beds', *Environmental Fluid Mechanics*, vol. 16, no. 3, pp. 659-93.
- Sheppard, D., Melville, B. & Demir, H. 2013, 'Evaluation of existing equations for local scour at bridge piers', *Journal of Hydraulic Engineering*, vol. 140, no. 1, pp. 14-23.
- Shrestha, C.K. 2015, 'Bridge pier flow interaction and its effect on the process of scouring', PhD Thesis, School of Civil and Environmental Engineering, University of Technology Sydney, Sydney, Australia.
- Sii, H.S., Ruxton, T. & Wang, J. 2001, 'Taguchi concepts and their applications in marine and offshore safety studies', *Journal of Engineering Design*, vol. 12, no. 4, pp. 331-58.

- Singh, C., Setia, B. & Verma, D. 2001, 'Collar-sleeve combination as a scour protection device around a circular pier', *29th IAHR World Congress*, Beijing, China, pp. 202-9.
- Singh, N.B., Devi, T.T. & Kumar, B. 2020, 'The local scour around bridge piers—a review of remedial techniques', *ISH Journal of Hydraulic Engineering*, pp. 1-14.
- Smith, D. 1976, 'Bridge failures', *Proceedings of the institution of civil engineers*, vol. 60, no. 3, pp. 367-82.
- Sontek, A. 1997, 'Operation manual, firmware version 4.0', *Sontek, San Diego*.
- Suaznabar, O., Bojanowski, C., Lottes, S., Shen, J., Kerenyi, K. & Kilgore, R. 2017, *Advanced Methodology to Assess Riprap Rock Stability at Bridge Piers and Abutments*, FHWA-HRT-17-054, Federal Highway Administration, Virginia, USA.
- Sumer, B.M. & Fredsøe, J. 2002, *The Mechanics of Scour in the Marine Environment*, vol. 17, World Scientific, Singapore.
- Sumner, D. 2010, 'Two circular cylinders in cross-flow: a review', *Journal of Fluids and Structures*, vol. 26, no. 6, pp. 849-99.
- Sumner, D., Price, S. & Paidoussis, M. 2000, 'Flow-pattern identification for two staggered circular cylinders in cross-flow', *Journal of Fluid Mechanics*, vol. 411, pp. 263-303.
- Tabarestani, M.K. & Zarrati, A. 2012, 'Design of stable riprap around aligned and skewed rectangular bridge piers', *Journal of hydraulic engineering*, vol. 139, no. 8, pp. 911-6.
- Tafarjnoruz, A., Gaudio, R. & Dey, S. 2010, 'Flow-altering countermeasures against scour at bridge piers: a review', *Journal of Hydraulic Research*, vol. 48, no. 4, pp. 441-52.
- Taricska, M. 2014, 'An Analysis of Recent Bridge Failures (2000-2012)', MSc Thesis, School of Civil Engineering, Ohio State University, Ohio, USA.
- Unger, J. & Hager, W.H. 2006, 'Riprap failure at circular bridge piers', *Journal of Hydraulic Engineering*, vol. 132, no. 4, pp. 354-62.
- Unger, J. & Hager, W.H. 2007, 'Down-flow and horseshoe vortex characteristics of sediment embedded bridge piers', *Experiments in Fluids*, vol. 42, no. 1, pp. 1-19.
- Van Rijn, L.C. 1993, *Principles of sediment transport in rivers, estuaries and coastal seas*, Aqua publications, Amsterdam, The Netherlands.

- Veerappadevaru, G., Gangadharaiyah, T. & Jagadeesh, T.R. 2011, 'Vortex scouring process around bridge pier with a caisson', *Journal of Hydraulic Research*, vol. 49, no. 3, pp. 378-83.
- Vijayasree, B., Eldho, T., Mazumder, B. & Ahmad, N. 2019, 'Influence of bridge pier shape on flow field and scour geometry', *International Journal of River Basin Management*, vol. 17, no. 1, pp. 109-29.
- Vittal, N., Kothiyari, U. & Haghigat, M. 1994, 'Clear-water scour around bridge pier group', *Journal of Hydraulic Engineering*, vol. 120, no. 11, pp. 1309-18.
- Wang, C., Yu, X. & Liang, F. 2017, 'A review of bridge scour: mechanism, estimation, monitoring and countermeasures', *Natural Hazards*, vol. 87, no. 3, pp. 1881-906.
- Wardhana, K. & Hadipriono, F.C. 2003, 'Analysis of Recent Bridge Failures in the United States', *Journal of Performance of Constructed Facilities*, vol. 17, no. 3, pp. 144-50.
- Wikipedia, *List of bridge failures*, https://en.wikipedia.org/wiki/List_of_bridge_failures
- Wörman, A. 1989, 'Riprap protection without filter layers', *Journal of Hydraulic engineering*, vol. 115, no. 12, pp. 1615-30.
- Wu, X.-f. & Zhou, G. 2011, 'Application of improved Taguchi method to the multiresponse optimization', *18th International Conference on Industrial Engineering and Engineering Management*, IEEE, Changchun, China, pp. 1829-32.
- Yoon, T.H. & Kim, D.-H. 2001, 'Bridge pier scour protection by sack gabions', *World Water and Environmental Resources Congress*, ASCE, Orlando, Florida, United States, pp. 1-8.
- Zarrati, A., Nazariha, M. & Mashahir, M. 2006, 'Reduction of local scour in the vicinity of bridge pier groups using collars and riprap', *Journal of Hydraulic Engineering*, vol. 132, no. 2, pp. 154-62.
- Zarrati, A.R., Gholami, H. & Mashahir, M. 2004, 'Application of collar to control scouring around rectangular bridge piers', *Journal of Hydraulic Research*, vol. 42, no. 1, pp. 97-103.
- Zdravkovich, M. 1977, 'Review of flow interference between two circular cylinders in various arrangements', *Journal of Fluids Engineering*, vol. 99, no. 4, pp. 618-33.
- Zdravkovich, M. 1987, 'The effects of interference between circular cylinders in cross flow', *Journal of fluids and structures*, vol. 1, no. 2, pp. 239-61.

- Zdravkovich, M.M. 1997, *Flow around Circular Cylinders: Volume 2: Applications*, vol. 2, Oxford University Press.
- Zhao, W. & Huhe, A. 2006, 'Experimental investigation of scour mechanism around a circular cylinder', *Acta Mechanica Sinica*, vol. 38, no. 5, p. 577.
- Zhou, Y. & Yiu, M.W. 2006, 'Flow structure, momentum and heat transport in a two-tandem-cylinder wake', *Journal of Fluid Mechanics*, vol. 548, pp. 17-48.

APPENDIX A

The Captured Models of Scour Holes and Photographs of Scour Tests

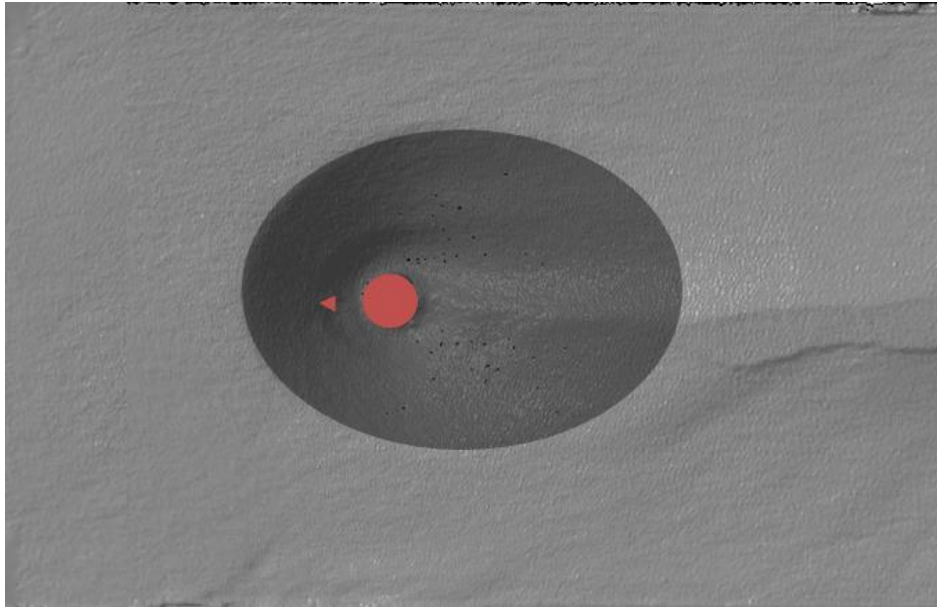


Figure A.1. Captured model of scour hole for Run 1



Figure A.2. A photograph of Run 1

Table A.1. The results of local scour tests for Run 1

Run No	B/D	L/D	H/y	d/D	Max scour depth (mm)	Max scour depth reduction (%)	Scour volume (1000mm ³)	Scour volume reduction (%)
1	0.2	0.2	0.25	0.5	67.45	18	2457	42

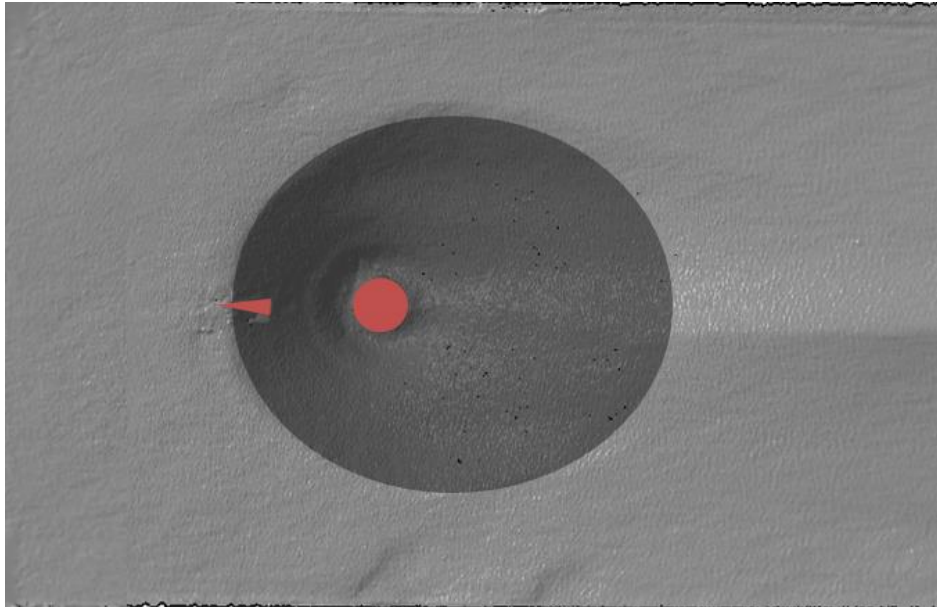


Figure A.3. Captured model of scour hole for Run 2



Figure A.4. A photograph of Run 2

Table A.2. The results of local scour tests for Run 2

Run No	B/D	L/D	H/y	d/D	Max scour depth (mm)	Max scour depth reduction (%)	Scour volume (1000mm ³)	Scour volume reduction (%)
2	0.2	1.0	1.00	1.5	72.62	11	2643	38

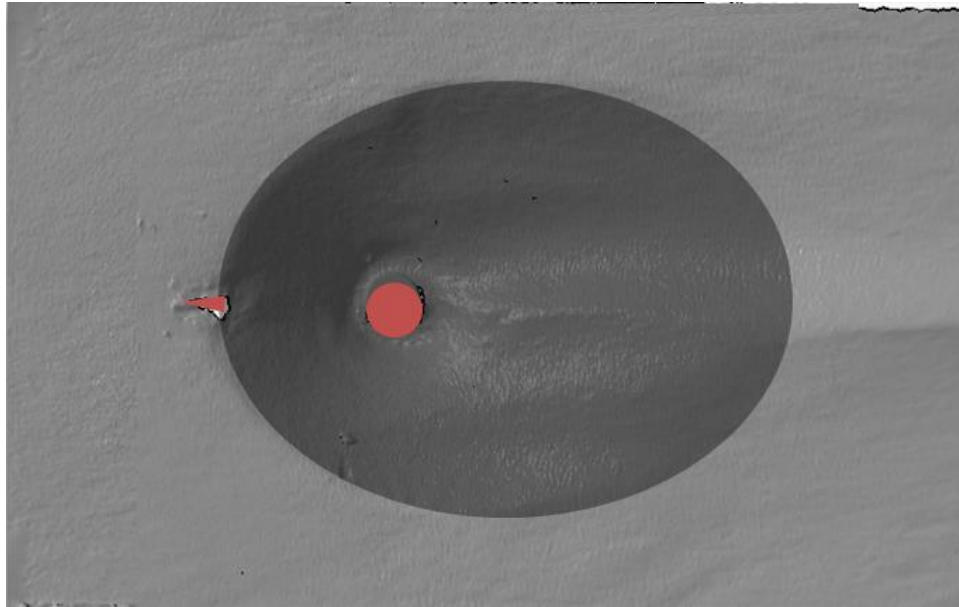


Figure A.5. Captured model of scour hole for Run 3



Figure A.6. A photograph of Run 3

Table A.3. The results of local scour tests for Run 3

Run No	B/D	L/D	H/y	d/D	Max scour depth (mm)	Max scour depth reduction (%)	Scour volume (1000mm ³)	Scour volume reduction (%)
3	0.2	0.8	0.50	2.5	73.87	10	3123	26

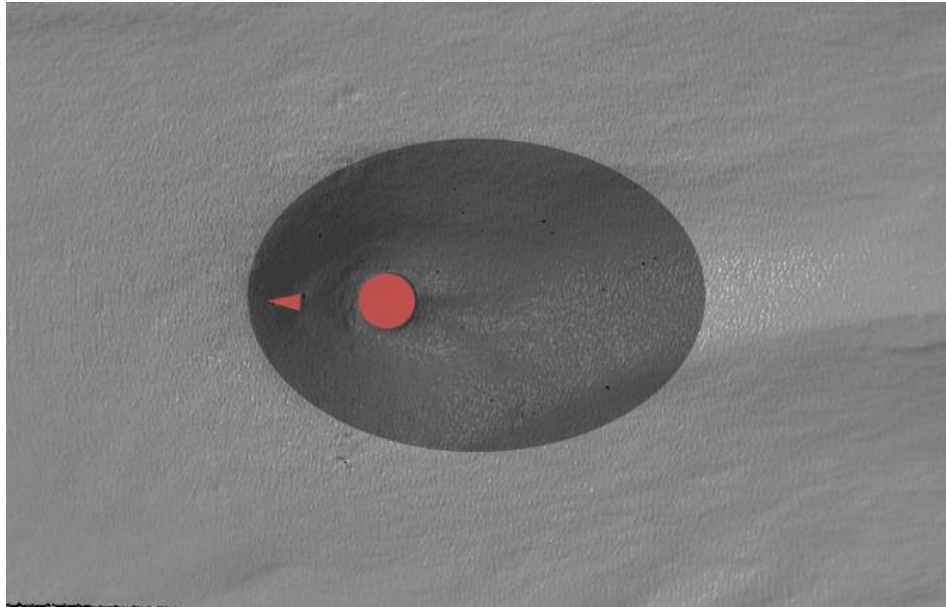


Figure A.7. Captured model of scour hole for Run 4



Figure A.8. A photograph of Run 4

Table A.4. The results of local scour tests for Run 4

Run No	B/D	L/D	H/y	d/D	Max scour depth (mm)	Max scour depth reduction (%)	Scour volume (1000mm ³)	Scour volume reduction (%)
4	0.2	0.6	>1.00	1.0	61.44	25	2221	48

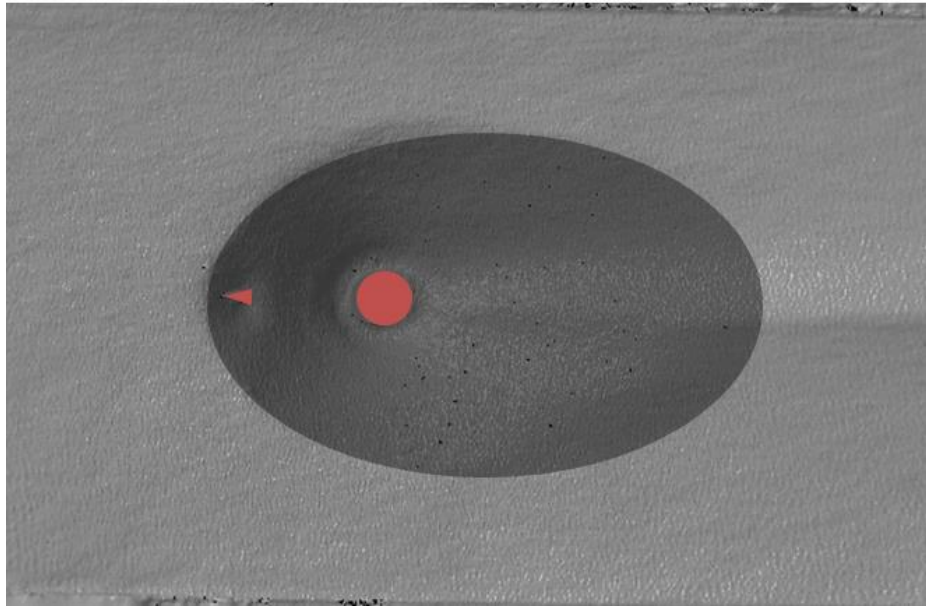


Figure A.9. Captured model of scour hole for Run 5



Figure A.10. A photograph of Run 5

Table A.5. The results of local scour tests for Run 5

Run No	B/D	L/D	H/y	d/D	Max scour depth (mm)	Max scour depth reduction (%)	Scour volume (1000mm ³)	Scour volume reduction (%)
5	0.2	0.4	0.75	2.0	70.83	14	2856	33

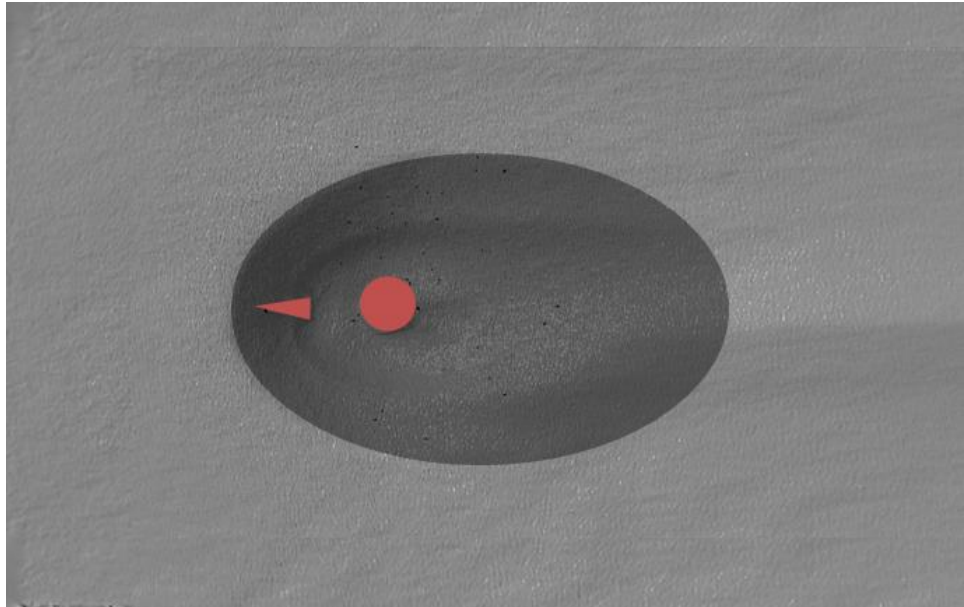


Figure A.11. Captured model of scour hole for Run 6



Figure A.12. A photograph of Run 6

Table A.6. The results of local scour tests for Run 6

Run No	B/D	L/D	H/y	d/D	Max scour depth (mm)	Max scour depth reduction (%)	Scour volume (1000mm ³)	Scour volume reduction (%)
6	0.4	1.0	0.75	1.0	57.9	29	2142	50

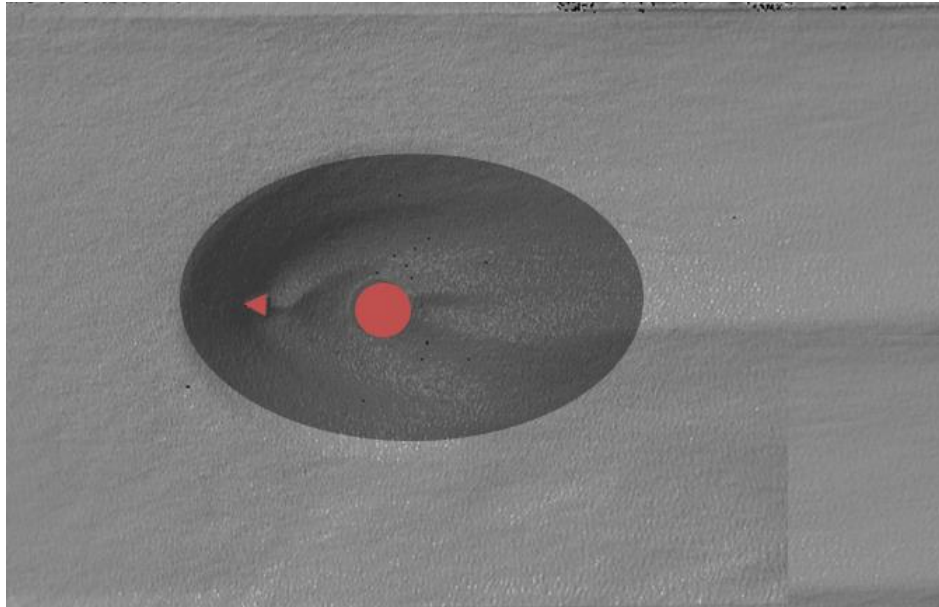


Figure A.13. Captured model of scour hole for Run 7



Figure A.14. A photograph of Run 7

Table A.7. The results of local scour tests for Run 7

Run No	B/D	L/D	H/y	d/D	Max scour depth (mm)	Max scour depth reduction (%)	Scour volume (1000mm ³)	Scour volume reduction (%)
7	0.4	0.4	0.50	1.5	55.16	33	2022	52

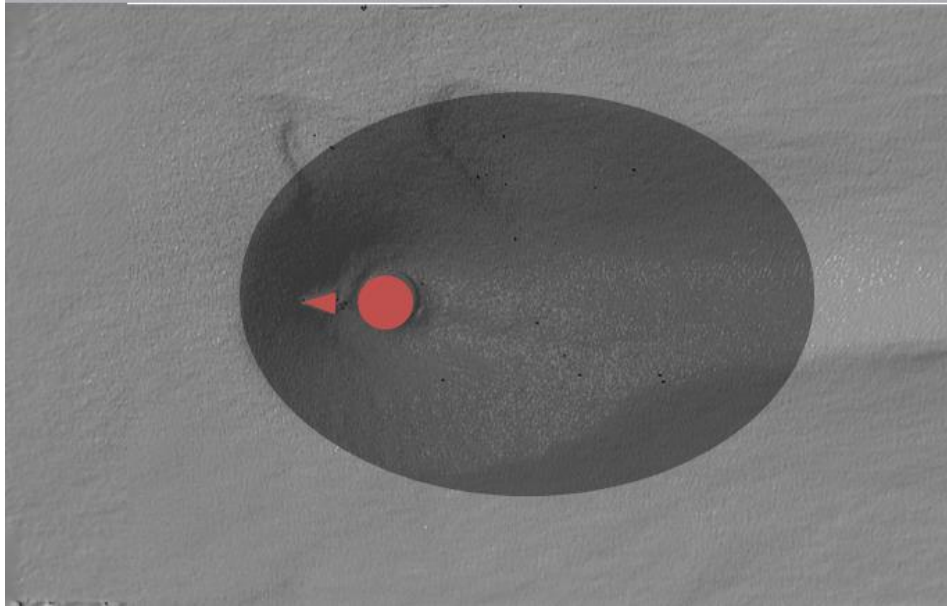


Figure A.15. Captured model of scour hole for Run 8



Figure A.16. A photograph of Run 8

Table A.8. The results of local scour tests for Run 8

Run No	B/D	L/D	H/y	d/D	Max scour depth (mm)	Max scour depth reduction (%)	Scour volume (1000mm ³)	Scour volume reduction (%)
8	0.4	0.6	1.00	0.5	65.41	20	2647	38

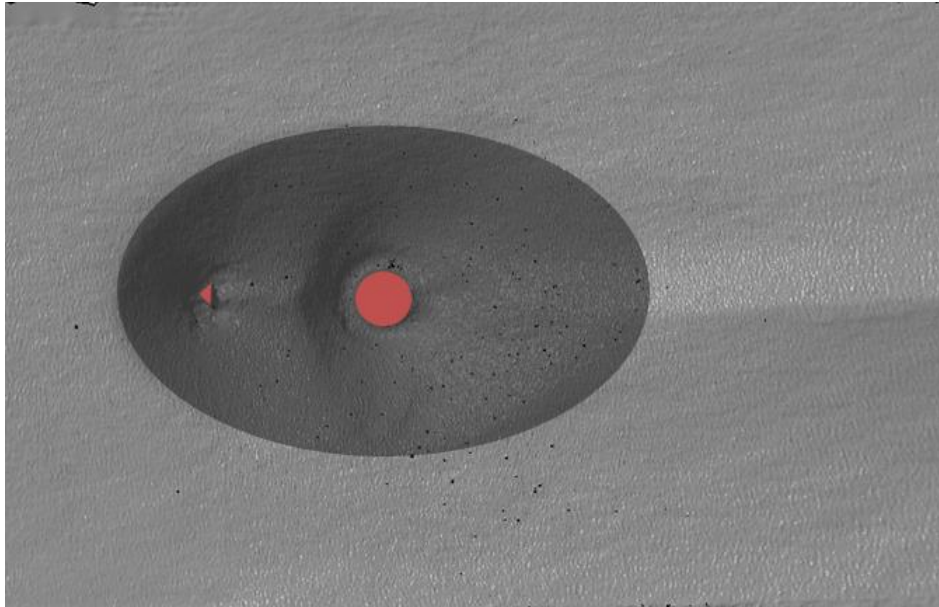


Figure A.17. Captured model of scour hole for Run 9



Figure A.18. A photograph of Run 9

Table A.9. The results of local scour tests for Run 9

Run No	B/D	L/D	H/y	d/D	Max scour depth (mm)	Max scour depth reduction (%)	Scour volume (1000mm ³)	Scour volume reduction (%)
9	0.4	0.2	>1.00	2.5	68.11	17	2756	35

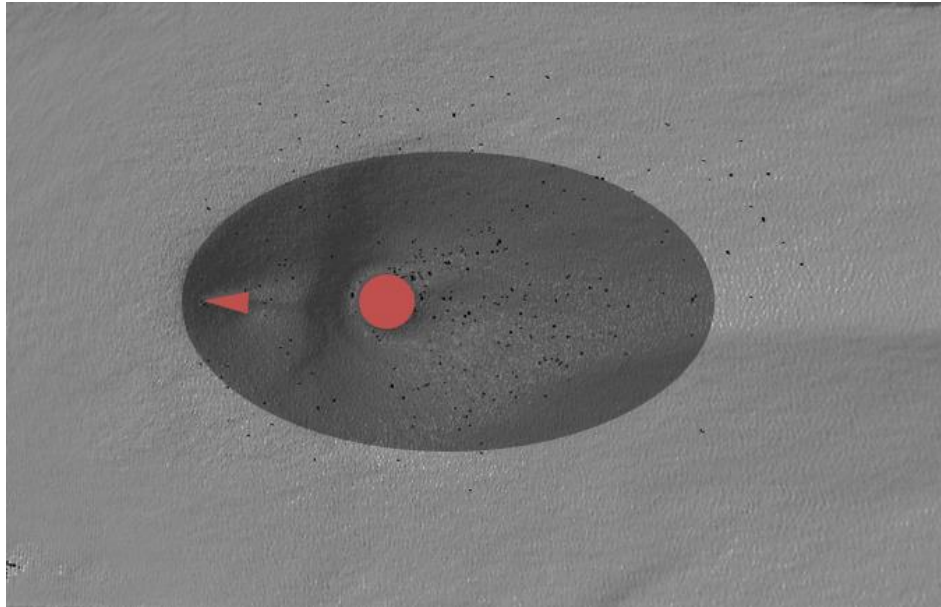


Figure A.19. Captured model of scour hole for Run 10



Figure A.20. A photograph of Run 10

Table A.10. The results of local scour tests for Run 10

Run No	B/D	L/D	H/y	d/D	Max scour depth (mm)	Max scour depth reduction (%)	Scour volume (1000mm ³)	Scour volume reduction (%)
10	0.4	0.8	0.25	2.0	60.78	26	2111	50

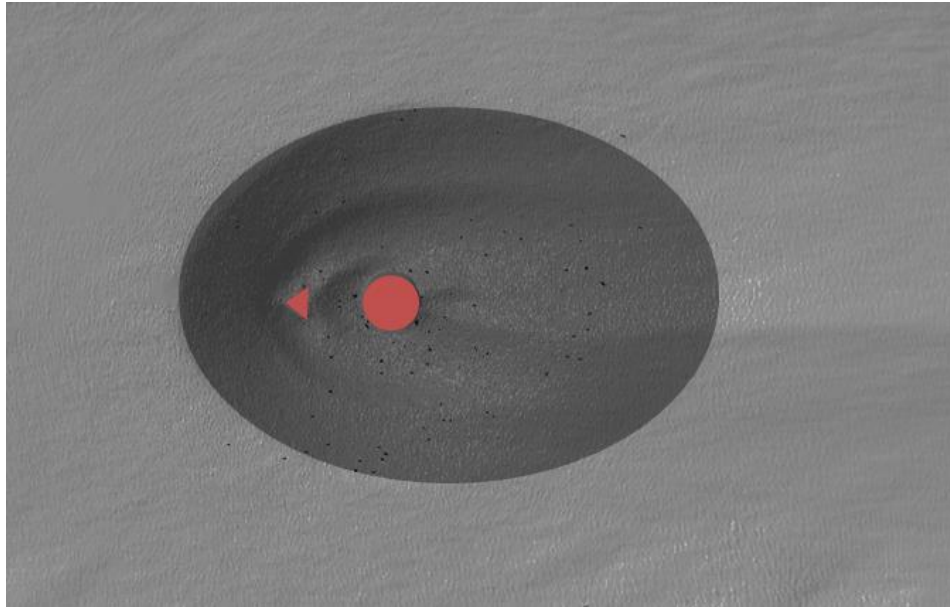


Figure A.21. Captured model of scour hole for Run 11



Figure A.22. A photograph of Run 11

Table A.11. The results of local scour tests for Run 11

Run No	B/D	L/D	H/y	d/D	Max scour depth (mm)	Max scour depth reduction (%)	Scour volume (1000mm ³)	Scour volume reduction (%)
11	0.6	0.4	0.25	1.0	58.53	29	1913	55

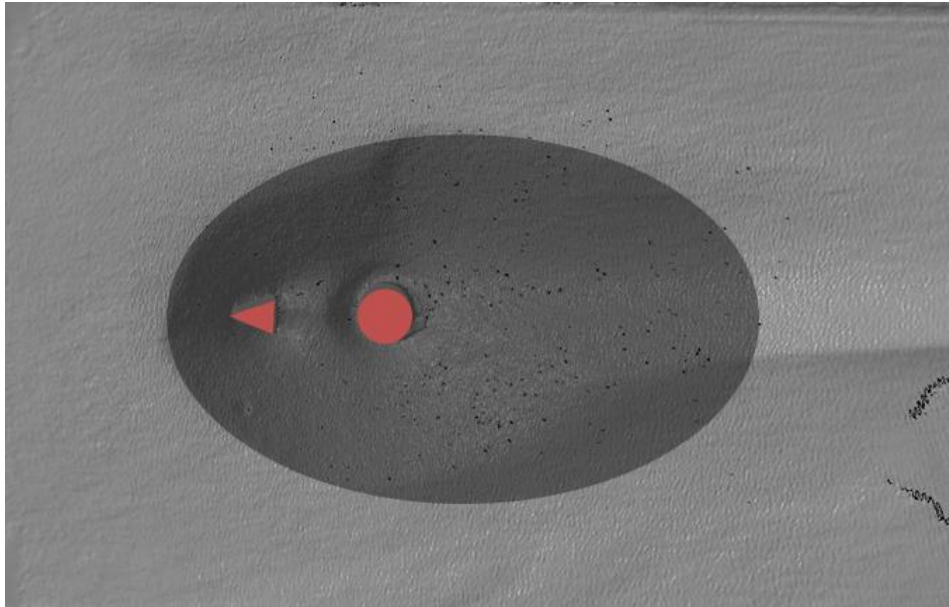


Figure A.23. Captured model of scour hole for Run 12



Figure A.24. A photograph of Run 12

Table A.12. The results of local scour tests for Run 12

Run No	B/D	L/D	H/y	d/D	Max scour depth (mm)	Max scour depth reduction (%)	Scour volume (1000mm ³)	Scour volume reduction (%)
12	0.6	0.8	>1.00	1.5	65.89	20	2574	39

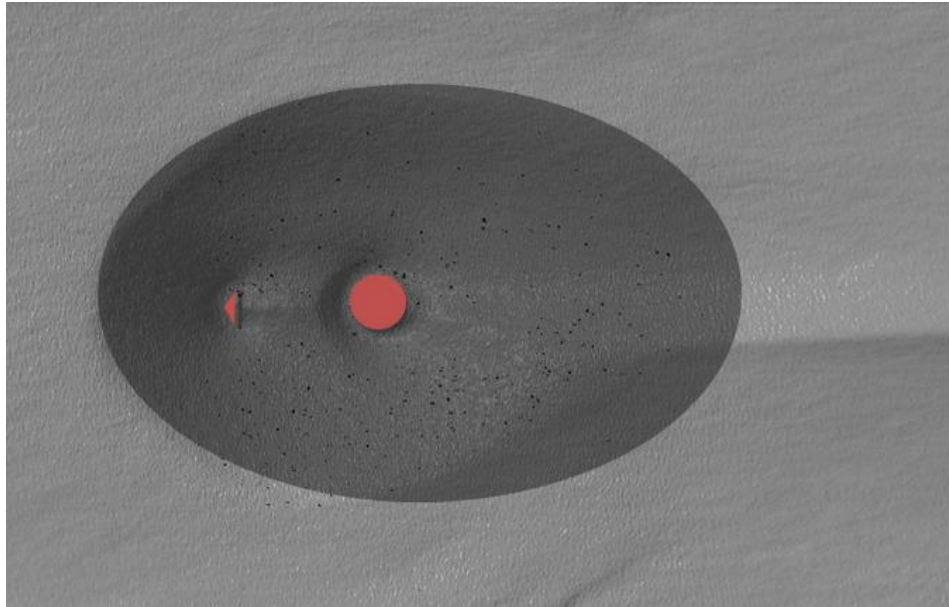


Figure A.25. Captured model of scour hole for Run 13



Figure A.26. A photograph of Run 13

Table A.13. The results of local scour tests for Run 13

Run No	B/D	L/D	H/y	d/D	Max scour depth (mm)	Max scour depth reduction (%)	Scour volume (1000mm ³)	Scour volume reduction (%)
13	0.6	0.2	1.00	2.0	66.89	18	2812	34

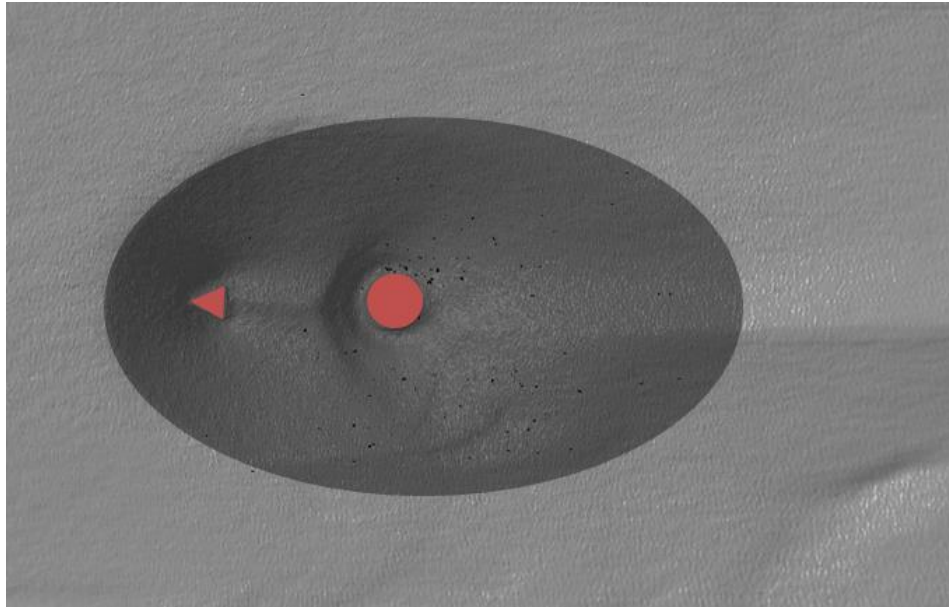


Figure A.27. Captured model of scour hole for Run 14



Figure A.28. A photograph of Run 14

Table A.14. The results of local scour tests for Run 14

Run No	B/D	L/D	H/y	d/D	Max scour depth (mm)	Max scour depth reduction (%)	Scour volume (1000mm ³)	Scour volume reduction (%)
14	0.6	0.6	0.75	2.5	65.01	21	2720	36

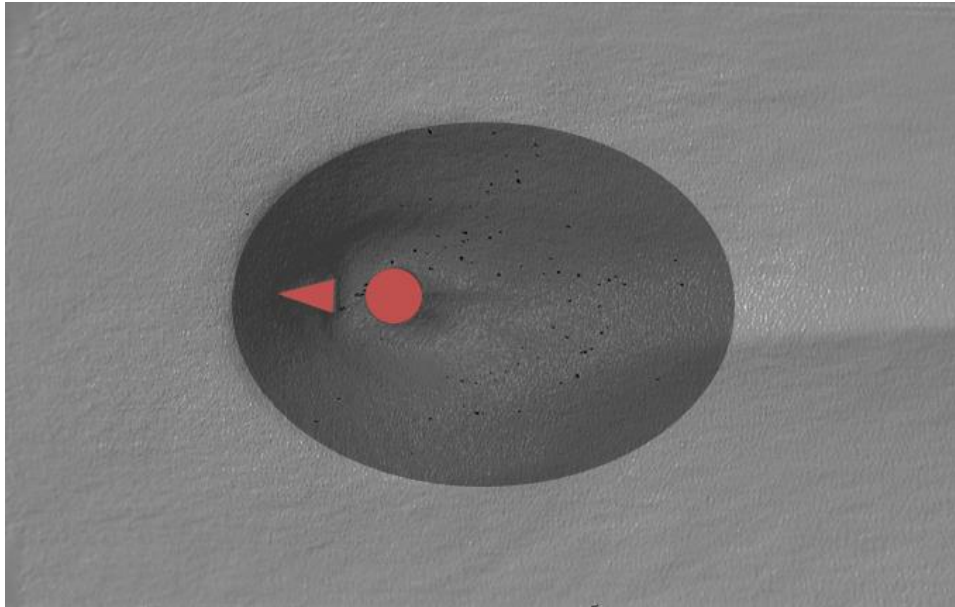


Figure A.29. Captured model of scour hole for Run 15



Figure A.30. A photograph of Run 15

Table A.15. The results of local scour tests for Run 15

Run No	B/D	L/D	H/y	d/D	Max scour depth (mm)	Max scour depth reduction (%)	Scour volume (1000mm ³)	Scour volume reduction (%)
15	0.6	1.0	0.50	0.5	65.83	20	2754	35

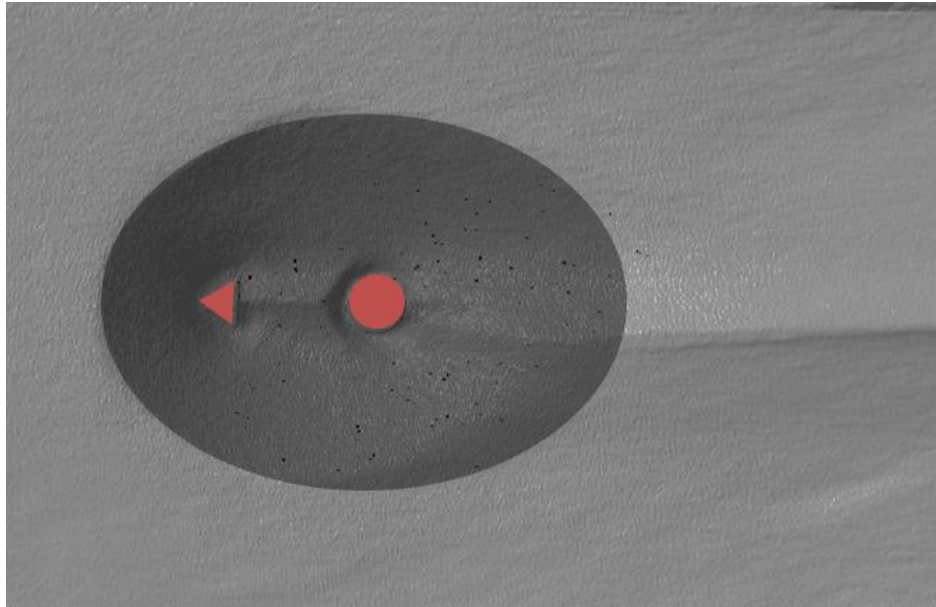


Figure A.31. Captured model of scour hole for Run 16



Figure A.32. A photograph of Run 16

Table A.16. The results of local scour tests for Run 16

Run No	B/D	L/D	H/y	d/D	Max scour depth (mm)	Max scour depth reduction (%)	Scour volume (1000mm ³)	Scour volume reduction (%)
16	0.8	0.6	0.50	2.0	53.8	34	2051	52

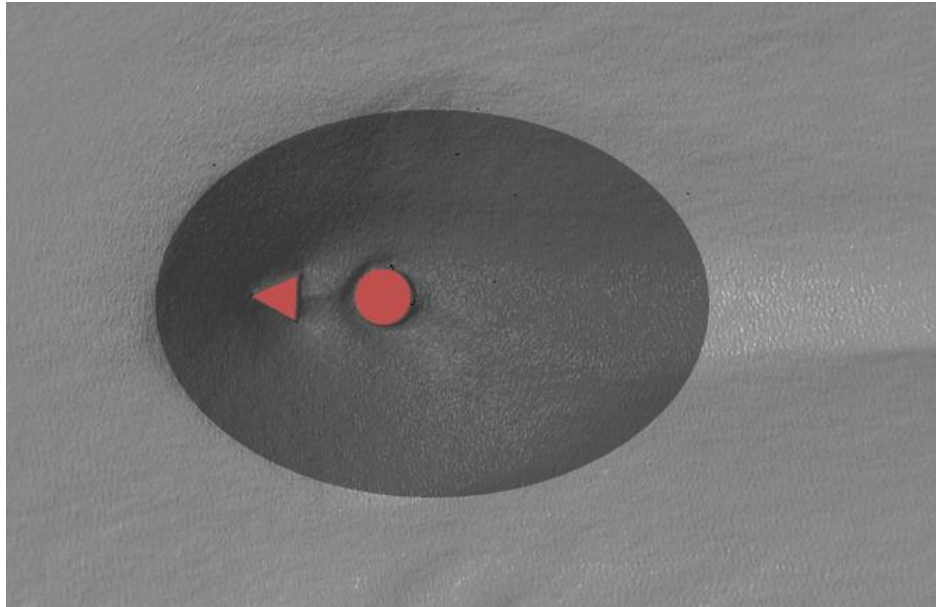


Figure A.33. Captured model of scour hole for Run 17



Figure A.34. A photograph of Run 17

Table A.17. The results of local scour tests for Run 17

Run No	B/D	L/D	H/y	d/D	Max scour depth (mm)	Max scour depth reduction (%)	Scour volume (1000mm ³)	Scour volume reduction (%)
17	0.8	0.8	1.00	1.0	65.83	20	2909	31

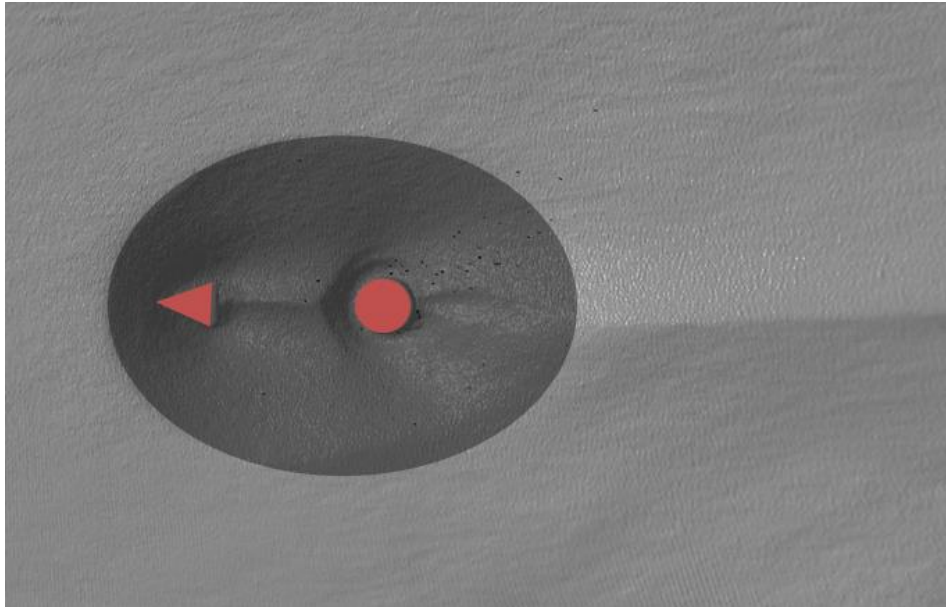


Figure A.35. Captured model of scour hole for Run 18



Figure A.36. A photograph of Run 18

Table A.18. The results of local scour tests for Run 18

Run No	B/D	L/D	H/y	d/D	Max scour depth (mm)	Max scour depth reduction (%)	Scour volume (1000mm ³)	Scour volume reduction (%)
18	0.8	1.0	0.25	2.5	55.02	33	2080	51

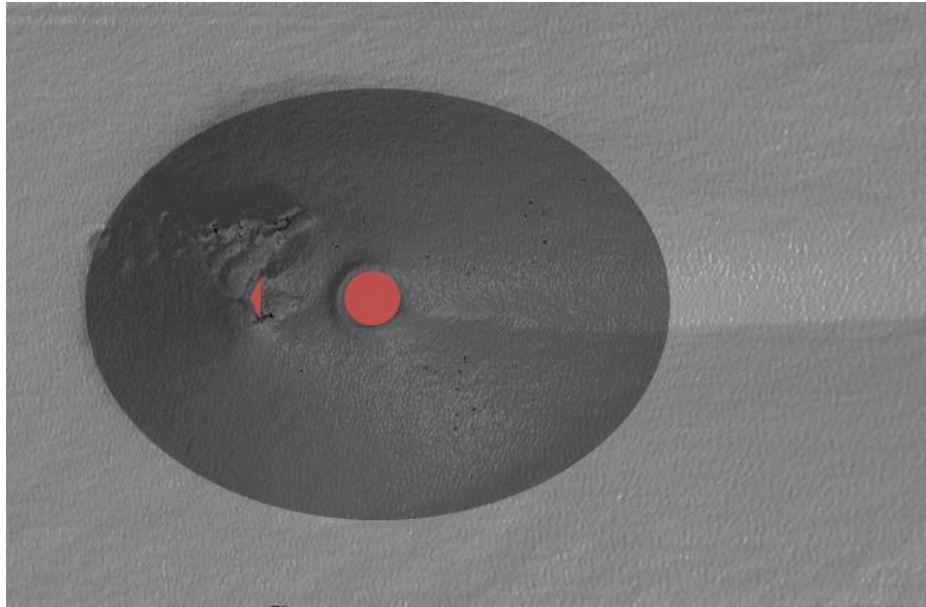


Figure A.37. Captured model of scour hole for Run 19



Figure A.38. A photograph of Run 19

Table A.19. The results of local scour tests for Run 19

Run No	B/D	L/D	H/y	d/D	Max scour depth (mm)	Max scour depth reduction (%)	Scour volume (1000mm ³)	Scour volume reduction (%)
19	0.8	0.2	0.75	1.5	66.53	19	3293	22

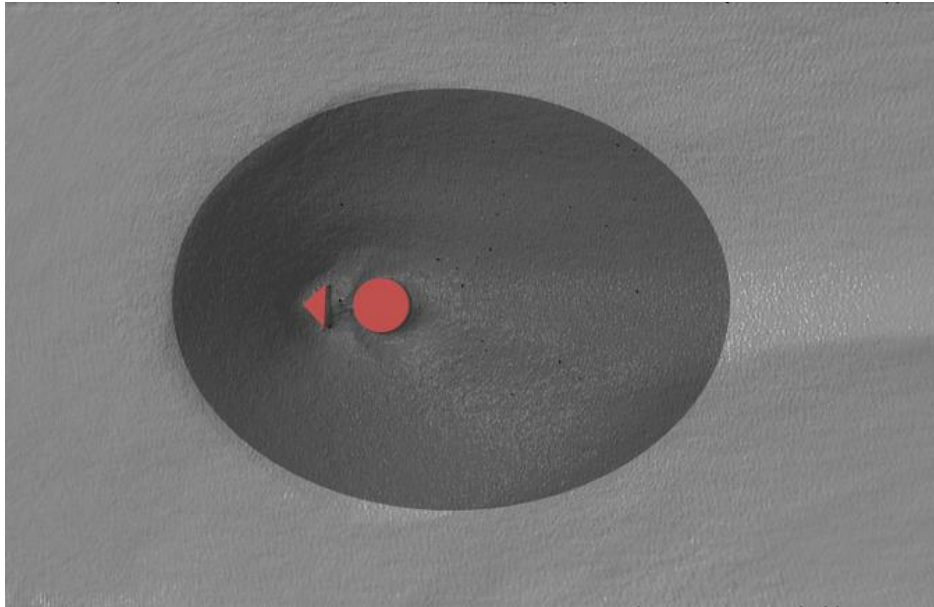


Figure A.39. Captured model of scour hole for Run 20



Figure A.40. A photograph of Run 20

Table A.20. The results of local scour tests for Run 20

Run No	B/D	L/D	H/y	d/D	Max scour depth (mm)	Max scour depth reduction (%)	Scour volume (1000mm ³)	Scour volume reduction (%)
20	0.8	0.4	>1.00	0.5	72.91	11	3718	12

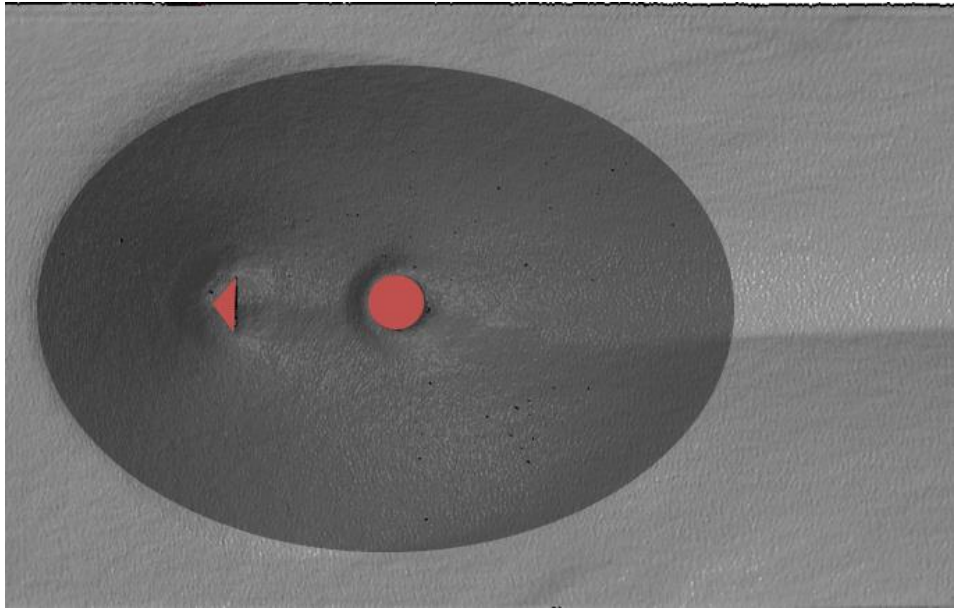


Figure A.41. Captured model of scour hole for Run 21



Figure A.42. A photograph of Run 21

Table A.21. The results of local scour tests for Run 21

Run No	B/D	L/D	H/y	d/D	Max scour depth (mm)	Max scour depth reduction (%)	Scour volume (1000mm ³)	Scour volume reduction (%)
21	1.0	0.4	1.00	2.5	70.41	14	3591	15

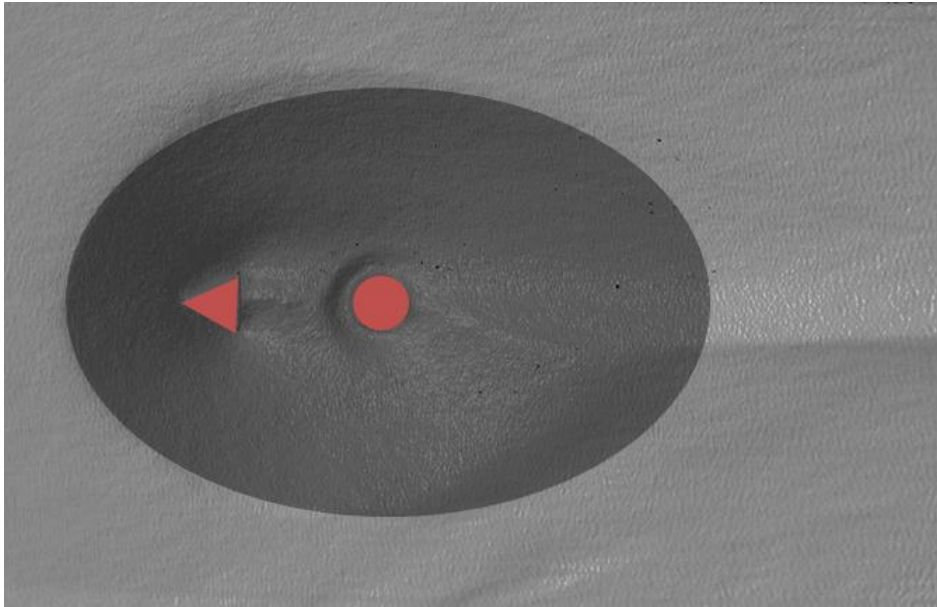


Figure A.43. Captured model of scour hole for Run 22



Figure A.44. A photograph of Run 22

Table A.22. The results of local scour tests for Run 22

Run No	B/D	L/D	H/y	d/D	Max scour depth (mm)	Max scour depth reduction (%)	Scour volume (1000mm ³)	Scour volume reduction (%)
22	1.0	1.0	>1.00	2.0	70.46	14	3760	11

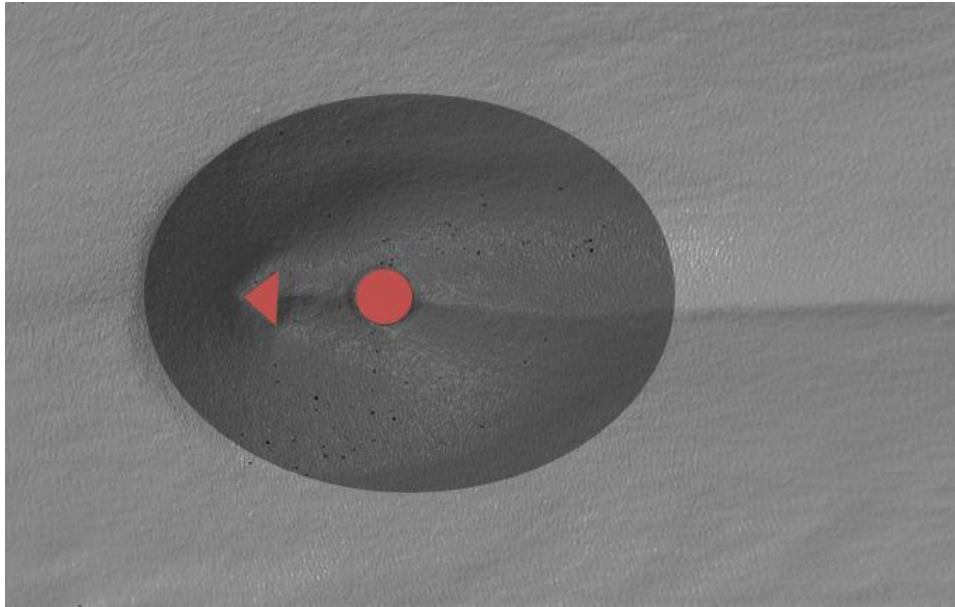


Figure A.45. Captured model of scour hole for Run 23



Figure A.46. A photograph of Run 23

Table A.23. The results of local scour tests for Run 23

Run No	B/D	L/D	H/y	d/D	Max scour depth (mm)	Max scour depth reduction (%)	Scour volume (1000mm ³)	Scour volume reduction (%)
23	1.0	0.6	0.25	1.5	51.9	37	2023	52

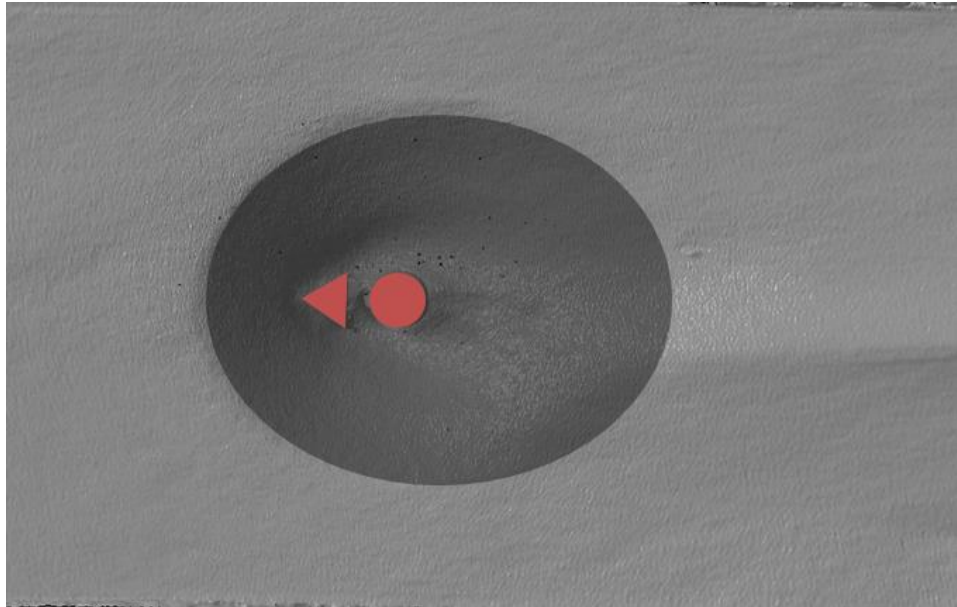


Figure A.47. Captured model of scour hole for Run 24



Figure A.48. A photograph of Run 24

Table A.24. The results of local scour tests for Run 24

Run No	B/D	L/D	H/y	d/D	Max scour depth (mm)	Max scour depth reduction (%)	Scour volume (1000mm ³)	Scour volume reduction (%)
24	1.0	0.8	0.75	0.5	75.93	7	4099	3

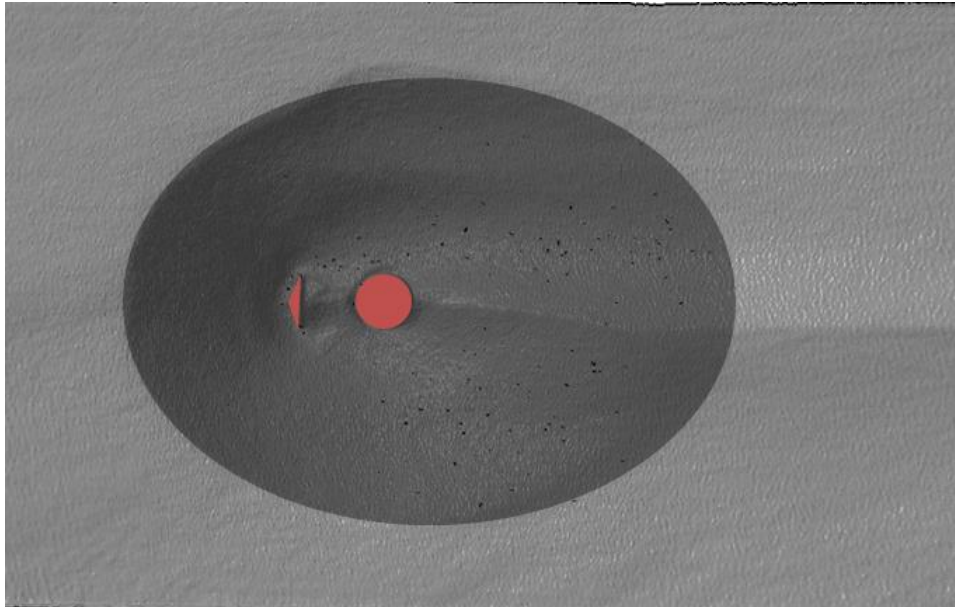


Figure A.49. Captured model of scour hole for Run 25



Figure A.50. A photograph of Run 25

Table A.25. The results of local scour tests for Run 25

Run No	B/D	L/D	H/y	d/D	Max scour depth (mm)	Max scour depth reduction (%)	Scour volume (1000mm ³)	Scour volume reduction (%)
25	1.0	0.2	0.50	1.0	68.05	17	3646	14

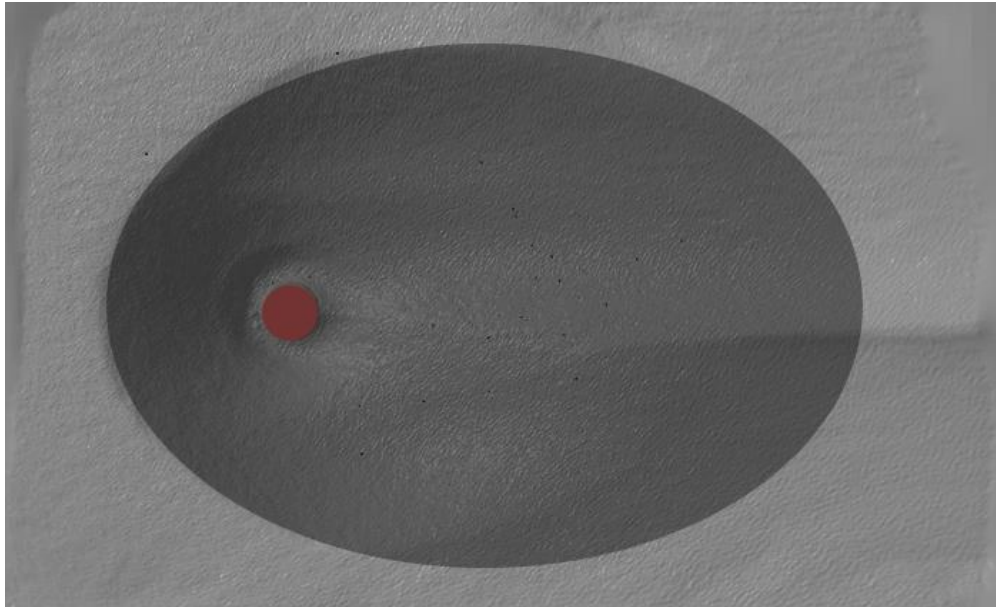


Figure A.51. Captured model of scour hole for control test



Figure A.52. A photograph of control test

Table A.1. The results of local scour tests for control test

Run No	B/D	L/D	H/y	d/D	Max scour depth (mm)	Max scour depth reduction (%)	Scour volume (1000mm ³)	Scour volume reduction (%)
0	-	-	-	-	81.9	0	4242	0

APPENDIX B

Flow Field Plots

B.1. Plots of Streamwise Velocity Component

B.2. Plots of Vertical Velocity Component

B.3. Plots of Absolute Flow Velocity and Streamlines

B.4. Plots of Streamwise Turbulence Intensity

B.5. Plots of Vertical Turbulence Intensity

B.6. Plots of Turbulent Kinetic Energy

B.7. Plots of Reynolds Shear Stress

B.1. Plots of Streamwise Velocity Component

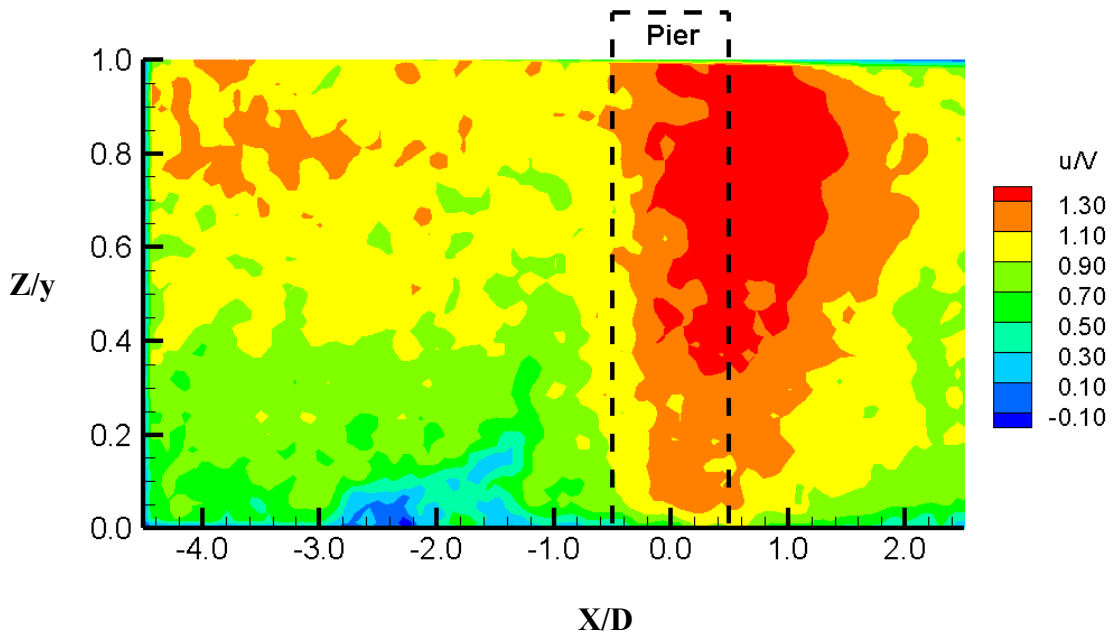


Figure B.1. Normalised streamwise velocity for the single pier case at $Y/D = 1$

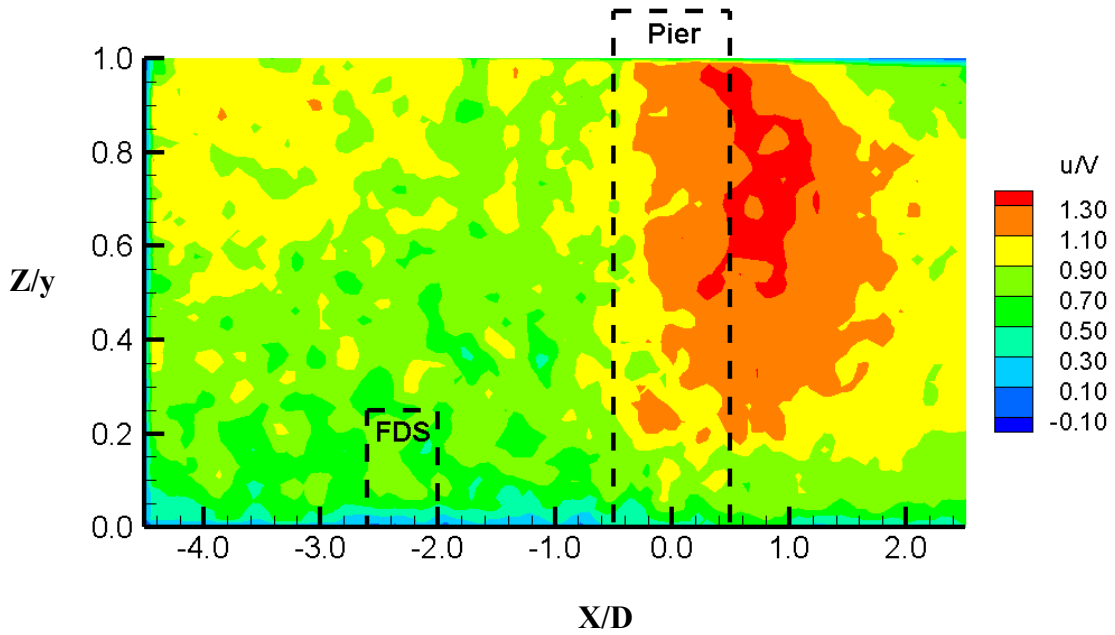


Figure B.2. Normalised streamwise velocity for the single pier case and FDS with $H/y=0.25$ at $Y/D = 1$

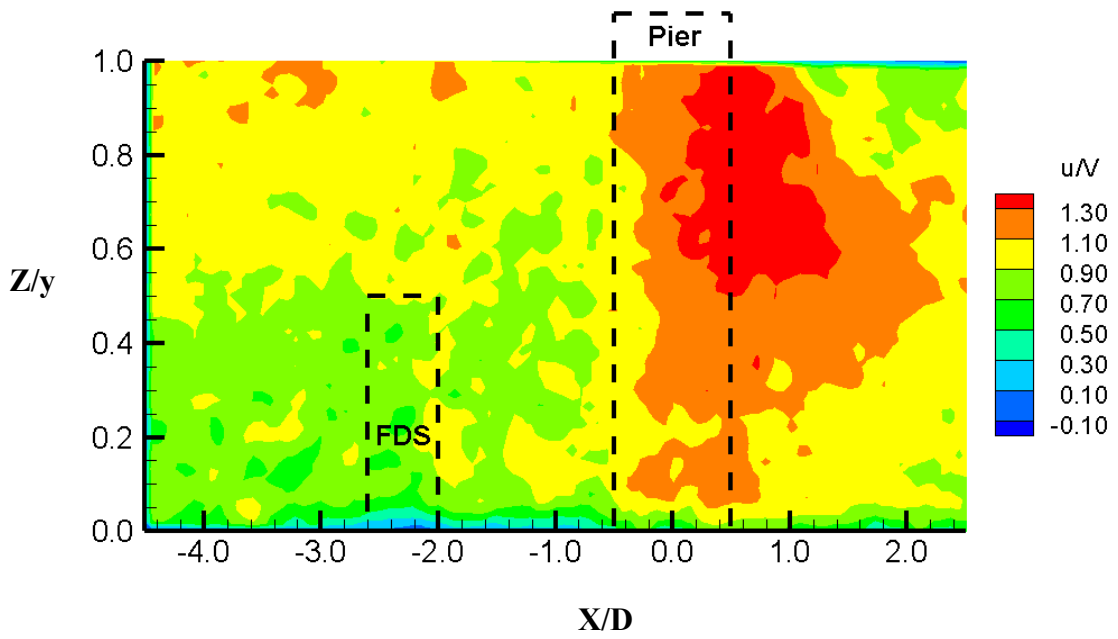


Figure B.3. Normalised streamwise velocity for the single pier case and FDS with $H/y=0.50$ at $Y/D = 1$

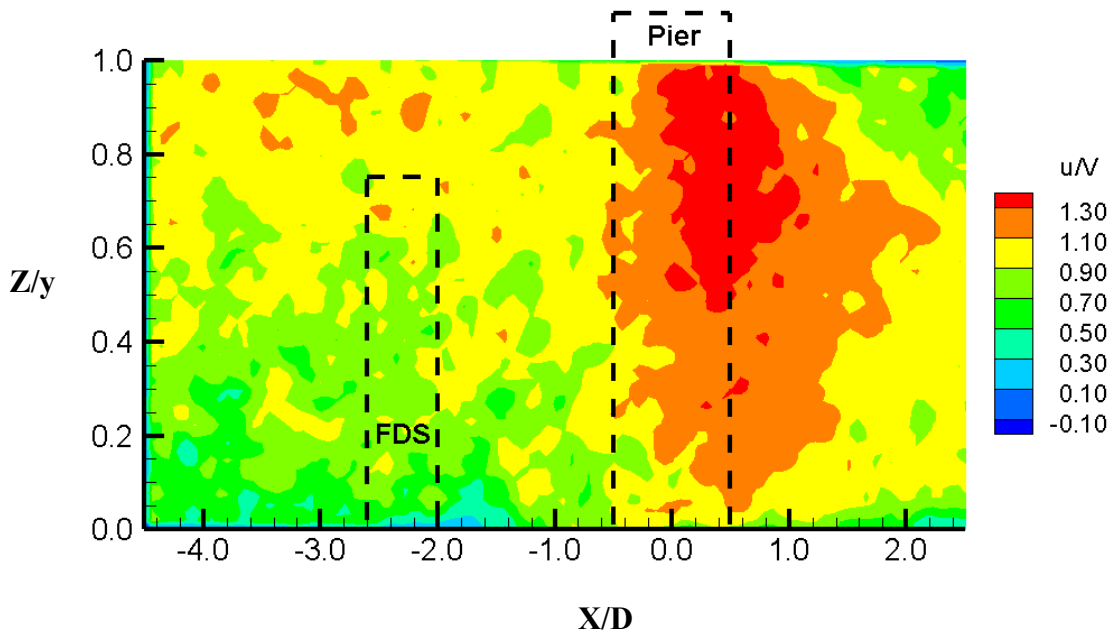


Figure B.4. Normalised streamwise velocity for the single pier case and FDS with $H/y=0.75$ at $Y/D = 1$

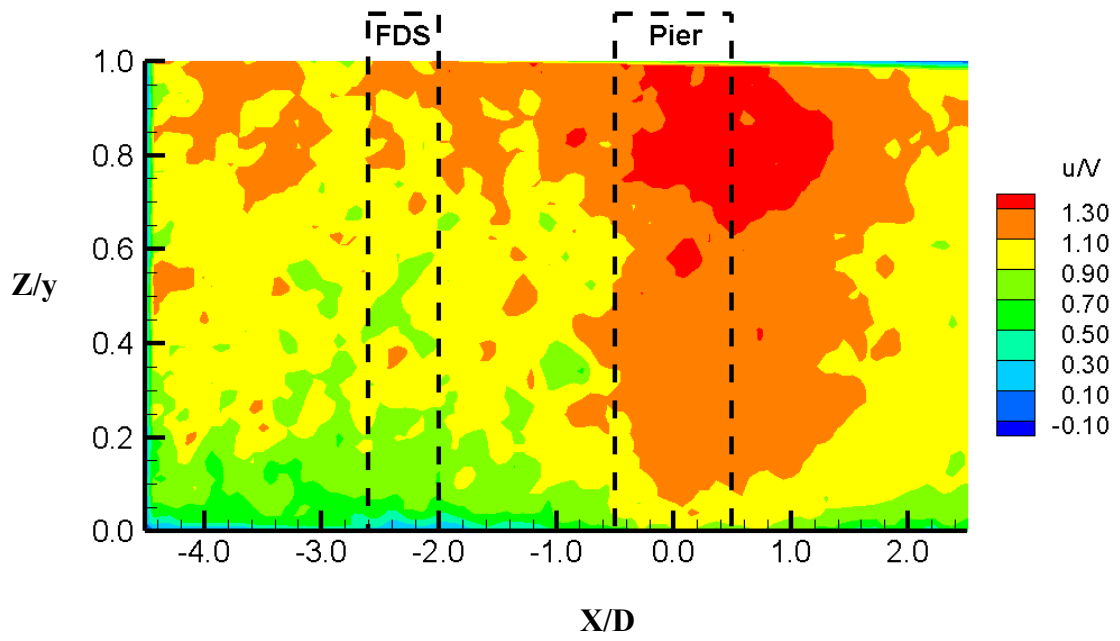


Figure B.5. Normalised streamwise velocity for the single pier case and FDS with $H/y > 1$ at $Y/D = 1$

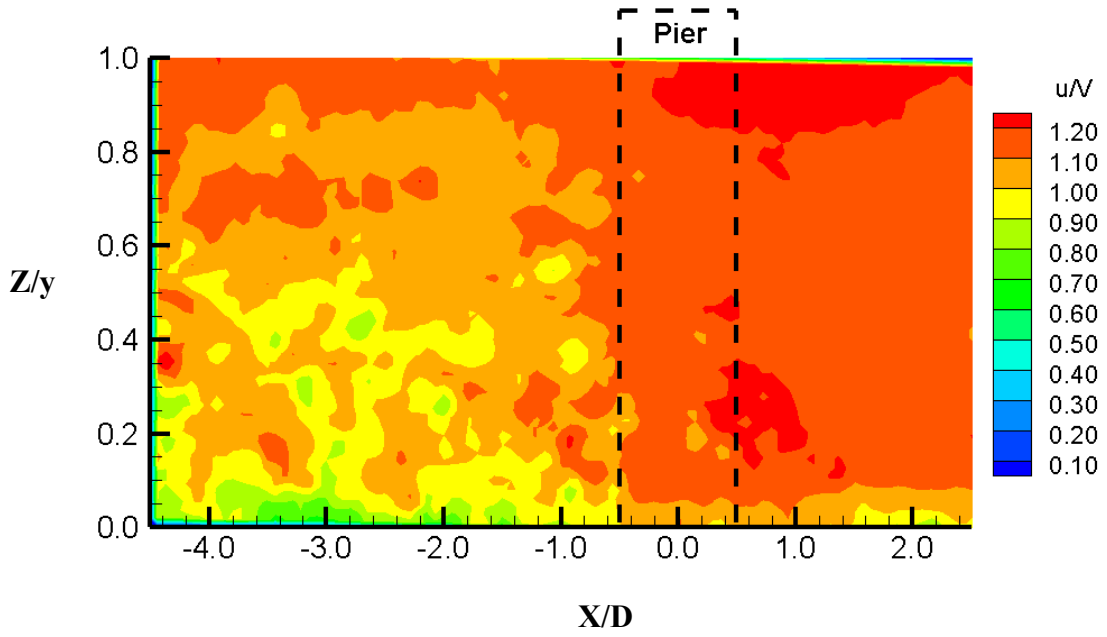


Figure B.6. Normalised streamwise velocity for the single pier case at $Y/D = 2$

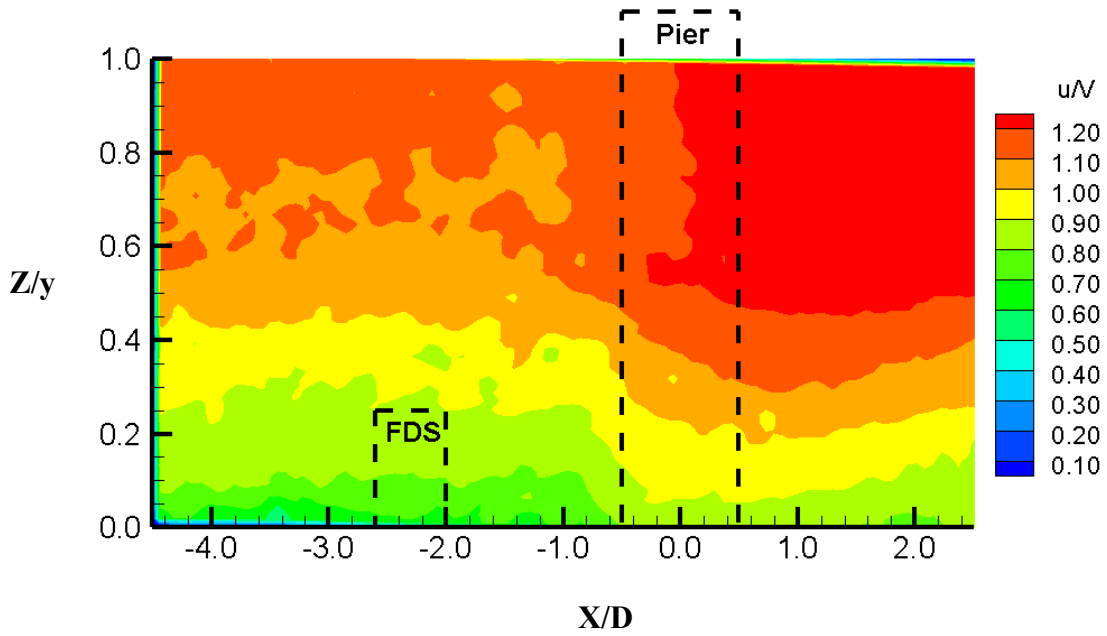


Figure B.7. Normalised streamwise velocity for the single pier case and FDS with $H/y = 0.25$ at $Y/D = 2$

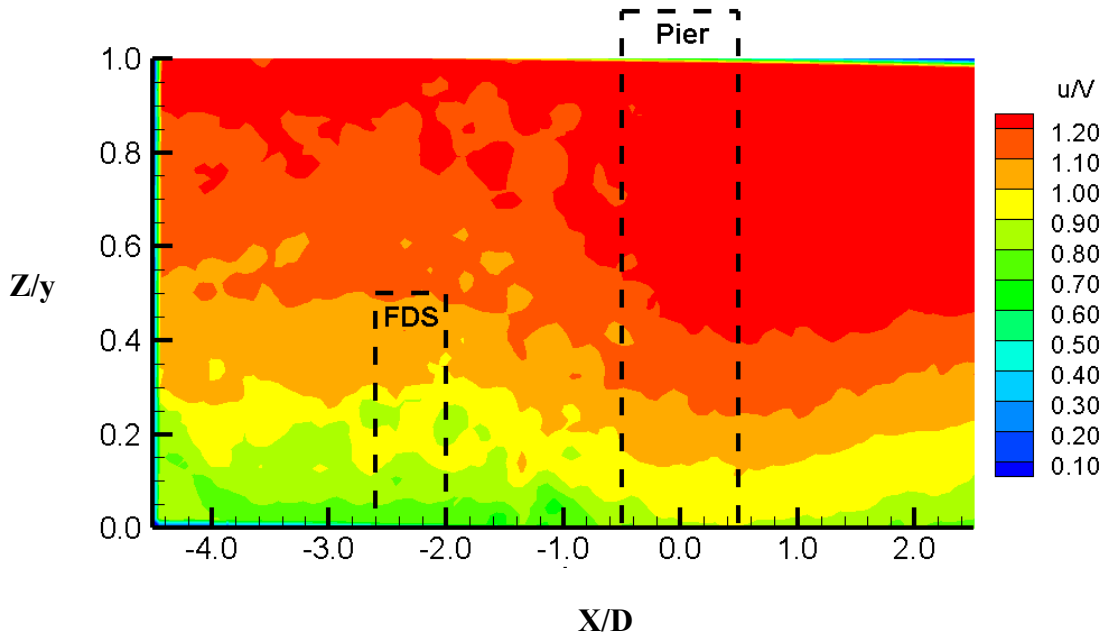


Figure B.8. Normalised streamwise velocity for the single pier case and FDS with $H/y=0.50$ at $Y/D = 2$

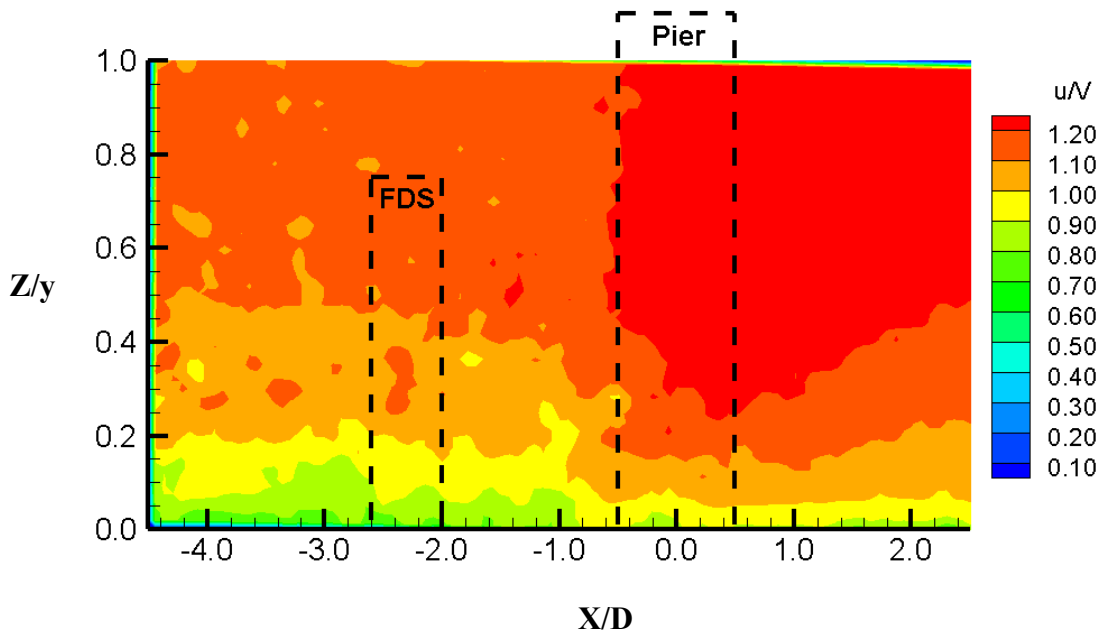


Figure B.9. Normalised streamwise velocity for the single pier case and FDS with $H/y=0.75$ at $Y/D = 2$

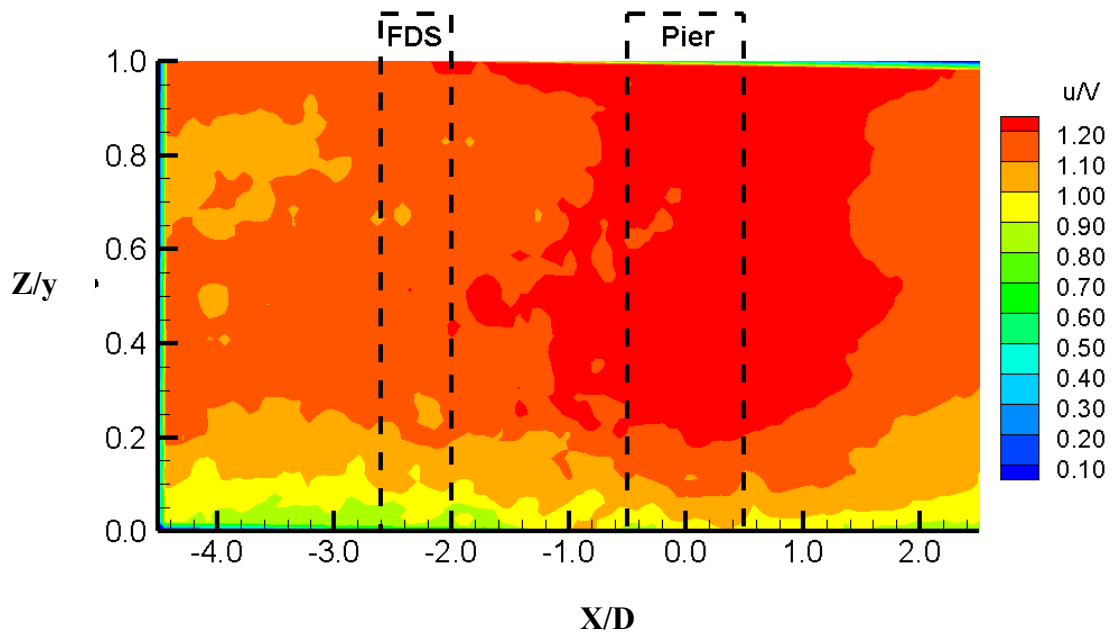


Figure B.10. Normalised streamwise velocity for the single pier case and FDS with $H/y > 1$ at $Y/D = 2$

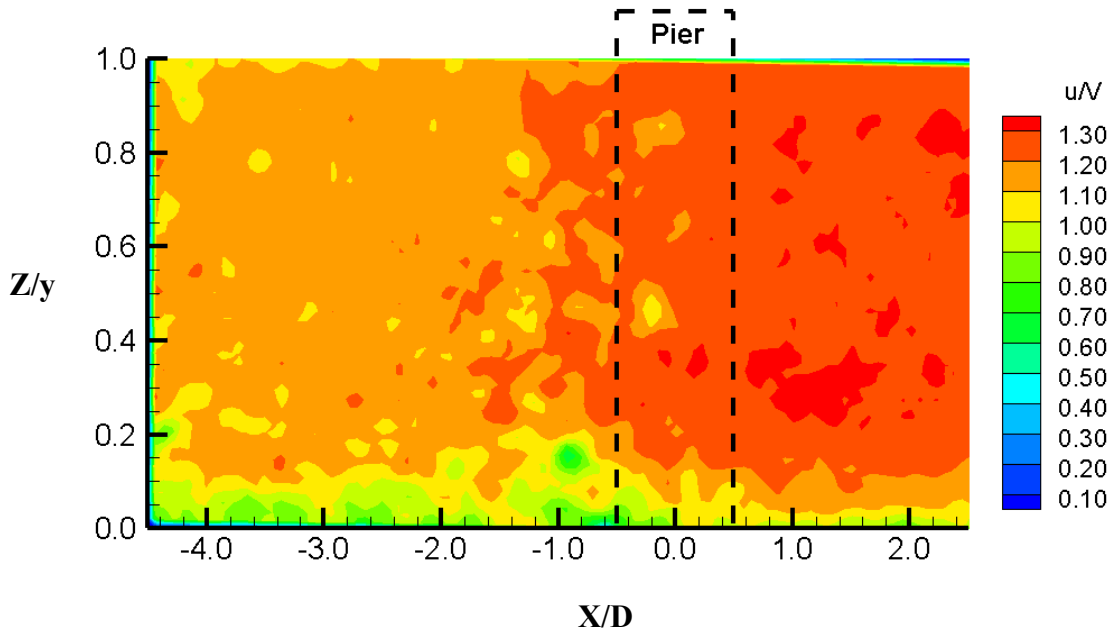


Figure B.11. Normalised streamwise velocity for the single pier case at $Y/D = 3$

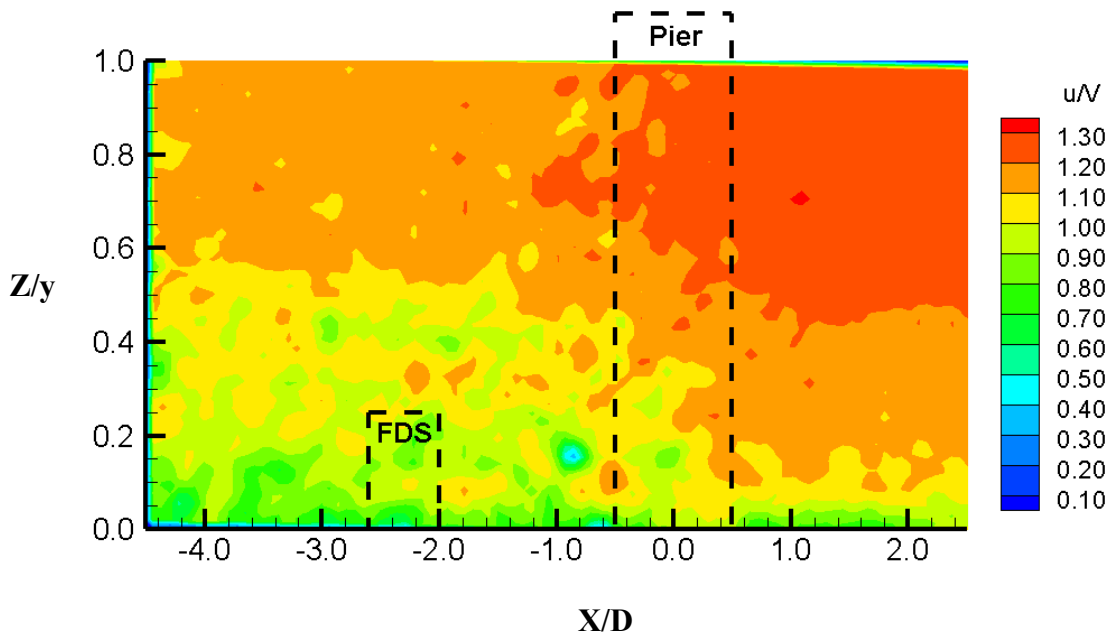


Figure B.12. Normalised streamwise velocity for the single pier case and FDS with $H/y = 0.25$ at $Y/D = 3$

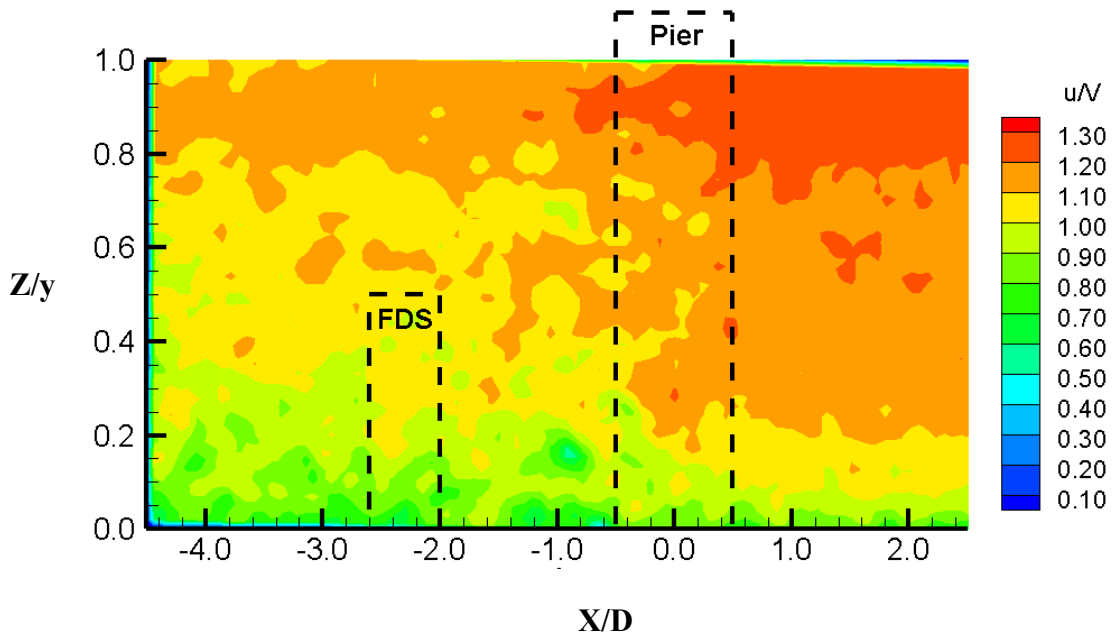


Figure B.13. Normalised streamwise velocity for the single pier case and FDS with $H/y=0.50$ at $Y/D = 3$

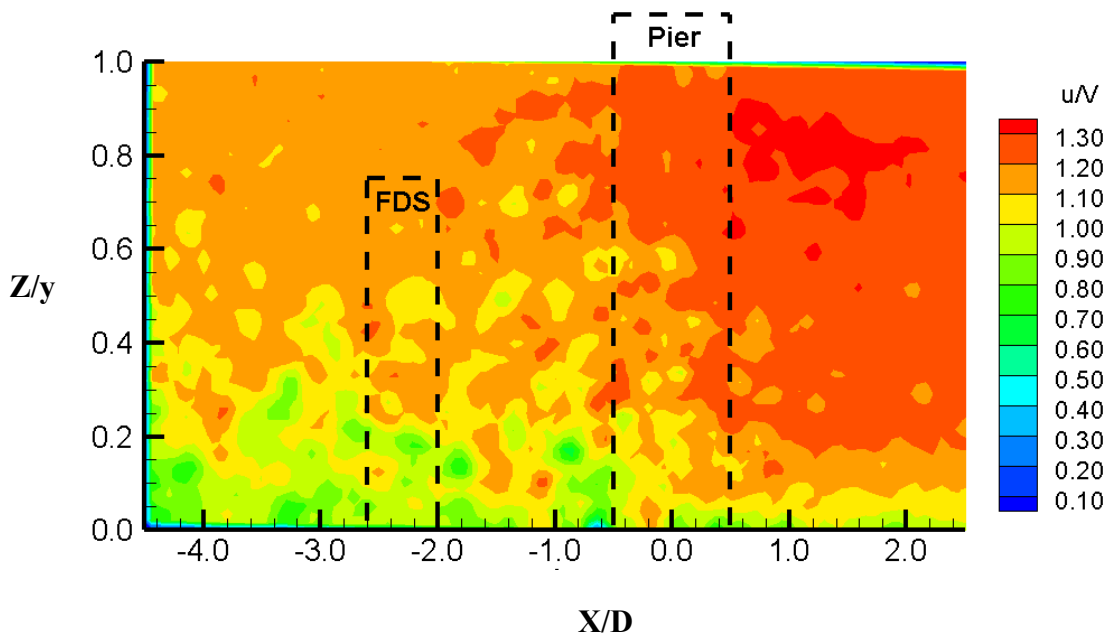


Figure B.14. Normalised streamwise velocity for the single pier case and FDS with $H/y=0.75$ at $Y/D = 3$

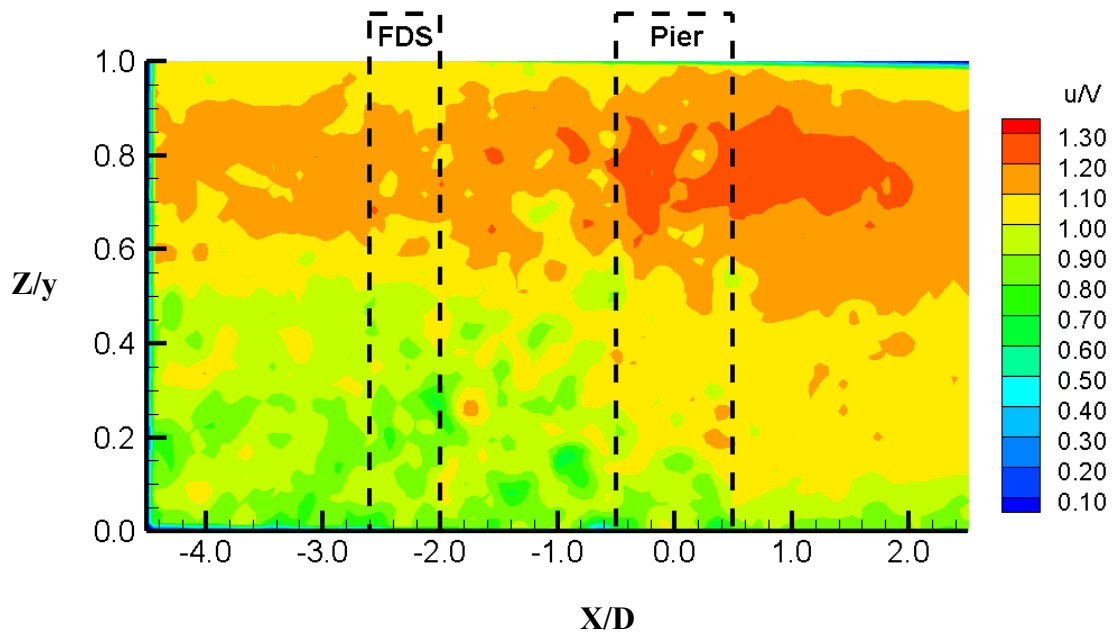


Figure B.15. Normalised streamwise velocity for the single pier case and FDS with $H/y > 1$ at $Y/D = 3$

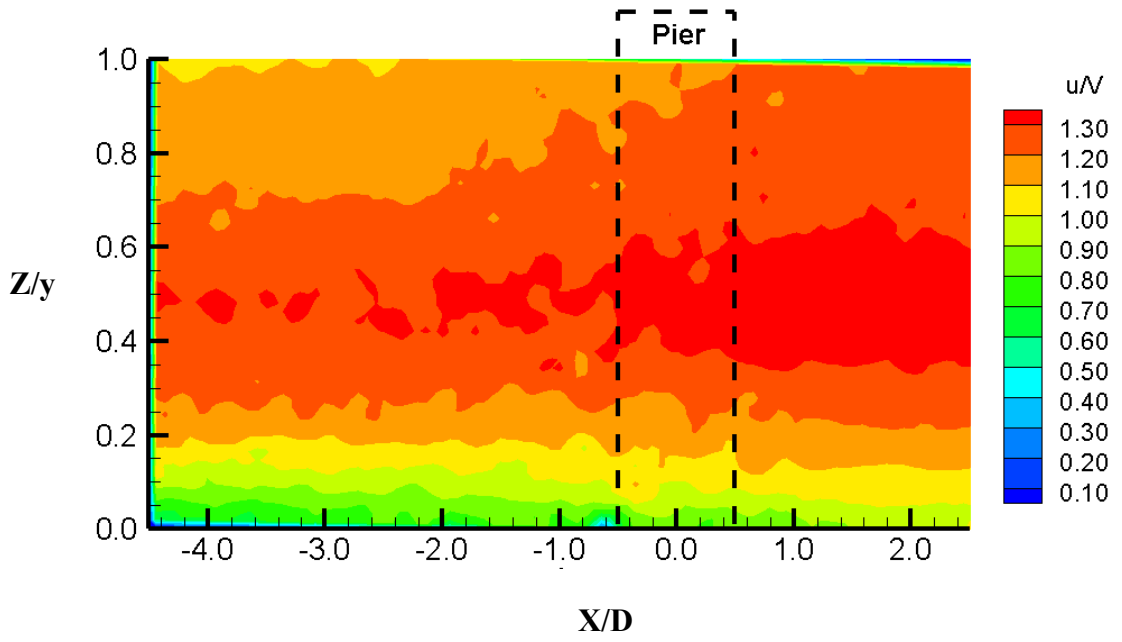


Figure B.16. Normalised streamwise velocity for the single pier case at $Y/D = 4$

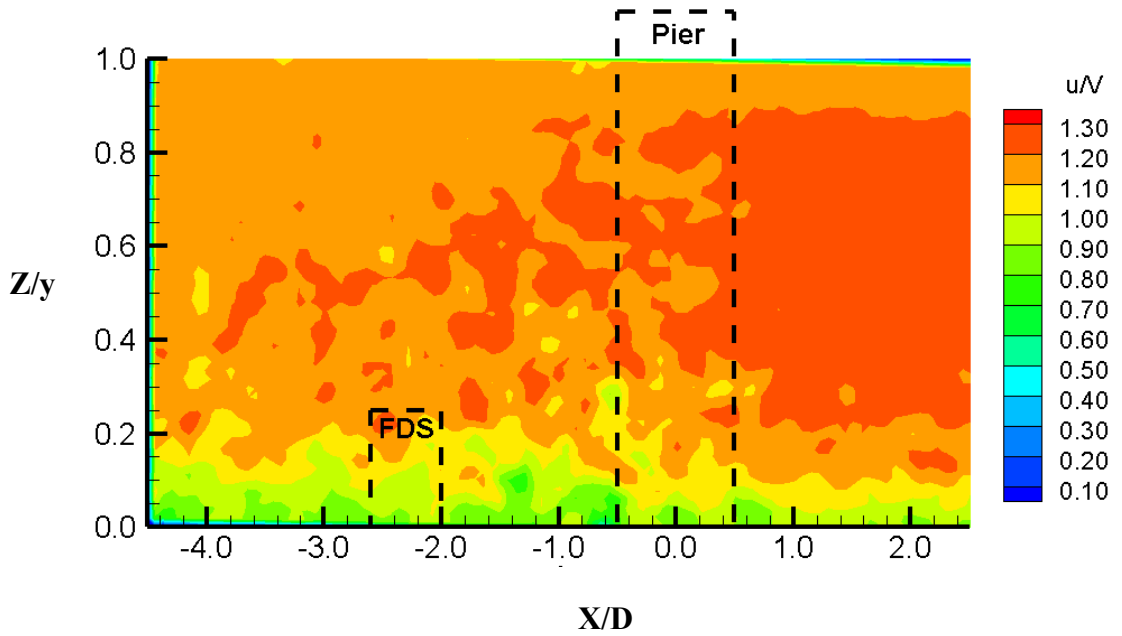


Figure B.17. Normalised streamwise velocity for the single pier case and FDS with $H/y = 0.25$ at $Y/D = 4$

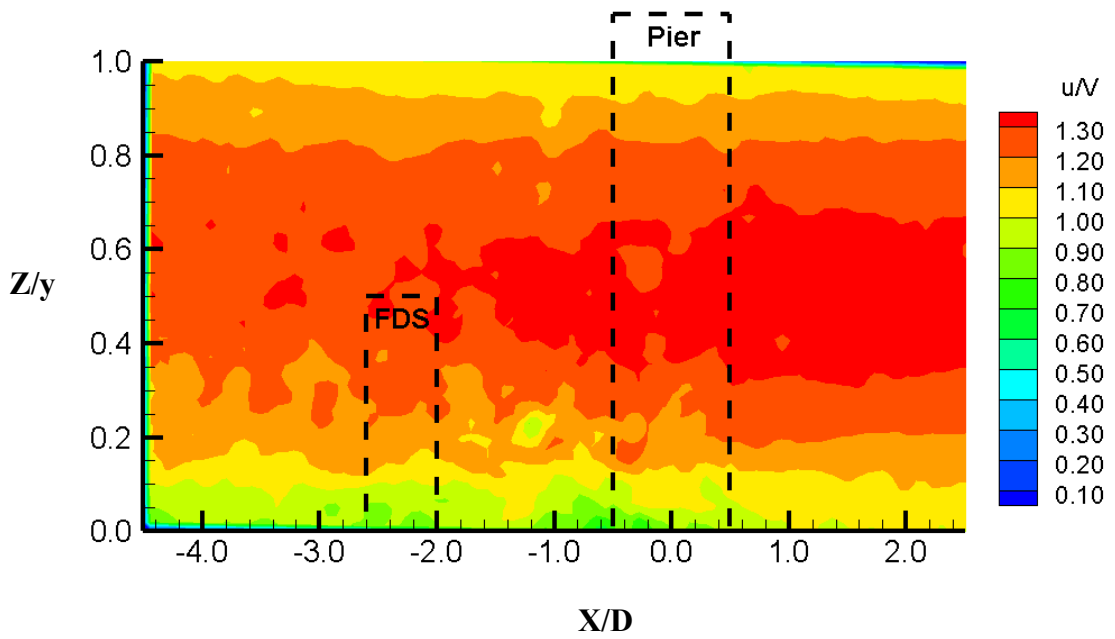


Figure B.18. Normalised streamwise velocity for the single pier case and FDS with $H/y=0.50$ at $Y/D = 4$

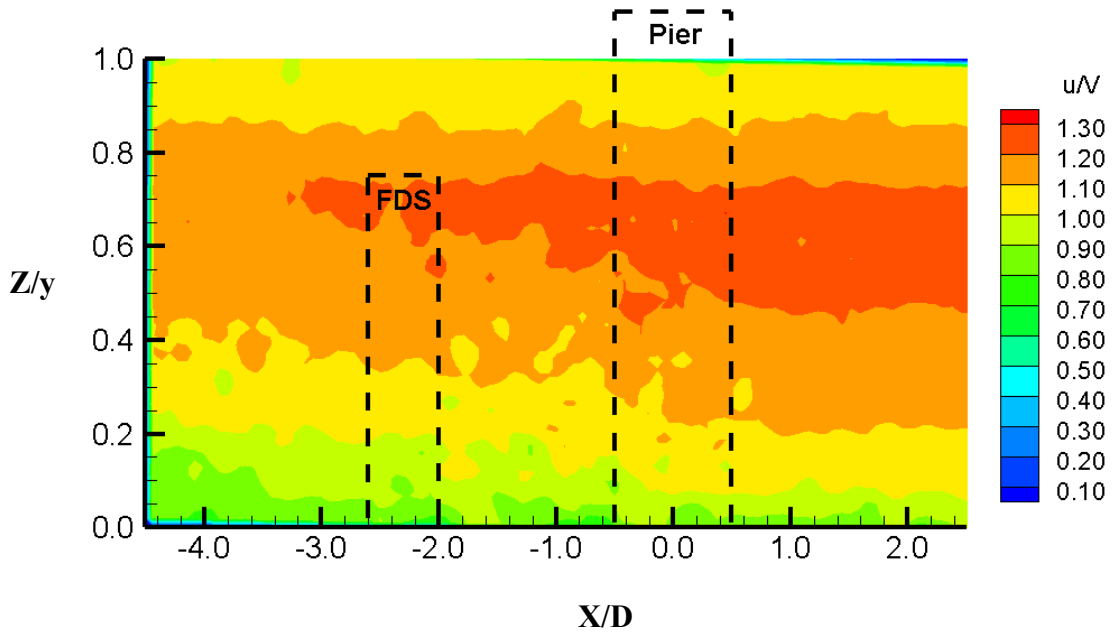


Figure B.19. Normalised streamwise velocity for the single pier case and FDS with $H/y=0.75$ at $Y/D = 4$

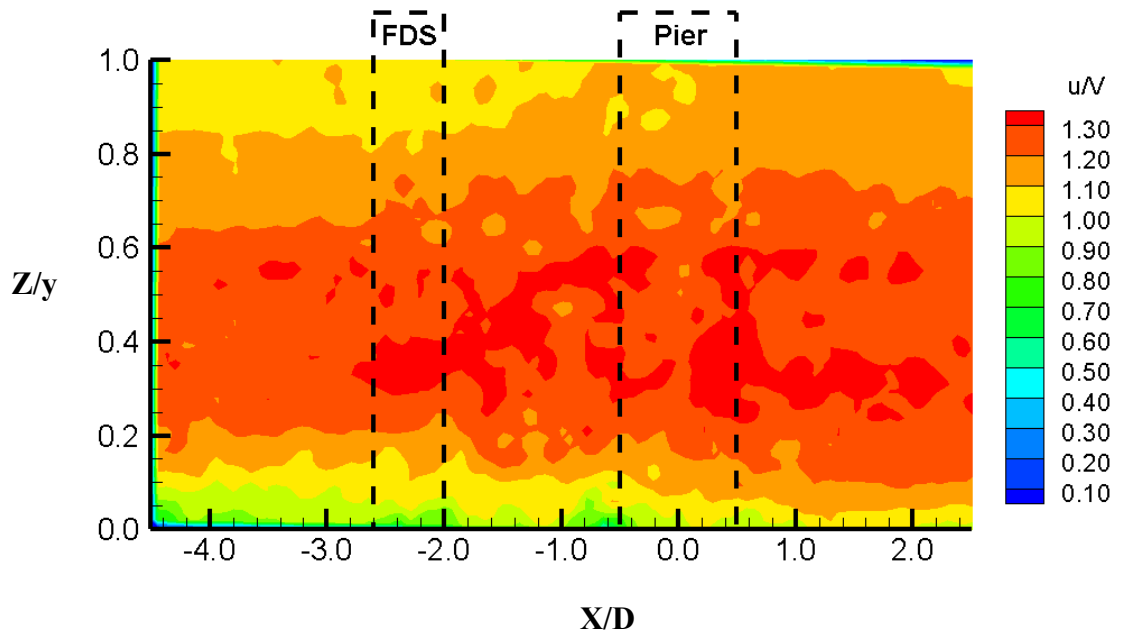


Figure B.20. Normalised streamwise velocity for the single pier case and FDS with $H/y > 1$ at $Y/D = 4$

B.2. Plots of Vertical Velocity Component

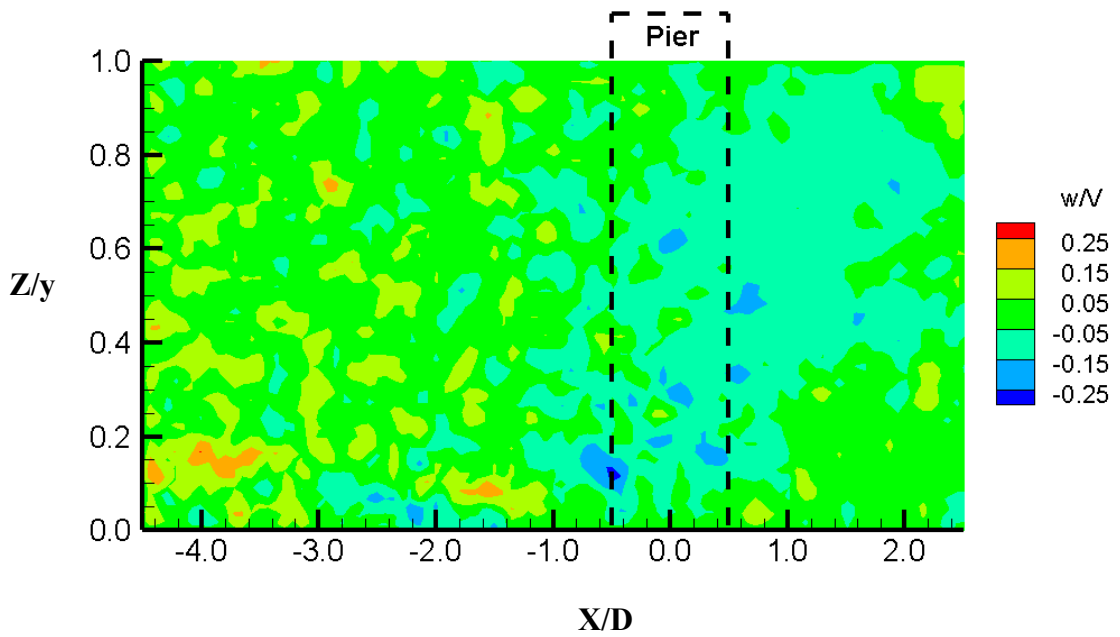


Figure B.21. Normalised vertical velocity for the single pier case at $Y/D = 1$

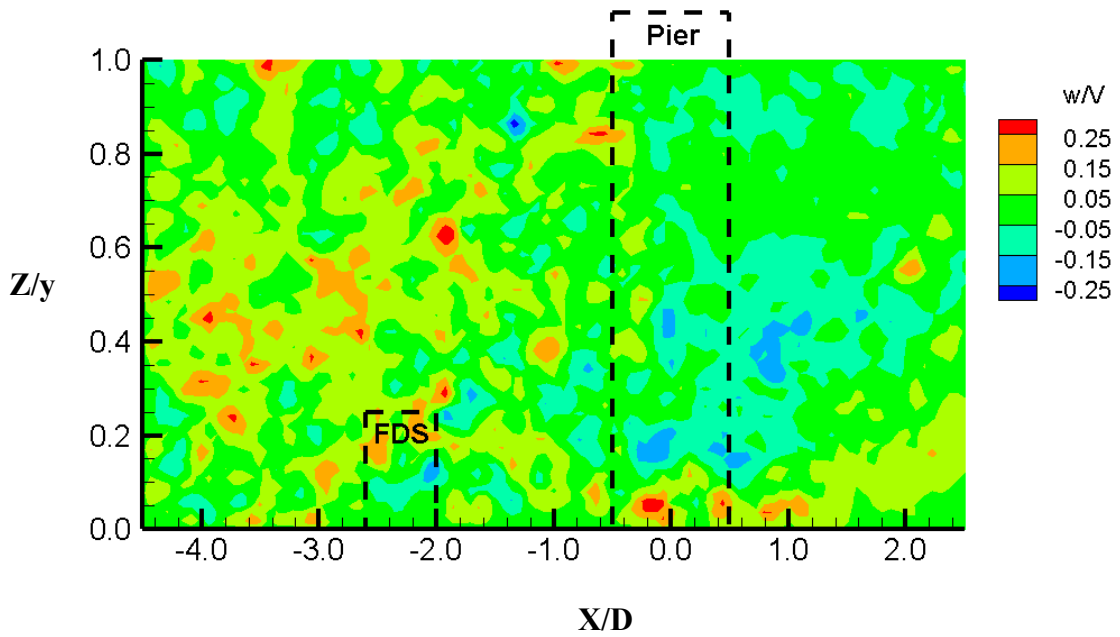


Figure B.22. Normalised vertical velocity for the single pier case and FDS with $H/y = 0.25$ at $Y/D = 1$

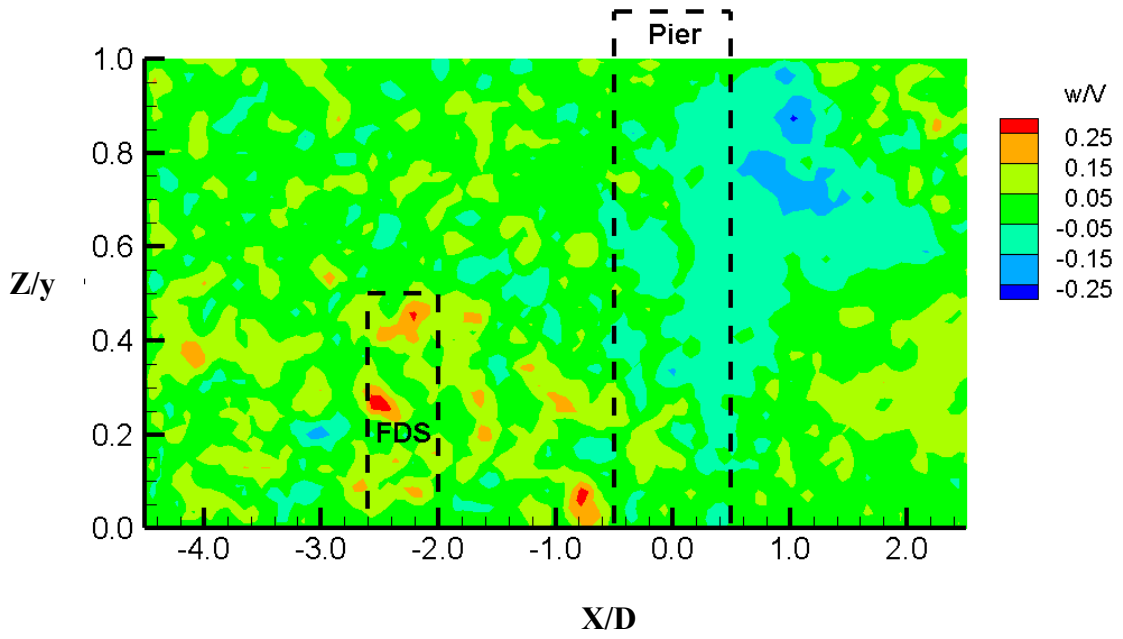


Figure B.23. Normalised vertical velocity for the single pier case and FDS with $H/y=0.50$ at $Y/D = 1$

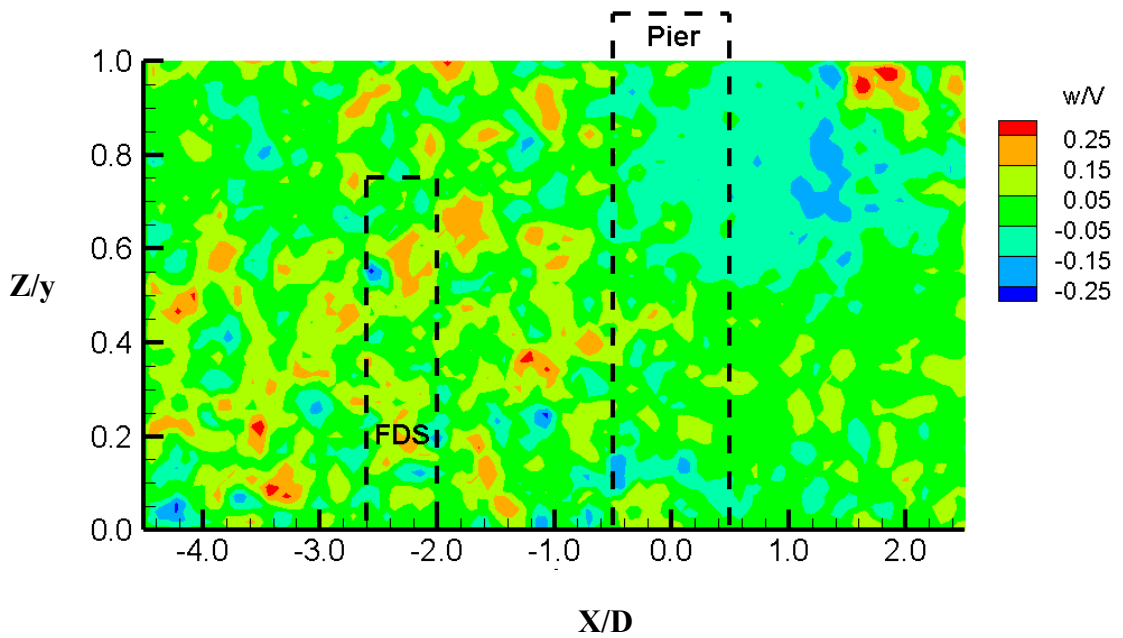


Figure B.24. Normalised vertical velocity for the single pier case and FDS with $H/y=0.75$ at $Y/D = 1$

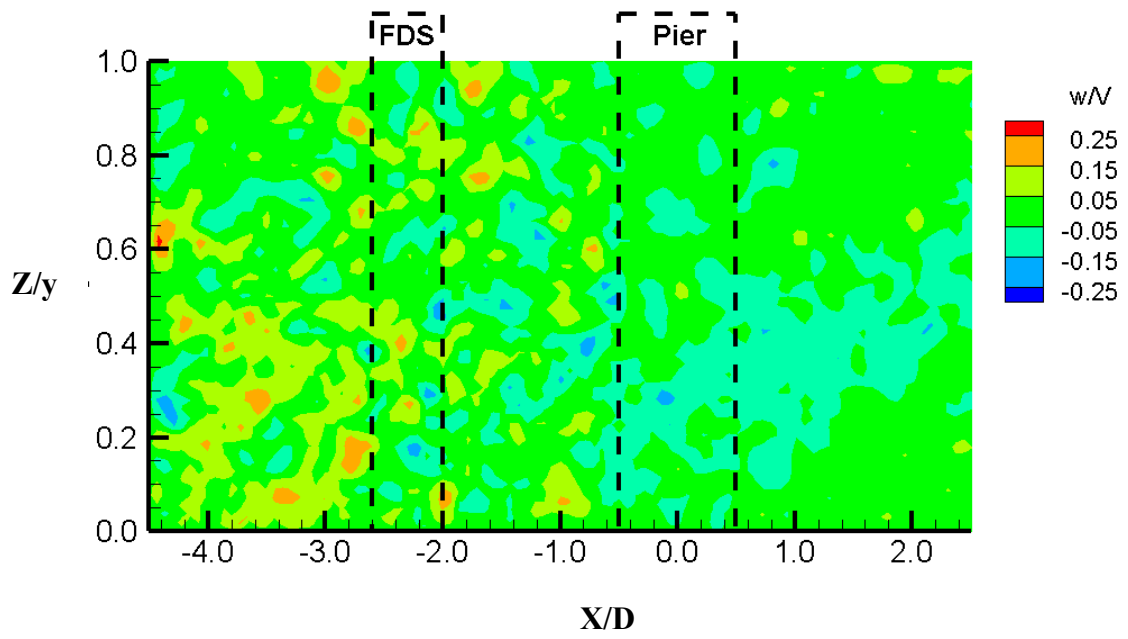


Figure B.25. Normalised vertical velocity for the single pier case and FDS with $H/y > 1$ at $Y/D = 1$

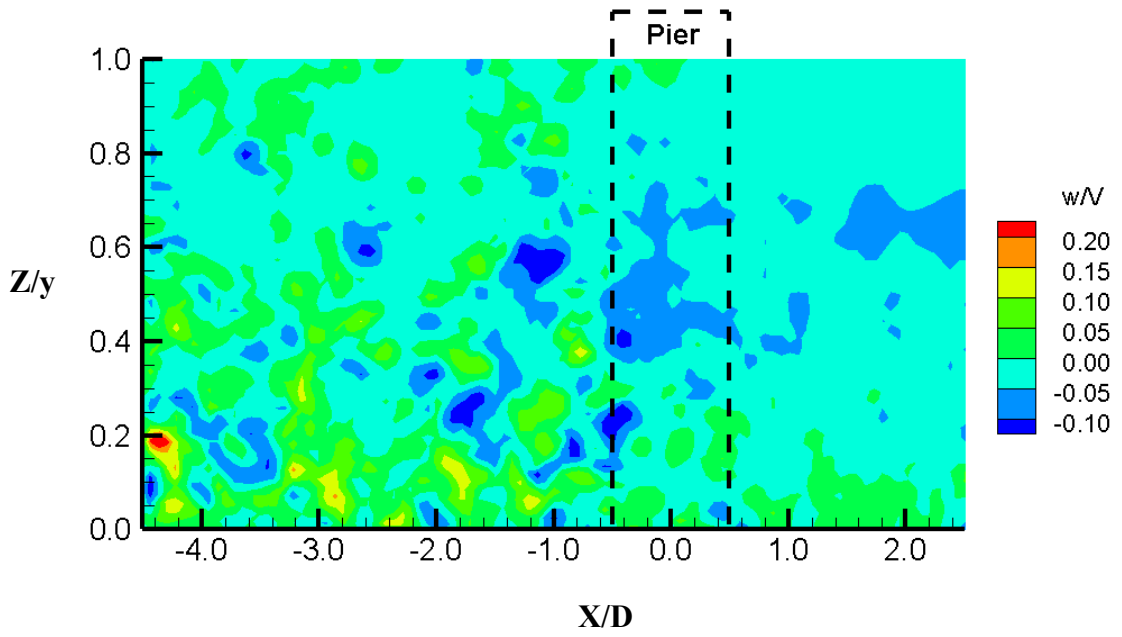


Figure B.26. Normalised vertical velocity for the single pier case at $Y/D = 2$

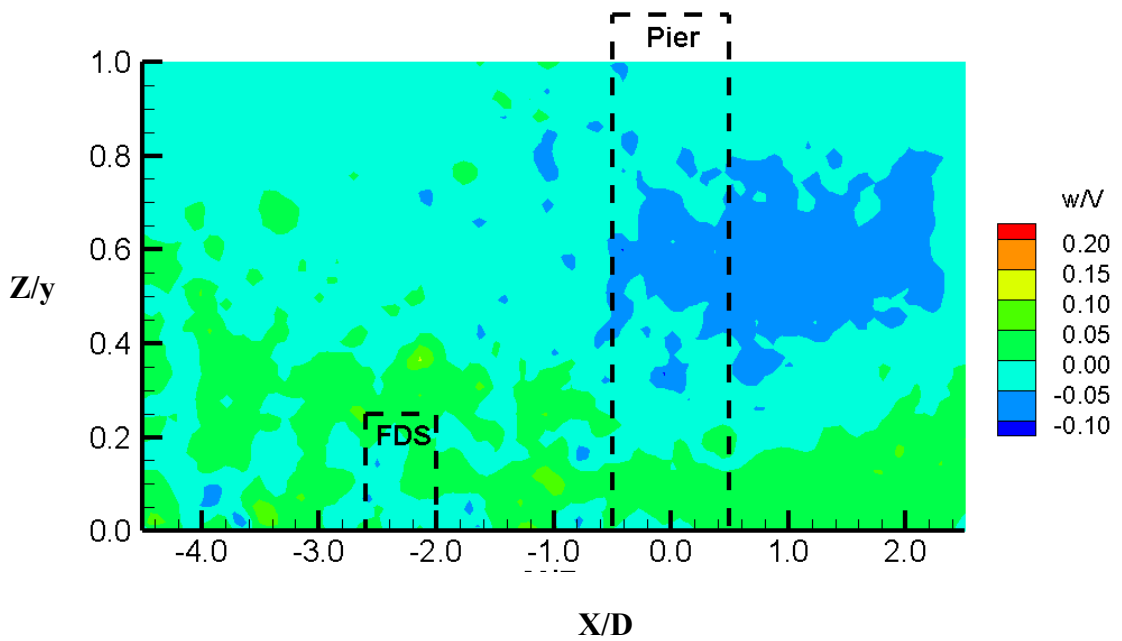


Figure B.27. Normalised vertical velocity for the single pier case and FDS with $H/y=0.25$ at $Y/D = 2$

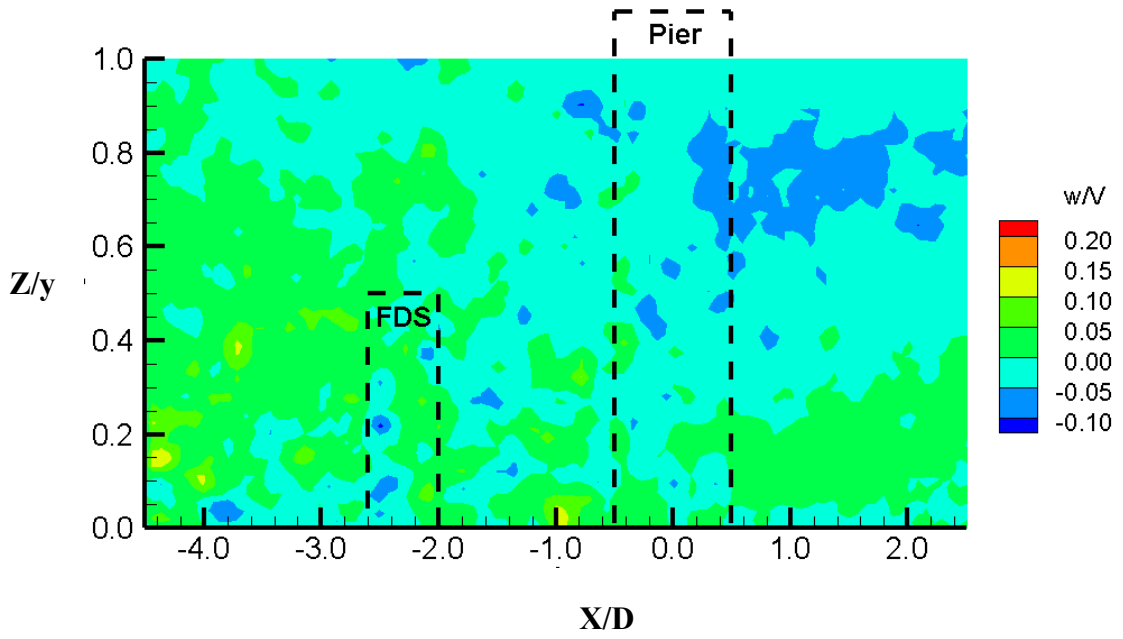


Figure B.28. Normalised vertical velocity for the single pier case and FDS with $H/y=0.50$ at $Y/D = 2$

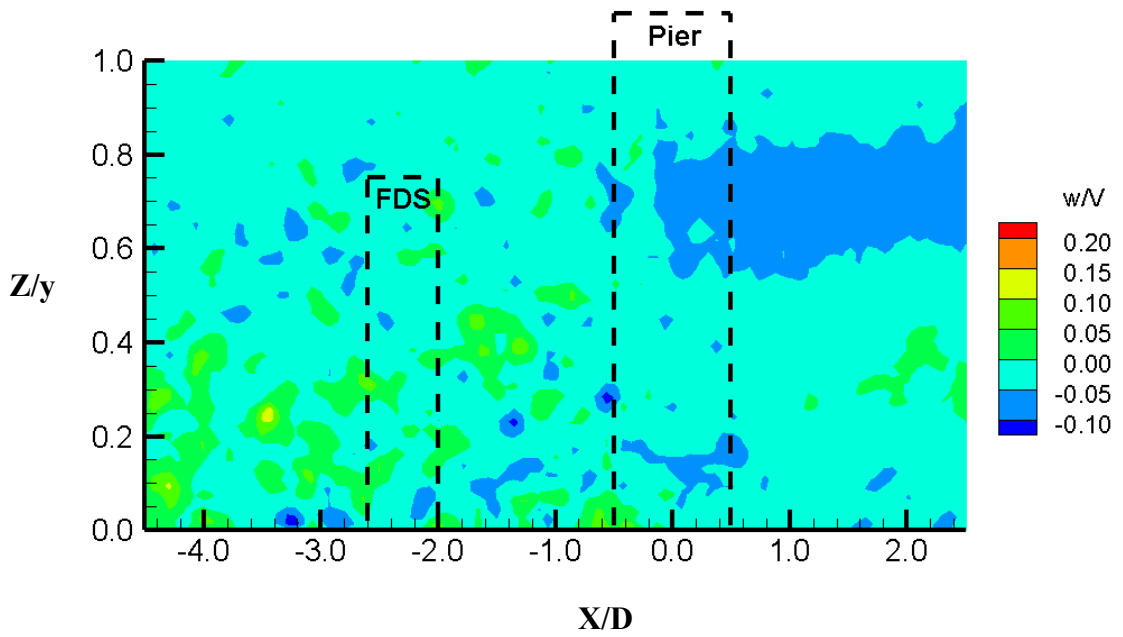


Figure B.29. Normalised vertical velocity for the single pier case and FDS with $H/y=0.75$ at $Y/D = 2$

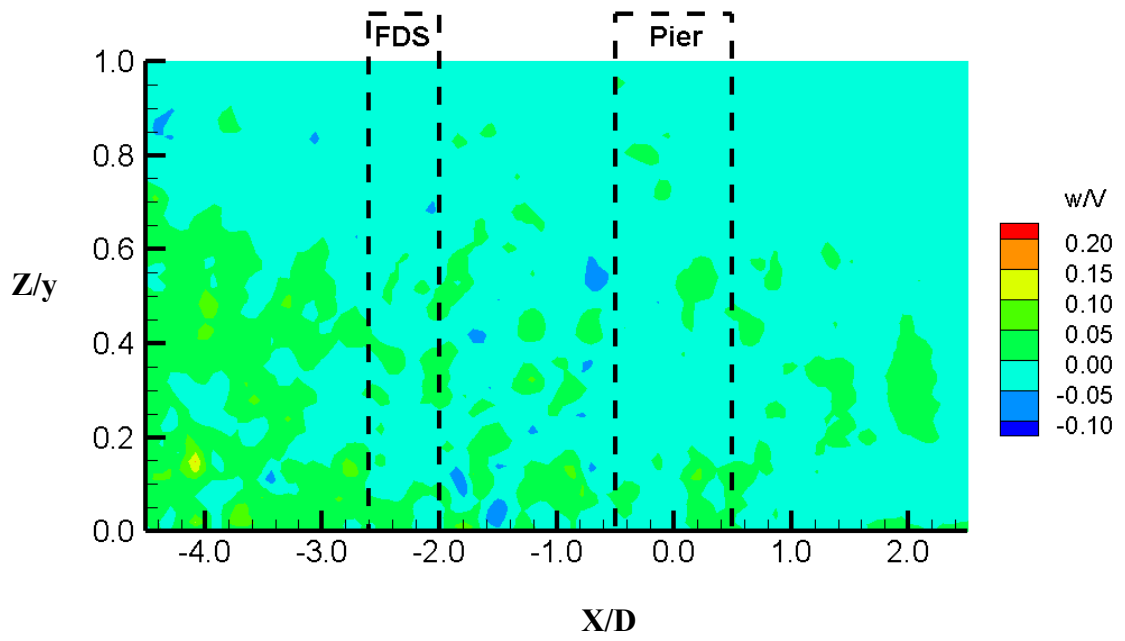


Figure B.30. Normalised vertical velocity for the single pier case and FDS with $H/y > 1$ at $Y/D = 2$

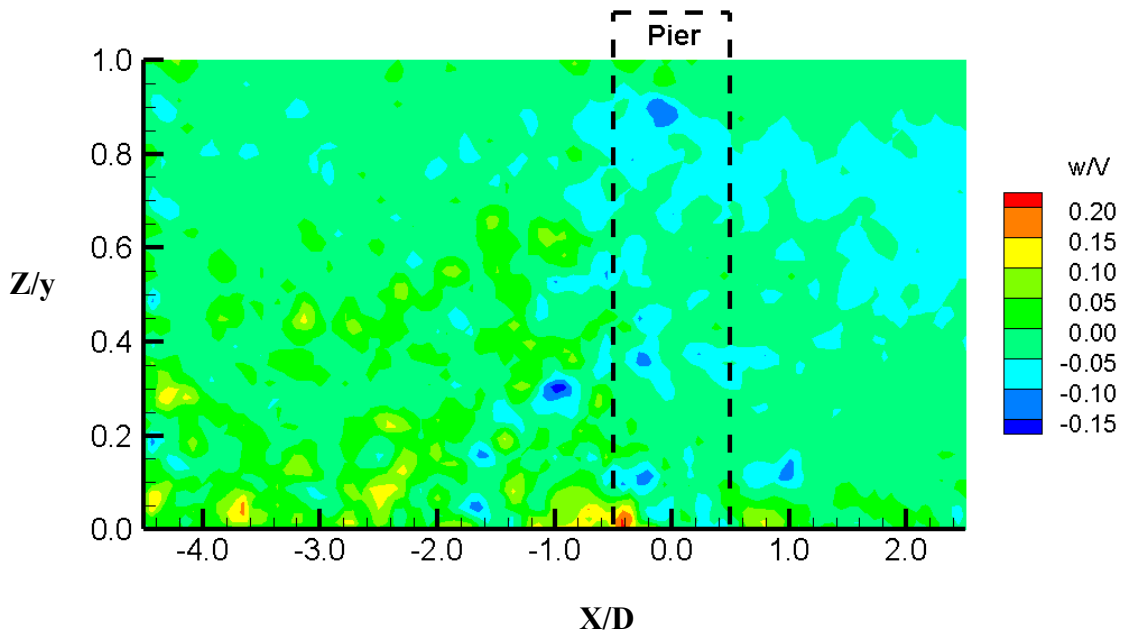


Figure B.31. Normalised vertical velocity for the single pier case at $Y/D = 3$

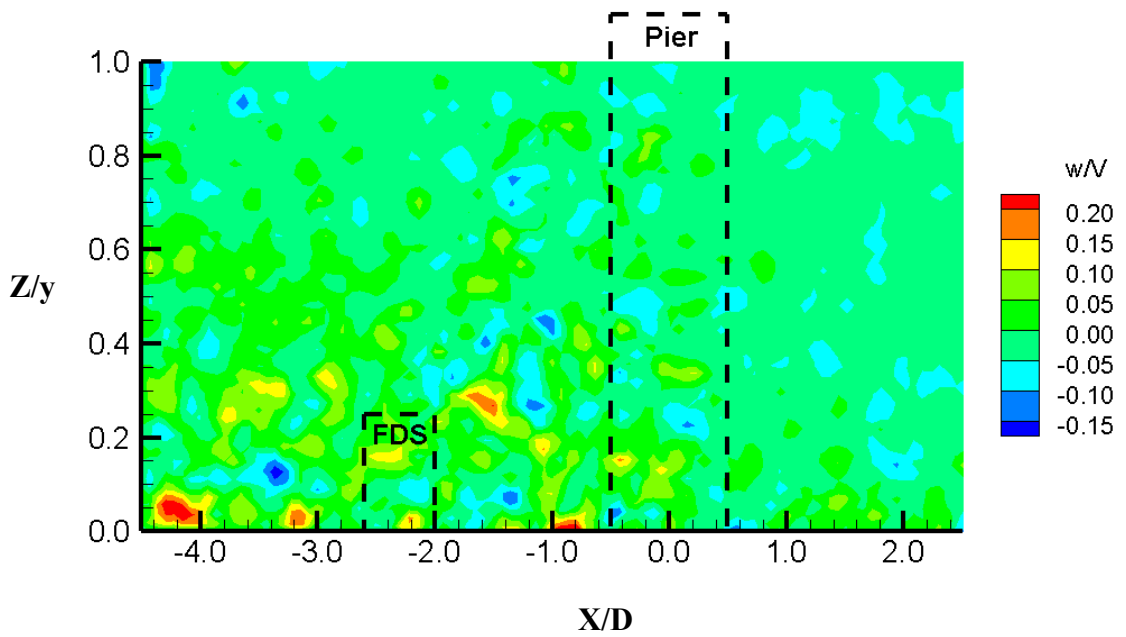


Figure B.32. Normalised vertical velocity for the single pier case and FDS with $H/y=0.25$ at $Y/D = 3$

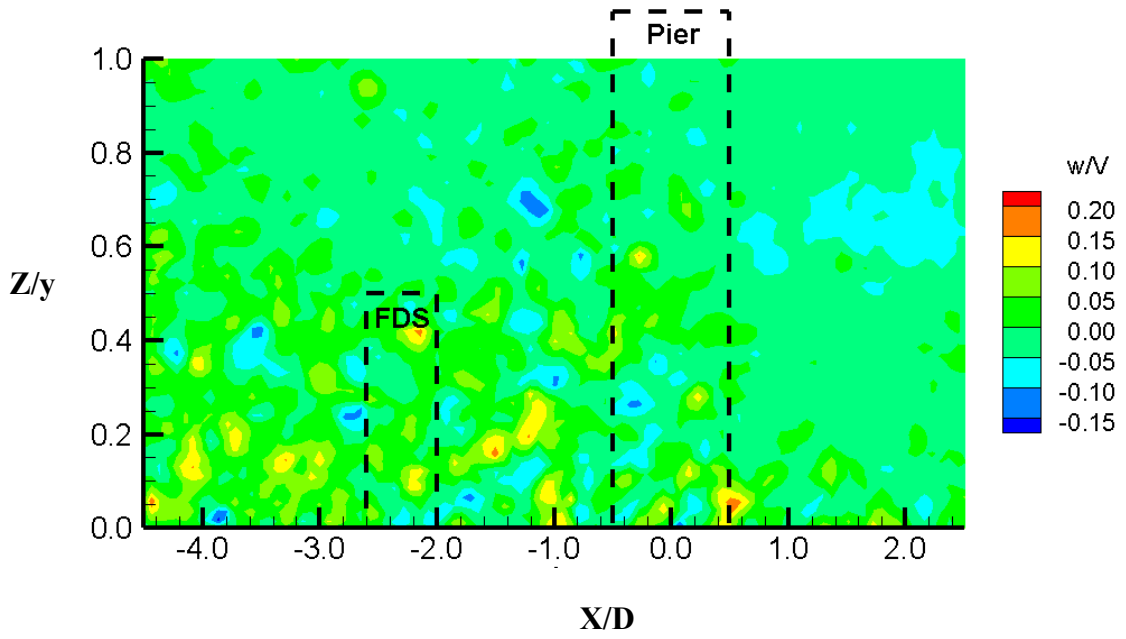


Figure B.33. Normalised vertical velocity for the single pier case and FDS with $H/y=0.50$ at $Y/D = 3$

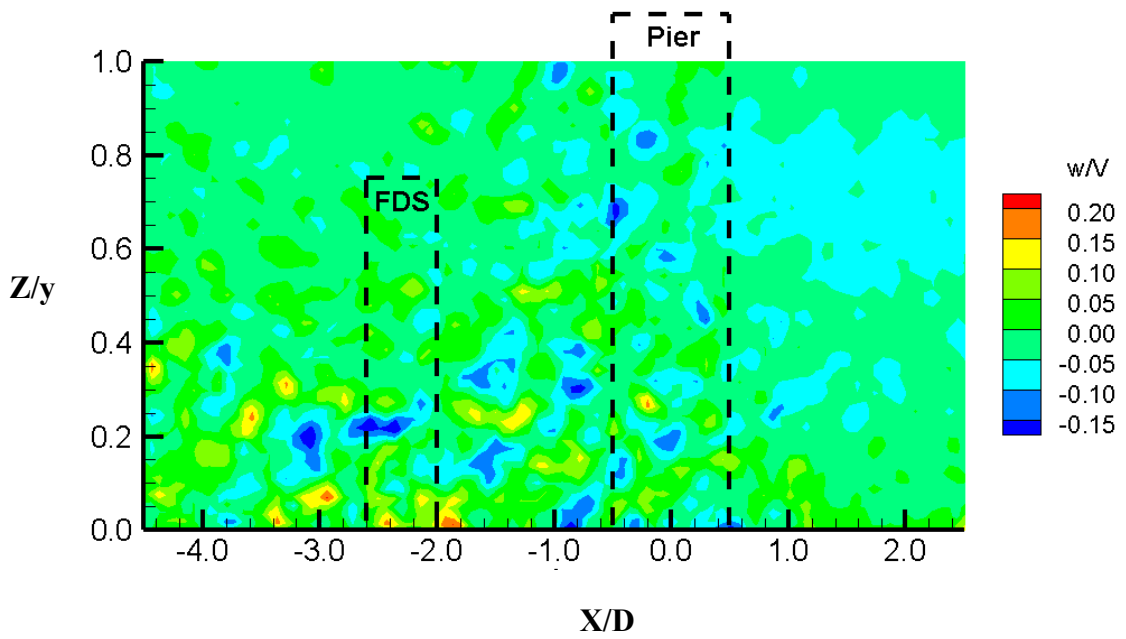


Figure B.34. Normalised vertical velocity for the single pier case and FDS with $H/y=0.75$ at $Y/D = 3$

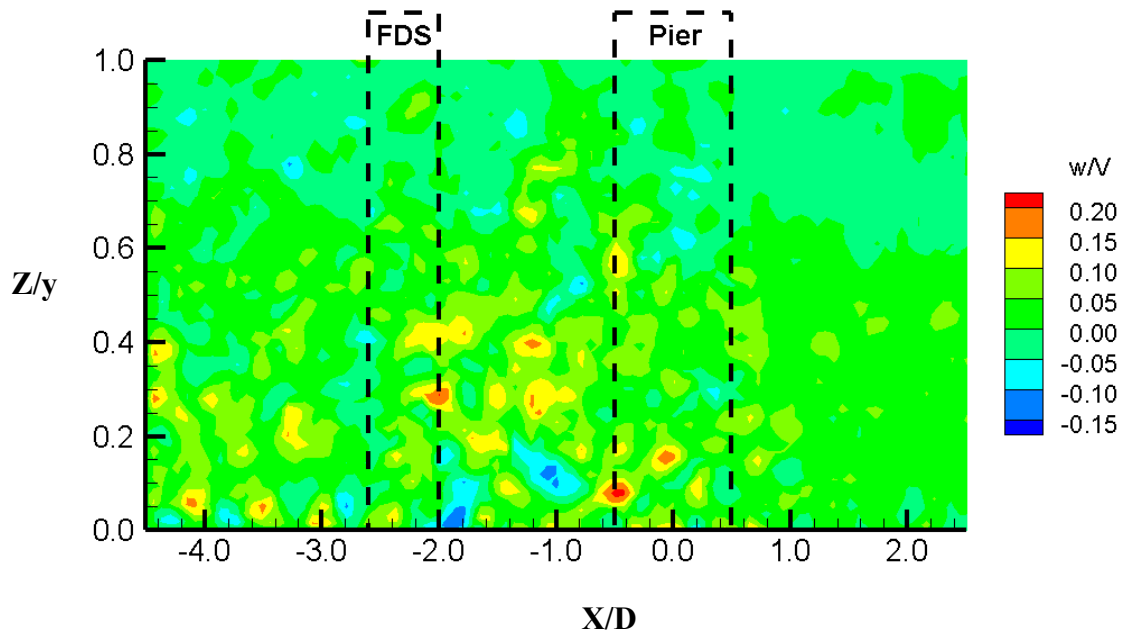


Figure B.35. Normalised vertical velocity for the single pier case and FDS with $H/y > 1$ at $Y/D = 3$

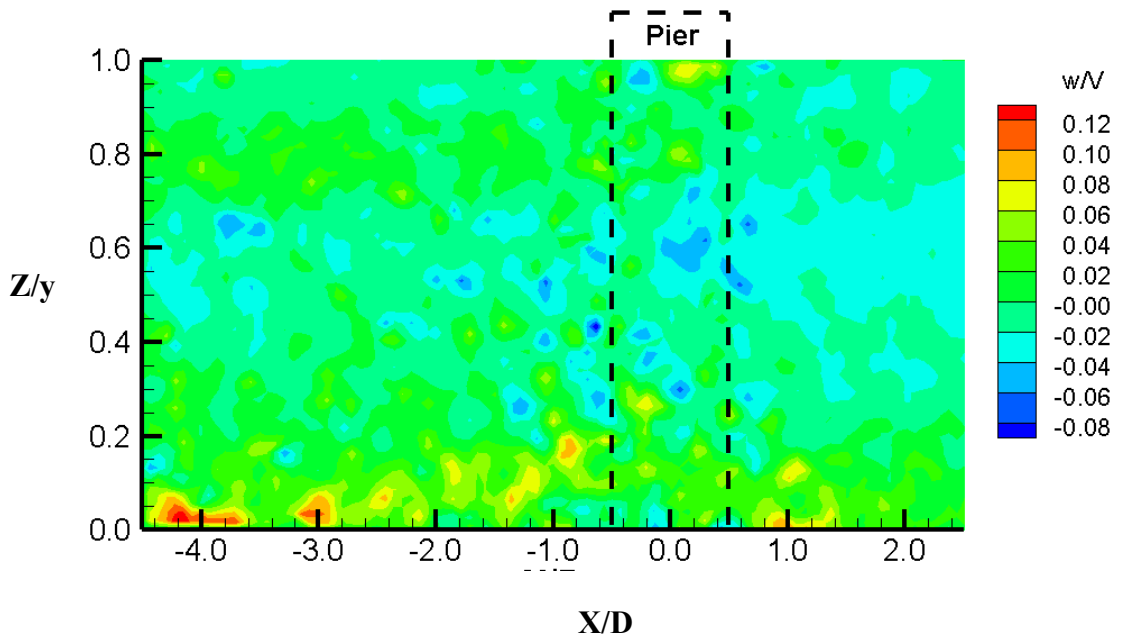


Figure B.36. Normalised vertical velocity for the single pier case at $Y/D = 4$

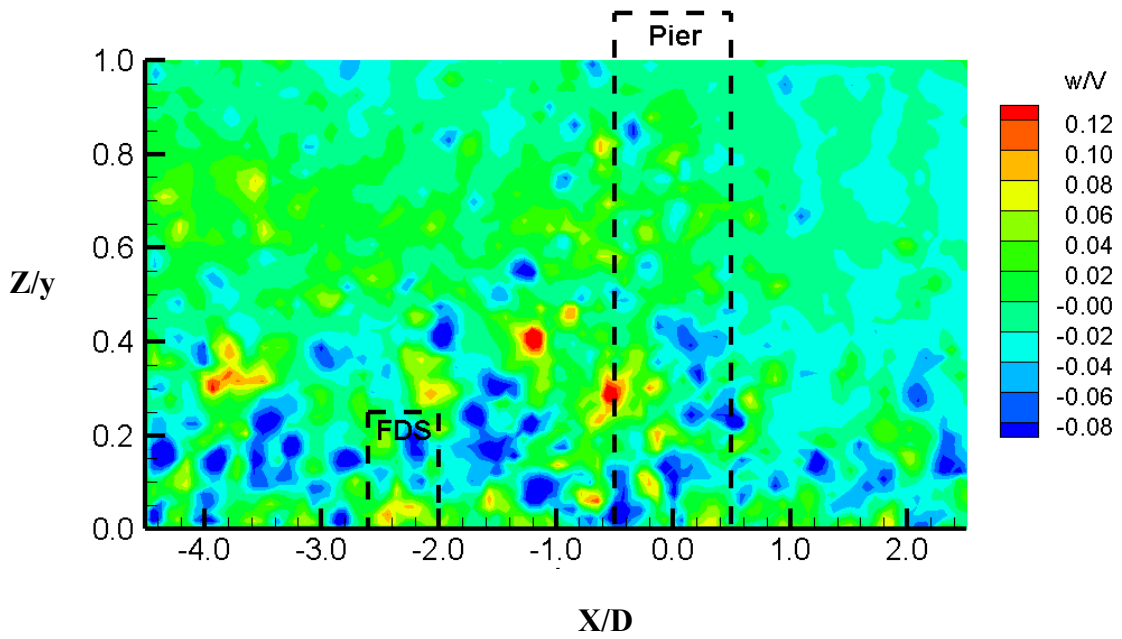


Figure B.37. Normalised vertical velocity for the single pier case and FDS with $H/y=0.25$ at $Y/D = 4$

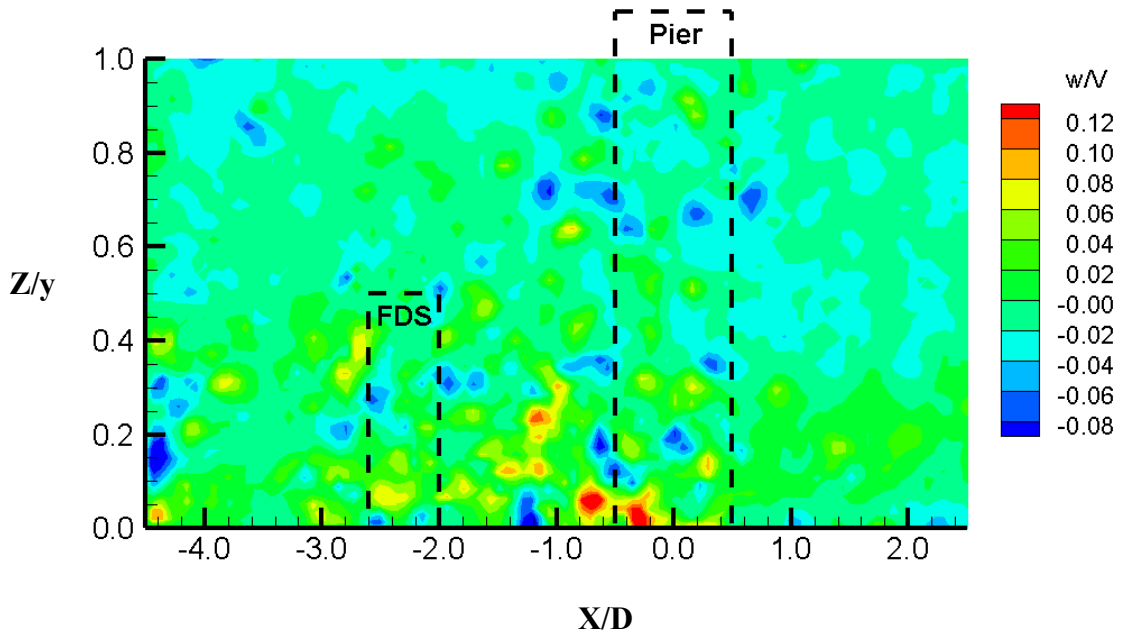


Figure B.38. Normalised vertical velocity for the single pier case and FDS with $H/y=0.50$ at $Y/D = 4$

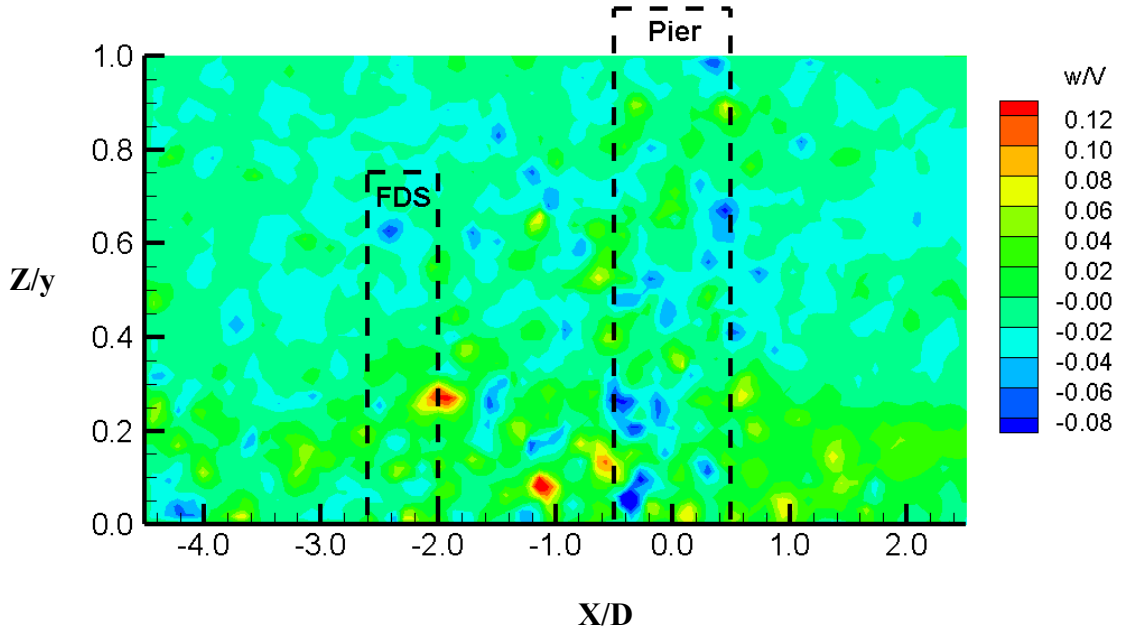


Figure B.39. Normalised vertical velocity for the single pier case and FDS with $H/y=0.75$ at $Y/D = 4$

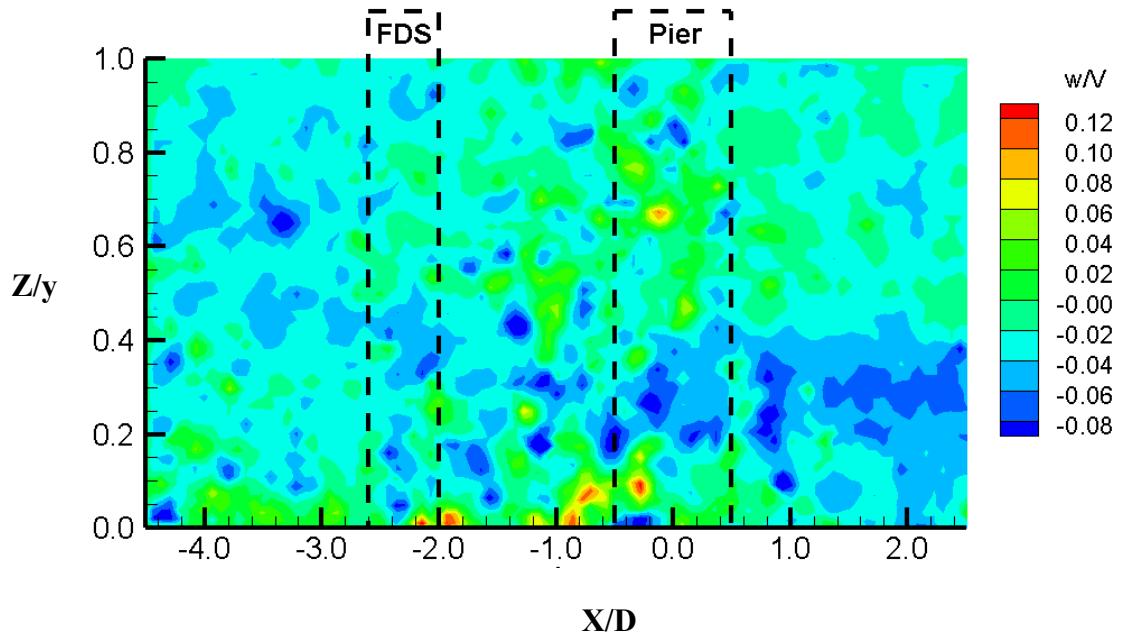


Figure B.40. Normalised vertical velocity for the single pier case and FDS with $H/y > 1$ at $Y/D = 4$

B.3. Plots of Absolute Flow Velocity and Streamlines

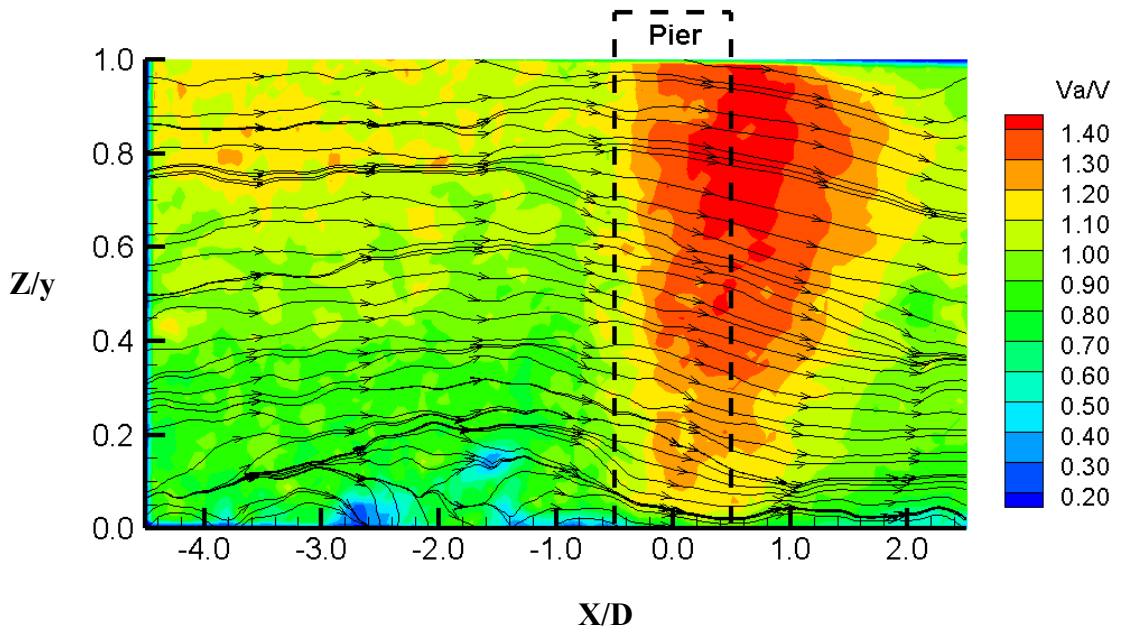


Figure B.41. Normalised absolute flow velocity and Streamlines for the single pier case at $Y/D = 1$

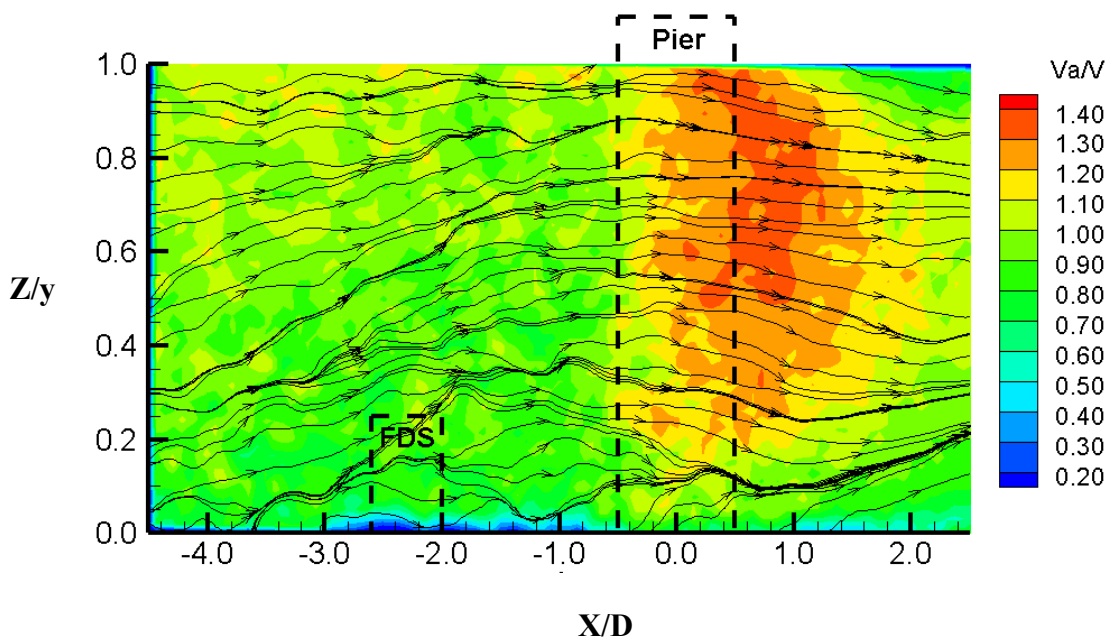


Figure B.42. Normalised absolute flow velocity and Streamlines for the single pier case and FDS with $H/y = 0.25$ at $Y/D = 1$

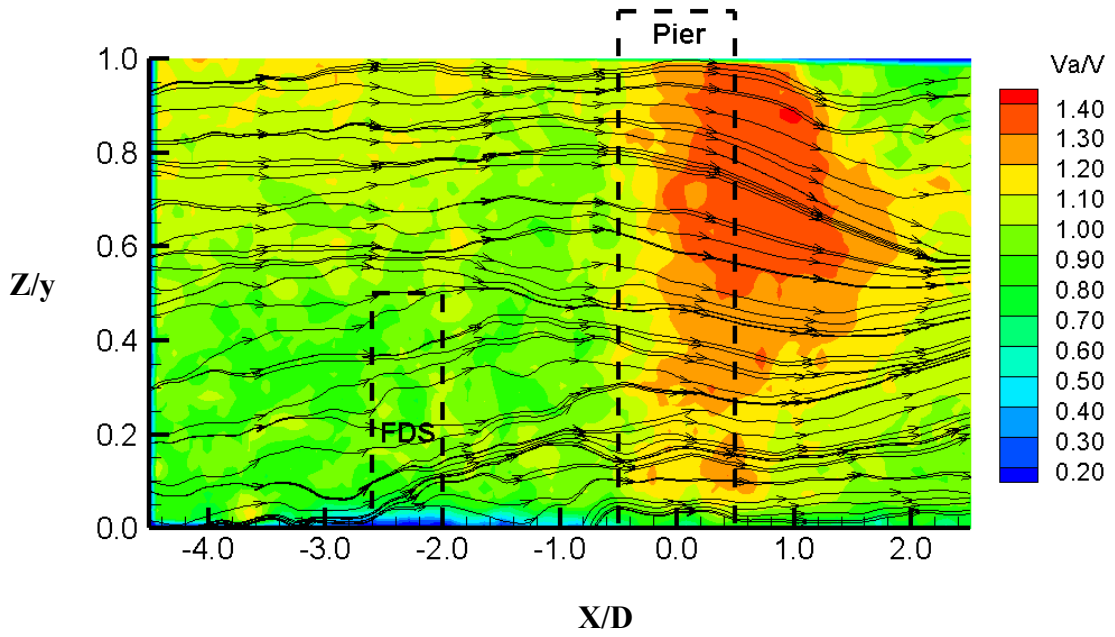


Figure B.43. Normalised absolute flow velocity and Streamlines for the single pier case and FDS with $H/y=0.50$ at $Y/D = 1$

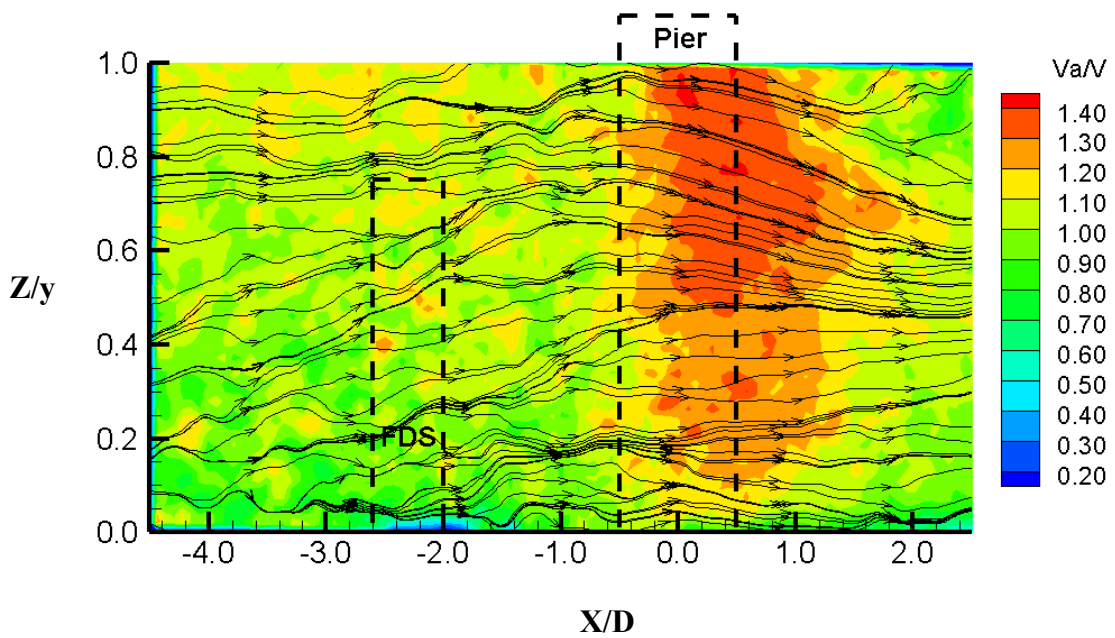


Figure B.44. Normalised absolute flow velocity and Streamlines for the single pier case and FDS with $H/y=0.75$ at $Y/D = 1$

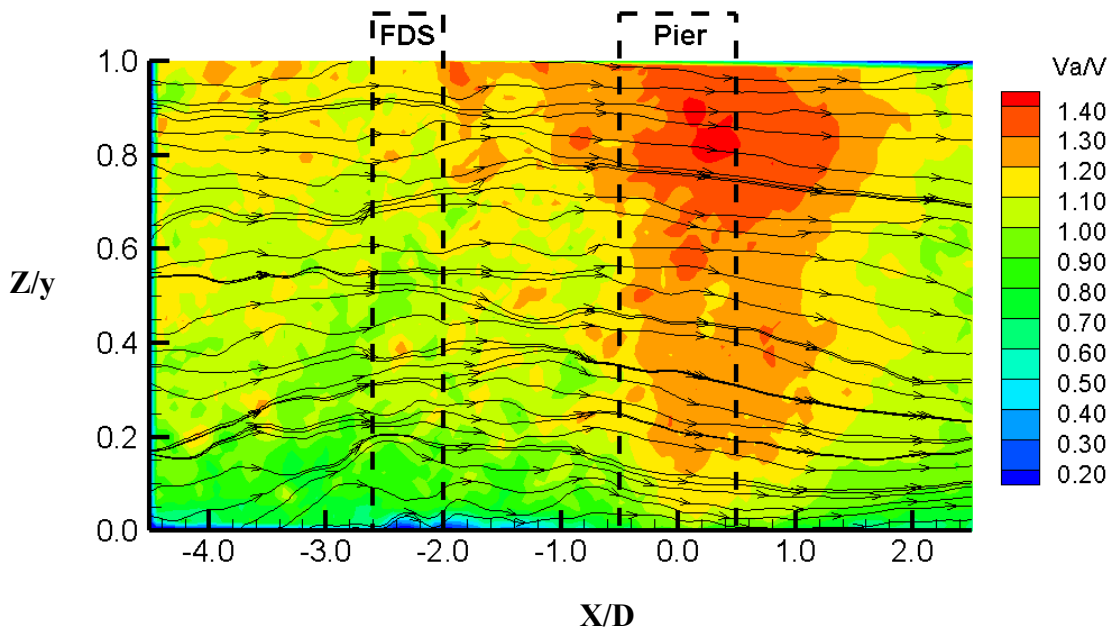


Figure B.45. Normalised absolute flow velocity and Streamlines for the single pier case and FDS with $H/y > 1$ at $Y/D = 1$

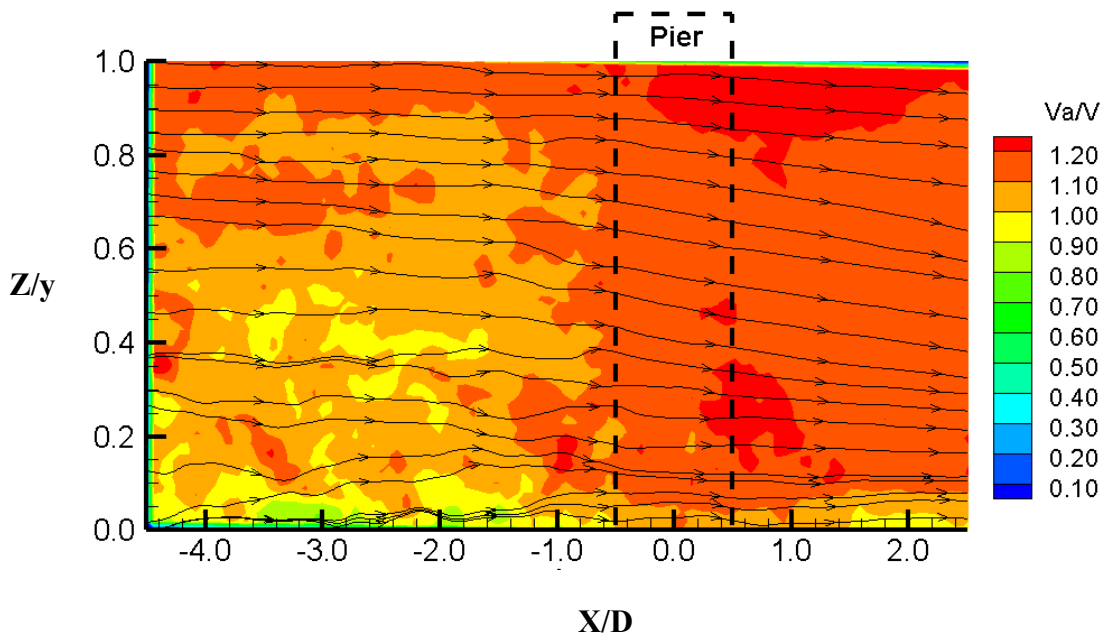


Figure B.46. Normalised absolute flow velocity and Streamlines for the single pier case at $Y/D = 2$

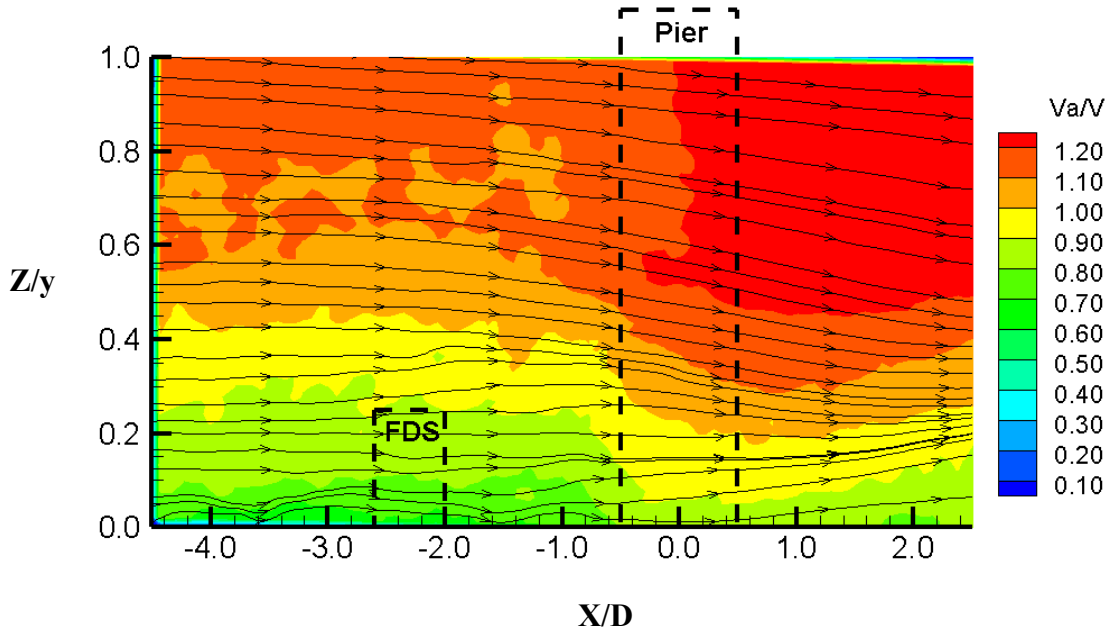


Figure B.47. Normalised absolute flow velocity and Streamlines for the single pier case and FDS with $H/y = 0.25$ at $Y/D = 2$

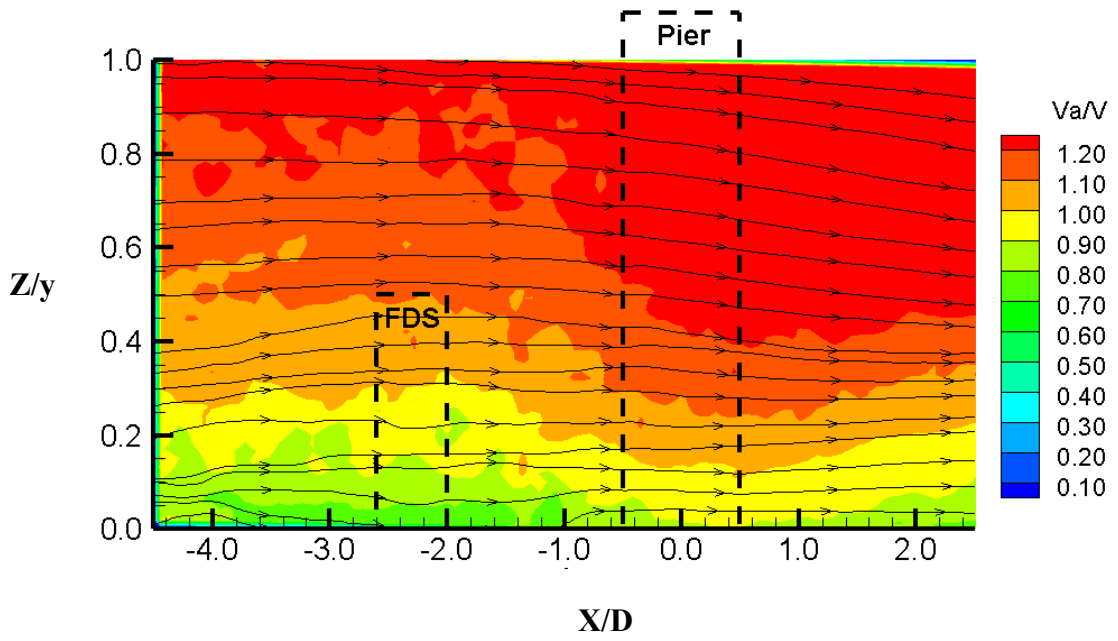


Figure B.48. Normalised absolute flow velocity and Streamlines for the single pier case and FDS with $H/y=0.50$ at $Y/D = 2$

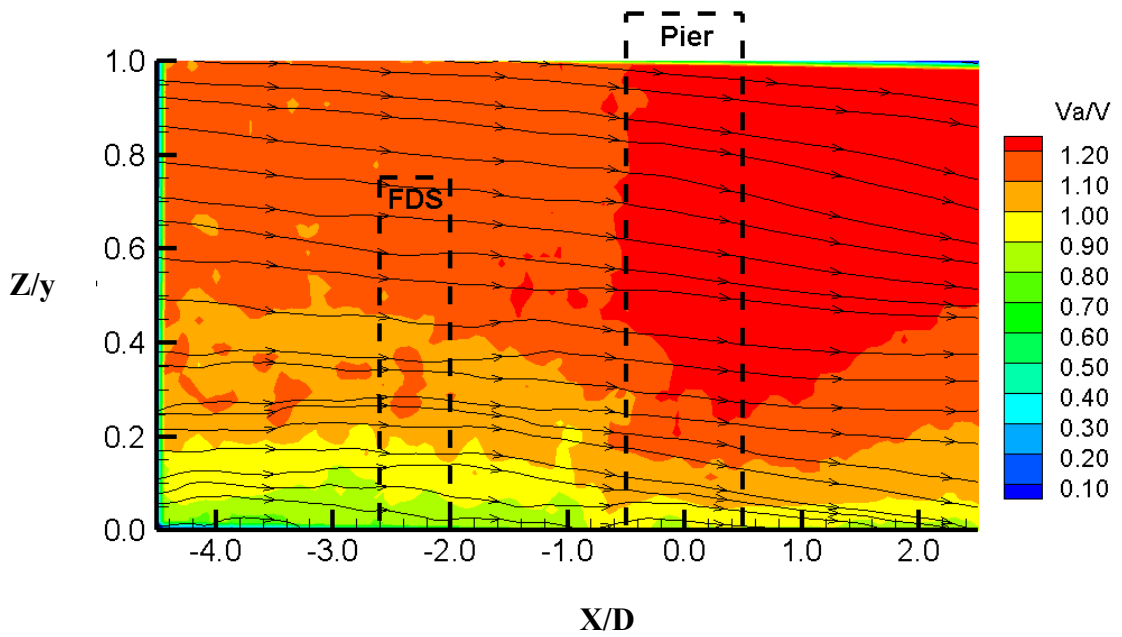


Figure B.49. Normalised absolute flow velocity and Streamlines for the single pier case and FDS with $H/y=0.75$ at $Y/D = 2$

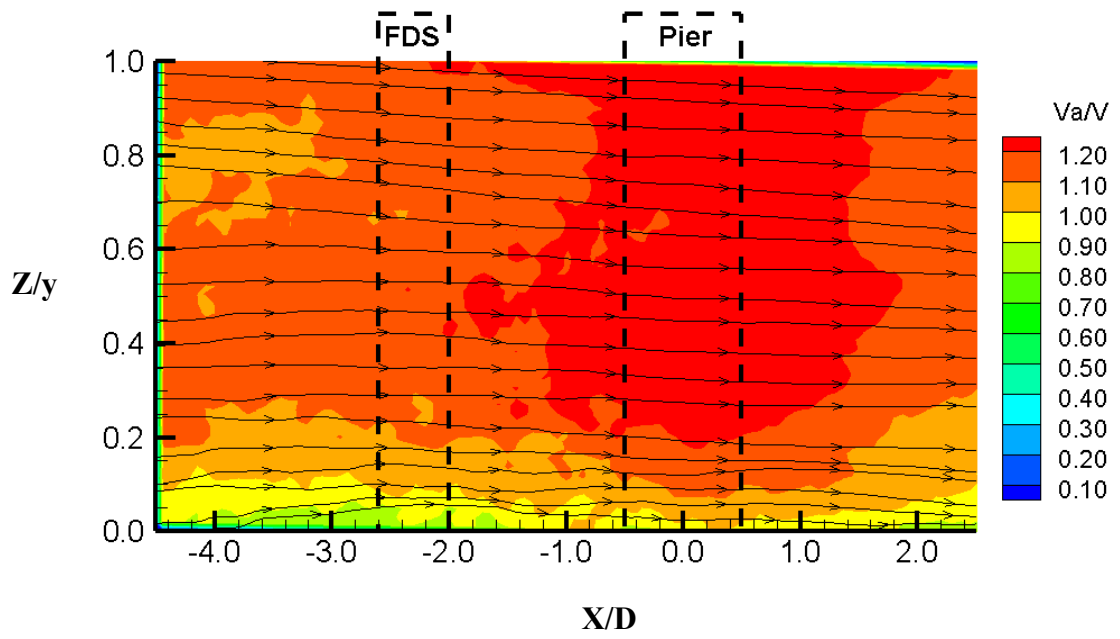


Figure B.50. Normalised absolute flow velocity and Streamlines for the single pier case and FDS with $H/y > 1$ at $Y/D = 2$

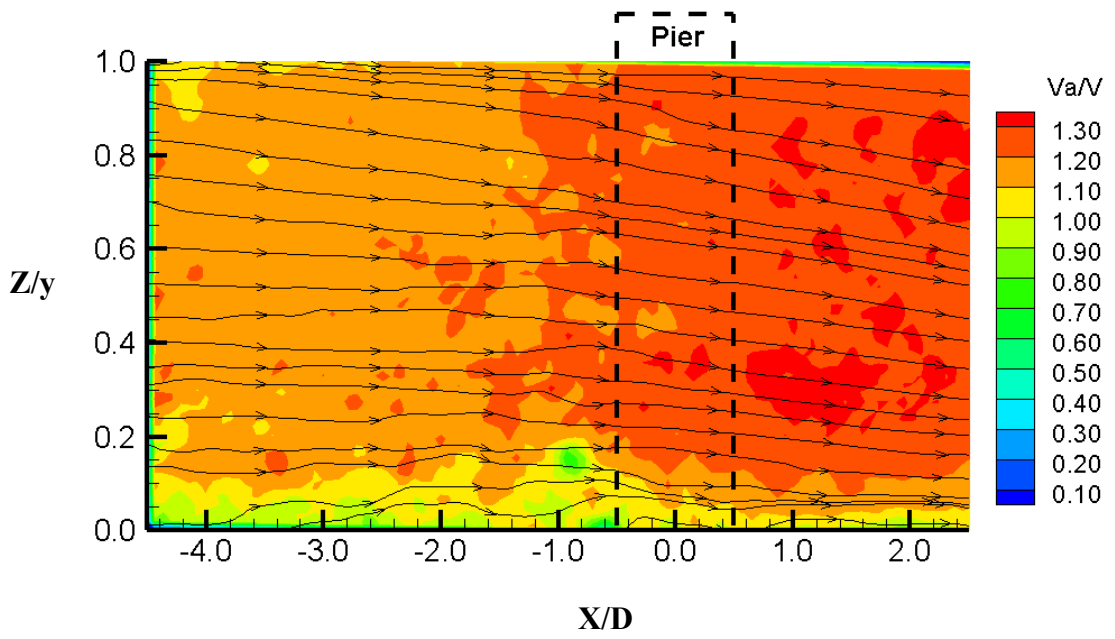


Figure B.51. Normalised absolute flow velocity and Streamlines for the single pier case at $Y/D = 3$

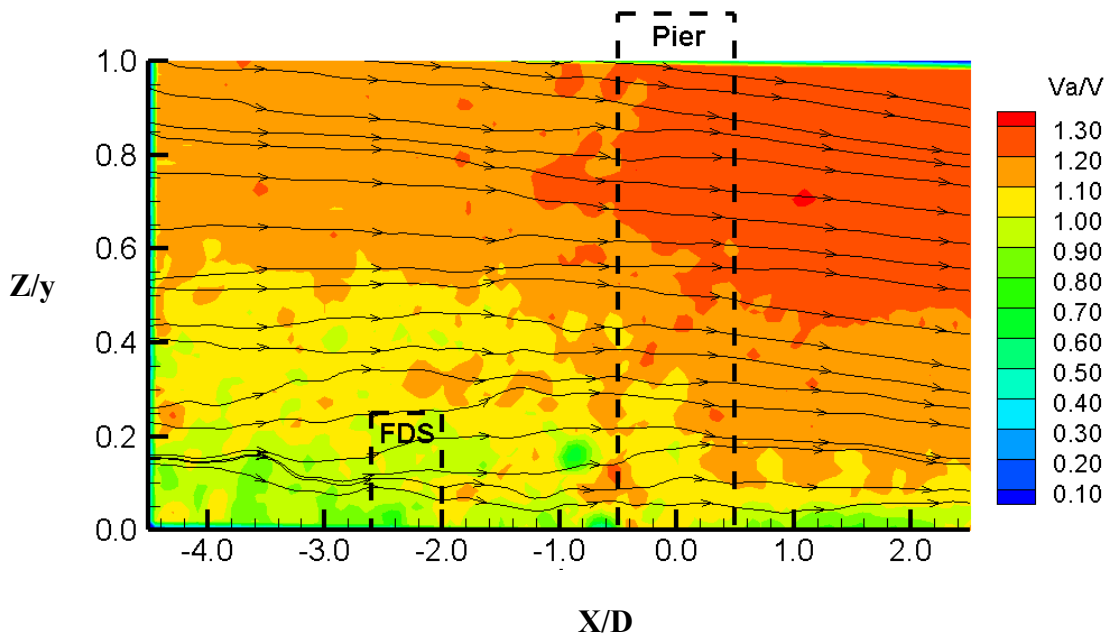


Figure B.52. Normalised absolute flow velocity and Streamlines for the single pier case and FDS with $H/y = 0.25$ at $Y/D = 3$

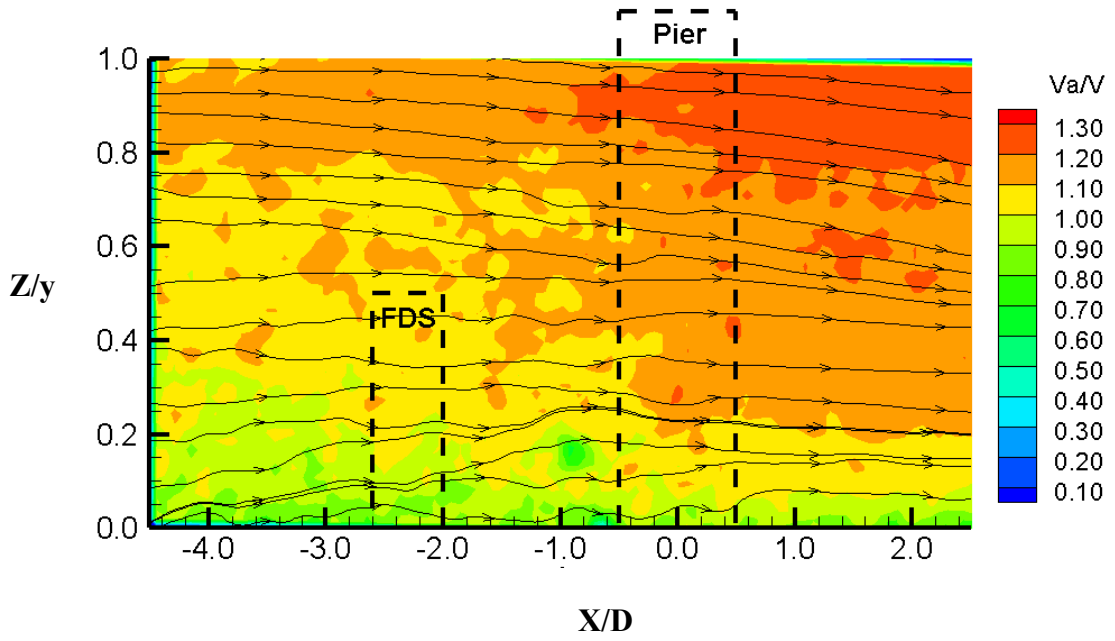


Figure B.53. Normalised absolute flow velocity and Streamlines for the single pier case and FDS with $H/y=0.50$ at $Y/D = 3$

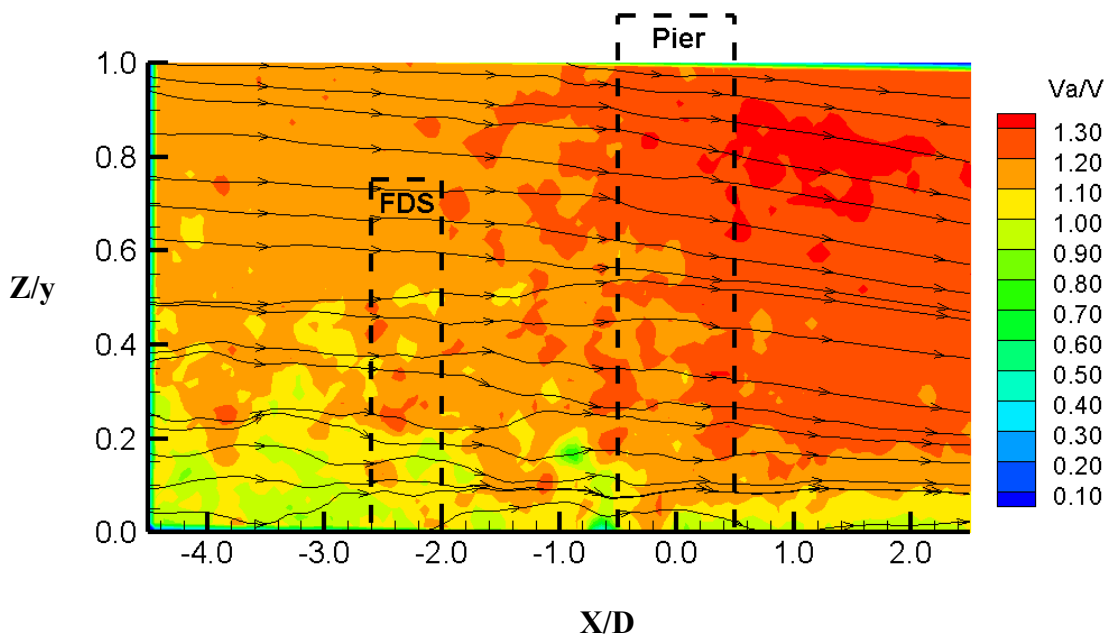


Figure B.54. Normalised absolute flow velocity and Streamlines for the single pier case and FDS with $H/y=0.75$ at $Y/D = 3$

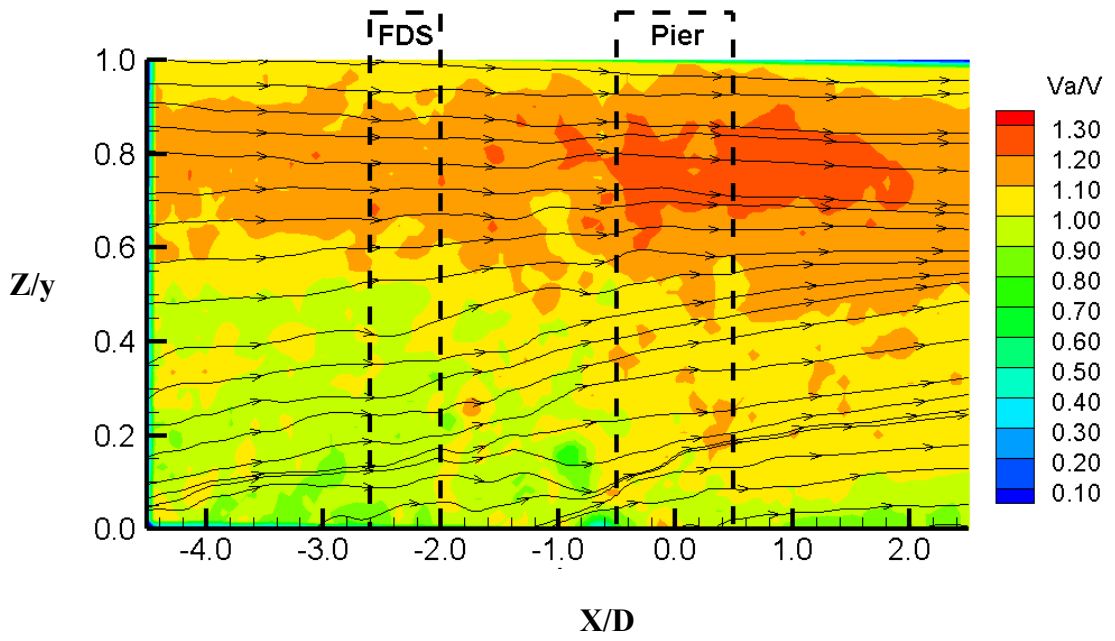


Figure B.55. Normalised absolute flow velocity and Streamlines for the single pier case and FDS with $H/y > 1$ at $Y/D = 3$

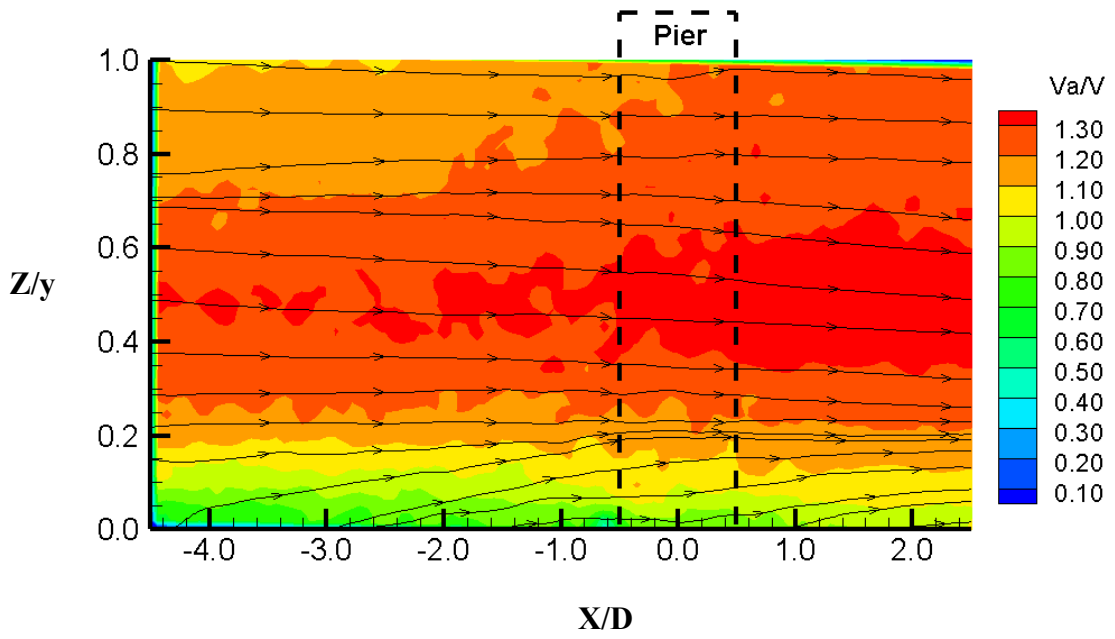


Figure B.56. Normalised absolute flow velocity and Streamlines for the single pier case at $Y/D = 4$

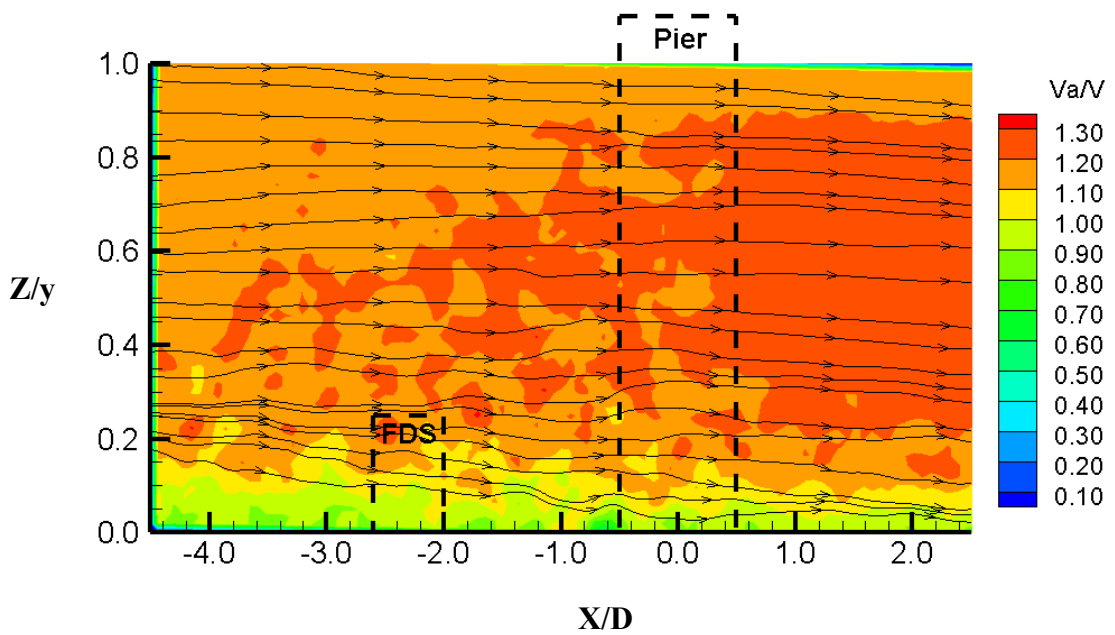


Figure B.57. Normalised absolute flow velocity and Streamlines for the single pier case and FDS with $H/y = 0.25$ at $Y/D = 4$

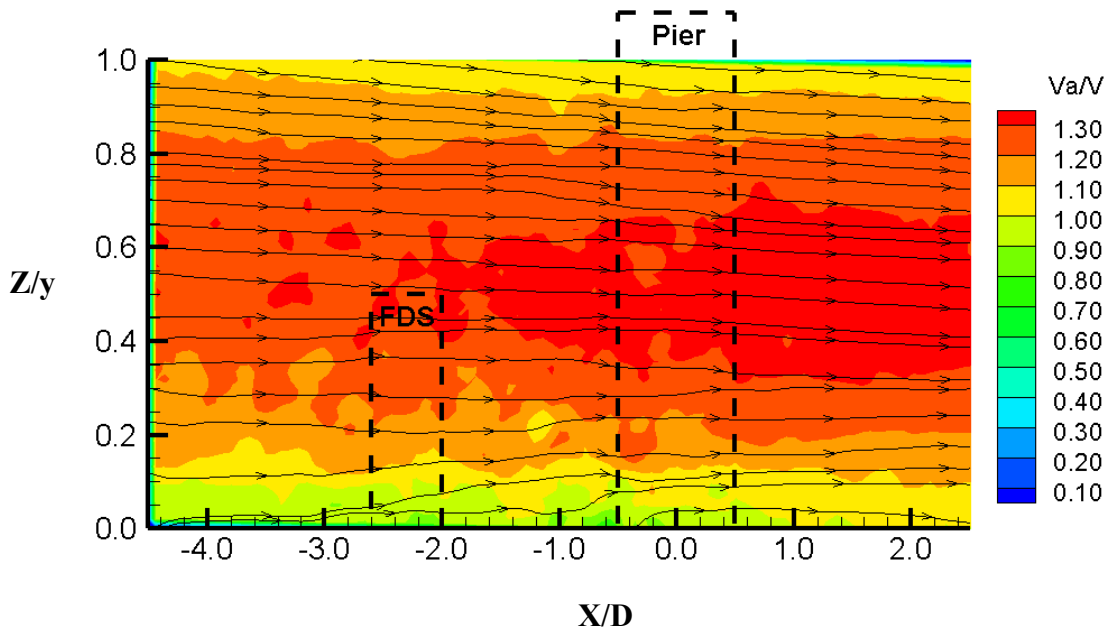


Figure B.58. Normalised absolute flow velocity and Streamlines for the single pier case and FDS with $H/y=0.50$ at $Y/D = 4$

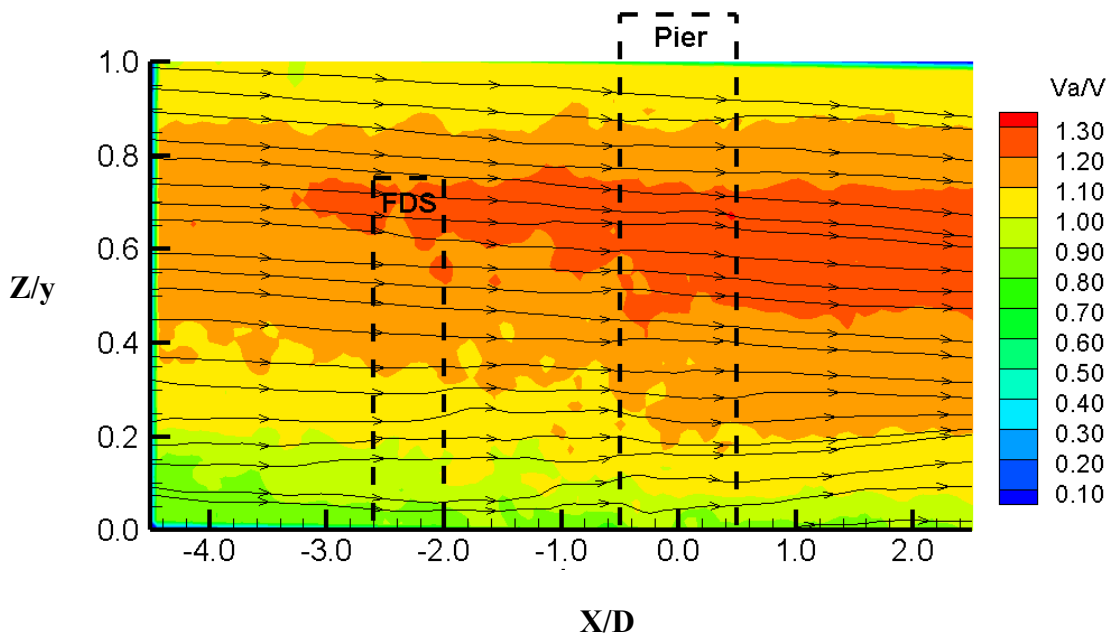


Figure B.59. Normalised absolute flow velocity and Streamlines for the single pier case and FDS with $H/y=0.75$ at $Y/D = 4$

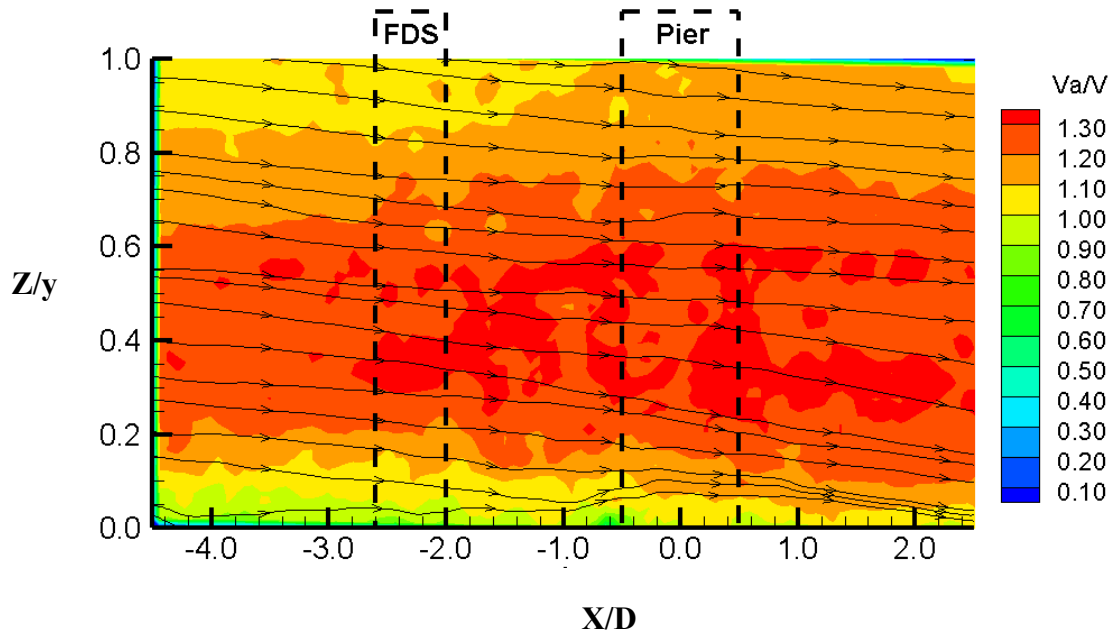


Figure B.60. Normalised absolute flow velocity and Streamlines for the single pier case and FDS with $H/y > 1$ at $Y/D = 4$

B.4. Plots of Streamwise Turbulence Intensity

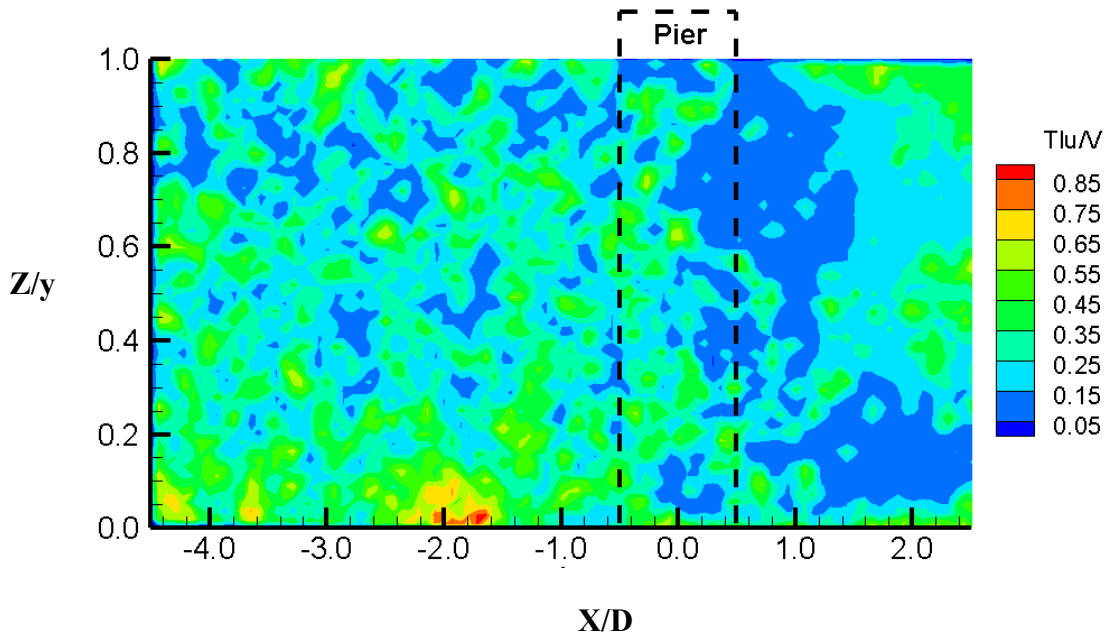


Figure B.61. Normalised streamwise turbulence intensity for the single pier case at $Y/D = 1$

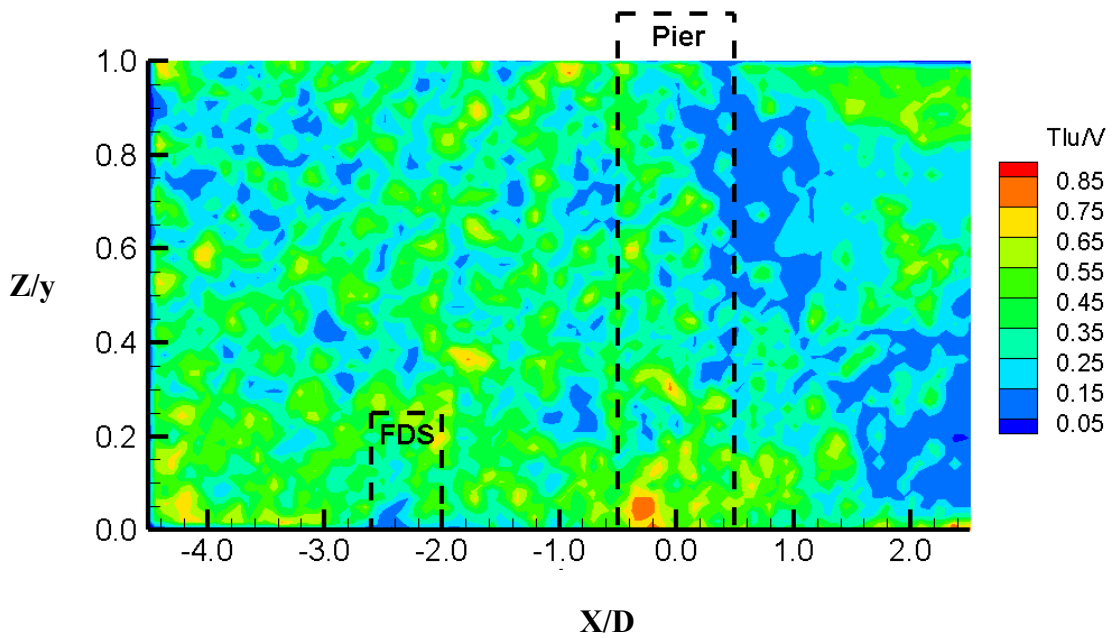


Figure B.62. Normalised streamwise turbulence intensity for the single pier case and FDS with $H/y = 0.25$ at $Y/D = 1$

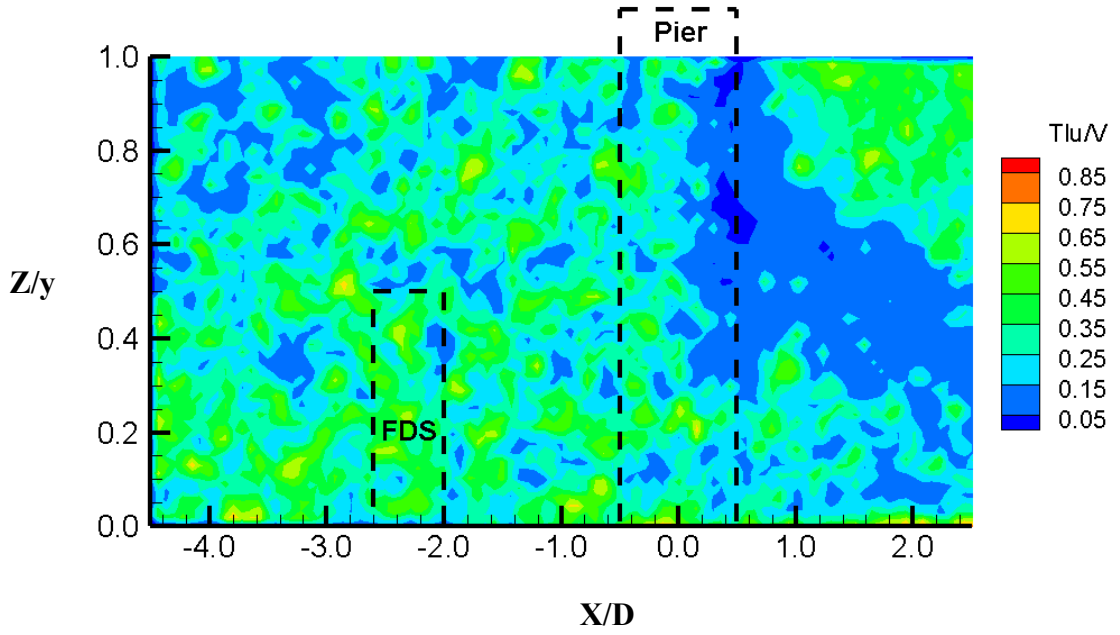


Figure B.63. Normalised streamwise turbulence intensity for the single pier case and FDS with $H/y=0.50$ at $Y/D = 1$

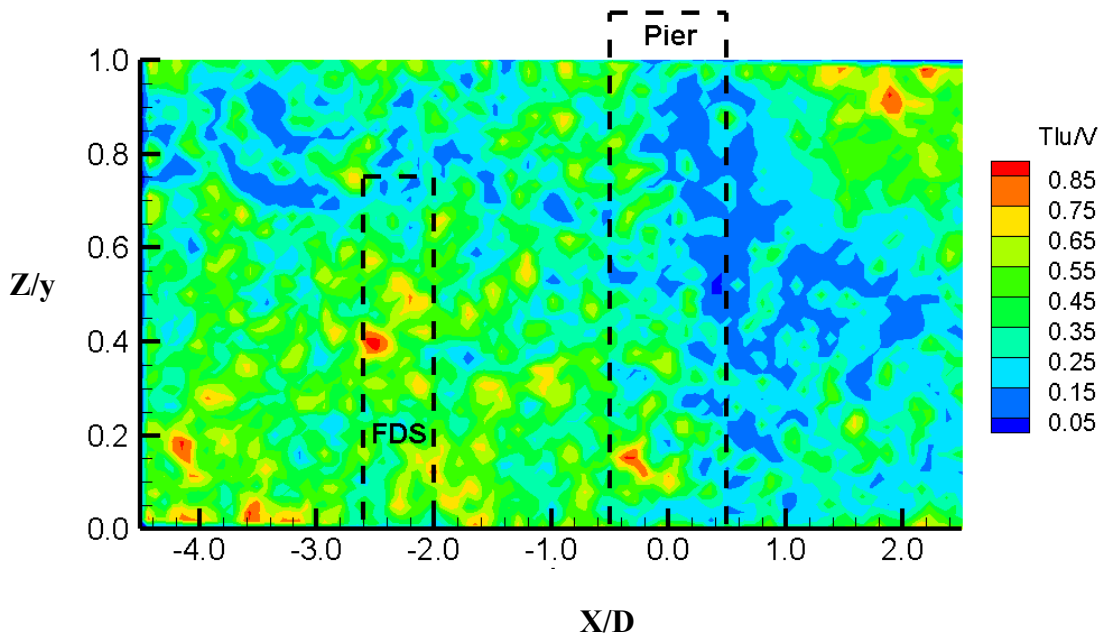


Figure B.64. Normalised streamwise turbulence intensity for the single pier case and FDS with $H/y=0.75$ at $Y/D = 1$

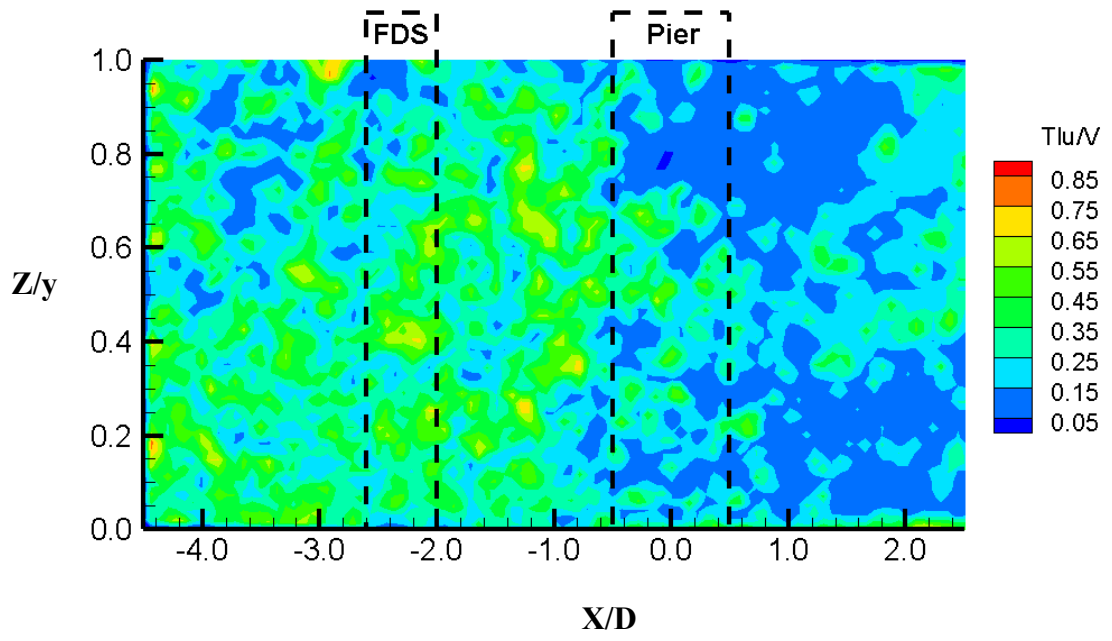


Figure B.65. Normalised streamwise turbulence intensity for the single pier case and FDS with $H/y > 1$ at $Y/D = 1$

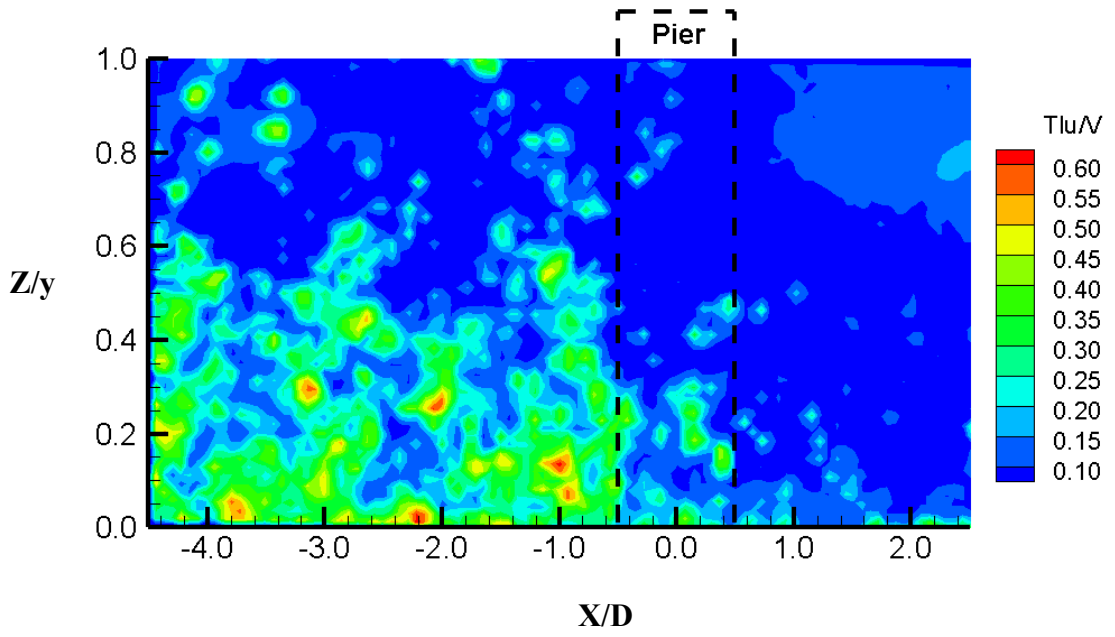


Figure B.66. Normalised streamwise turbulence intensity for the single pier case at $Y/D = 2$

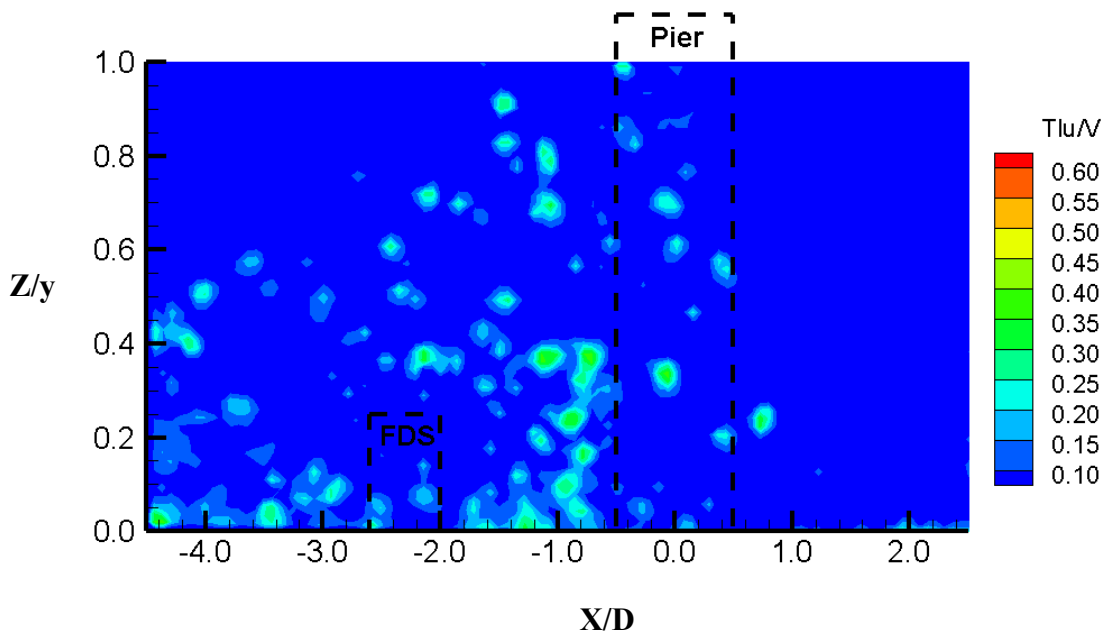


Figure B.67. Normalised streamwise turbulence intensity for the single pier case and FDS with $H/y=0.25$ at $Y/D = 2$

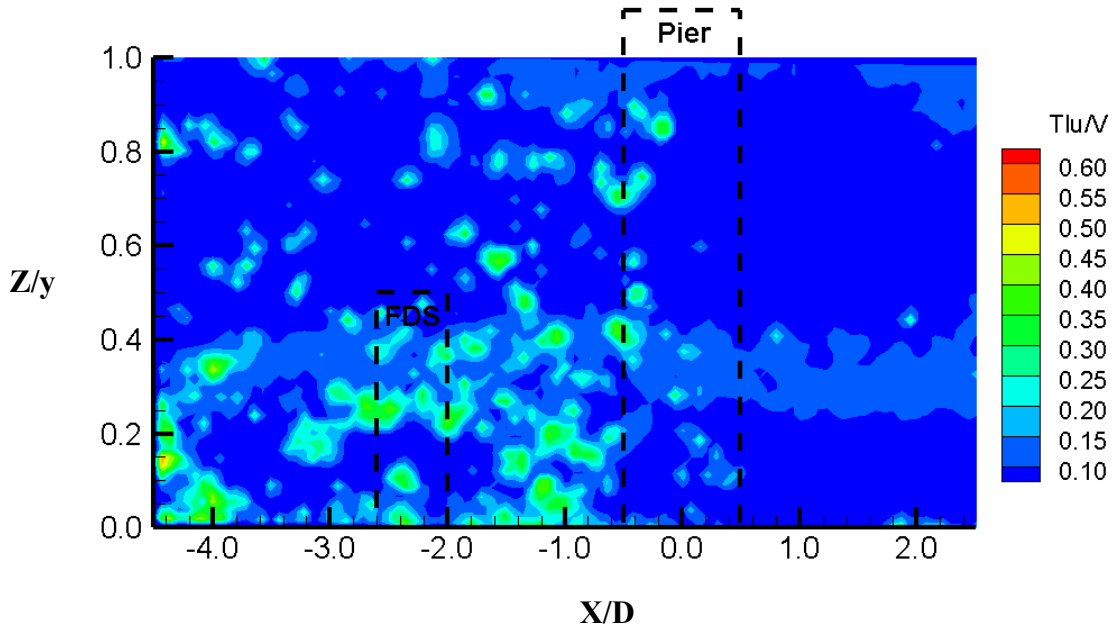


Figure B.68. Normalised streamwise turbulence intensity for the single pier case and FDS with $H/y=0.50$ at $Y/D = 2$

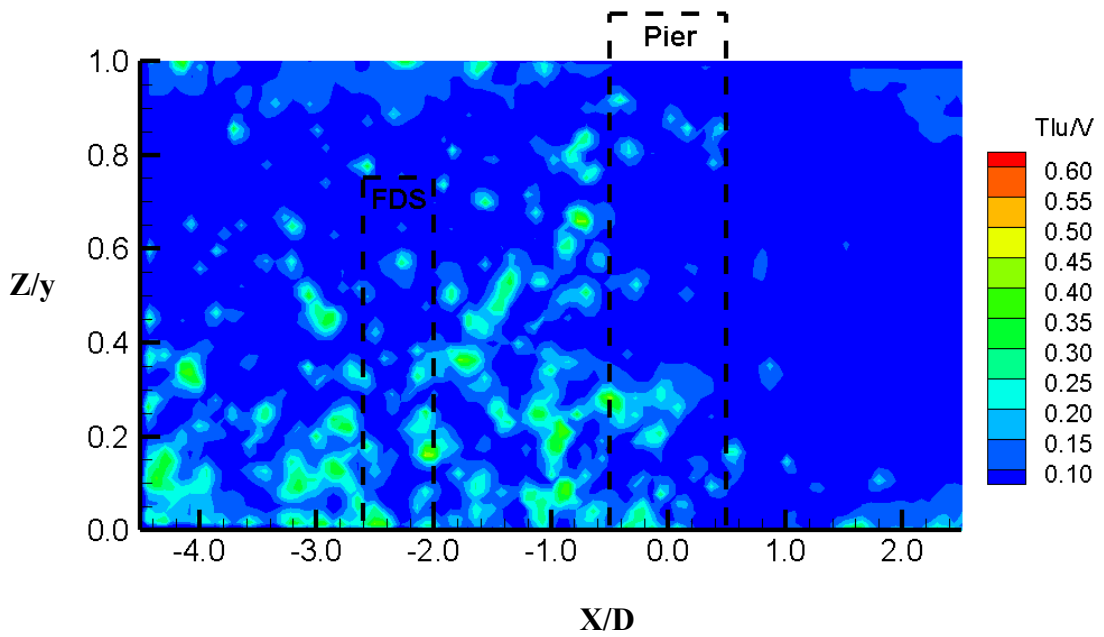


Figure B.69. Normalised streamwise turbulence intensity for the single pier case and FDS with $H/y=0.75$ at $Y/D = 2$

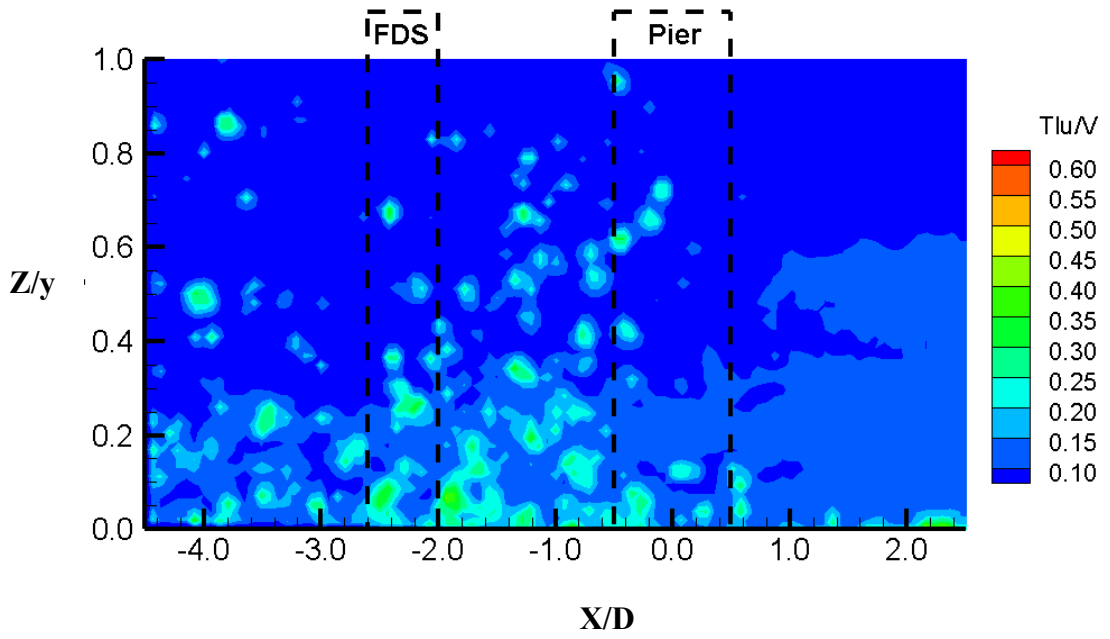


Figure B.70. Normalised streamwise turbulence intensity for the single pier case and FDS with $H/y > 1$ at $Y/D = 2$

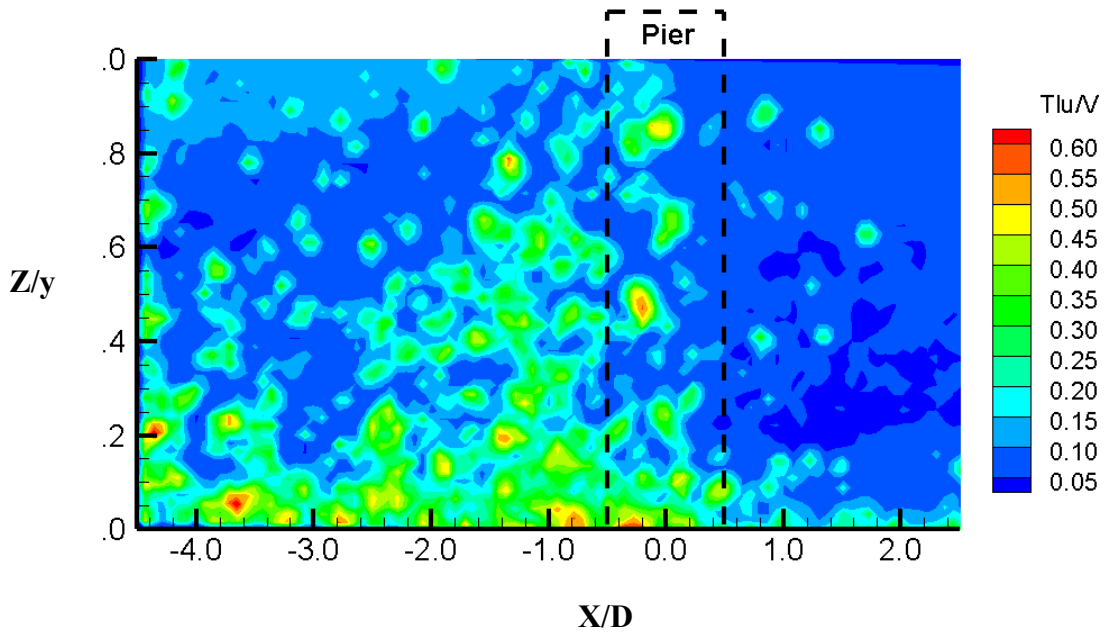


Figure B.71. Normalised streamwise turbulence intensity for the single pier case at $Y/D = 3$

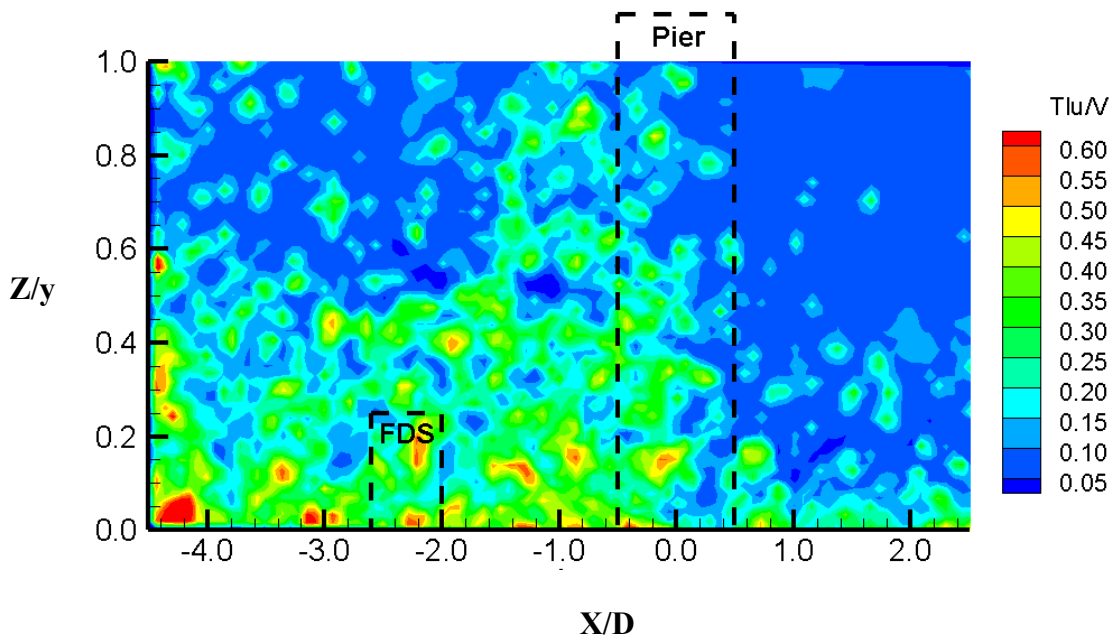


Figure B.72. Normalised streamwise turbulence intensity for the single pier case and FDS with $H/y = 0.25$ at $Y/D = 3$

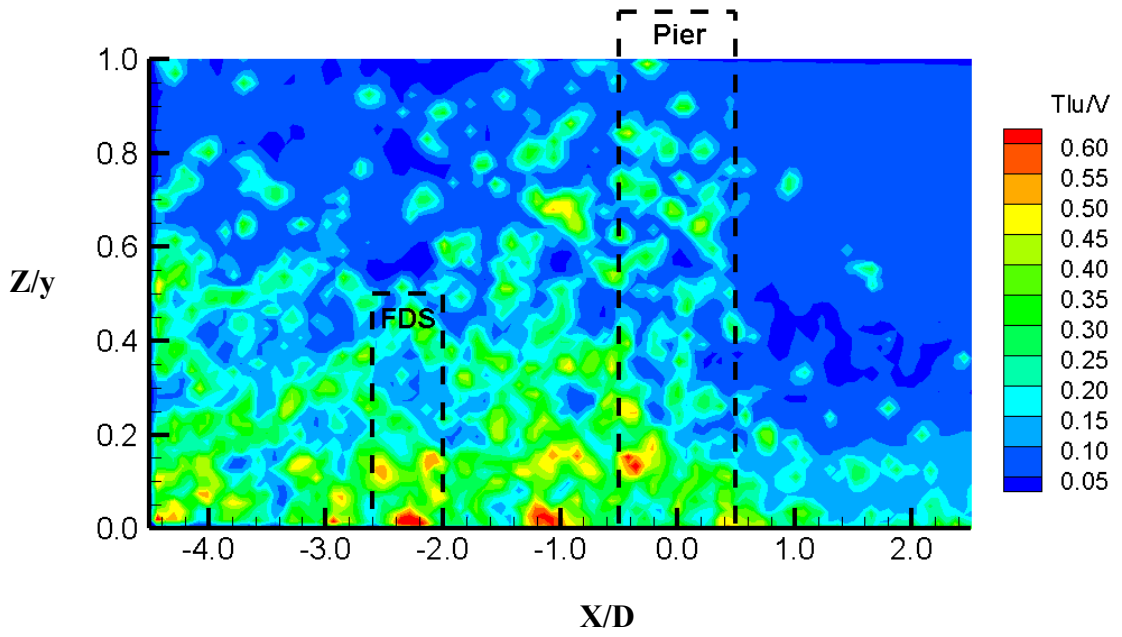


Figure B.73. Normalised streamwise turbulence intensity for the single pier case and FDS with $H/y=0.50$ at $Y/D = 3$

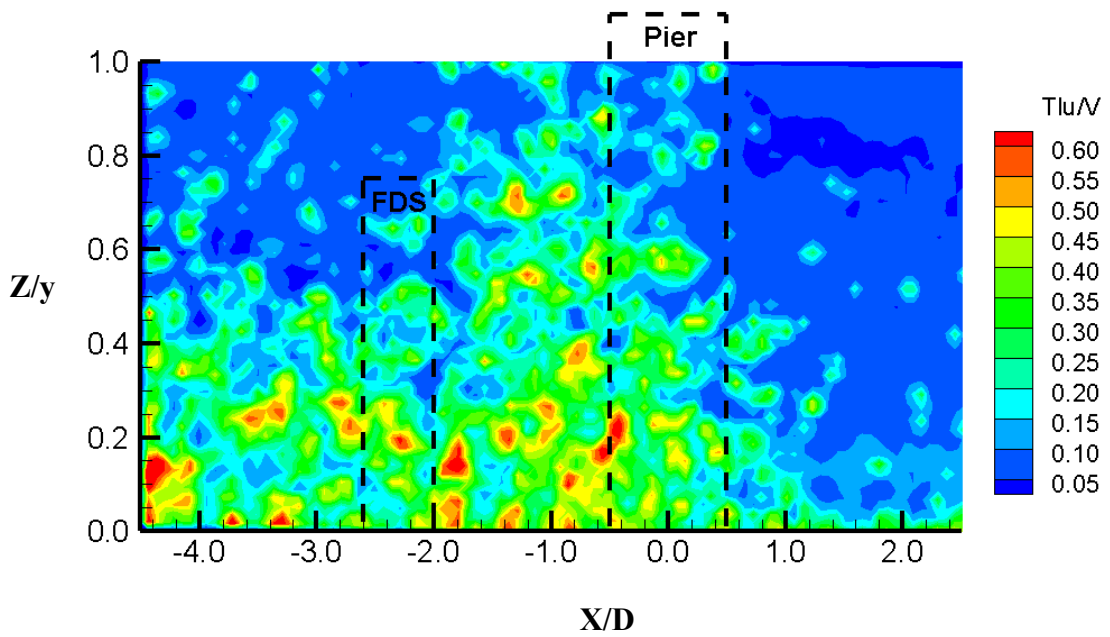


Figure B.74. Normalised streamwise turbulence intensity for the single pier case and FDS with $H/y=0.75$ at $Y/D = 3$

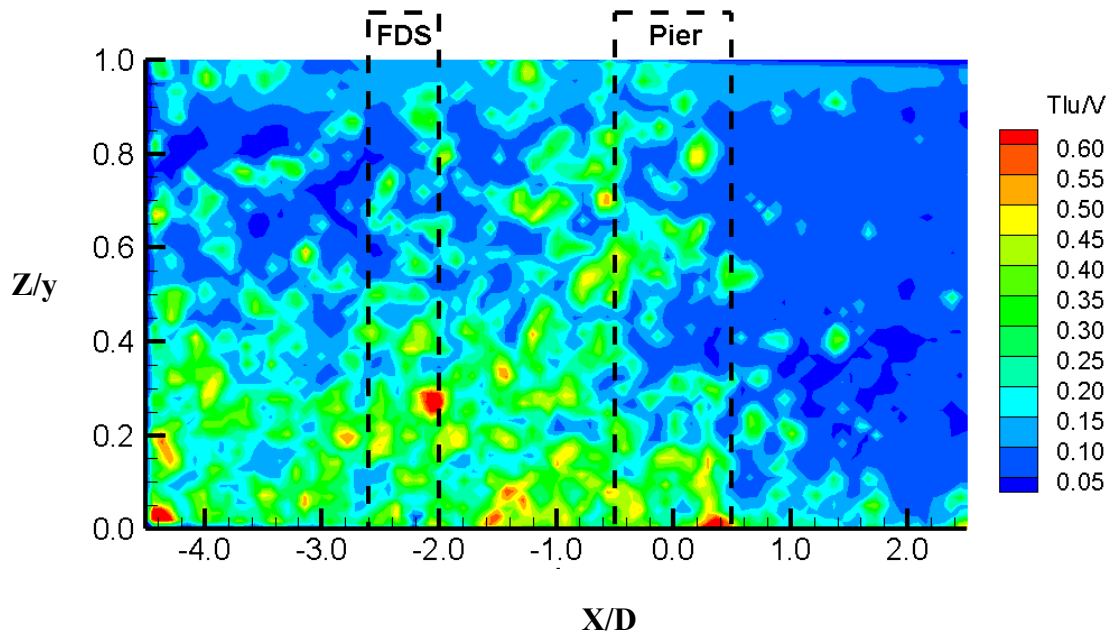


Figure B.75. Normalised streamwise turbulence intensity for the single pier case and FDS with $H/y > 1$ at $Y/D = 3$

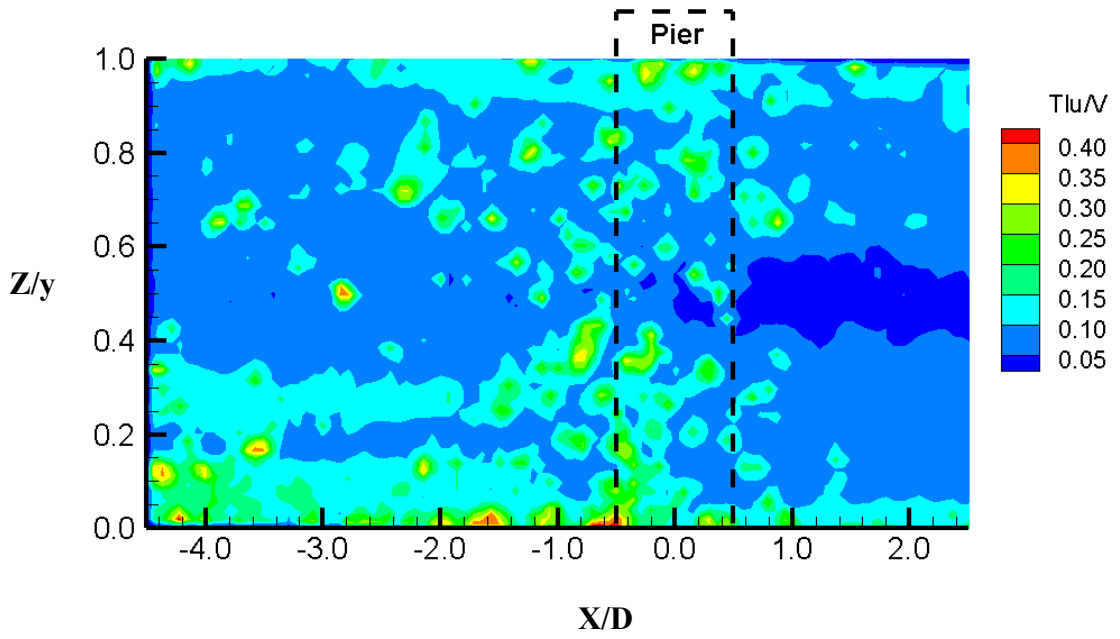


Figure B.76. Normalised streamwise turbulence intensity for the single pier case at $Y/D = 4$

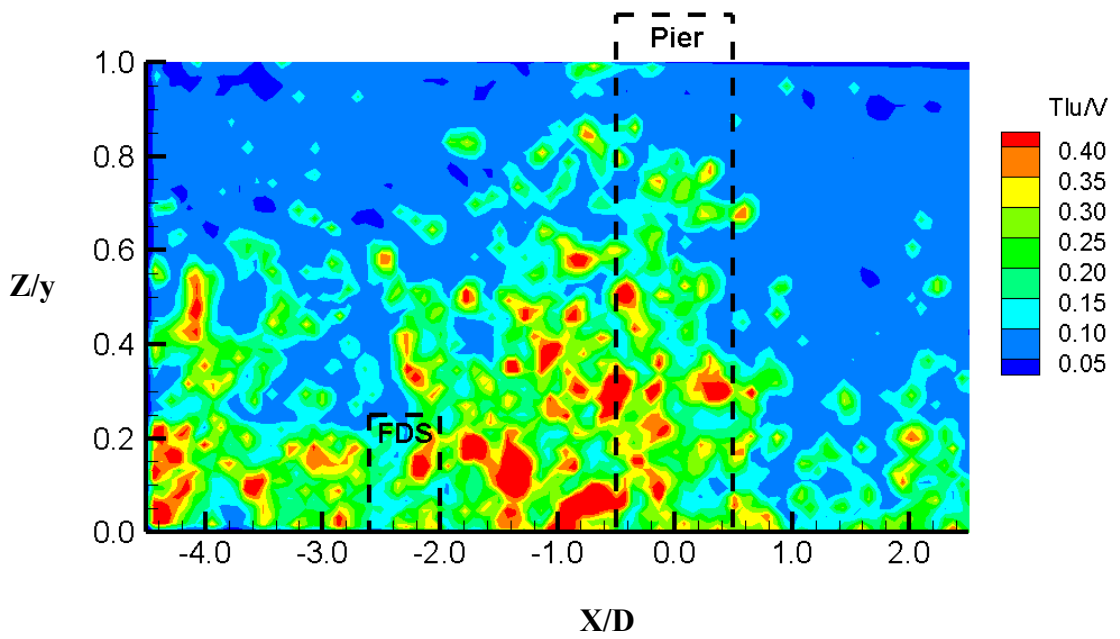


Figure B.77. Normalised streamwise turbulence intensity for the single pier case and FDS with $H/y = 0.25$ at $Y/D = 4$

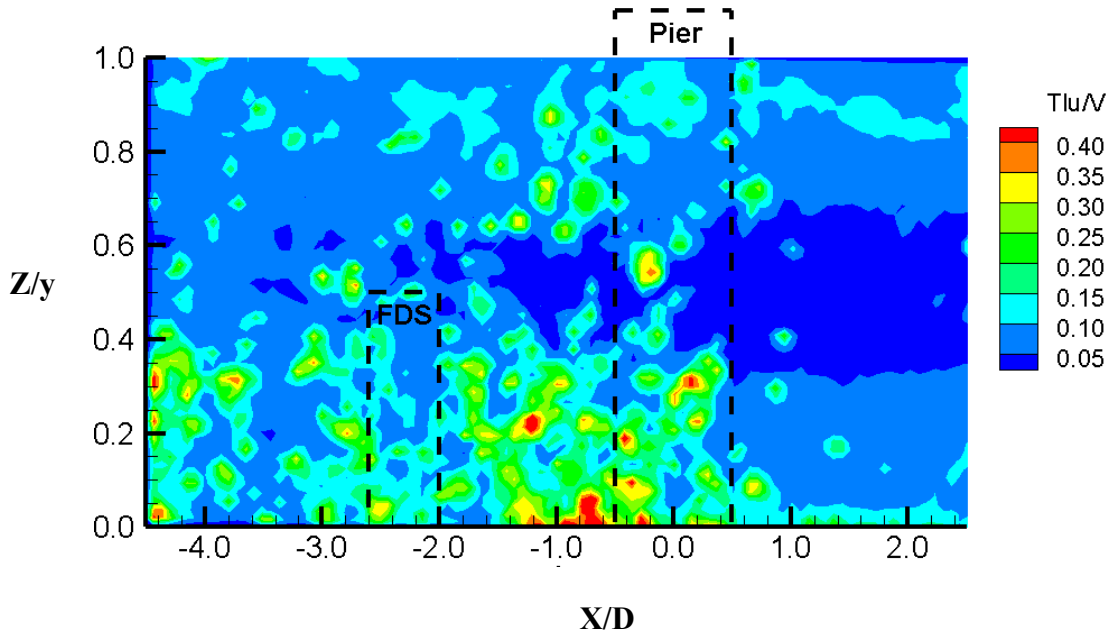


Figure B.78. Normalised streamwise turbulence intensity for the single pier case and FDS with $H/y=0.50$ at $Y/D = 4$

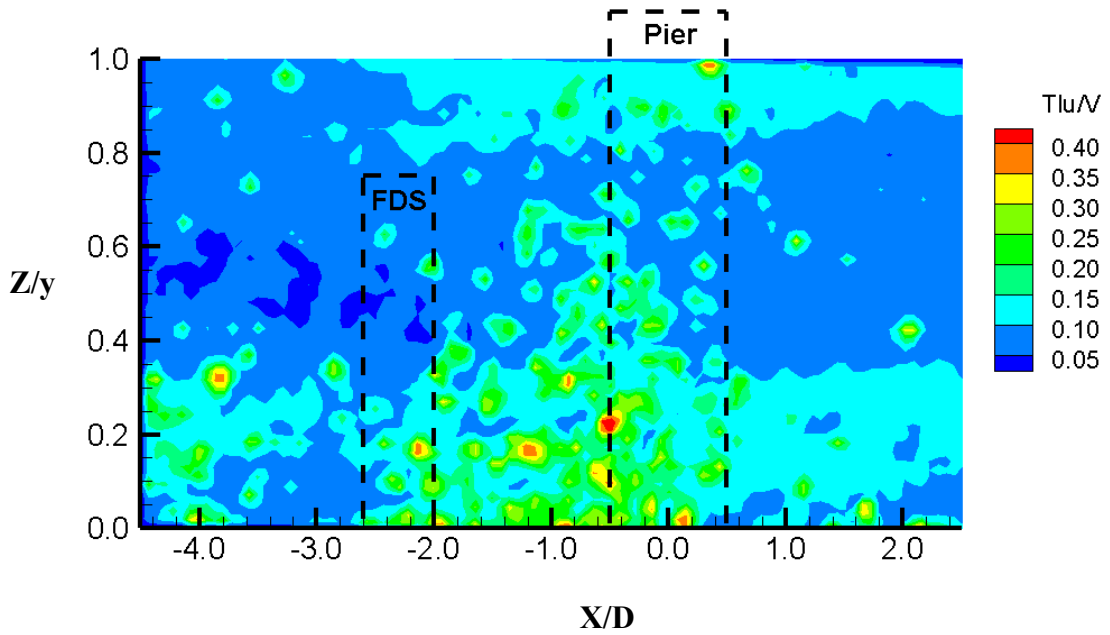


Figure B.79. Normalised streamwise turbulence intensity for the single pier case and FDS with $H/y=0.75$ at $Y/D = 4$

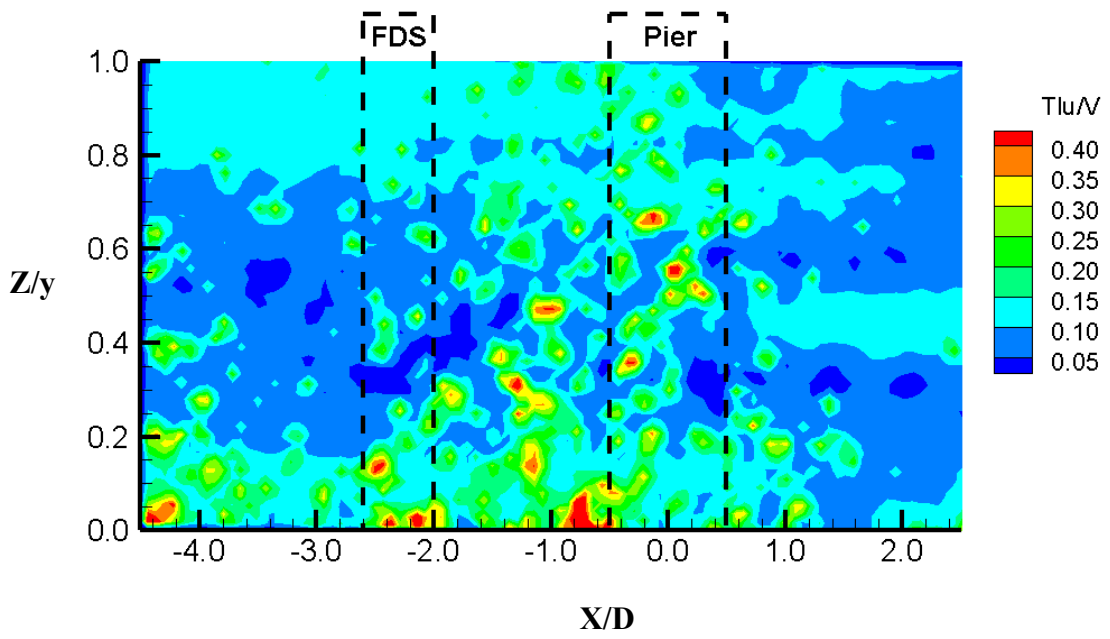


Figure B.80. Normalised streamwise turbulence intensity for the single pier case and FDS with $H/y > 1$ at $Y/D = 4$

B.5. Plots of Vertical Turbulence Intensity

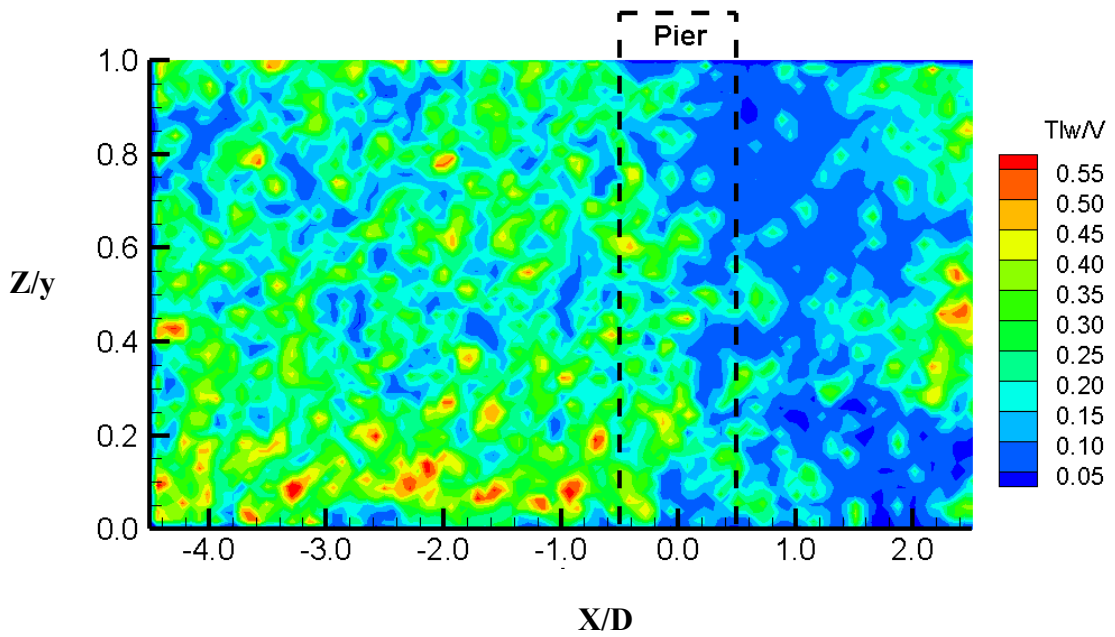


Figure B.81. Normalised vertical turbulence intensity for the single pier case at $Y/D = 1$

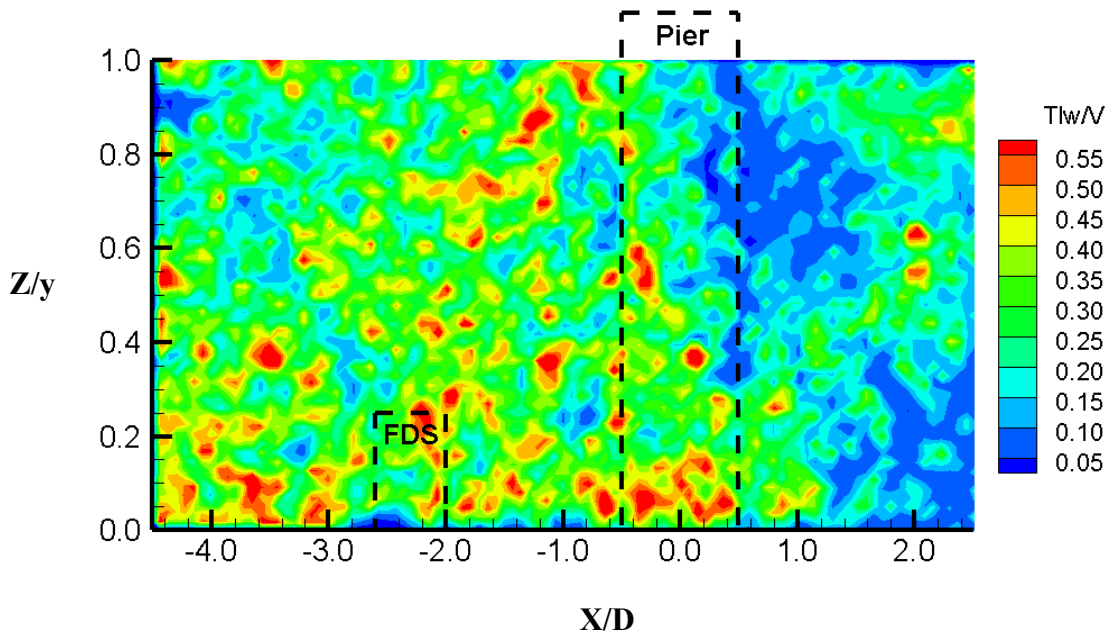


Figure B.82. Normalised vertical turbulence intensity for the single pier case and FDS with $H/y = 0.25$ at $Y/D = 1$

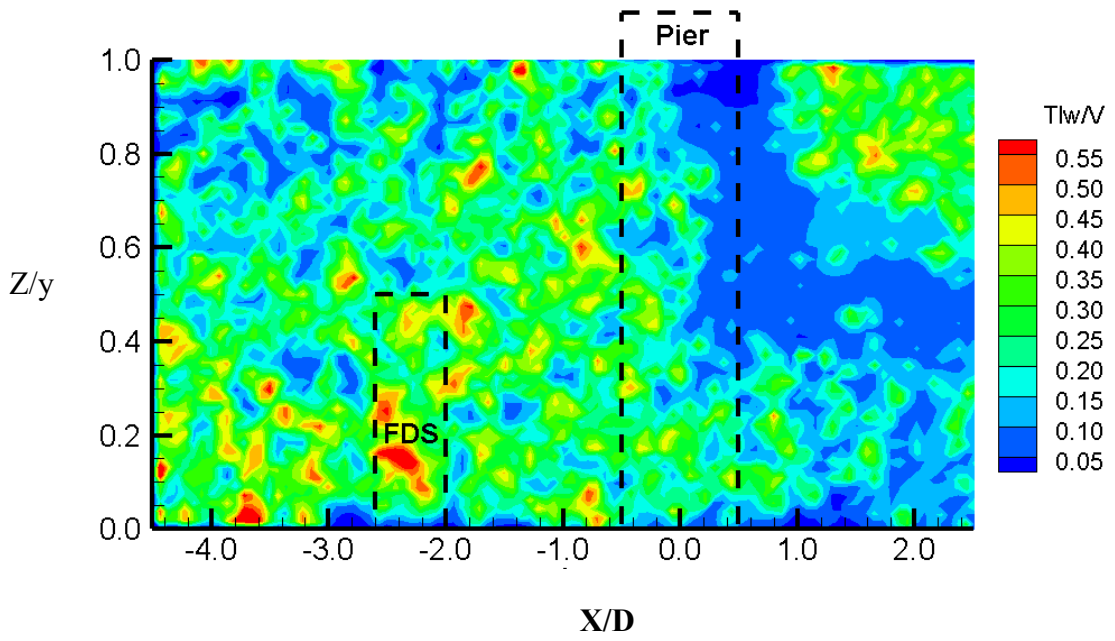


Figure B.83. Normalised vertical turbulence intensity for the single pier case and FDS with $H/y=0.50$ at $Y/D = 1$

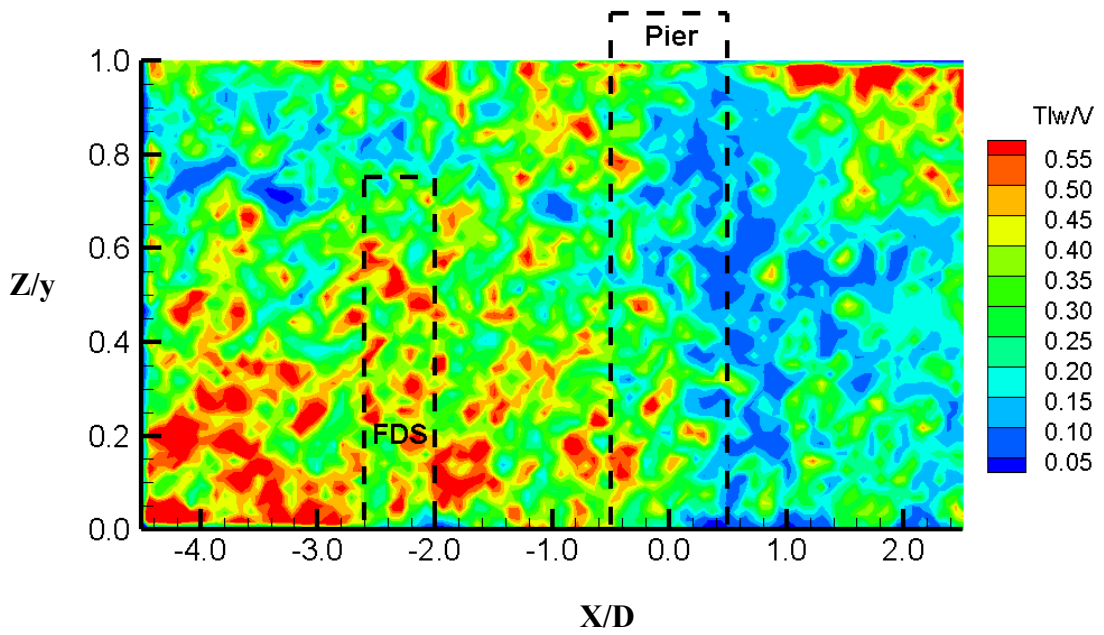


Figure B.84. Normalised vertical turbulence intensity for the single pier case and FDS with $H/y=0.75$ at $Y/D = 1$

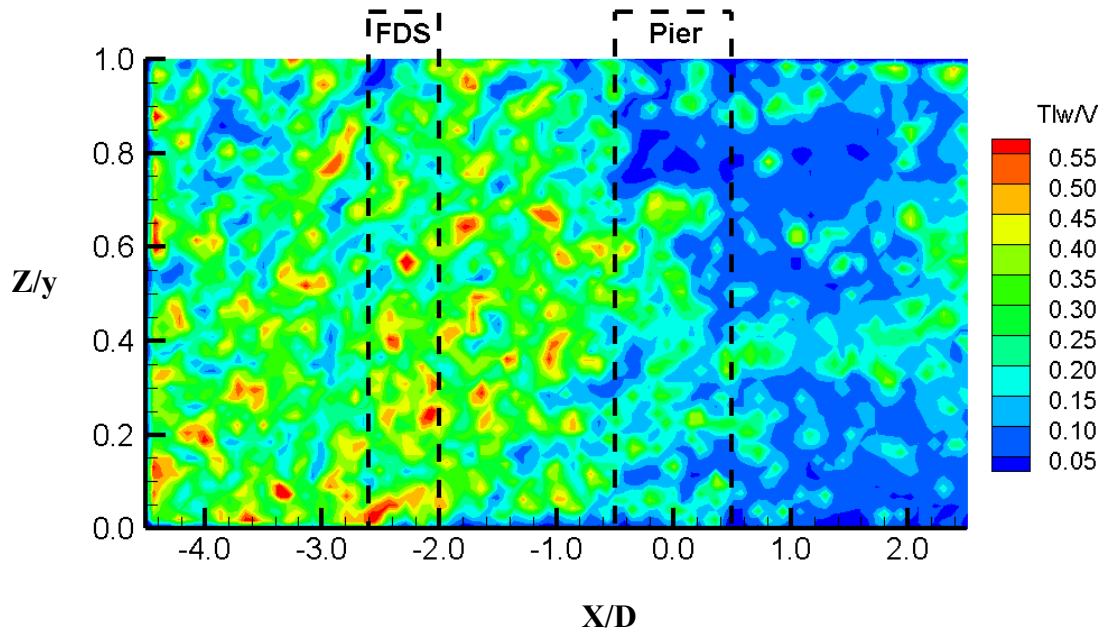


Figure B.85. Normalised vertical turbulence intensity for the single pier case and FDS with $H/y > 1$ at $Y/D = 1$

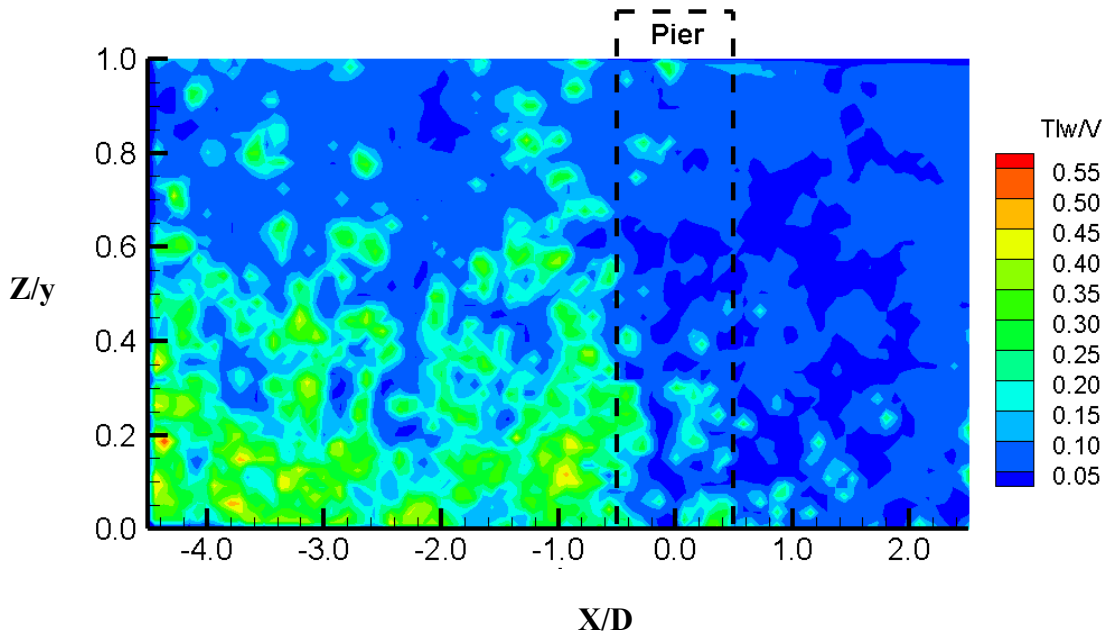


Figure B.86. Normalised vertical turbulence intensity for the single pier case at $Y/D = 2$

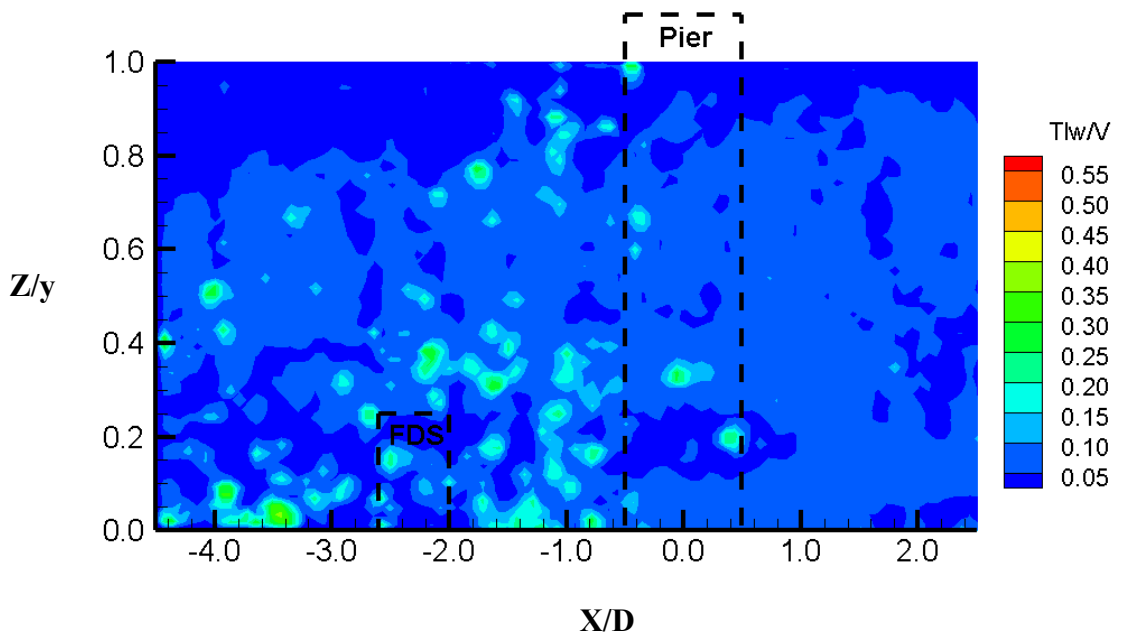


Figure B.87. Normalised vertical turbulence intensity for the single pier case and FDS with $H/y = 0.25$ at $Y/D = 2$

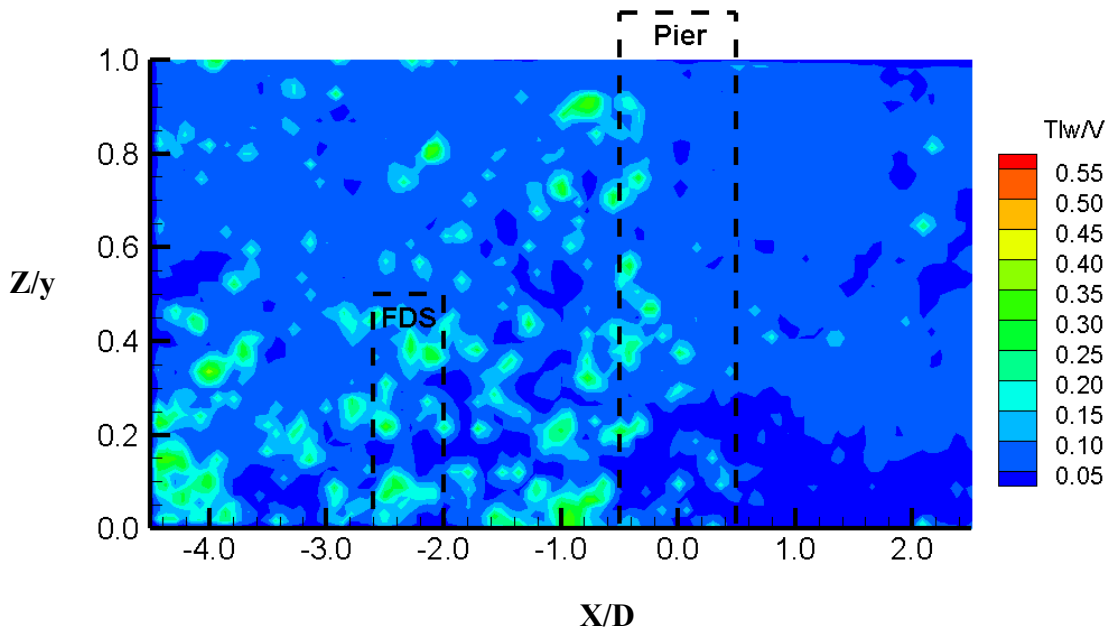


Figure B.88. Normalised vertical turbulence intensity for the single pier case and FDS with $H/y=0.50$ at $Y/D = 2$

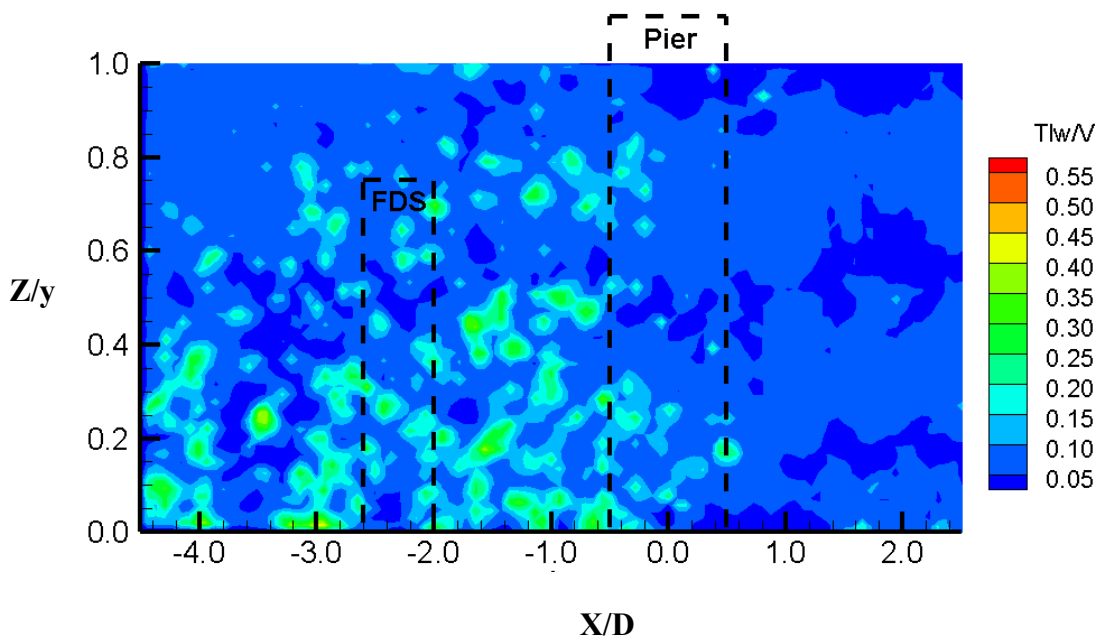


Figure B.89. Normalised vertical turbulence intensity for the single pier case and FDS with $H/y=0.75$ at $Y/D = 2$

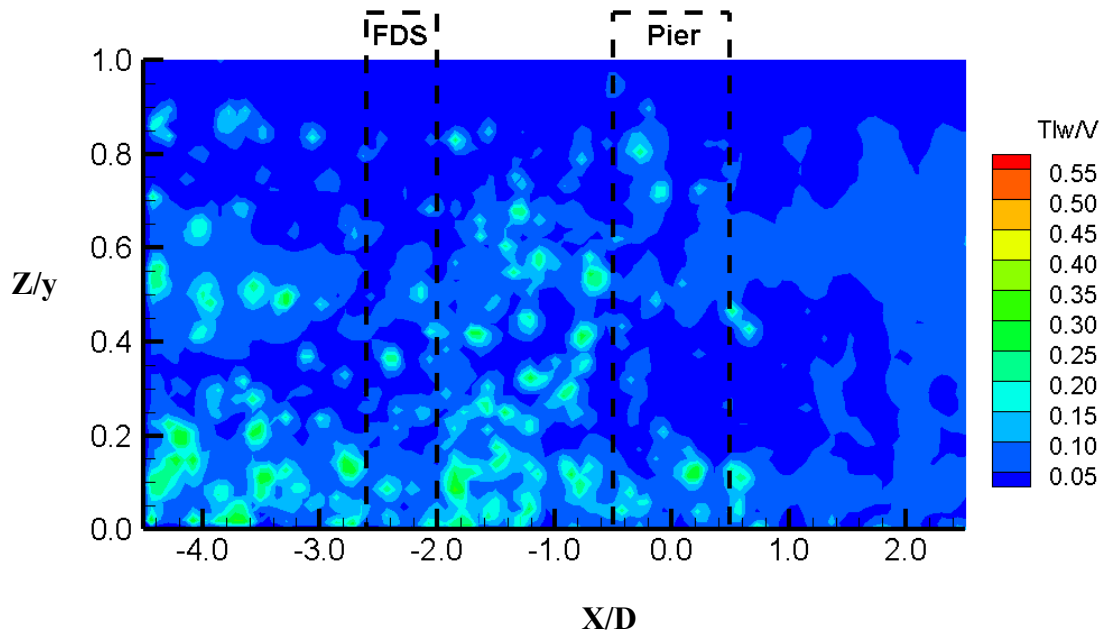


Figure B.90. Normalised vertical turbulence intensity for the single pier case and FDS with $H/y > 1$ at $Y/D = 2$

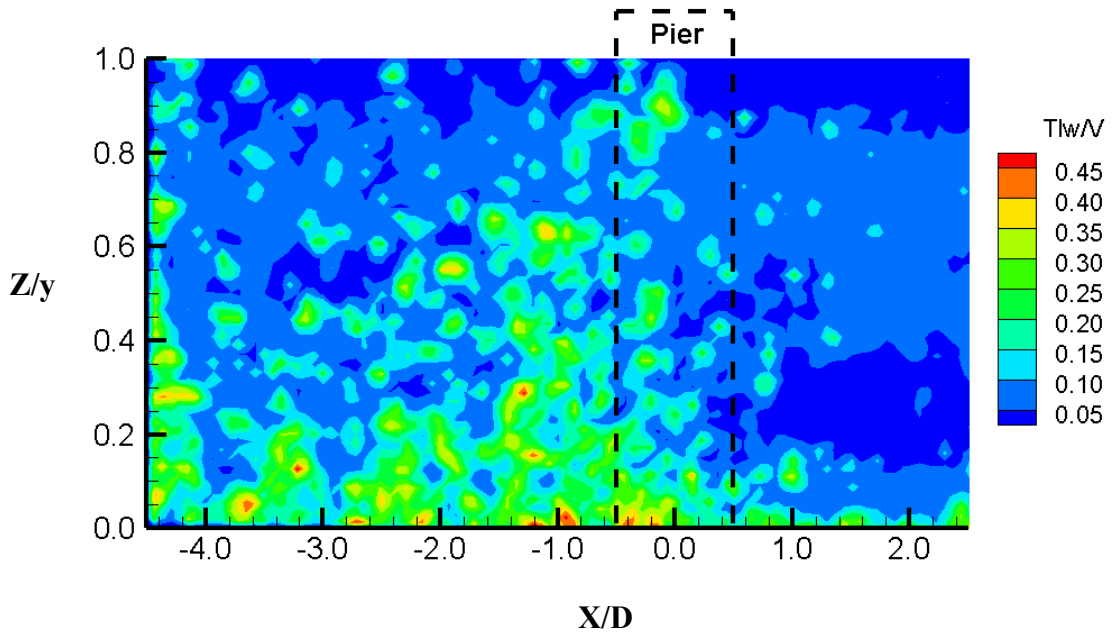


Figure B.91. Normalised vertical turbulence intensity for the single pier case at $Y/D = 3$

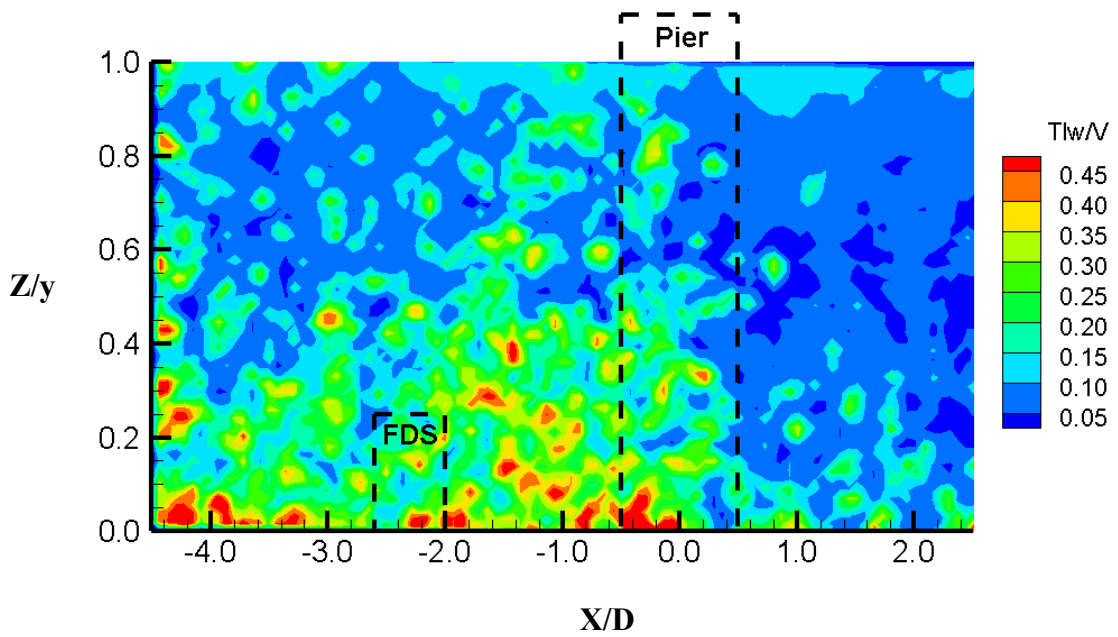


Figure B.92. Normalised vertical turbulence intensity for the single pier case and FDS with $H/y = 0.25$ at $Y/D = 3$

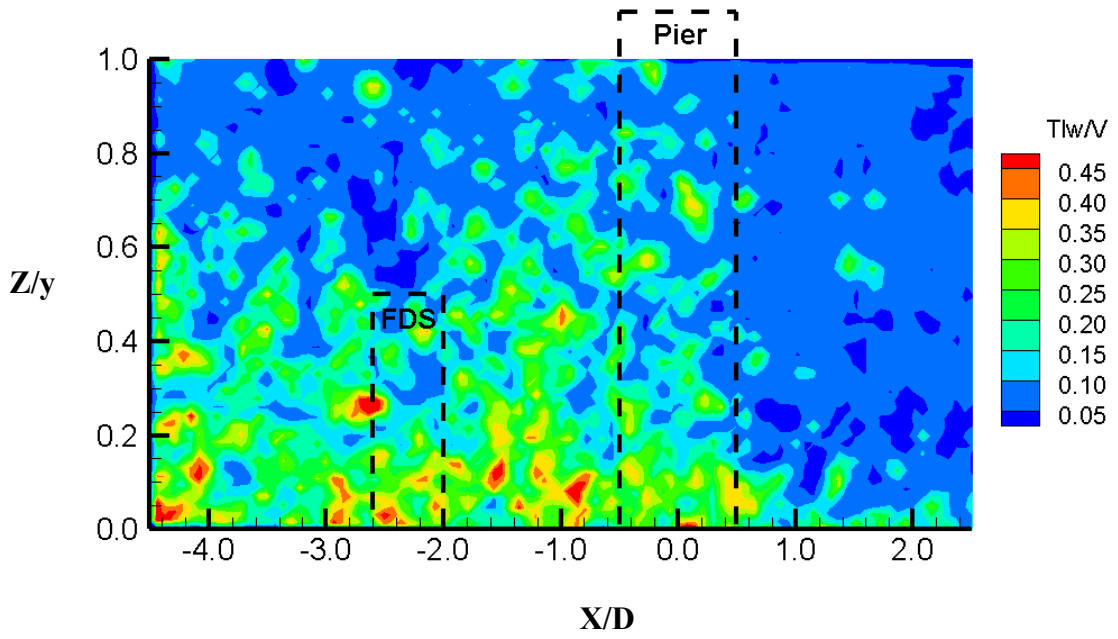


Figure B.93. Normalised vertical turbulence intensity for the single pier case and FDS with $H/y=0.50$ at $Y/D = 3$

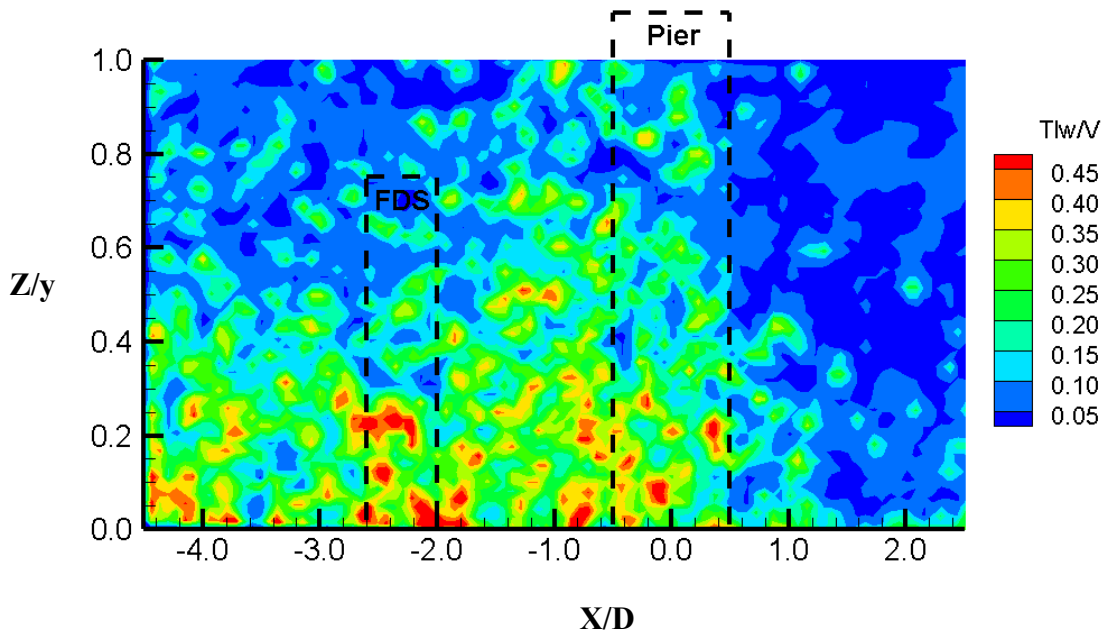


Figure B.94. Normalised vertical turbulence intensity for the single pier case and FDS with $H/y=0.75$ at $Y/D = 3$

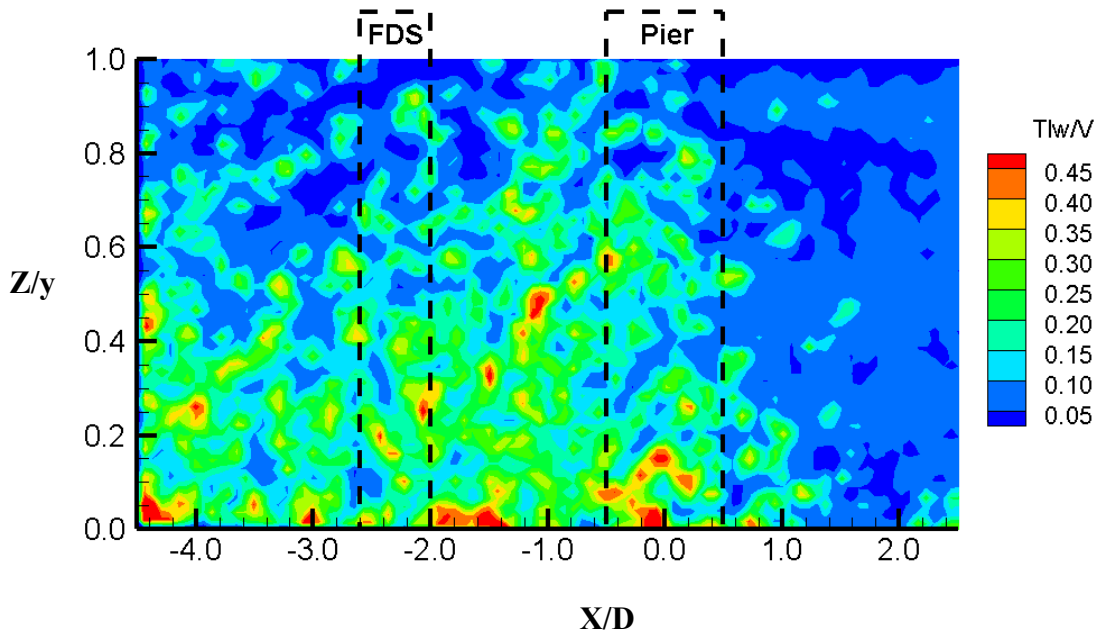


Figure B.95. Normalised vertical turbulence intensity for the single pier case and FDS with $H/y > 1$ at $Y/D = 3$

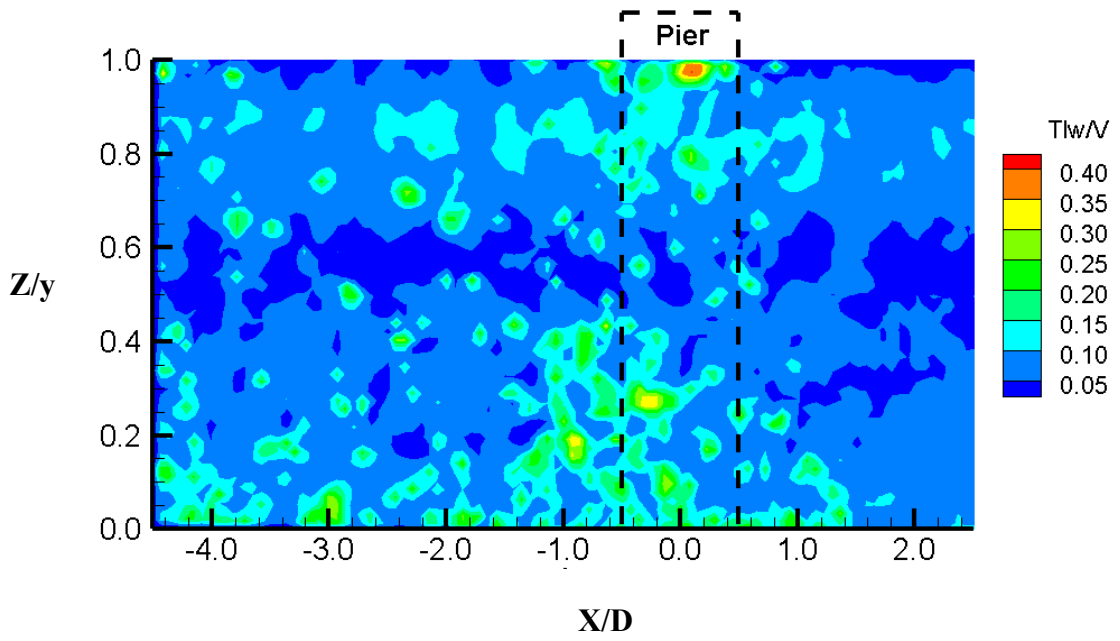


Figure B.96. Normalised vertical turbulence intensity for the single pier case at $Y/D = 4$

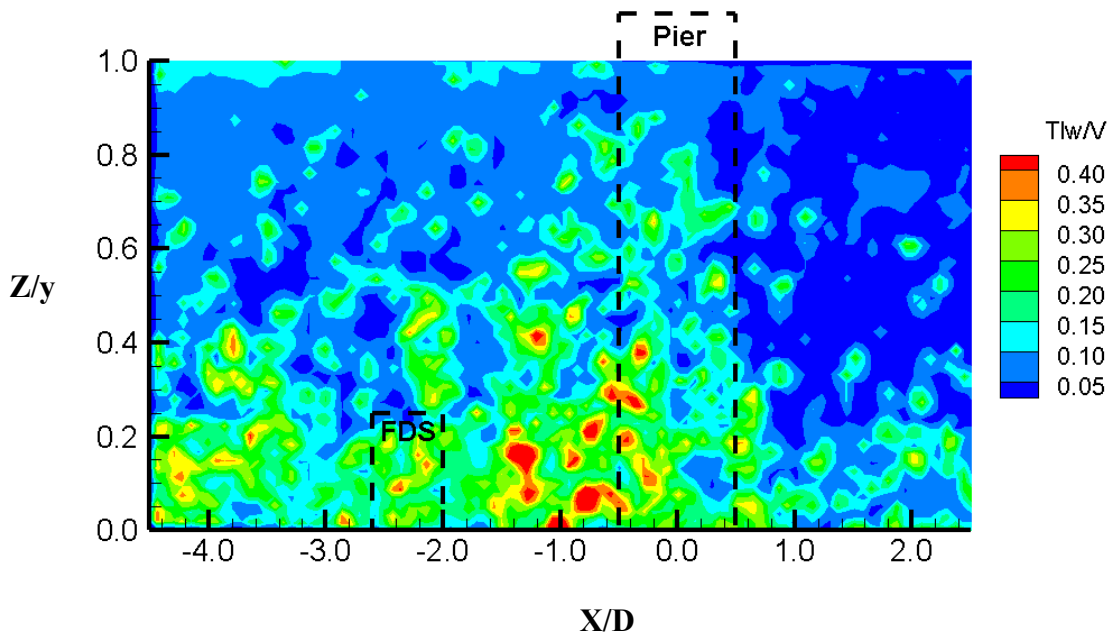


Figure B.97. Normalised vertical turbulence intensity for the single pier case and FDS with $H/y = 0.25$ at $Y/D = 4$

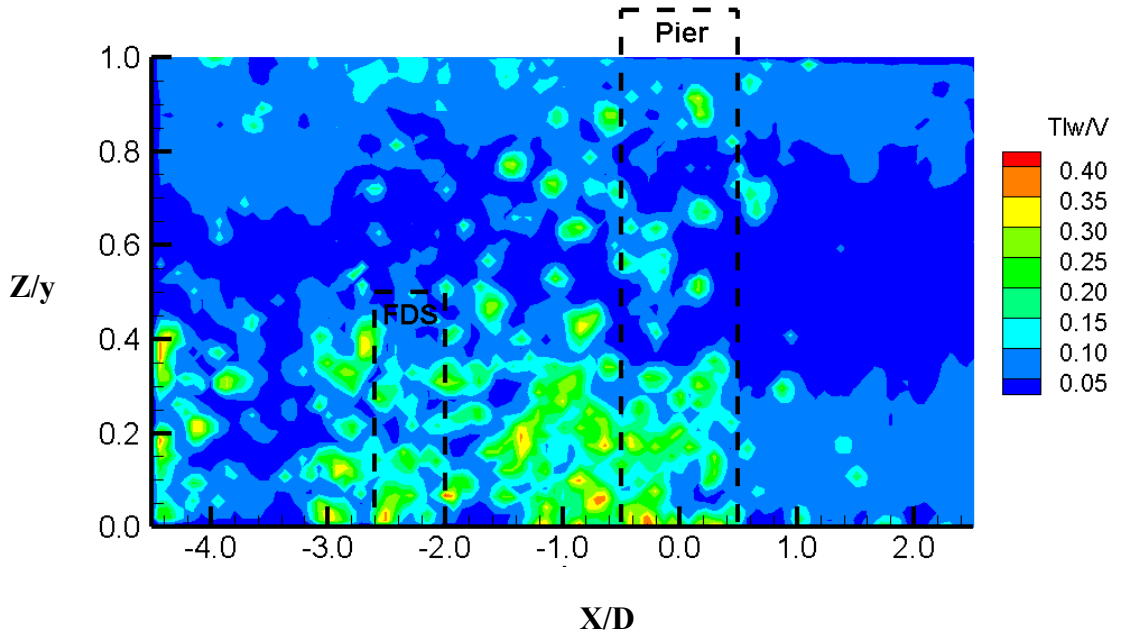


Figure B.98. Normalised vertical turbulence intensity for the single pier case and FDS with $H/y=0.50$ at $Y/D = 4$

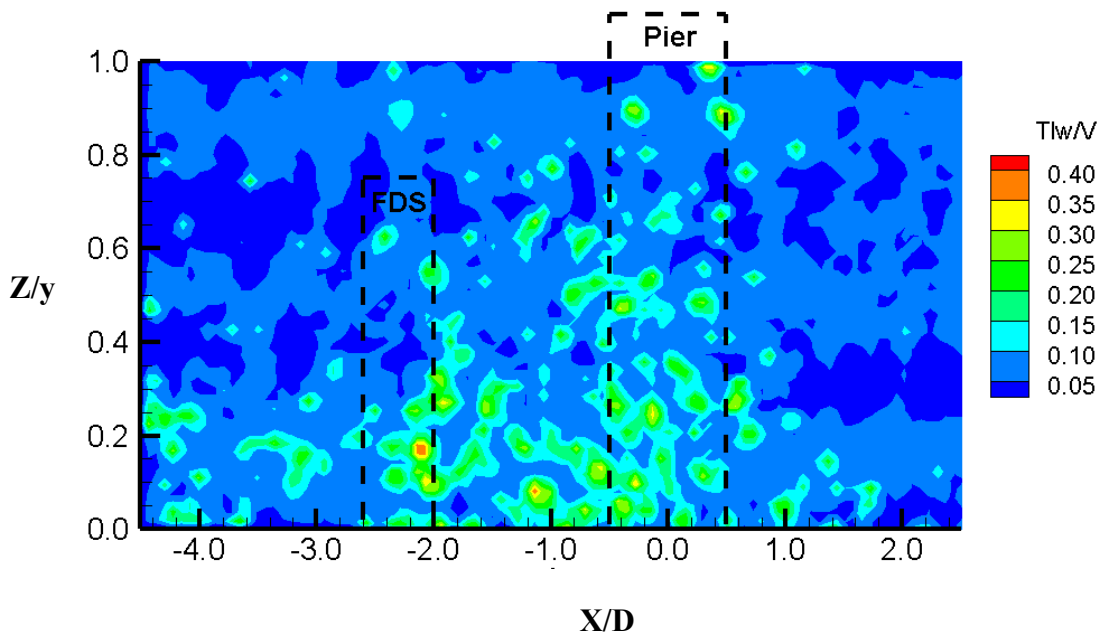


Figure B.99. Normalised vertical turbulence intensity for the single pier case and FDS with $H/y=0.75$ at $Y/D = 4$

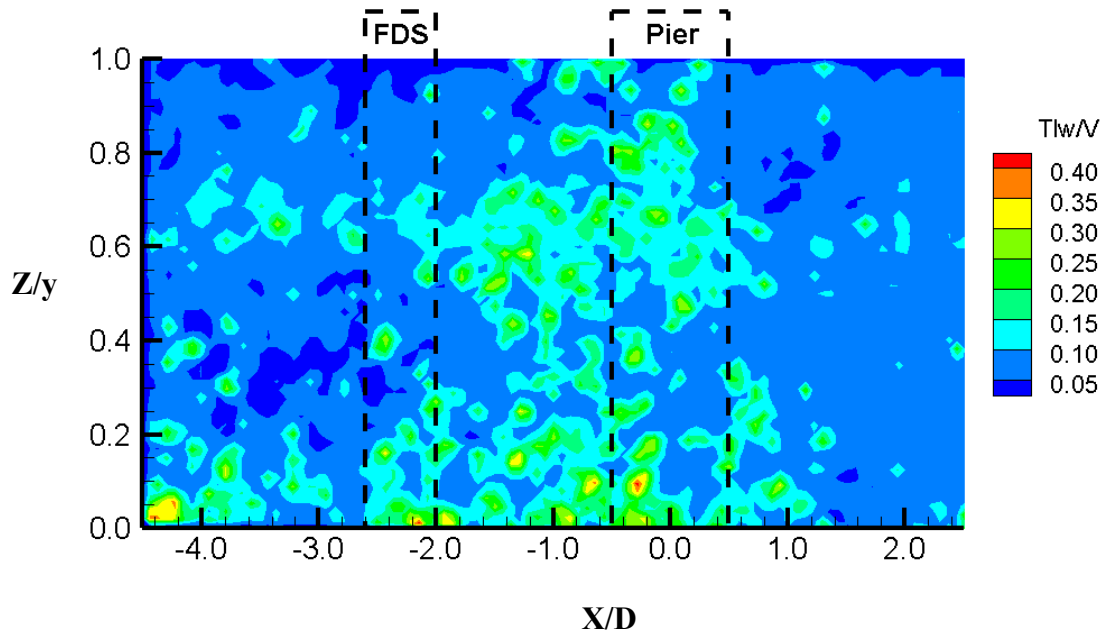


Figure B.100. Normalised vertical turbulence intensity for the single pier case and FDS with $H/y > 1$ at $Y/D = 4$

B.6. Plots of Turbulent Kinetic Energy

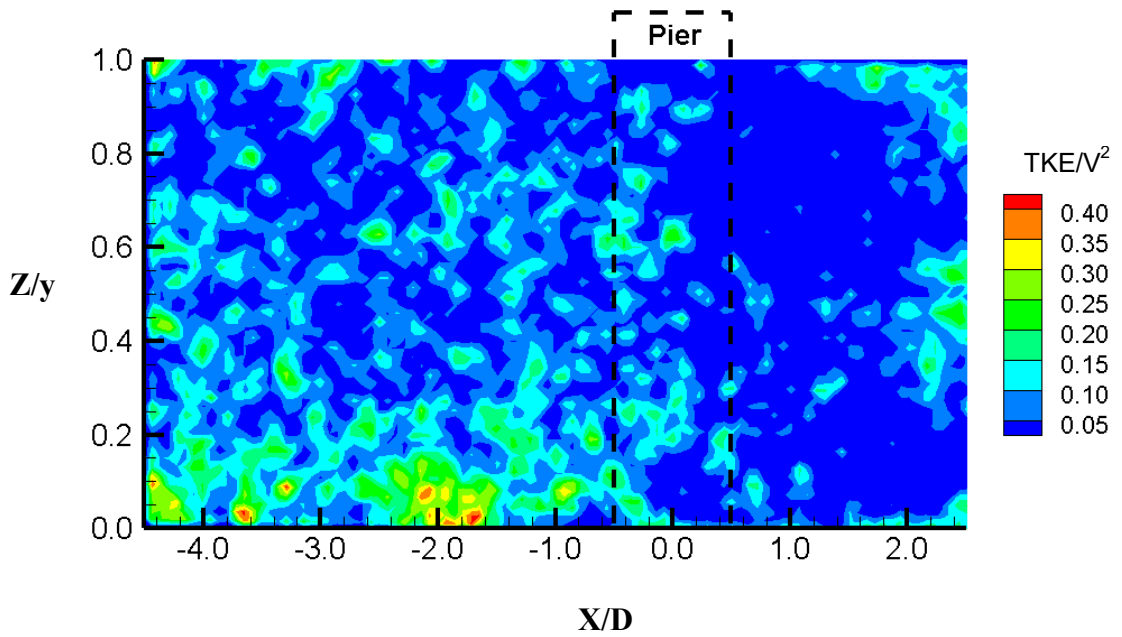


Figure B.101. Normalised turbulent kinetic energy for the single pier case at $Y/D = 1$

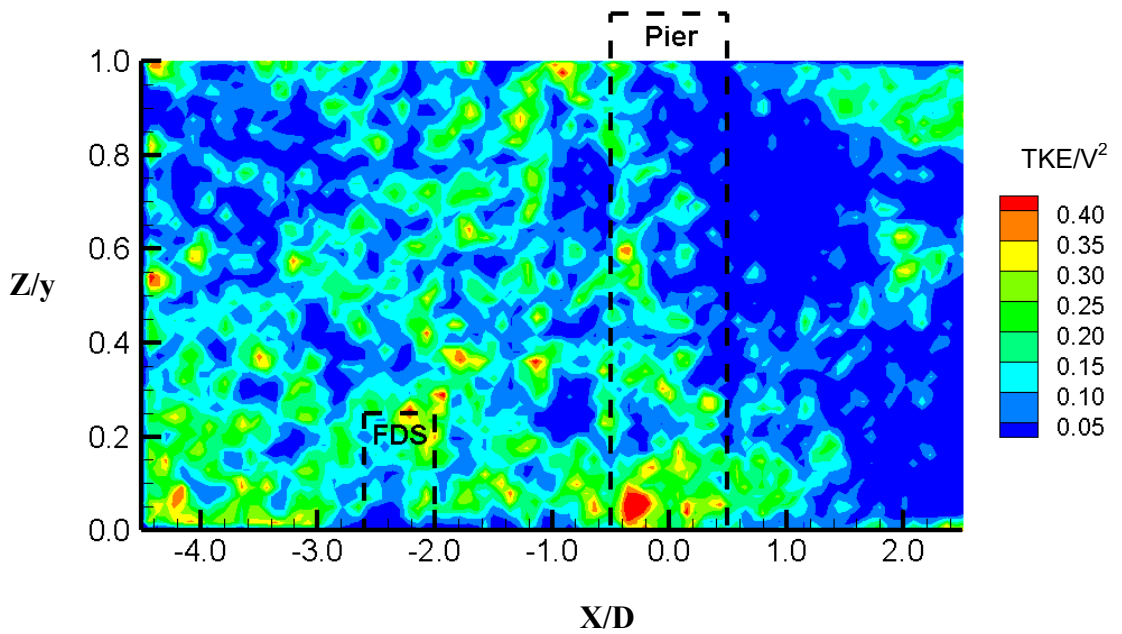


Figure B.102. Normalised turbulent kinetic energy for the single pier case and FDS with $H/y = 0.25$ at $Y/D = 1$

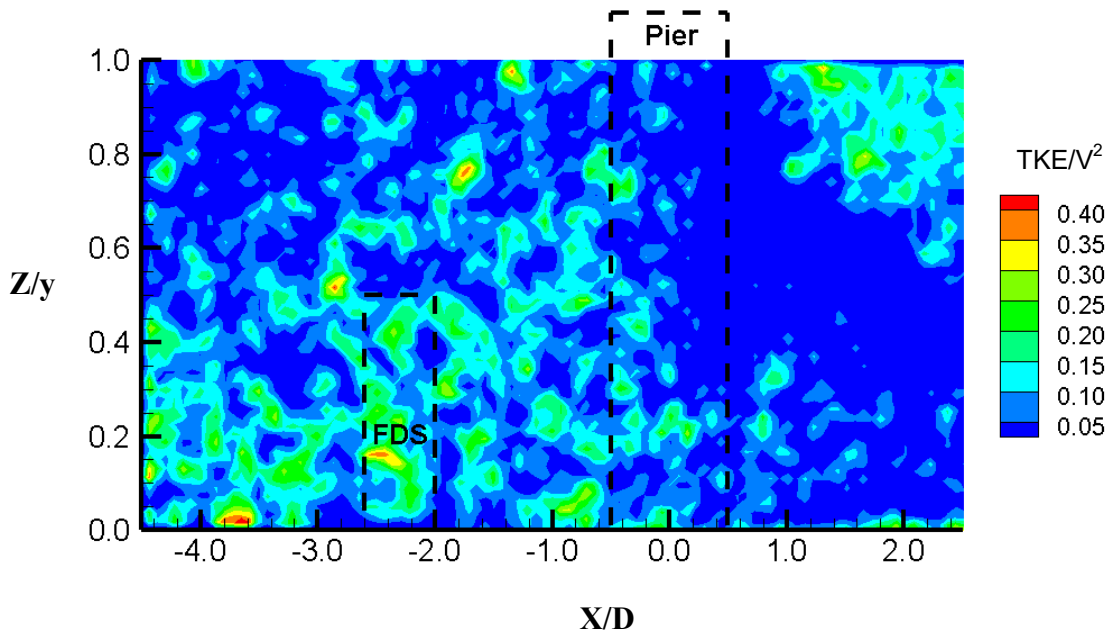


Figure B.103. Normalised turbulent kinetic energy for the single pier case and FDS with $H/y=0.50$ at $Y/D = 1$

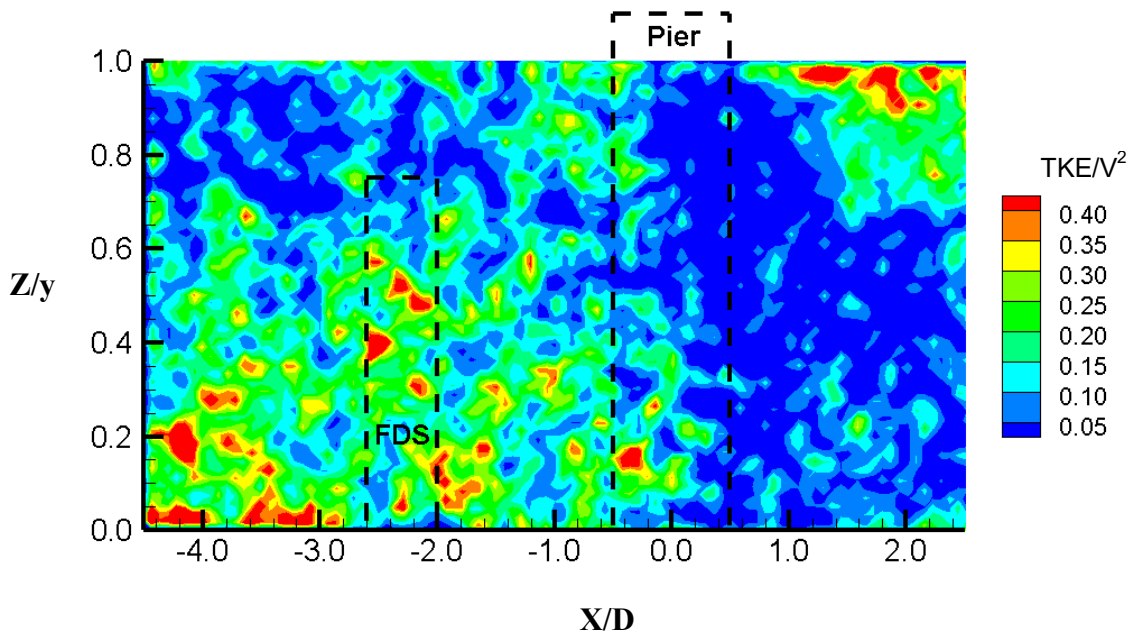


Figure B.104. Normalised turbulent kinetic energy for the single pier case and FDS with $H/y=0.75$ at $Y/D = 1$

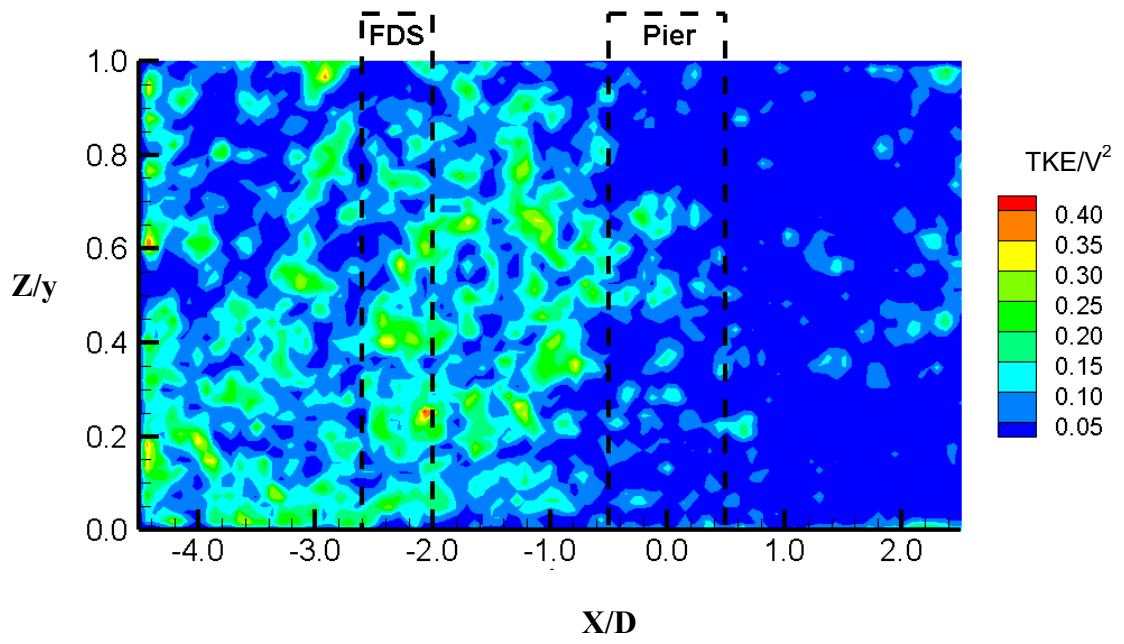


Figure B.105. Normalised turbulent kinetic energy for the single pier case and FDS with $H/y > 1$ at $Y/D = 1$

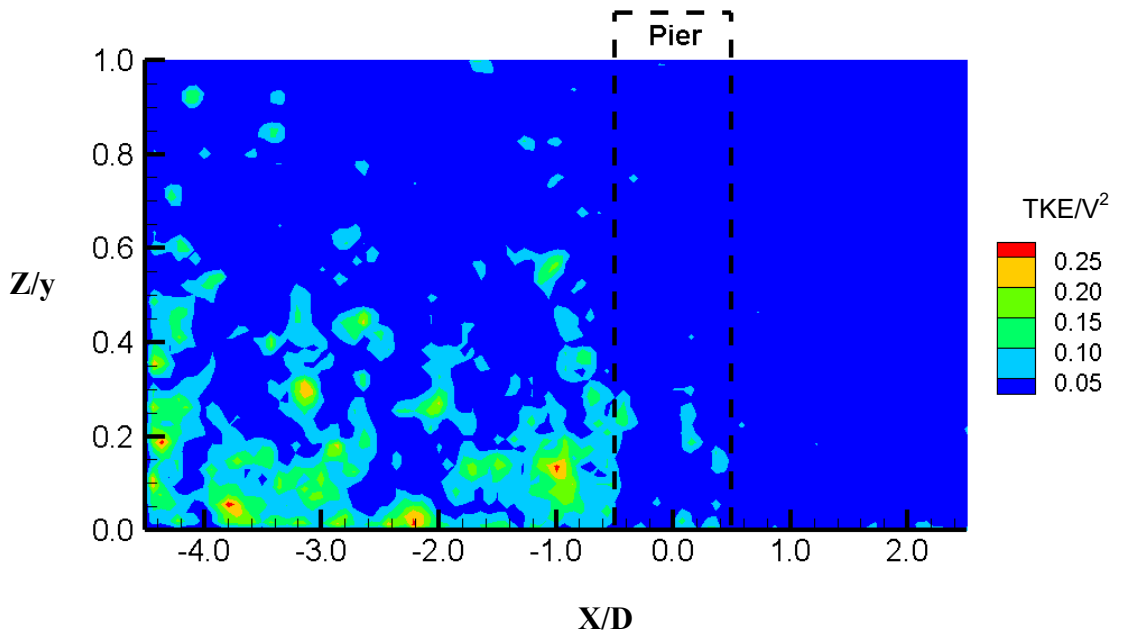


Figure B.106. Normalised turbulent kinetic energy for the single pier case at $Y/D = 2$

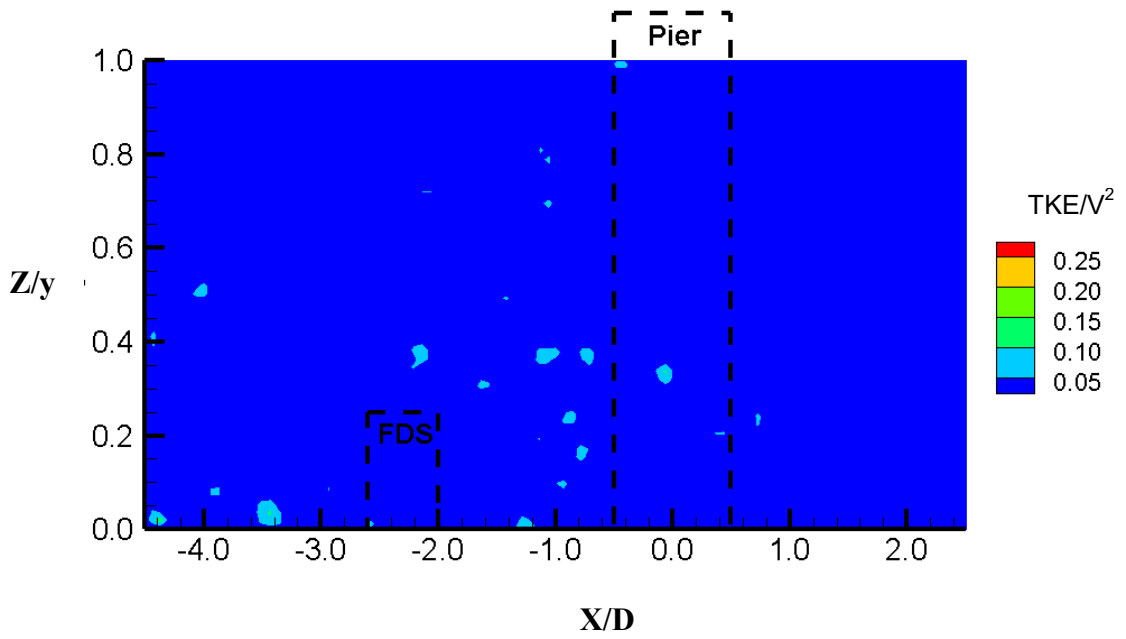


Figure B.107. Normalised turbulent kinetic energy for the single pier case and FDS with $H/y = 0.25$ at $Y/D = 2$

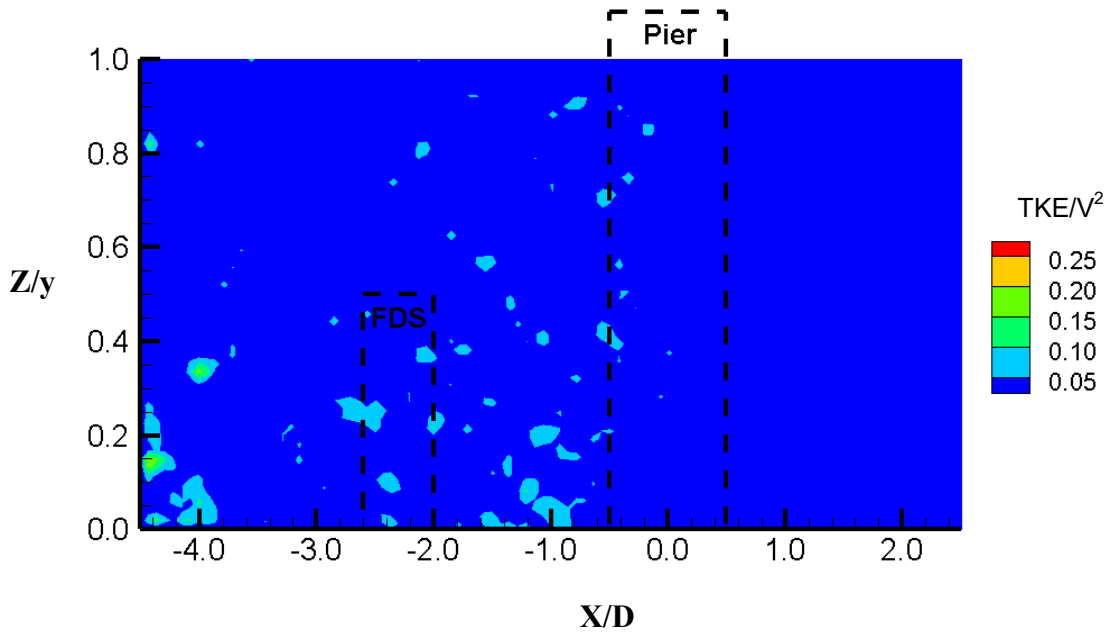


Figure B.108. Normalised turbulent kinetic energy for the single pier case and FDS with $H/y=0.50$ at $Y/D = 2$

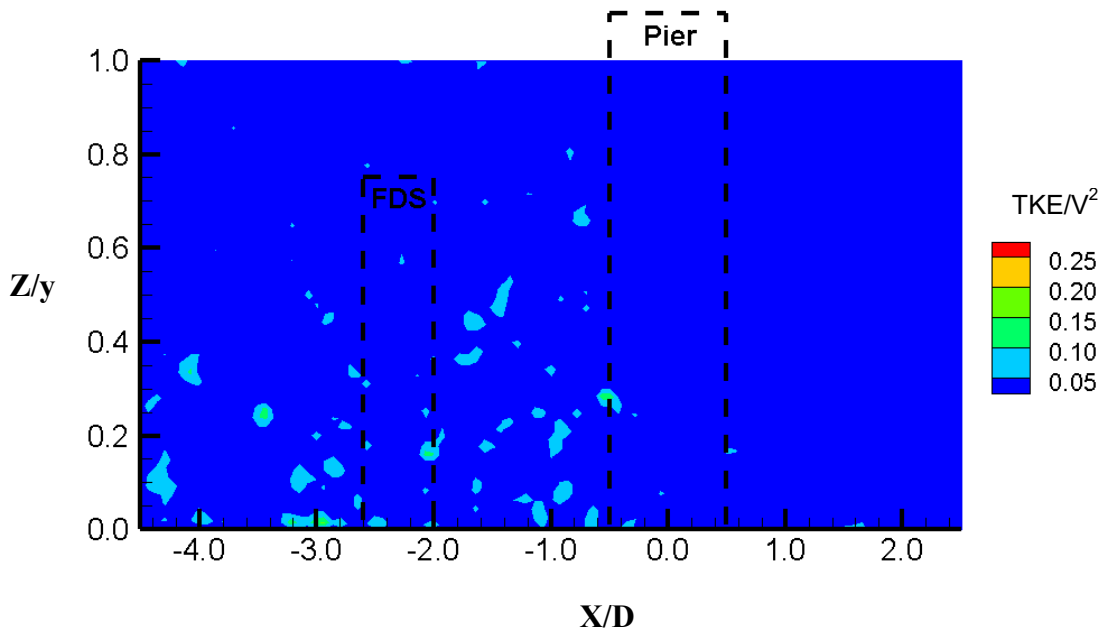


Figure B.109. Normalised turbulent kinetic energy for the single pier case and FDS with $H/y=0.75$ at $Y/D = 2$

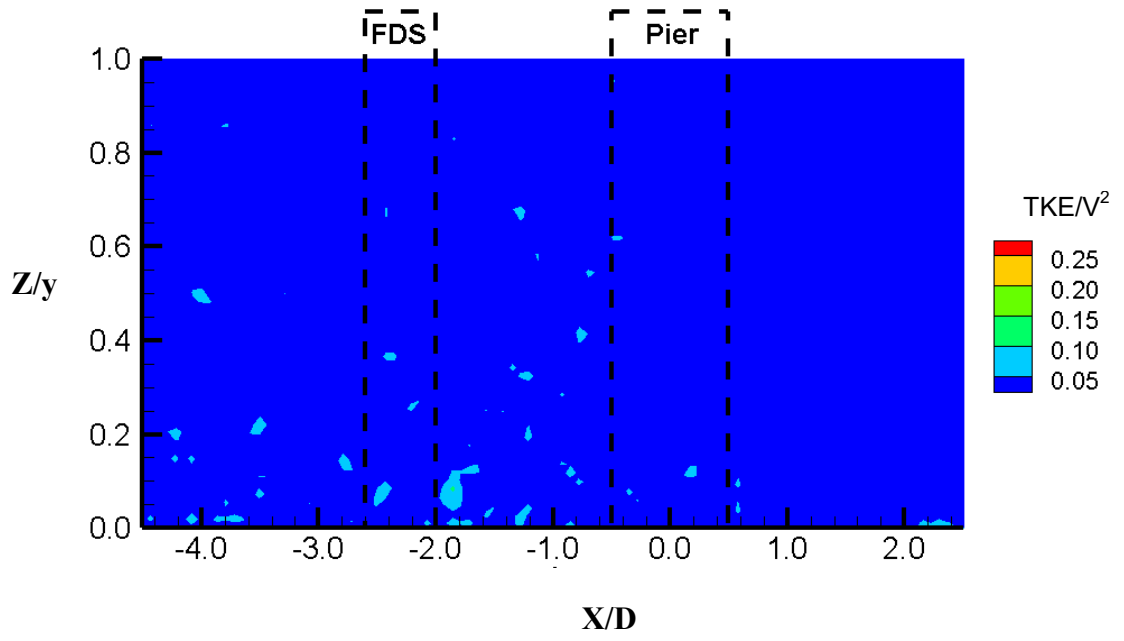


Figure B.110. Normalised turbulent kinetic energy for the single pier case and FDS with $H/y > 1$ at $Y/D = 2$

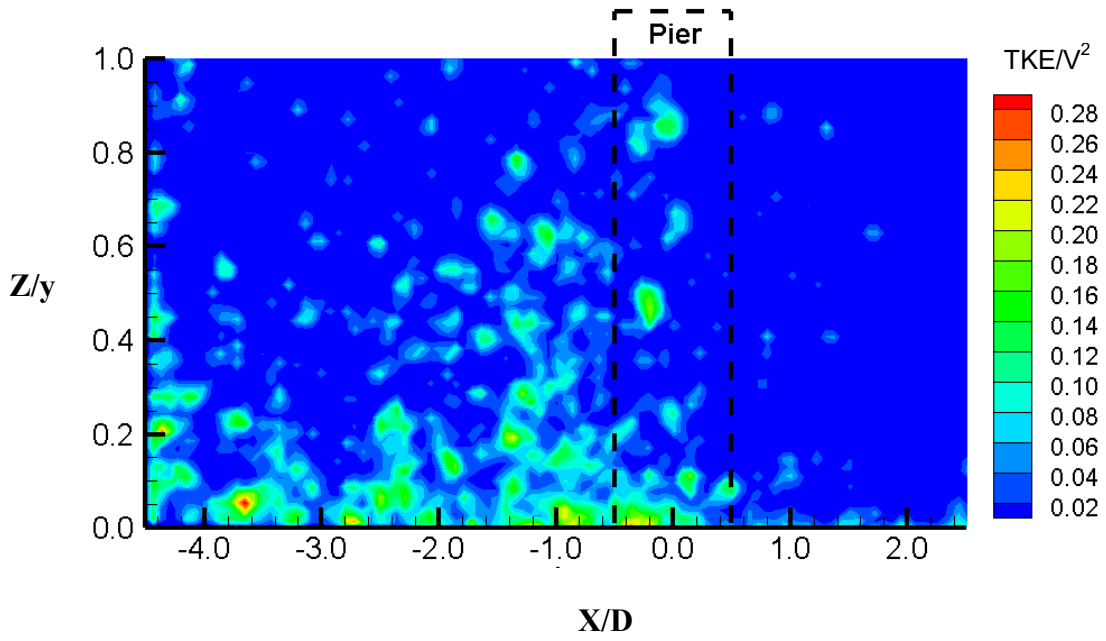


Figure B.111. Normalised turbulent kinetic energy for the single pier case at $Y/D = 3$

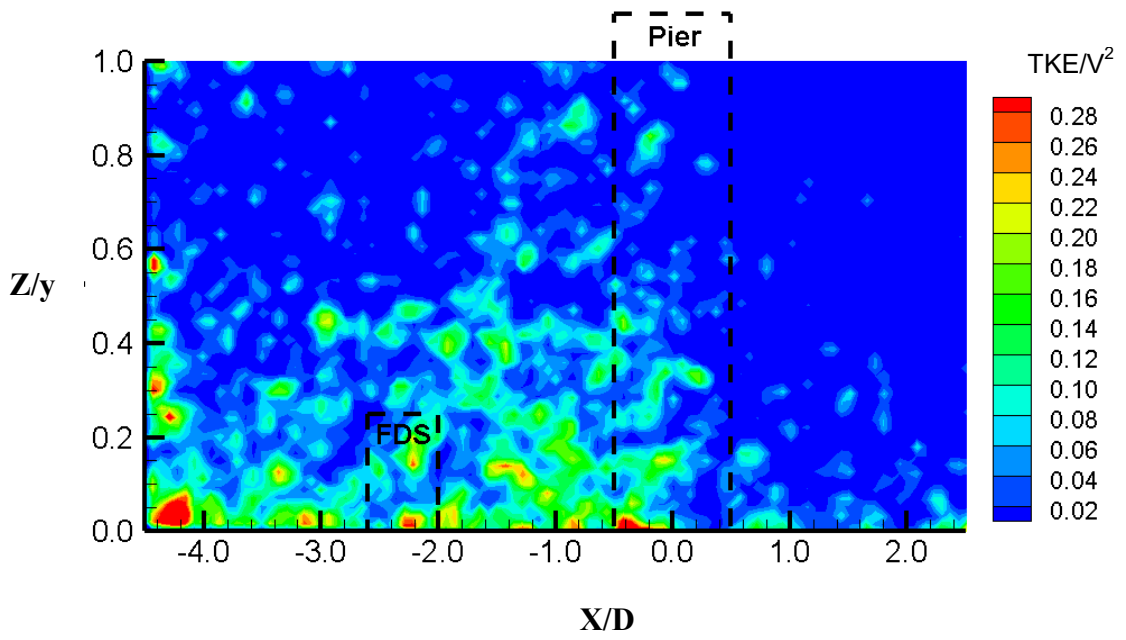


Figure B.112. Normalised turbulent kinetic energy for the single pier case and FDS with $H/y=0.25$ at $Y/D = 3$

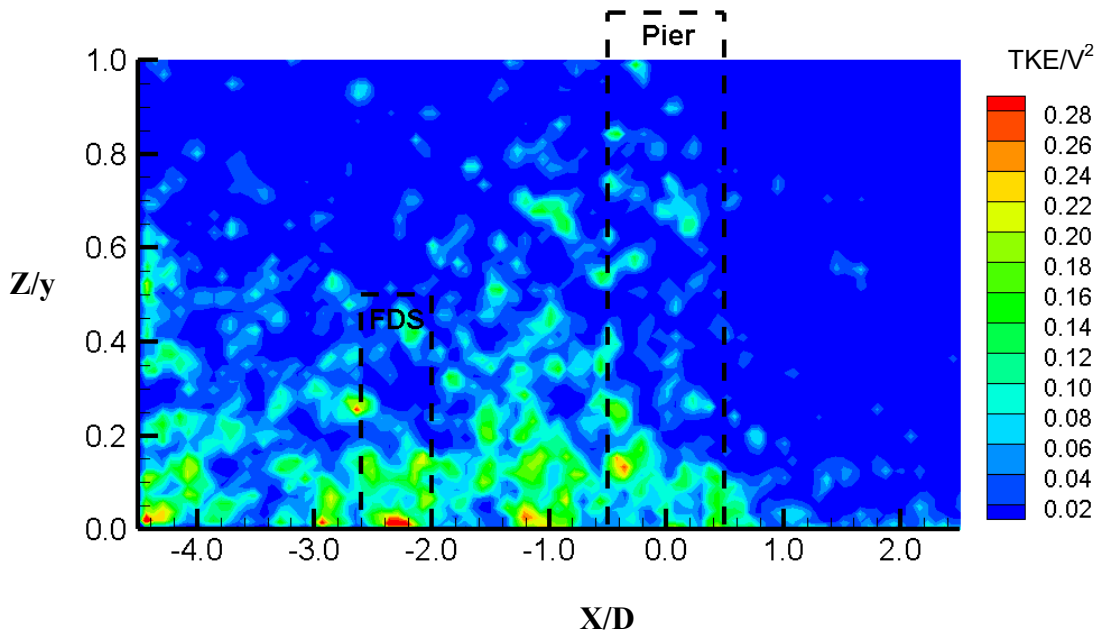


Figure B.113. Normalised turbulent kinetic energy for the single pier case and FDS with $H/y=0.50$ at $Y/D=3$

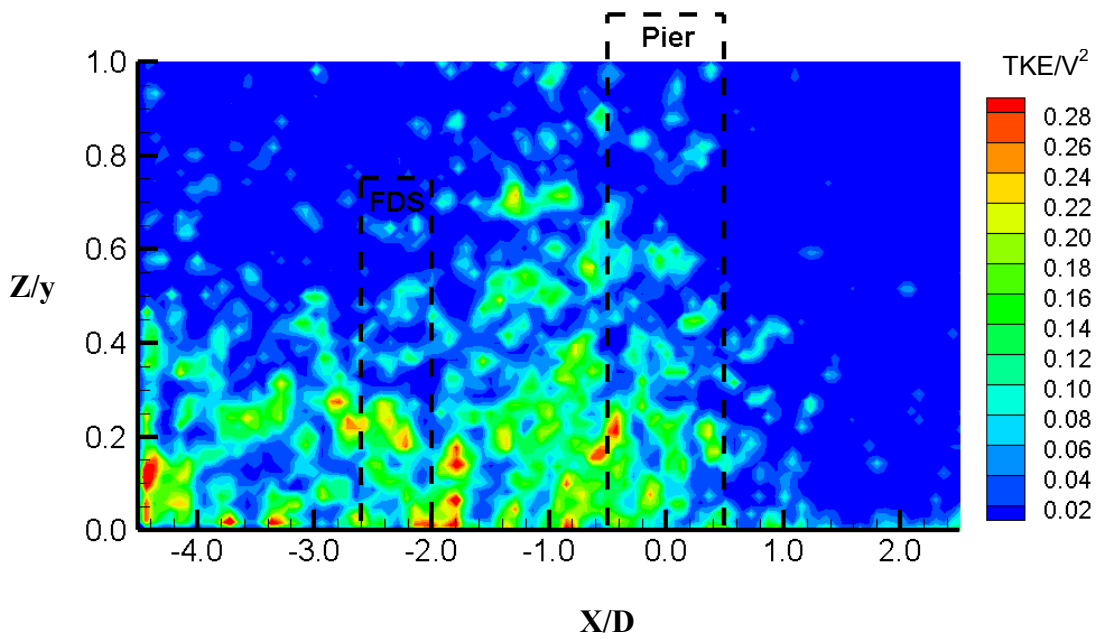


Figure B.114. Normalised turbulent kinetic energy for the single pier case and FDS with $H/y=0.75$ at $Y/D=3$

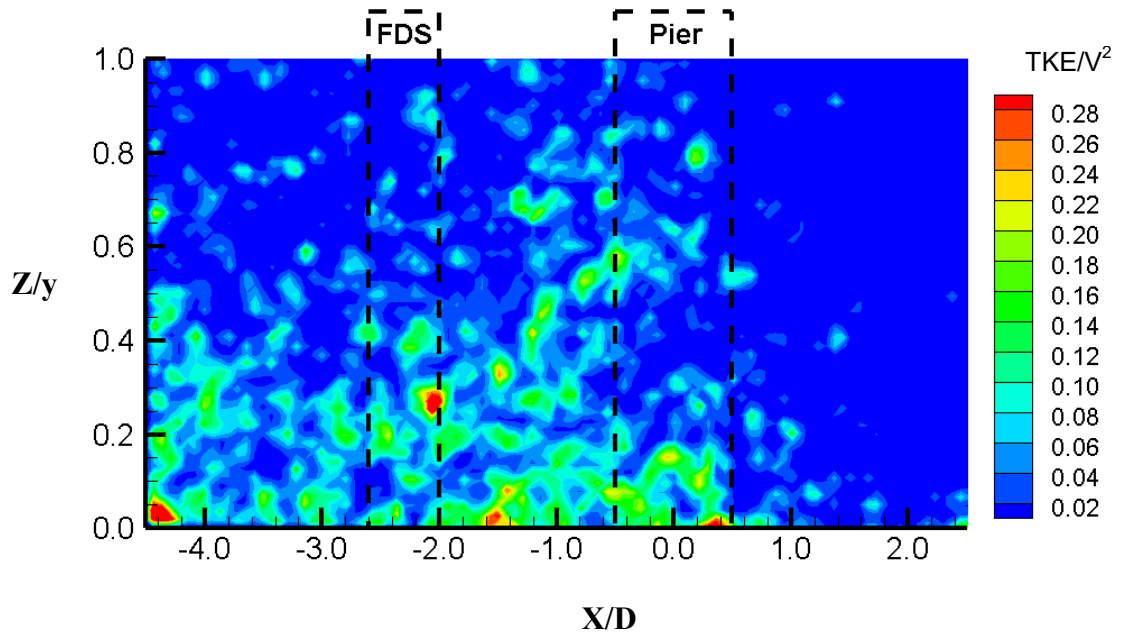


Figure B.114. Normalised turbulent kinetic energy for the single pier case and FDS with $H/y > 1$ at $Y/D = 3$

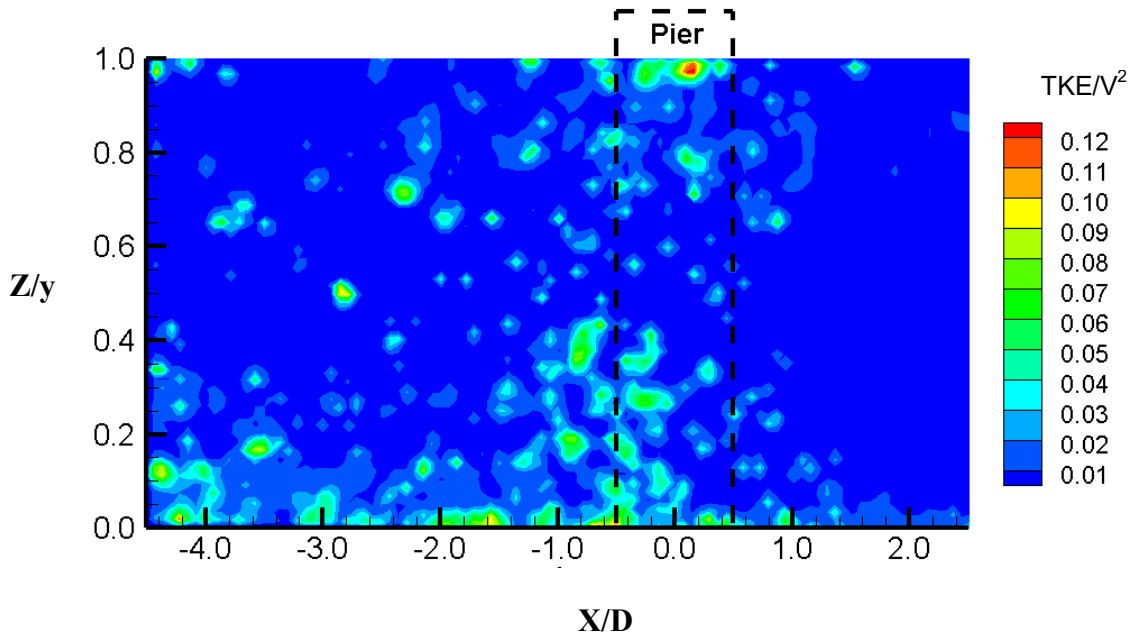


Figure B.116. Normalised turbulent kinetic energy for the single pier case at $Y/D = 4$

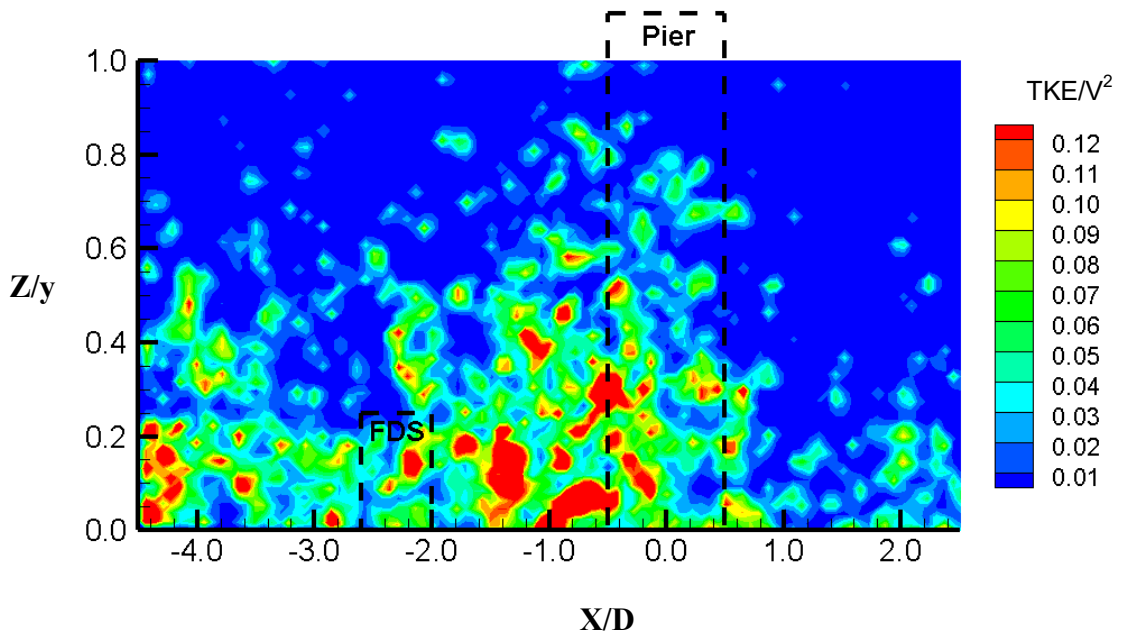


Figure B.117. Normalised turbulent kinetic energy for the single pier case and FDS with $H/y=0.25$ at $Y/D = 4$

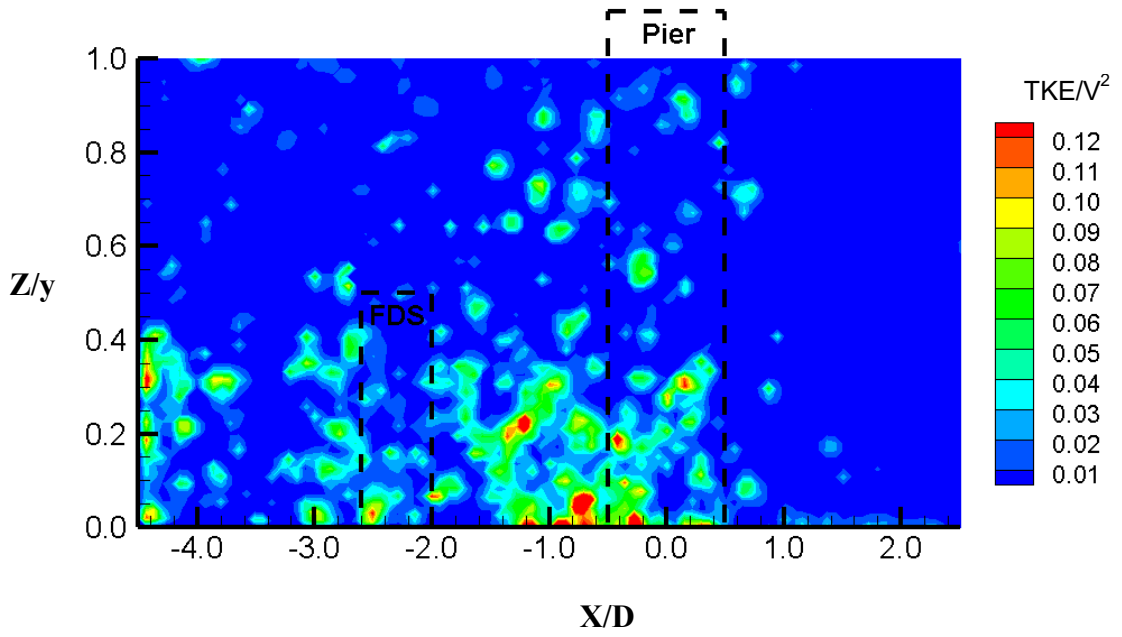


Figure B.118. Normalised turbulent kinetic energy for the single pier case and FDS with $H/y=0.50$ at $Y/D = 4$

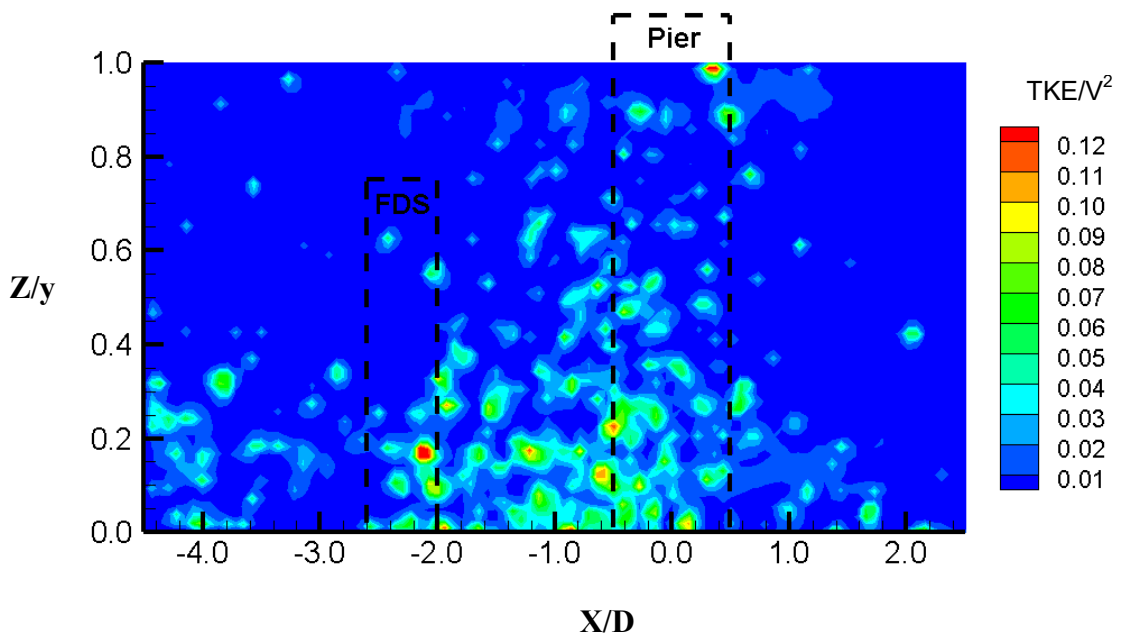


Figure B.119. Normalised turbulent kinetic energy for the single pier case and FDS with $H/y=0.75$ at $Y/D = 4$

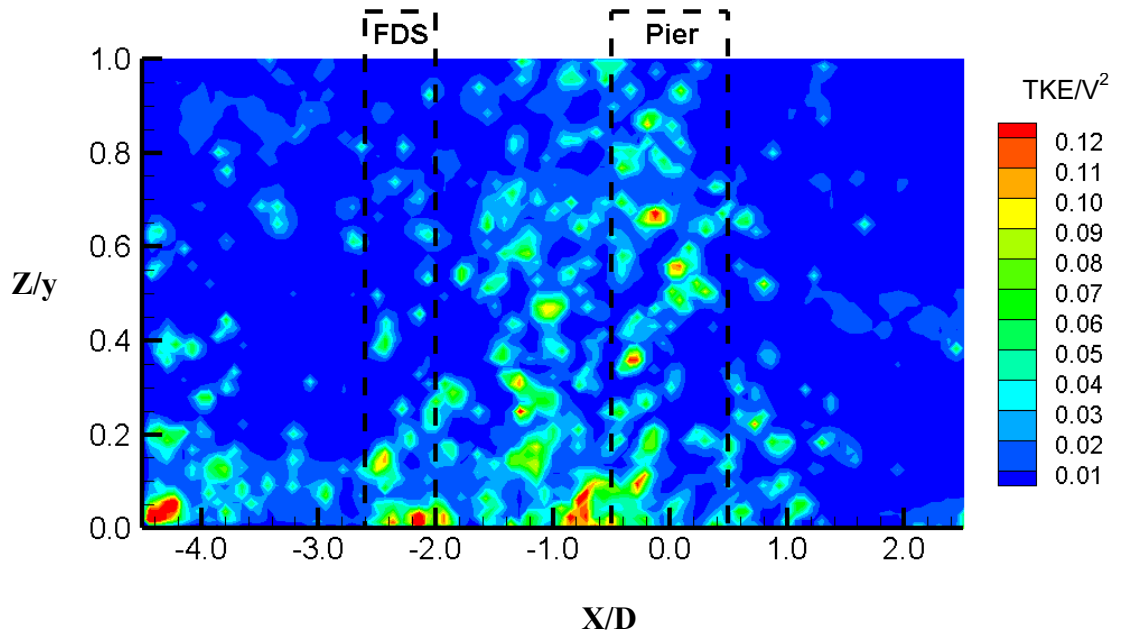


Figure B.120. Normalised turbulent kinetic energy for the single pier case and FDS with $H/y > 1$ at $Y/D = 4$

B.7. Plots of Reynolds Shear Stress

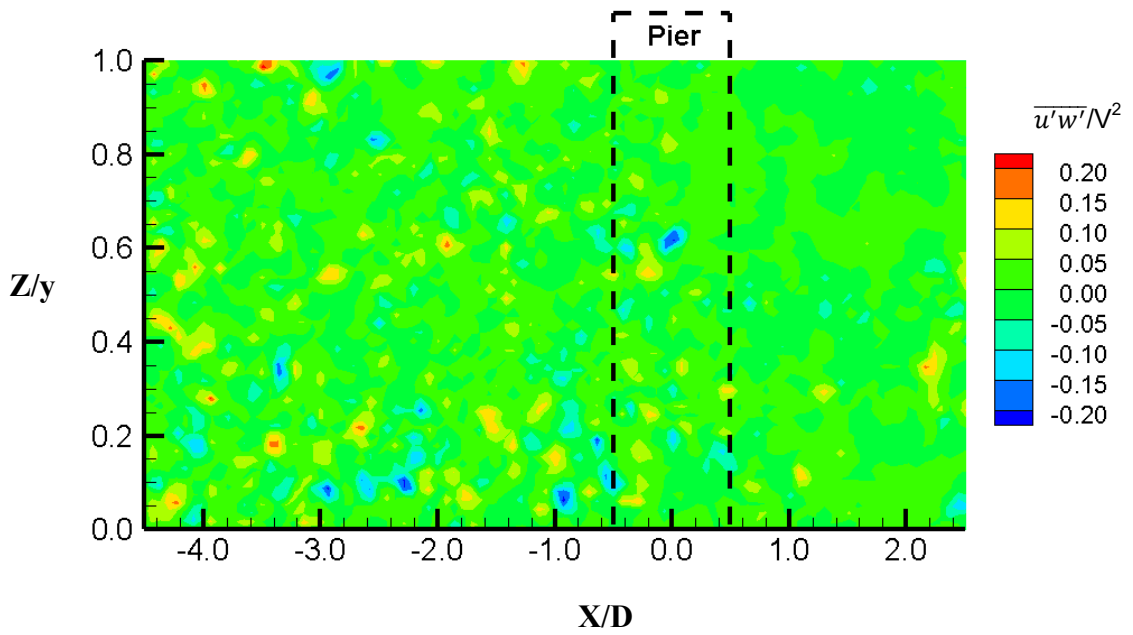


Figure B.121. Normalised Reynolds Shear Stress for the single pier case at $Y/D = 1$

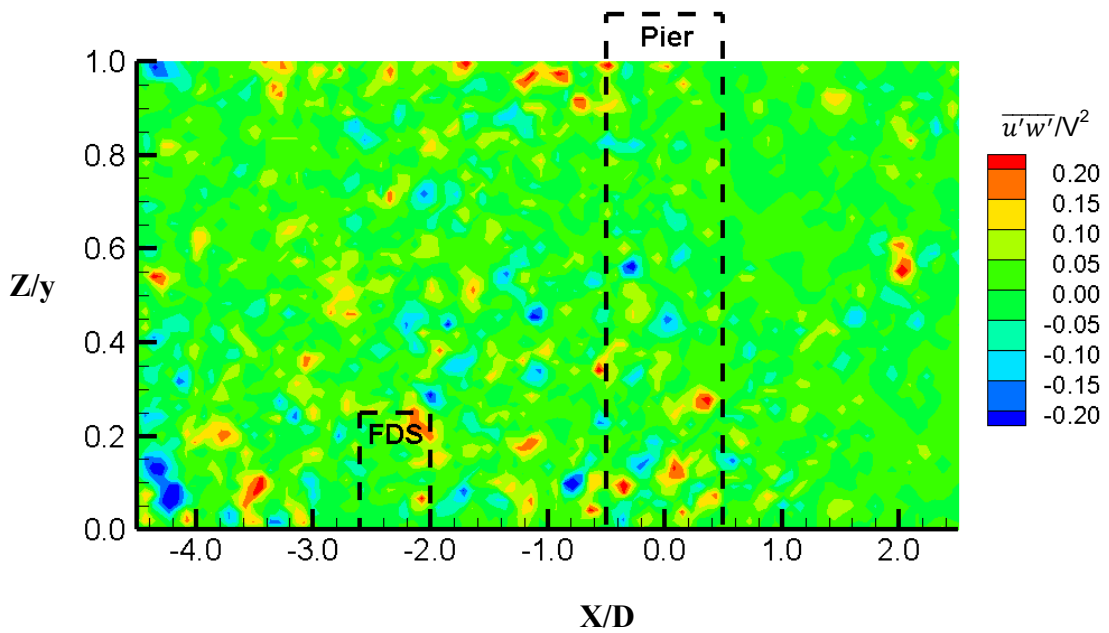


Figure B.122. Normalised Reynolds Shear Stress for the single pier case and FDS with $H/y=0.25$ at $Y/D = 1$

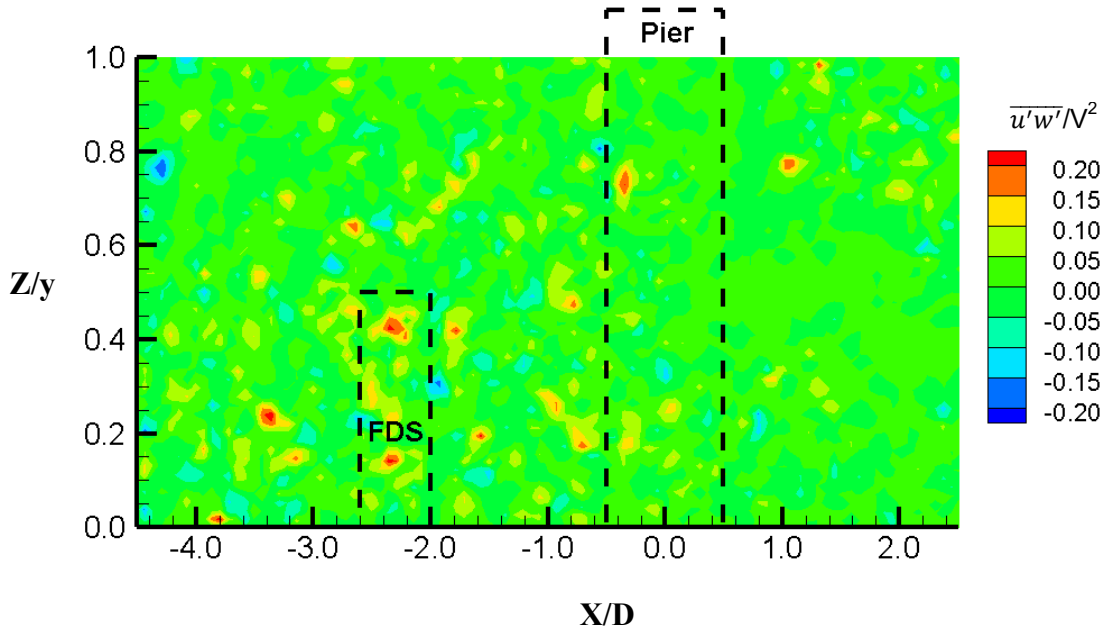


Figure B.123. Normalised Reynolds Shear Stress for the single pier case and FDS with $H/y=0.50$ at $Y/D = 1$

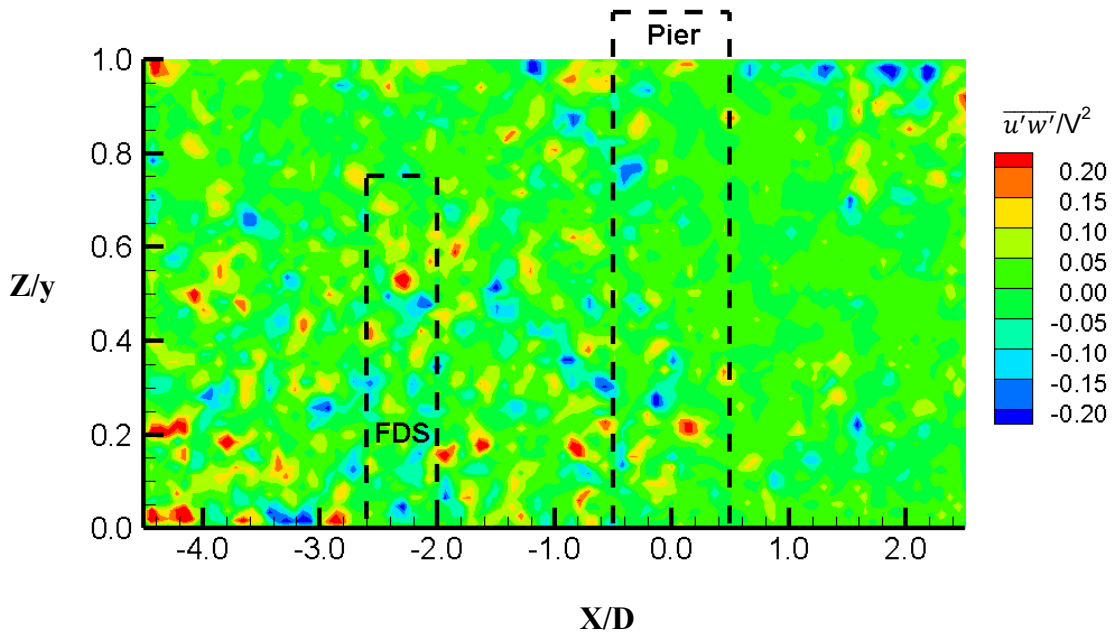


Figure B.124. Normalised Reynolds Shear Stress for the single pier case and FDS with $H/y=0.75$ at $Y/D = 1$

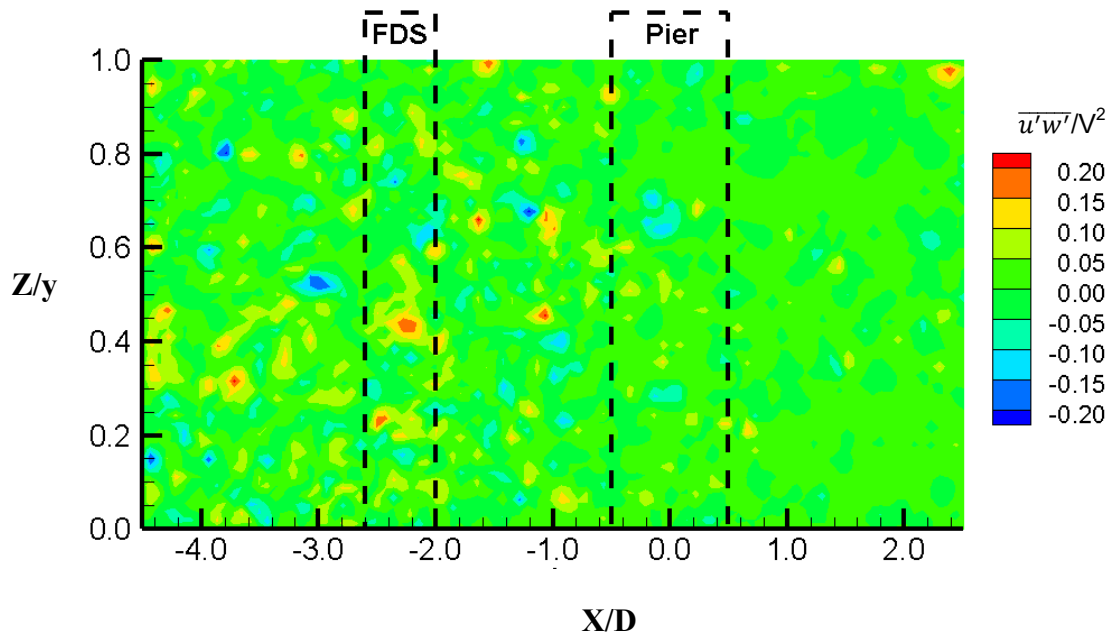


Figure B.125. Normalised Reynolds Shear Stress for the single pier case and FDS with $H/y > 1$ at $Y/D = 1$

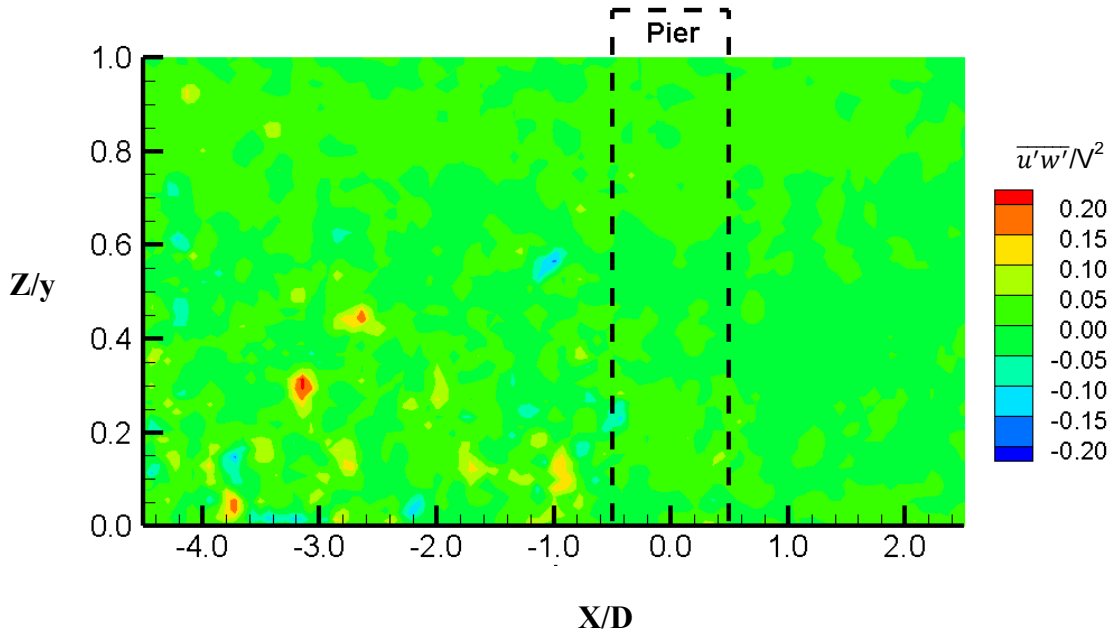


Figure B.126. Normalised Reynolds Shear Stress for the single pier case at $Y/D = 2$

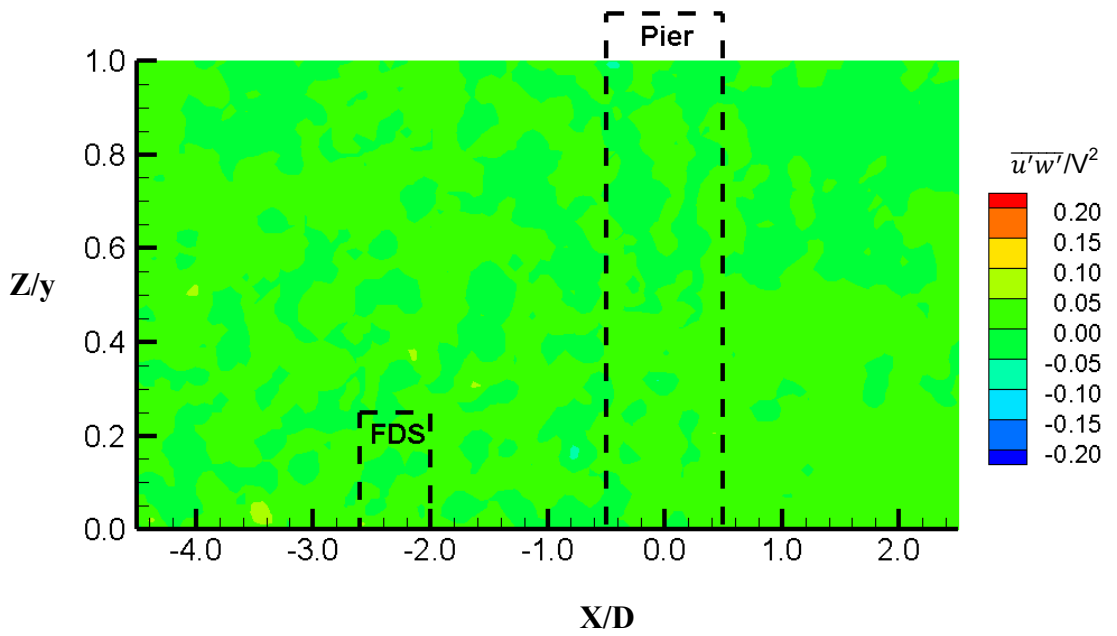


Figure B.127. Normalised Reynolds Shear Stress for the single pier case and FDS with $H/y=0.25$ at $Y/D = 2$

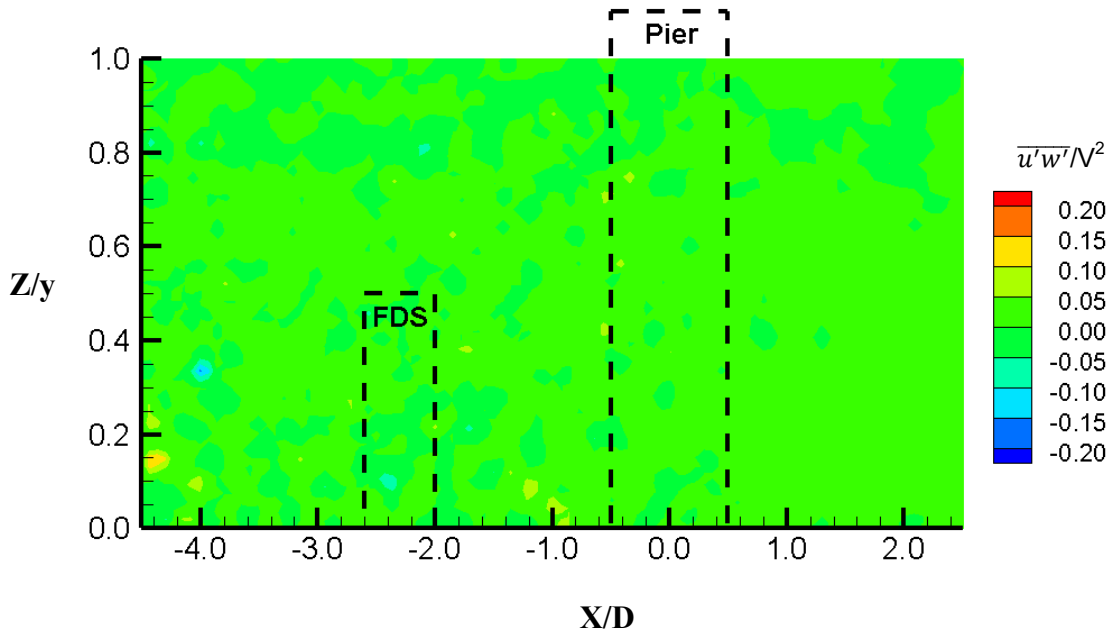


Figure B.128. Normalised Reynolds Shear Stress for the single pier case and FDS with $H/y=0.50$ at $Y/D = 2$

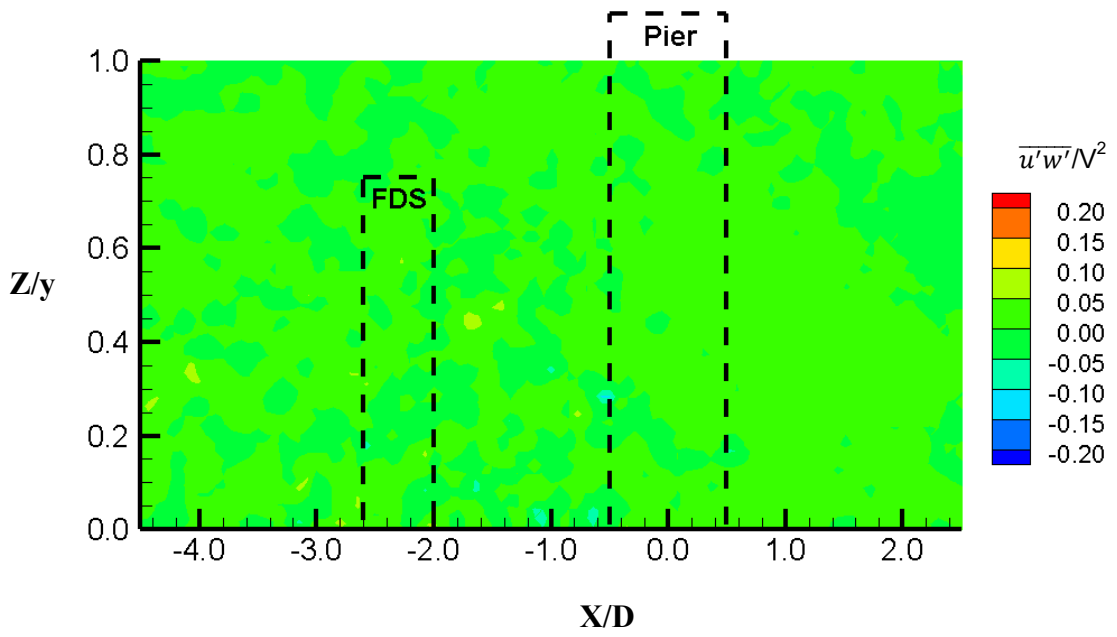


Figure B.129. Normalised Reynolds Shear Stress for the single pier case and FDS with $H/y=0.75$ at $Y/D = 2$

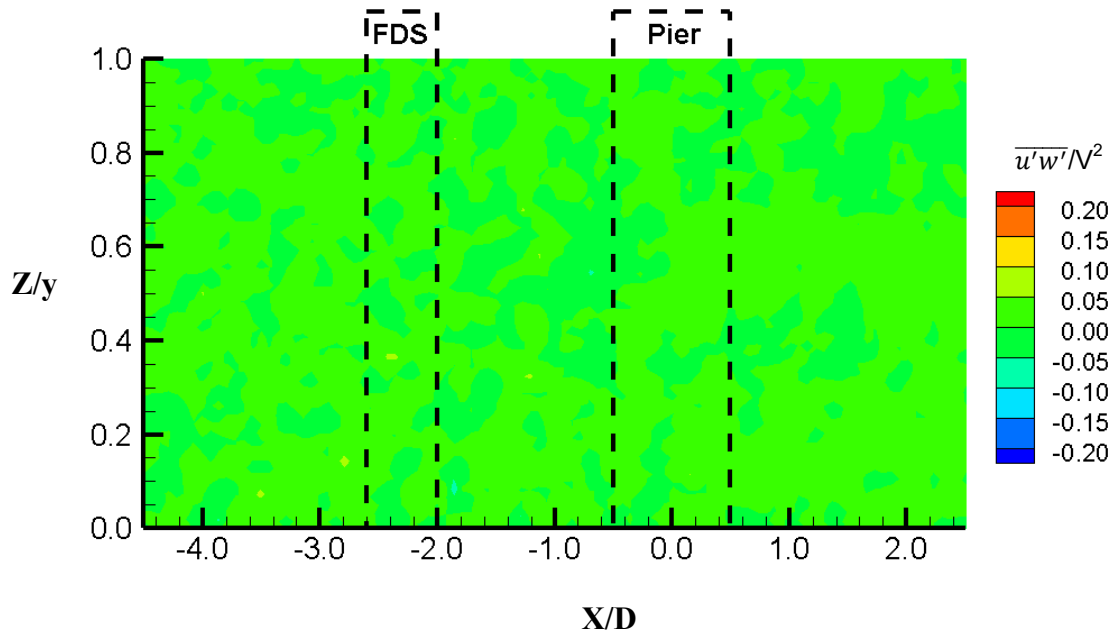


Figure B.130. Normalised Reynolds Shear Stress for the single pier case and FDS with $H/y > 1$ at $Y/D = 2$

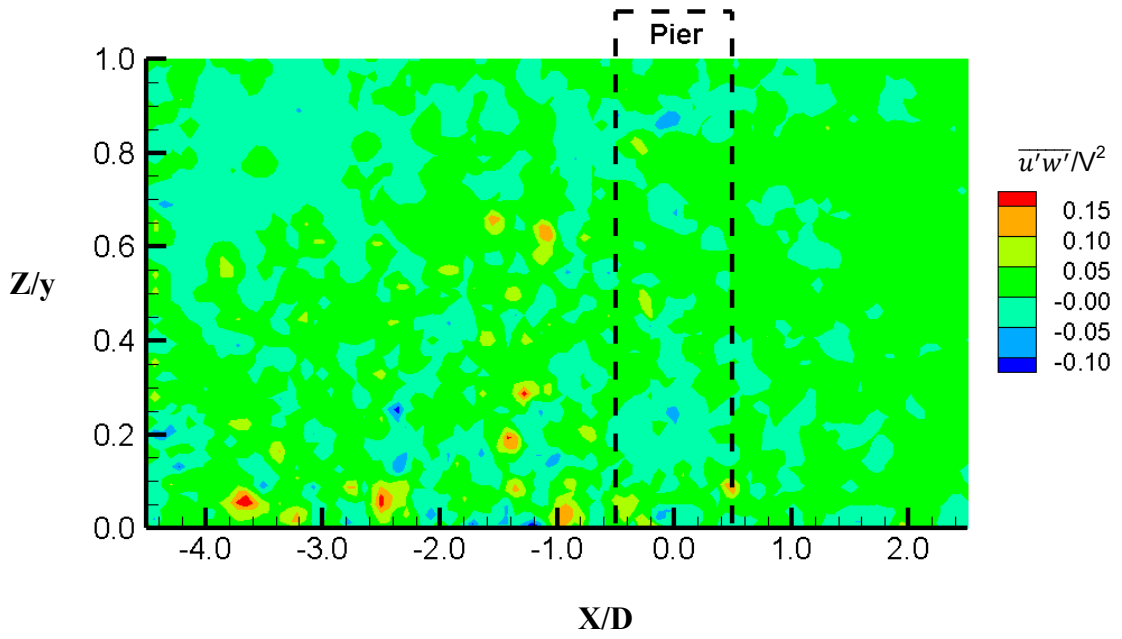


Figure B.131. Normalised Reynolds Shear Stress for the single pier case at $Y/D = 3$

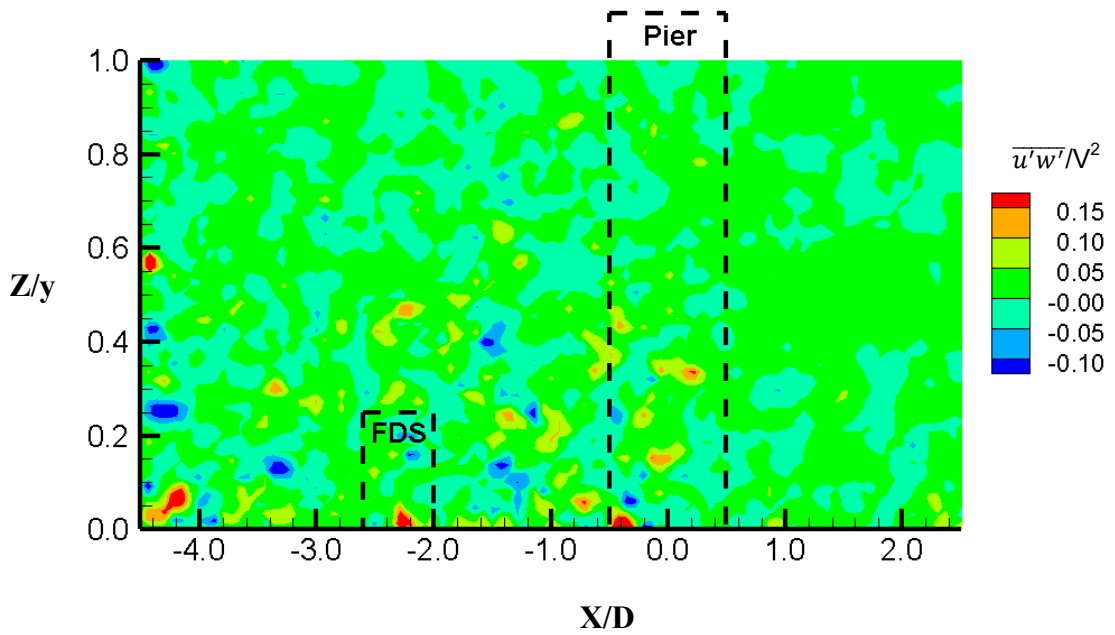


Figure B.132. Normalised Reynolds Shear Stress for the single pier case and FDS with $H/y = 0.25$ at $Y/D = 3$

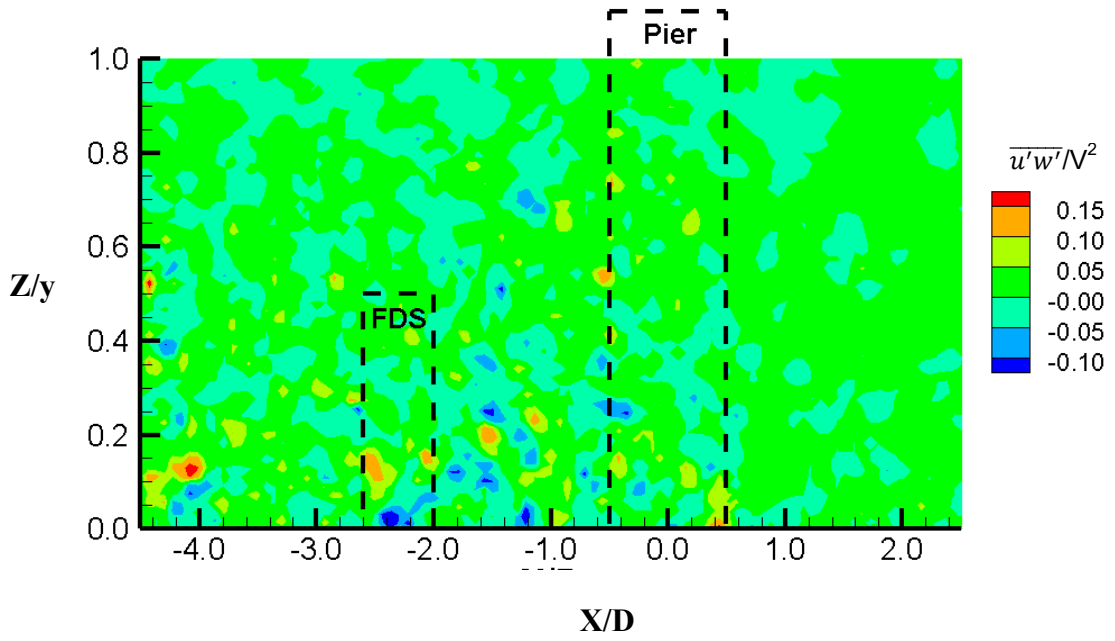


Figure B.133. Normalised Reynolds Shear Stress for the single pier case and FDS with $H/y=0.50$ at $Y/D = 3$

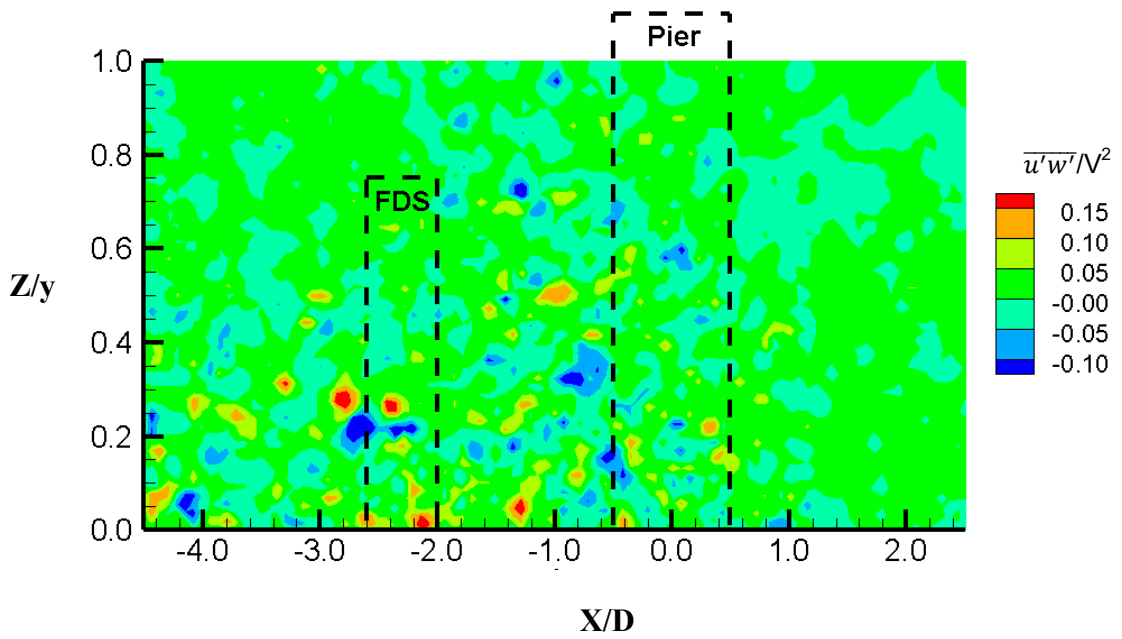


Figure B.134. Normalised Reynolds Shear Stress for the single pier case and FDS with $H/y=0.75$ at $Y/D = 3$

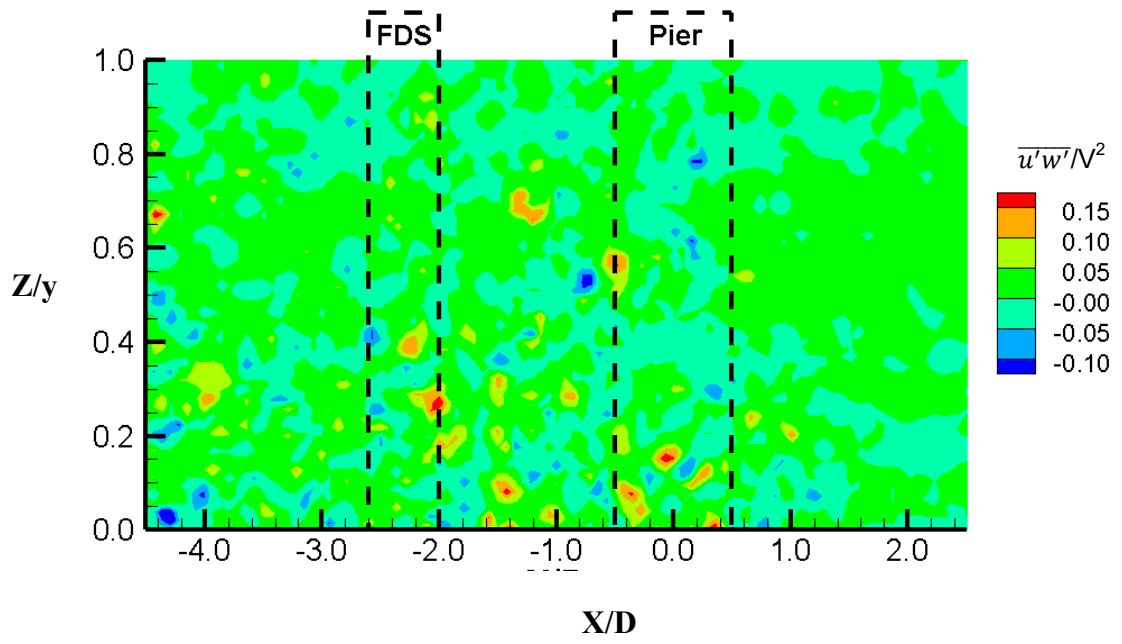


Figure B.135. Normalised Reynolds Shear Stress for the single pier case and FDS with $H/y > 1$ at $Y/D = 3$

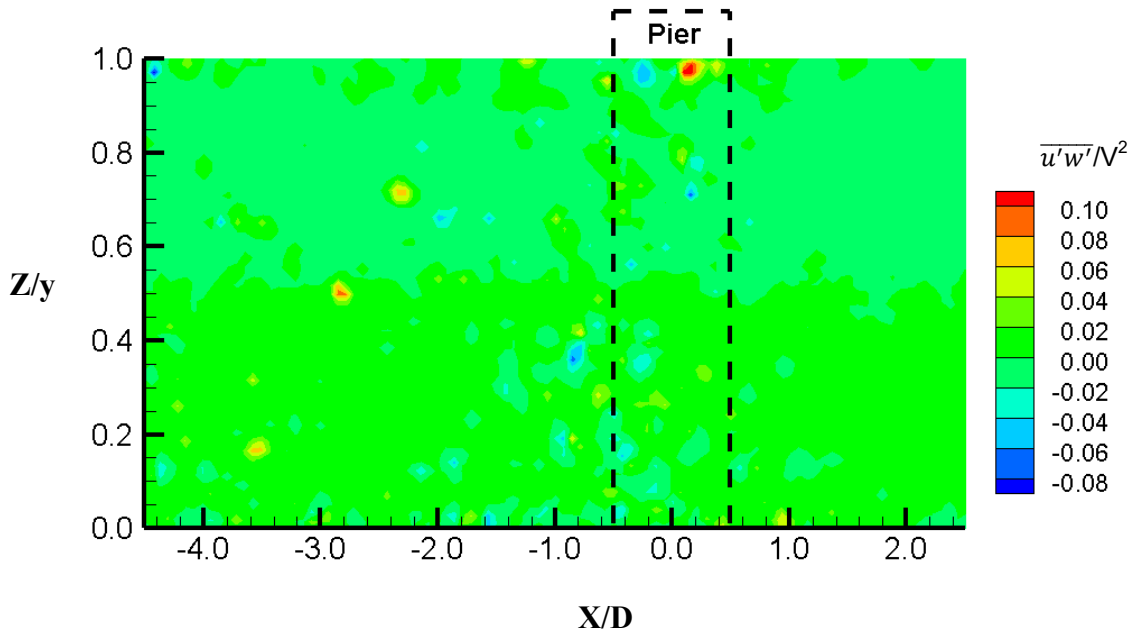


Figure B.136. Normalised Reynolds Shear Stress for the single pier case at $Y/D = 4$

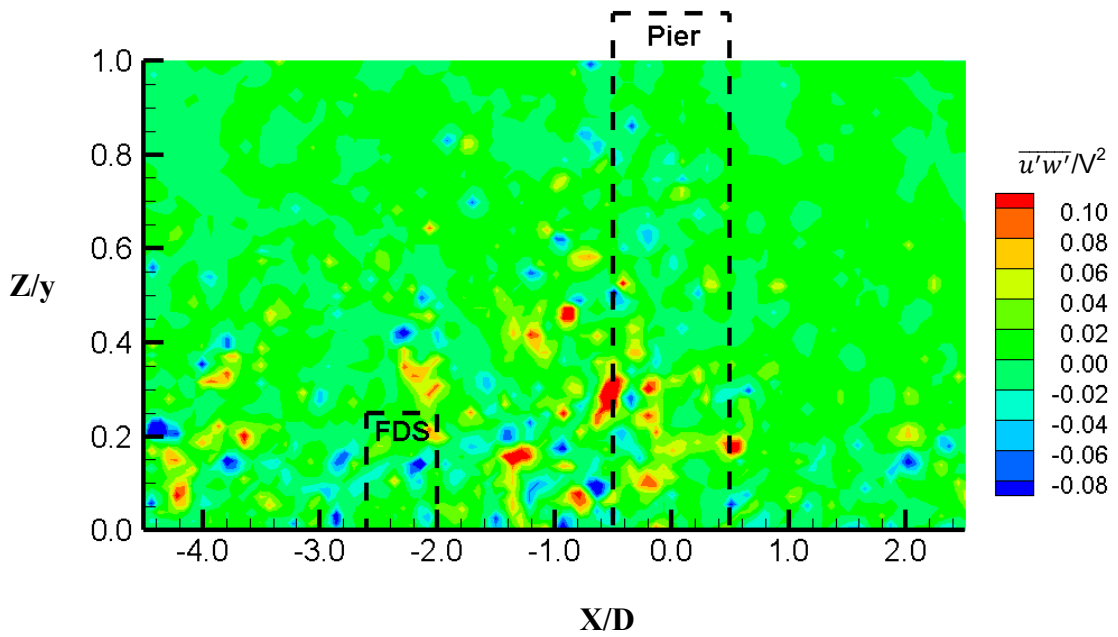


Figure B.137. Normalised Reynolds Shear Stress for the single pier case and FDS with $H/y=0.25$ at $Y/D = 4$

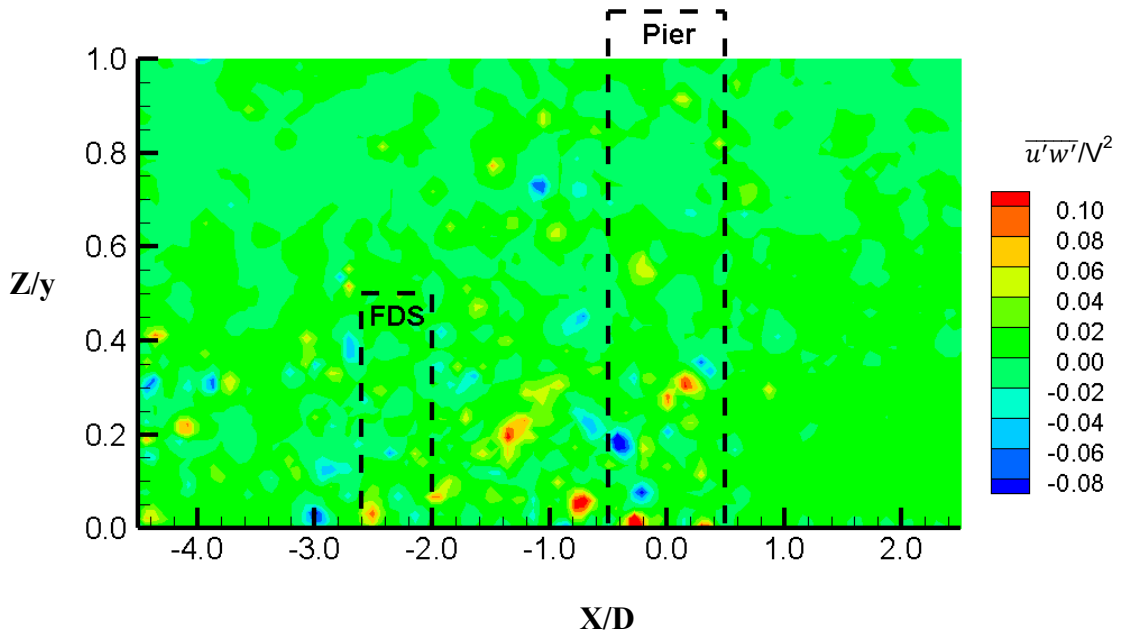


Figure B.138. Normalised Reynolds Shear Stress for the single pier case and FDS with $H/y=0.50$ at $Y/D = 4$

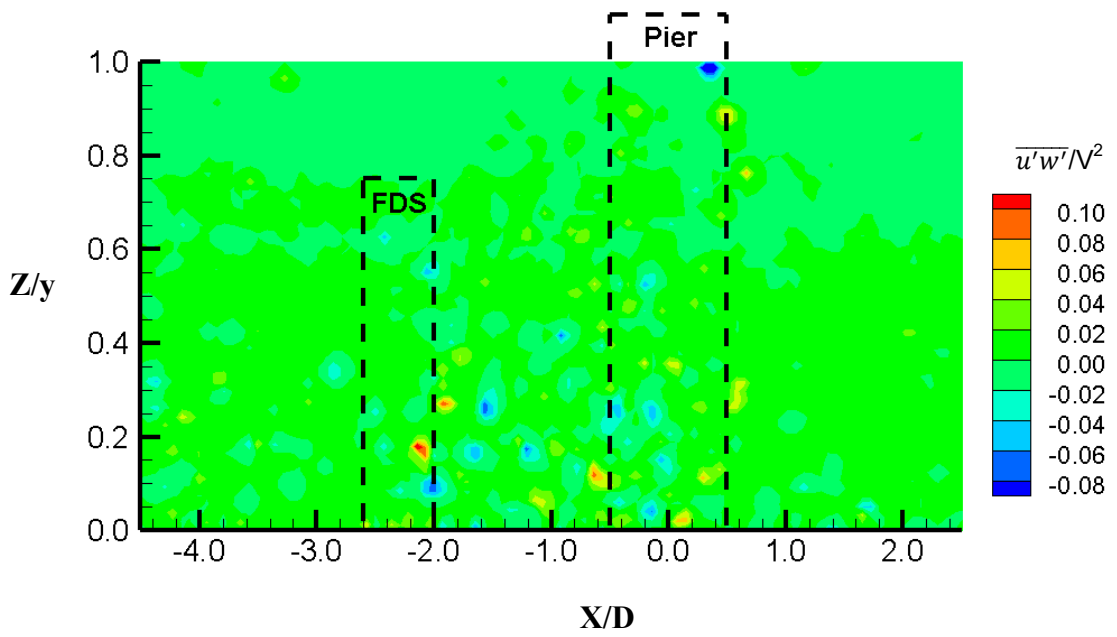


Figure B.139. Normalised Reynolds Shear Stress for the single pier case and FDS with $H/y=0.75$ at $Y/D = 4$

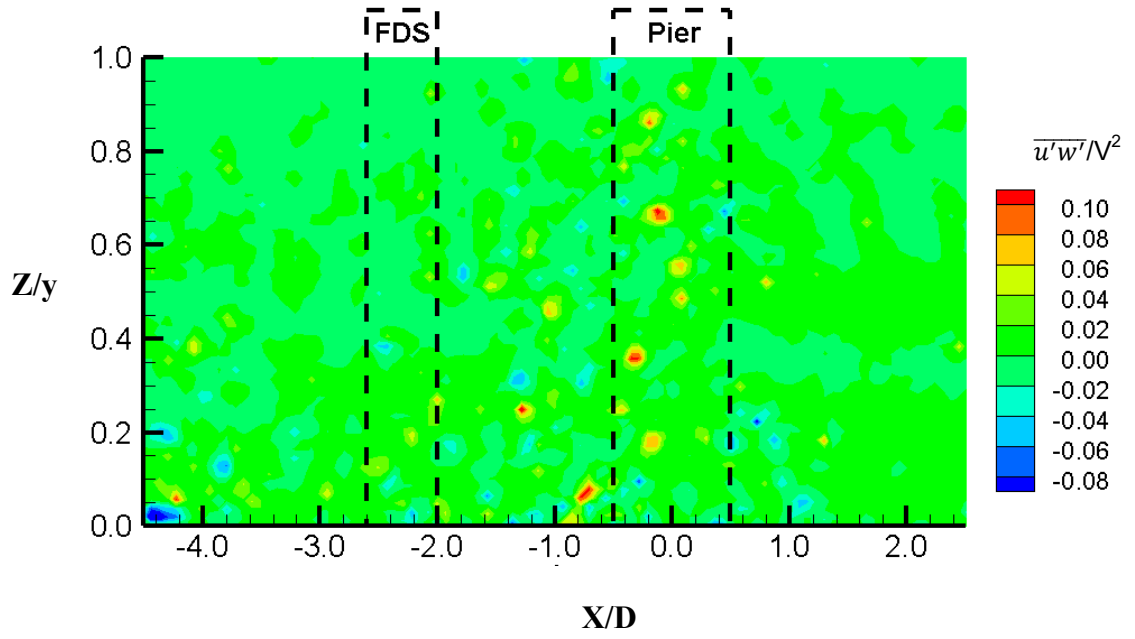


Figure B.140. Normalised Reynolds Shear Stress for the single pier case and FDS with $H/y > 1$ at $Y/D = 4$

APPENDIX C

F-Distribution Table

C.1. F-Distribution Table for 95% Confidence Intervals

C.2. F-Distribution Table for 90% Confidence Intervals

Table C.1. F-Distribution for 95% confidence intervals

DF2	DF1																		
	1	2	3	4	5	6	7	8	9	10	12	15	20	24	30	40	60	120	Inf
1	161.45	199.5	215.71	224.58	230.16	233.99	236.77	238.88	240.54	241.88	243.91	245.95	248.01	249.05	250.1	251.14	252.2	253.25	254.31
2	18.513	19	19.164	19.247	19.296	19.33	19.353	19.371	19.385	19.396	19.413	19.429	19.446	19.454	19.462	19.471	19.479	19.487	19.496
3	10.128	9.5521	9.2766	9.1172	9.0135	8.9406	8.8867	8.8452	8.8123	8.7855	8.7446	8.7029	8.6602	8.6385	8.6166	8.5944	8.572	8.5494	8.5264
4	7.7086	6.9443	6.5914	6.3882	6.2561	6.1631	6.0942	6.041	5.9988	5.9644	5.9117	5.8578	5.8025	5.7744	5.7459	5.717	5.6877	5.6581	5.6281
5	6.6079	5.7861	5.4095	5.1922	5.0503	4.9503	4.8759	4.8183	4.7725	4.7351	4.6777	4.6188	4.5581	4.5272	4.4957	4.4638	4.4314	4.3985	4.365
6	5.9874	5.1433	4.7571	4.5337	4.3874	4.2839	4.2067	4.1468	4.099	4.06	3.9999	3.9381	3.8742	3.8415	3.8082	3.7743	3.7398	3.7047	3.6689
7	5.5914	4.7374	4.3468	4.1203	3.9715	3.866	3.787	3.7257	3.6767	3.6365	3.5747	3.5107	3.4445	3.4105	3.3758	3.3404	3.3043	3.2674	3.2298
8	5.3177	4.459	4.0662	3.8379	3.6875	3.5806	3.5005	3.4381	3.3881	3.3472	3.2839	3.2184	3.1503	3.1152	3.0794	3.0428	3.0053	2.9669	2.9276
9	5.1174	4.2565	3.8625	3.6331	3.4817	3.3738	3.2927	3.2296	3.1789	3.1373	3.0729	3.0061	2.9365	2.9005	2.8637	2.8259	2.7872	2.7475	2.7067
10	4.9646	4.1028	3.7083	3.478	3.3258	3.2172	3.1355	3.0717	3.0204	2.9782	2.913	2.845	2.774	2.7372	2.6996	2.6609	2.6211	2.5801	2.5379
11	4.8443	3.9823	3.5874	3.3567	3.2039	3.0946	3.0123	2.948	2.8962	2.8536	2.7876	2.7186	2.6464	2.609	2.5705	2.5309	2.4901	2.448	2.4045
12	4.7472	3.8853	3.4903	3.2592	3.1059	2.9961	2.9134	2.8486	2.7964	2.7534	2.6866	2.6169	2.5436	2.5055	2.4663	2.4259	2.3842	2.341	2.2962
13	4.6672	3.8056	3.4105	3.1791	3.0254	2.9153	2.8321	2.7669	2.7144	2.671	2.6037	2.5331	2.4589	2.4202	2.3803	2.3392	2.2966	2.2524	2.2064
14	4.6001	3.7389	3.3439	3.1122	2.9582	2.8477	2.7642	2.6987	2.6458	2.6022	2.5342	2.463	2.3879	2.3487	2.3082	2.2664	2.2229	2.1778	2.1307
15	4.5431	3.6823	3.2874	3.0556	2.9013	2.7905	2.7066	2.6408	2.5876	2.5437	2.4753	2.4034	2.3275	2.2878	2.2468	2.2043	2.1601	2.1141	2.0658
16	4.494	3.6337	3.2389	3.0069	2.8524	2.7413	2.6572	2.5911	2.5377	2.4935	2.4247	2.3522	2.2756	2.2354	2.1938	2.1507	2.1058	2.0589	2.0096
17	4.4513	3.5915	3.1968	2.9647	2.81	2.6987	2.6143	2.548	2.4943	2.4499	2.3807	2.3077	2.2304	2.1898	2.1477	2.104	2.0584	2.0107	1.9604
18	4.4139	3.5546	3.1599	2.9277	2.7729	2.6613	2.5767	2.5102	2.4563	2.4117	2.3421	2.2686	2.1906	2.1497	2.1071	2.0629	2.0166	1.9681	1.9168
19	4.3807	3.5219	3.1274	2.8951	2.7401	2.6283	2.5435	2.4768	2.4227	2.3779	2.308	2.2341	2.1555	2.1141	2.0712	2.0264	1.9795	1.9302	1.878
20	4.3512	3.4928	3.0984	2.8661	2.7109	2.599	2.514	2.4471	2.3928	2.3479	2.2776	2.2033	2.1242	2.0825	2.0391	1.9938	1.9464	1.8963	1.8432
21	4.3248	3.4668	3.0725	2.8401	2.6848	2.5727	2.4876	2.4205	2.366	2.321	2.2504	2.1757	2.096	2.054	2.0102	1.9645	1.9165	1.8657	1.8117
22	4.3009	3.4434	3.0491	2.8167	2.6613	2.5491	2.4638	2.3965	2.3419	2.2967	2.2258	2.1508	2.0707	2.0283	1.9842	1.938	1.8894	1.838	1.7831
23	4.2793	3.4221	3.028	2.7955	2.64	2.5277	2.4422	2.3748	2.3201	2.2747	2.2036	2.1282	2.0476	2.005	1.9605	1.9139	1.8648	1.8128	1.757
24	4.2597	3.4028	3.0088	2.7763	2.6207	2.5082	2.4226	2.3551	2.3002	2.2547	2.1834	2.1077	2.0267	1.9838	1.939	1.892	1.8424	1.7896	1.733
25	4.2417	3.3852	2.9912	2.7587	2.603	2.4904	2.4047	2.3371	2.2821	2.2365	2.1649	2.0889	2.0075	1.9643	1.9192	1.8718	1.8217	1.7684	1.711
26	4.2252	3.369	2.9752	2.7426	2.5868	2.4741	2.3883	2.3205	2.2655	2.2197	2.1479	2.0716	1.9898	1.9464	1.901	1.8533	1.8027	1.7488	1.6906
27	4.21	3.3541	2.9604	2.7278	2.5719	2.4591	2.3732	2.3053	2.2501	2.2043	2.1323	2.0558	1.9736	1.9299	1.8842	1.8361	1.7851	1.7306	1.6717
28	4.196	3.3404	2.9467	2.7141	2.5581	2.4453	2.3593	2.2913	2.236	2.19	2.1179	2.0411	1.9586	1.9147	1.8687	1.8203	1.7689	1.7138	1.6541
29	4.183	3.3277	2.934	2.7014	2.5454	2.4324	2.3463	2.2783	2.2229	2.1768	2.1045	2.0275	1.9446	1.9005	1.8543	1.8055	1.7537	1.6981	1.6376
30	4.1709	3.3158	2.9223	2.6896	2.5336	2.4205	2.3343	2.2662	2.2107	2.1646	2.0921	2.0148	1.9317	1.8874	1.8409	1.7918	1.7396	1.6835	1.6223
40	4.0847	3.2317	2.8387	2.606	2.4495	2.3359	2.249	2.1802	2.124	2.0772	2.0035	1.9245	1.8389	1.7929	1.7444	1.6928	1.6373	1.5766	1.5089
60	4.0012	3.1504	2.7581	2.5252	2.3683	2.2541	2.1665	2.097	2.0401	1.9926	1.9174	1.8364	1.748	1.7001	1.6491	1.5943	1.5343	1.4673	1.3893
120	3.9201	3.0718	2.6802	2.4472	2.2899	2.175	2.0868	2.0164	1.9588	1.9105	1.8337	1.7505	1.6587	1.6084	1.5543	1.4952	1.429	1.3519	1.2539
Inf	3.8415	2.9957	2.6049	2.3719	2.2141	2.0986	2.0096	1.9384	1.8799	1.8307	1.7522	1.6664	1.5705	1.5173	1.4591	1.394	1.318	1.2214	1

DF1: the numerator degrees of freedom

DF2: the denominator degrees of freedom

Table C.2. F-Distribution for 90% confidence intervals

DF2	DF1																		
	1	2	3	4	5	6	7	8	9	10	12	15	20	24	30	40	60	120	Inf
1	39.863	49.5	53.593	55.833	57.24	58.204	58.906	59.439	59.858	60.195	60.705	61.22	61.74	62.002	62.265	62.529	62.794	63.061	63.328
2	8.5263	9	9.1618	9.2434	9.2926	9.3255	9.3491	9.3668	9.3805	9.3916	9.4081	9.4247	9.4413	9.4496	9.4579	9.4662	9.4746	9.4829	9.4912
3	5.5383	5.4624	5.3908	5.3426	5.3092	5.2847	5.2662	5.2517	5.24	5.2304	5.2156	5.2003	5.1845	5.1764	5.1681	5.1597	5.1512	5.1425	5.1337
4	4.5448	4.3246	4.1909	4.1073	4.0506	4.0098	3.979	3.9549	3.9357	3.9199	3.8955	3.8704	3.8443	3.831	3.8174	3.8036	3.7896	3.7753	3.7607
5	4.0604	3.7797	3.6195	3.5202	3.453	3.4045	3.3679	3.3393	3.3163	3.2974	3.2682	3.238	3.2067	3.1905	3.1741	3.1573	3.1402	3.1228	3.105
6	3.776	3.4633	3.2888	3.1808	3.1075	3.0546	3.0145	2.983	2.9577	2.9369	2.9047	2.8712	2.8363	2.8183	2.8	2.7812	2.762	2.7423	2.7222
7	3.5894	3.2574	3.0741	2.9605	2.8833	2.8274	2.7849	2.7516	2.7247	2.7025	2.6681	2.6322	2.5947	2.5753	2.5555	2.5351	2.5142	2.4928	2.4708
8	3.4579	3.1131	2.9238	2.8064	2.7265	2.6683	2.6241	2.5894	2.5612	2.538	2.502	2.4642	2.4246	2.4041	2.383	2.3614	2.3391	2.3162	2.2926
9	3.3603	3.0065	2.8129	2.6927	2.6106	2.5509	2.5053	2.4694	2.4403	2.4163	2.3789	2.3396	2.2983	2.2768	2.2547	2.232	2.2085	2.1843	2.1592
10	3.285	2.9245	2.7277	2.6053	2.5216	2.4606	2.414	2.3772	2.3473	2.3226	2.2841	2.2435	2.2007	2.1784	2.1554	2.1317	2.1072	2.0818	2.0554
11	3.2252	2.8595	2.6602	2.5362	2.4512	2.3891	2.3416	2.304	2.2735	2.2482	2.2087	2.1671	2.1231	2.1	2.0762	2.0516	2.0261	1.9997	1.9721
12	3.1766	2.8068	2.6055	2.4801	2.394	2.331	2.2828	2.2446	2.2135	2.1878	2.1474	2.1049	2.0597	2.036	2.0115	1.9861	1.9597	1.9323	1.9036
13	3.1362	2.7632	2.5603	2.4337	2.3467	2.283	2.2341	2.1954	2.1638	2.1376	2.0966	2.0532	2.007	1.9827	1.9576	1.9315	1.9043	1.8759	1.8462
14	3.1022	2.7265	2.5222	2.3947	2.3069	2.2426	2.1931	2.1539	2.122	2.0954	2.0537	2.0095	1.9625	1.9377	1.9119	1.8852	1.8572	1.828	1.7973
15	3.0732	2.6952	2.4898	2.3614	2.273	2.2081	2.1582	2.1185	2.0862	2.0593	2.0171	1.9722	1.9243	1.899	1.8728	1.8454	1.8168	1.7876	1.7551
16	3.0481	2.6682	2.4618	2.3327	2.2438	2.1783	2.128	2.088	2.0553	2.0282	1.9854	1.9399	1.8913	1.8656	1.8388	1.8108	1.7816	1.7508	1.7182
17	3.0262	2.6446	2.4374	2.3078	2.2183	2.1524	2.1017	2.0613	2.0284	2.0009	1.9577	1.9117	1.8624	1.8362	1.809	1.7805	1.7506	1.7191	1.6856
18	3.007	2.624	2.416	2.2858	2.1958	2.1296	2.0785	2.0379	2.0047	1.977	1.9333	1.8868	1.8369	1.8104	1.7827	1.7537	1.7232	1.691	1.6567
19	2.9899	2.6056	2.397	2.2663	2.176	2.1094	2.058	2.0171	1.9836	1.9557	1.9117	1.8647	1.8142	1.7873	1.7592	1.7298	1.6988	1.6659	1.6308
20	2.9747	2.5893	2.3801	2.2489	2.1582	2.0913	2.0397	1.9985	1.9649	1.9367	1.8924	1.8449	1.7938	1.7667	1.7382	1.7083	1.6768	1.6433	1.6074
21	2.961	2.5746	2.3649	2.2333	2.1423	2.0751	2.0233	1.9819	1.948	1.9197	1.875	1.8272	1.7756	1.7481	1.7193	1.689	1.6569	1.6228	1.5862
22	2.9486	2.5613	2.3512	2.2193	2.1279	2.0605	2.0084	1.9668	1.9327	1.9043	1.8593	1.8111	1.759	1.7312	1.7021	1.6714	1.6389	1.6042	1.5668
23	2.9374	2.5493	2.3387	2.2065	2.1149	2.0472	1.9949	1.9531	1.9189	1.8903	1.845	1.7964	1.7439	1.7159	1.6864	1.6554	1.6224	1.5871	1.549
24	2.9271	2.5383	2.3274	2.1949	2.103	2.0351	1.9826	1.9407	1.9063	1.8775	1.8319	1.7831	1.7302	1.7019	1.6721	1.6407	1.6073	1.5715	1.5327
25	2.9177	2.5283	2.317	2.1842	2.0922	2.0241	1.9714	1.9293	1.8947	1.8658	1.82	1.7708	1.7175	1.689	1.659	1.6272	1.5934	1.557	1.5176
26	2.9091	2.5191	2.3075	2.1745	2.0822	2.0139	1.961	1.9188	1.8841	1.855	1.809	1.7596	1.7059	1.6771	1.6468	1.6147	1.5805	1.5437	1.5036
27	2.9012	2.5106	2.2987	2.1655	2.073	2.0045	1.9515	1.9091	1.8743	1.8451	1.7989	1.7492	1.6951	1.6662	1.6356	1.6032	1.5686	1.5313	1.4906
28	2.8939	2.5028	2.2906	2.1571	2.0645	1.9959	1.9427	1.9001	1.8652	1.8359	1.7895	1.7395	1.6852	1.656	1.6252	1.5925	1.5575	1.5198	1.4784
29	2.887	2.4955	2.2831	2.1494	2.0566	1.9878	1.9345	1.8918	1.8568	1.8274	1.7808	1.7306	1.6759	1.6466	1.6155	1.5825	1.5472	1.509	1.467
30	2.8807	2.4887	2.2761	2.1422	2.0493	1.9803	1.9269	1.8841	1.849	1.8195	1.7727	1.7223	1.6673	1.6377	1.6065	1.5732	1.5376	1.4989	1.4564
40	2.8354	2.4404	2.2261	2.091	1.9968	1.9269	1.8725	1.8289	1.7929	1.7627	1.7146	1.6624	1.6052	1.5741	1.5411	1.5056	1.4672	1.4248	1.3769
60	2.7911	2.3933	2.1774	2.041	1.9457	1.8747	1.8194	1.7748	1.738	1.707	1.6574	1.6034	1.5435	1.5107	1.4755	1.4373	1.3952	1.3476	1.2915
120	2.7478	2.3473	2.13	1.9923	1.8959	1.8238	1.7675	1.722	1.6843	1.6524	1.6012	1.545	1.4821	1.4472	1.4094	1.3676	1.3203	1.2646	1.1926
Inf	2.7055	2.3026	2.0838	1.9449	1.8473	1.7741	1.7167	1.6702	1.6315	1.5987	1.5458	1.4871	1.4206	1.3832	1.3419	1.2951	1.24	1.1686	1

APPENDIX D

Developed Code in MATLAB for PIV Data Analysis

```

clc, clear
d=dir(fullfile('c:\','Users','12174696','Documents','Matlab','Moh','PIV','*.dat'));%
important
n=length(d);
disp('=====')
disp([num2str(n),' files have been read.'])
disp('=====')
B = fopen(d(1).name,'r');
B2=textscan(B,'%f %f %f %f %f %f','delimiter',' ','delimiter','/n','headerlines',4);
B3=length(B2{1,1});
D=25;
y=100;
Vbar=100;
% D=input('input pier diameter (mm): ');
% y=input('input water depth (mm): ');
% Vbar=input('input approach flow velocity (mm/s): ');
I=1;
A{I}=zeros;
X{I}=zeros;
Y{I}=zeros;
u{I}=zeros;
w{I}=zeros;
V{I}=zeros;
XX=zeros(B3,n);
YY=zeros(B3,n);
uu=zeros(B3,n);
ww=zeros(B3,n);
VV=zeros(B3,n);
NAME(I)={' '};
for I=1:n
    fid = fopen(d(I).name,'r');
    [pathstr,name,ext] = fileparts(d(I).name);
    NAME(I)={name};

```

```

A{I}=textscan(fid,'%f%f%f%f%f%f','delimiter',' ','delimiter','/n','headerlines',4);
X{I}=A{1,I}(1,1);
Y{I}=A{1,I}(1,2);
u{I}=A{1,I}(1,3);
w{I}=A{1,I}(1,4);
V{I}=A{1,I}(1,6);
XX(:,I)=X{1,I}{:,1};
YY(:,I)=Y{1,I}{1,1};
uu(:,I)=u{1,I}{1,1};
ww(:,I)=w{1,I}{1,1};
VV(:,I)=V{1,I}{1,1};
fclose(fid);
end
Xa=mean(XX,2);
Ya=mean(YY,2);
ua=mean(uu,2);
wa=mean(ww,2);
Va=mean(VV,2);
Ma=[Xa Ya ua wa Va];
fu=uu-ua;
fw=ww-wa;
fu2=fu.^2;
fw2=fw.^2;
fuw=-fu.*fw;
fu2a=mean(fu2,2);
fw2a=mean(fw2,2);
TIu=(fu2a.^0.5);
TIw=(fw2a.^0.5);
TI=(0.5.*(fu2a+fw2a)).^0.5;
TKE=0.5.*(fu2a+fw2a);
RSS=mean(fuw,2);
MF=[(Xa-15)./D Ya./y ua./Vbar wa./Vbar Va./Vbar TIu./Vbar TIw./Vbar TI./Vbar
TKE./(Vbar.^2) RSS./(Vbar.^2)];

```

```

% disp(Ma);
%
col_header={'X/D','Y/y','u/V','w/V','Va/V','TIu/V','TIw/V','TI/V','TKE/V^2','RSS/V^2'};
% xlswrite('Output4.xlsx',MF,'Sheet1','A2');
% xlswrite('Output4.xlsx',col_header,'Sheet1','A1');
% % figure
% plot((Xa-15)./D, Ya./y, '-ro'); grid('on');
% ylim([0,1])
% xlim([0,37.5])
% quiver((Xa-15)./D, Ya./y, ua./Vbar, wa./Vbar)
% xlabel('X/D'); ylabel('Y/y')
% ylim([0,1])
plot((Xa-15)./D, Ya./y)
% xlim([-6,2.5])
% plot(ischange(the_tab.posY), '-ro')
% xlim([90, 110]); grid on
%% Open the text file.
% fileID = fopen(d(I).name,'r');
%% Read columns of data according to the format.
% This call is based on the structure of the file used to generate this
% code. If an error occurs for a different file, try regenerating the code
% from the Import Tool.
%% dataArray = textscan(fileID, formatSpec, 'Delimiter', delimiter, 'TextType', 'string',
'EmptyValue', NaN, 'HeaderLines', startRow-1, 'ReturnOnError', false, 'EndOfLine',
'\r\n');
%% Close the text file.
% % fclose(fileID);
%% Post processing for unimportable data.
% No unimportable data rules were applied during the import, so no post
% processing code is included. To generate code which works for
% unimportable data, select unimportable cells in a file and regenerate the
% script.

```

```
%% Create output variable
% % Export000 = [dataArray{1:end-1}];
%% Clear temporary variables
% % clearvars filename delimiter startRow formatSpec fileID dataArray ans;
```